Investigation of energy flow in earthquake response of structures
Hao, Tzong-Ying
ProQuest Dissertations and Theses; 2002; ProQuest
pg. n/a

INFORMATION TO USERS

This manuscript has been reproduced from the microfilm master. UMI films the text directly from the original or copy submitted. Thus, some thesis and dissertation copies are in typewriter face, while others may be from any type of computer printer.

The quality of this reproduction is dependent upon the quality of the copy submitted. Broken or indistinct print, colored or poor quality illustrations and photographs, print bleedthrough, substandard margins, and improper alignment can adversely affect reproduction.

In the unlikely event that the author did not send UMI a complete manuscript and there are missing pages, these will be noted. Also, if unauthorized copyright material had to be removed, a note will indicate the deletion.

Oversize materials (e.g., maps, drawings, charts) are reproduced by sectioning the original, beginning at the upper left-hand corner and continuing from left to right in equal sections with small overlaps.

ProQuest Information and Learning
300 North Zeeb Road, Ann Arbor, MI 48106-1346 USA
800-521-0600

Reproduced with permission of the copyright owner. Further reproduction prohibited without permission.

Reproduced with permission of the copyright owner. Further reproduction prohibited without permission.

INVESTIGATION OF ENERGY FLOW IN EARTHQUAKE RESPONSE OF STRUCTURES

by

Tzong-Ying Hao

A Dissertation Presented to the
FACULTY OF THE GRADUATE SCHOOL
UNIVERSITY OF SOUTHERN CALIFORNIA
In Partial Fulfillment of the
Requirements for the Degree
DOCTOR OF PHILOSOPHY
(CIVIL ENGINEERING)

May 2002

Copyright 2002 Tzong-Ying Hao

Reproduced with permission of the copyright owner. Further reproduction prohibited without permission.

UMI Number: 3073789

UMI®

UMI Microform 3073789
Copyright 2003 by ProQuest Information and Learning Company.
All rights reserved. This microform edition is protected against unauthorized copying under Title 17, United States Code.

ProQuest Information and Learning Company
300 North Zeeb Road
P.O. Box 1346
Ann Arbor, MI 48106-1346

Reproduced with permission of the copyright owner. Further reproduction prohibited without permission.

UNIVERSITY OF SOUTHERN CALIFORNIA
The Graduate School
University Park
LOS ANGELES, CALIFORNIA 90089-1695

This dissertation, written by

Tzong-Ying Hao

Under the direction of h.ex... Dissertation Committee, and approved by all its members, has been presented to and accepted by The Graduate School, in partial fulfillment of requirements for the degree of

DOCTOR OF PHILOSOPHY

Dean of Graduate Studies

Date May 10, 2002

DISSERTATION COMMITTEE

Chairperson

Reproduced with permission of the copyright owner. Further reproduction prohibited without permission.

ACKNOWLEDGEMENTS

Foremost, I am indebted to my advisor, Prof. M. D. Trifunac, for providing continuous guidance during my studies at USC. He imbibed in me many important facets of scientific research and I realize that it is up to me to carry on those great ideas and dedication in future.

I am very grateful to the members of my Guidance and Defense Committee. Their comments and suggestions were of great help for the completion of this dissertation. I would also like to thank all the faculty and staff members of the Department of Civil Engineering at the University of Southern California and all my fellow graduate friends for their concern and help during this work.

I own a particular debt to Dr. M. I. Todorovska and Mr. C-H. Lin. It was them, more than anyone else, who provided support and encouragement when they were most needed.

Last but not least, I wish to express my deep gratitude to my family, especially to my beloved grandparents.

Reproduced with permission of the copyright owner. Further reproduction prohibited without permission.

TABLE OF CONTENTS

Reproduced with permission of the copyright owner. Further reproduction prohibited without permission.

Reproduced with permission of the copyright owner. Further reproduction prohibited without permission.

LIST OF TABLES

Reproduced with permission of the copyright owner. Further reproduction prohibited without permission.

LIST OF FIGURES

Reproduced with permission of the copyright owner. Further reproduction prohibited without permission.

Reproduced with permission of the copyright owner. Further reproduction prohibited without permission.

Reproduced with permission of the copyright owner. Further reproduction prohibited without permission.

Reproduced with permission of the copyright owner. Further reproduction prohibited without permission.

Reproduced with permission of the copyright owner. Further reproduction prohibited without permission.

Reproduced with permission of the copyright owner. Further reproduction prohibited without permission.

Reproduced with permission of the copyright owner. Further reproduction prohibited without permission.

ABSTRACT

The use of energy concepts is studied as an alternative to the traditional design methods, in the analyses of seismic demands imposed by the earthquake, and of structural capacities to meet such demands. It is shown how the earthquake energy at the source is converted into relative response of a structure, with a focus on the energy balance during soil-foundation-structure system response. A two-dimensional model is used to represent soil-foundation-structure systems. It is applied to five case studies: a 14-story reinforced concrete storage building in Hollywood, a 7-story reinforced concrete hotel in Van Nuys, a 12-story reinforced concrete commercial building in Sherman Oaks, a 9-story reinforced concrete library building in Pasadena, and an 8-story steel building in Santa Susana. For these buildings, the correspondence between the total incident wave energy and the sum of all energies associated with the response of their soil-structure systems is analyzed. Then, a realistic energy demand is defined. It is shown how this demand leads to deformation of the building and how the soil-foundation interaction effects can be included in the response analysis. Some elementary aspects of energy absorption capacity of a structure and the design advantages of not ignoring soil-structure interaction are demonstrated.

Reproduced with permission of the copyright owner. Further reproduction prohibited without permission.

1. INTRODUCTION

1.1 General

Traditionally, displacement ductility has been used as a criterion for earthquake resistant design of structures. Alternative energy-related concepts were discussed by Benioff (1934), Sezawa and Kanai (1936), Tanabashi (1937), and later by Tanabashi (1956), Housner (1956) and Blume (1960). Fig. 1.1 outlines the milestones of the work on earthquake-resistant design, the years of the major earthquakes (from earthquake engineering point of view), and of World Conferences on Earthquake Engineering (up to year 2000).

In 1934, Benioff proposed a measure of seismic destructiveness to be computed via the area under the relative displacement response spectrum. It can be shown that this result can be related to the energy of response to strong motion (Arias, 1970; Trifunac and Brady, 1975). Benioff (1934) introduced his paper on earthquake destructiveness by stating that "...*The problem of designing structures to withstand destructive earthquakes is not in a very satisfactory condition. On the one hand engineers do not know what characteristics of the ground motion are responsible for destruction, and on the other hand seismologists have no measurements of seismic motion which are sufficiently adequate to serve for design, even if the destructive characteristics were known. Consequently, engineers have been forced to proceed on an empirical basis. From past experience, chiefly in Japan, it has been found that buildings which are designed to withstand a constant horizontal acceleration of 0.1 gravity are, on the whole, fairly resistant to seismic damage. It is fortunate that such*

Reproduced with permission of the copyright owner. Further reproduction prohibited without permission.

a simple formula works at all, in view of its inadequacy from the point of view of precise computation..." Benioff did not discuss strong motion energy explicitly. However, his definition of destructiveness as "*the integral with respect to pendulum frequency of the maximum displacement of an infinite series of undamped pendulums*" is directly related to the energy of response.

Current seismic design codes describe earthquake excitation in the form of an acceleration response spectrum, which prescribes the required horizontal loads representing a design earthquake. Acceleration response spectrum displays the maximum absolute acceleration response, and its shape reflects the frequency content of excitation (Biot, 1932; 1933; 1934; 1941; 1942). Although acceleration response spectra provide a convenient tool for quantifying an earthquake input, research indicates that this is not sufficient for expressing the damage potential of earthquake ground motion. Seismic energy input, and seismic energy dissipation during strong shaking, can represent the damage potential of an earthquake ground motion more directly than spectral acceleration.

In this work, we consider an alternative to the spectral method in earthquake-resistant design by analyzing the flow of energy associated with strong motion, and by focusing on the energy during soil-foundation-structure system response. In Fig. 1.2, the principal stages of the earthquake wave energy flow, from the earthquake source, along the propagation path, and to the final work leading to relative response of the structure, are outlined. The losses of energy at every stage are also outlined. These

Reproduced with permission of the copyright owner. Further reproduction prohibited without permission.

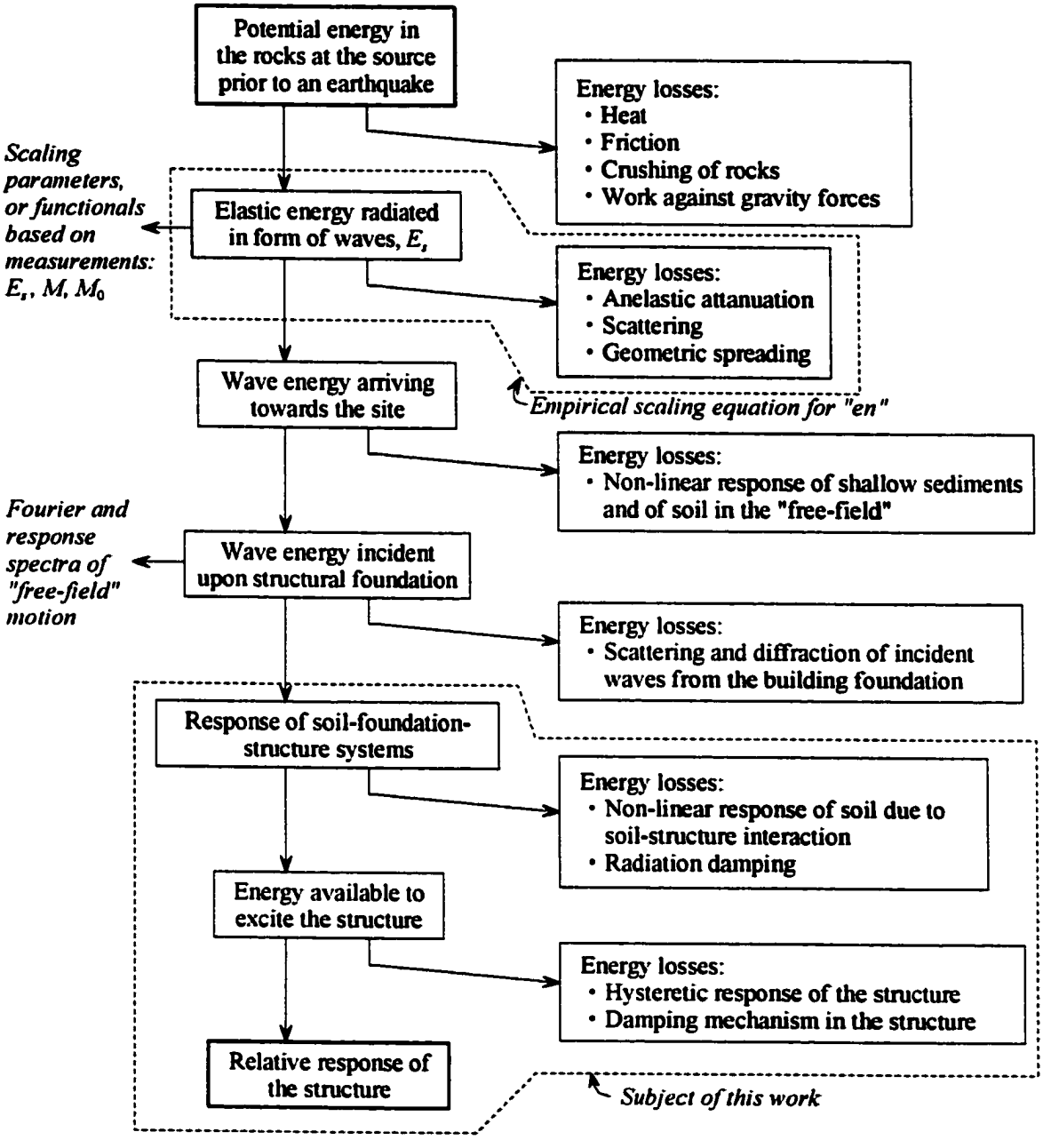

Fig. 1.2 An outline of principal stages in the flow of earthquake wave energy, from the earthquake source to a structure.

Reproduced with permission of the copyright owner. Further reproduction prohibited without permission.

losses must be accounted for to accurately quantify the remaining energy, which will excite the structure.

1.2 Literature Review and Key Issues in Energy of Structural Response

The formulation of a rational design approach based on energy concepts requires the understanding of the effects of the incident energy and other relevant parameters external to the structure (e.g. earthquake magnitude, distance to the causative fault and in-situ soil properties) on the response of earthquake-resisting structures.

The energy associated with elastic waves radiated from the earthquake source, E_s (Gutenberg and Richter, 1956), is attenuated with increasing epicentral distance, R, through mechanisms of inelastic attenuation, scattering, and geometric spreading (Trifunac, 1994; Trifunac et al., 2001f). The earthquake wave energy arriving towards the site is next dissipated by nonlinear response of shallow sediments and soil in the free-field (Joyner, 1975; Joyner and Chen, 1975; Trifunac and Todorovska, 1996, 1998), before it begins to excite the foundation. Once the foundation is excited by the incident earthquake waves, the response of the soil-structure system is initiated. The available incident wave energy is reduced by nonlinear deformation of the soil during soil-structure interaction (Trifunac et al., 1999a; 2001a, b) and by radiation damping (Luco et al., 1986; Todorovska and Trifunac, 1991). The earthquake wave energy flow and distribution involving the last three stages in Fig. 1.2: (1) the response of soil-foundation-structure system, (2) the energy available to excite the structure, and (3) the relative response of the structure, will be considered in this work.

Reproduced with permission of the copyright owner. Further reproduction prohibited without permission.

The total energy input into a structure exerted by an earthquake depends mainly on the total mass and the fundamental natural period of the structure (Akiyama, 1985, 1988, 1997; Uang and Bertero, 1988). Energy dissipation as means of reducing the seismic response of structures has become also an important topic among the designers who develop friction dampers, fluid dampers, and isolators.

A natural form of energy dissipation occurs during interaction between a structure, its foundation, and the supporting soil medium. This dissipated energy can be significant and will contribute towards reduction in seismic response. Unfortunately, this energy sink is often disregarded by the researchers and engineers while creating a model representation of the prototype to proceed with design of earthquake-resistant structures. Moreover, most modern structures are designed to resist severe loading conditions for which inelastic action exists only in the superstructure response. Hence there is need to develop soil-foundation analysis models which can account for inelastic behavior of soil. The non-linearity can occur either in the superstructure, in the foundation, in the supporting soil medium, or in all of those simultaneously, depending upon the system properties and amplitudes of excitation. Consequently, a good and realistic model must have the features which will describe the response of the soil-foundation-structure system as completely and as accurately as possible.

For the majority of structures an inelastic behavior is accepted in the design for severe earthquake shaking. The effects of such inelastic behavior on the intensity and the spectral distribution of the energy demands were investigated by Decanini and

Reproduced with permission of the copyright owner. Further reproduction prohibited without permission.

Mollaioli (2001). Fajfar and Fischinger (1990), Uang and Bertero (1990), and Tembulkar and Nau (1987) evaluated the effects of nonlinear behavior on the seismic input energy of SDOF systems. Zahrah and Hall (1984) evaluated the nonlinear response of simple structures and the damage potential of an earthquake ground motion as measured in terms of the amount of energy imparted into a structure, the amount of energy dissipated by inelastic deformation and by damping, as well as assessment of the displacement ductility of the structure and the number of yielding excursions and reversals experienced during the excitation. Uang and Bertero (1988) discussed the derivation of the two "energy equations" (absolute and relative), and have shown that the maximum values of the absolute and relative energy input, E_I, for any given constant displacement ductility ratio are very close in the period range of practical interest for earthquake-resistant design of buildings (0.3 to 5.0 seconds).

In most published studies, the derivation of energy equations begins by integrating the differential equation of dynamic equilibrium of a single-degree-of-freedom system with respect to displacement, which results in

$$E_I = E_E + E_D = E_K + E_S + E_{H\xi} + E_{H\mu} \tag{1.1}$$

where E_I is the energy input at the foundation of the building due to the earthquake ground motions, E_E is the stored elastic energy, E_D is the dissipated energy through viscous-damping mechanisms, E_K is the kinetic energy, E_S is the elastic strain energy, $E_{H\xi}$ is the energy dissipated through hysteretic damping and $E_{H\mu}$ is the energy dissipated due to hysteretic plastic deformation.

Reproduced with permission of the copyright owner. Further reproduction prohibited without permission.

An important omission in many of the published studies is that the effects of soil-structure interaction are ignored. Because of that significant energy loss mechanisms (nonlinear response of the soil and radiation damping) are thus neglected (Fig. 1.2). The other extreme is to neglect the stiffness of the foundation system (and the soil-structure interaction), and assume that the wave energy in the soil drives the building to follow the motions specified by the wave propagation in the free-field. This approximate approach underestimates the scattering of incident wave energy by the foundation and overestimates the energy transmitted into the building. The reality is somewhere between these two extremes, and can be studied further in detail only by numerical methods. Other simplifications and omissions in eqn (1.1) are that the dynamic instability and the effects of gravity on nonlinear response are usually ignored (Husid, 1967; Lee, 1979; Todorovska and Trifunac, 1991, 1993).

At present, the model most commonly used by engineers for the design of buildings assumes the structure to be fixed to a rigid ground. Current design methods thus disregard the influence the flexibility of ground has on the response of a structure. Such a procedure simplifies the analysis. The assumption that there is no coupling or interaction between the structure, its foundation and the supporting soil is however contrary to recorded observations (Trifunac et al., 1999a; 2001a, b). The conceptual model proposed herein attempts to capture the main characteristics of the nonlinear behavior of soil in soil-structure systems.

Reproduced with permission of the copyright owner. Further reproduction prohibited without permission.

1.3 Organization of this Dissertation

Chapter 2 deals with the representation of the seismic energy flow through the last three stages outlined in Fig. 1.2: the response of soil-foundation-structure systems, the energy available to excite the structure, and the relative response of the structure. For this purpose, a model is used (presented in Fig. 2.1), which is calibrated in Chapter 3 against five case studies–a fourteen-story reinforced concrete building in Hollywood, a seven-story reinforced concrete building in Van Nuys, a twelve-story reinforced concrete building in Sherman Oaks, a nine-story reinforced concrete building in Pasadena, and an eight-story steel building in Santa Susana. For these buildings, the correspondence between the total incident wave energy and the sum of all energies associated with the response of the soil-structure system is demonstrated. In Chapter 4, some energy-based design considerations are discussed and a regression analysis to interpret the energy dissipation of nonlinear soil behavior as means of reducing the seismic response of structures is explored. Chapter 5 presents a summary and conclusions of this study. Appendix A presents details of the approximate analysis for cases in which the earthquake motions at the base were not avaibale. Appendix B presents chosen values of the equation parameters of the model. Appendix C presents results for the relative response and its energies for the Sherman Oaks, Pasadena and Santa Susana buildings.

Reproduced with permission of the copyright owner. Further reproduction prohibited without permission.

2. ENERGY DURING SOIL-FOUNDATION-STRUCTURE SYSTEM RESPONSE

2.1 Model

To describe the energy flow through a soil-foundation-structure system, we use the idealized mathematical model shown in Fig. 2.1. In this model, the building is represented by an equivalent single-degree-of-freedom (SDOF) oscillator founded on a rigid embedded rectangular foundation. The top of the foundation is at the same level as the surface of the soil. The soil has shear modulus G, shear wave velocity β, Poisson's ratio ν, and mass density ρ_s. The oscillator has only one degree-of-freedom with respect to the foundation, θ^{rel}. The mass of the oscillator is m_b. It has height H and radius of gyration r_b. The oscillator is connected to the foundation at point O through a rotational spring and a viscous damper. The spring has stiffness K_b, and the viscous damper has damping constant C_b. The stiffness is chosen such that the natural period of the oscillator, T_1, is equal to the corresponding fixed-base period of the fundamental mode of the building. Assuming that the equivalent SDOF oscillator has same mass per unit length as the real building, then, H and r_b are related to H_{sb} and W_{sb}, the height and width of the real building (Todorovska and Trifunac, 1993), as

$$H = \frac{H_{sb}}{\sqrt{3}}, \quad r_b = \frac{W_{sb}}{\sqrt{3}}. \tag{2.1}$$

The rectangular foundation has width W_{sb}, depth D, mass m_f, and mass moment of inertia I_f. To simplify the analysis, we assume that the stiffness of the soil in the vertical direction is infinite. The foundation has two degrees-of-freedom with respect

Reproduced with permission of the copyright owner. Further reproduction prohibited without permission.

Reproduced with permission of the copyright owner. Further reproduction prohibited without permission.

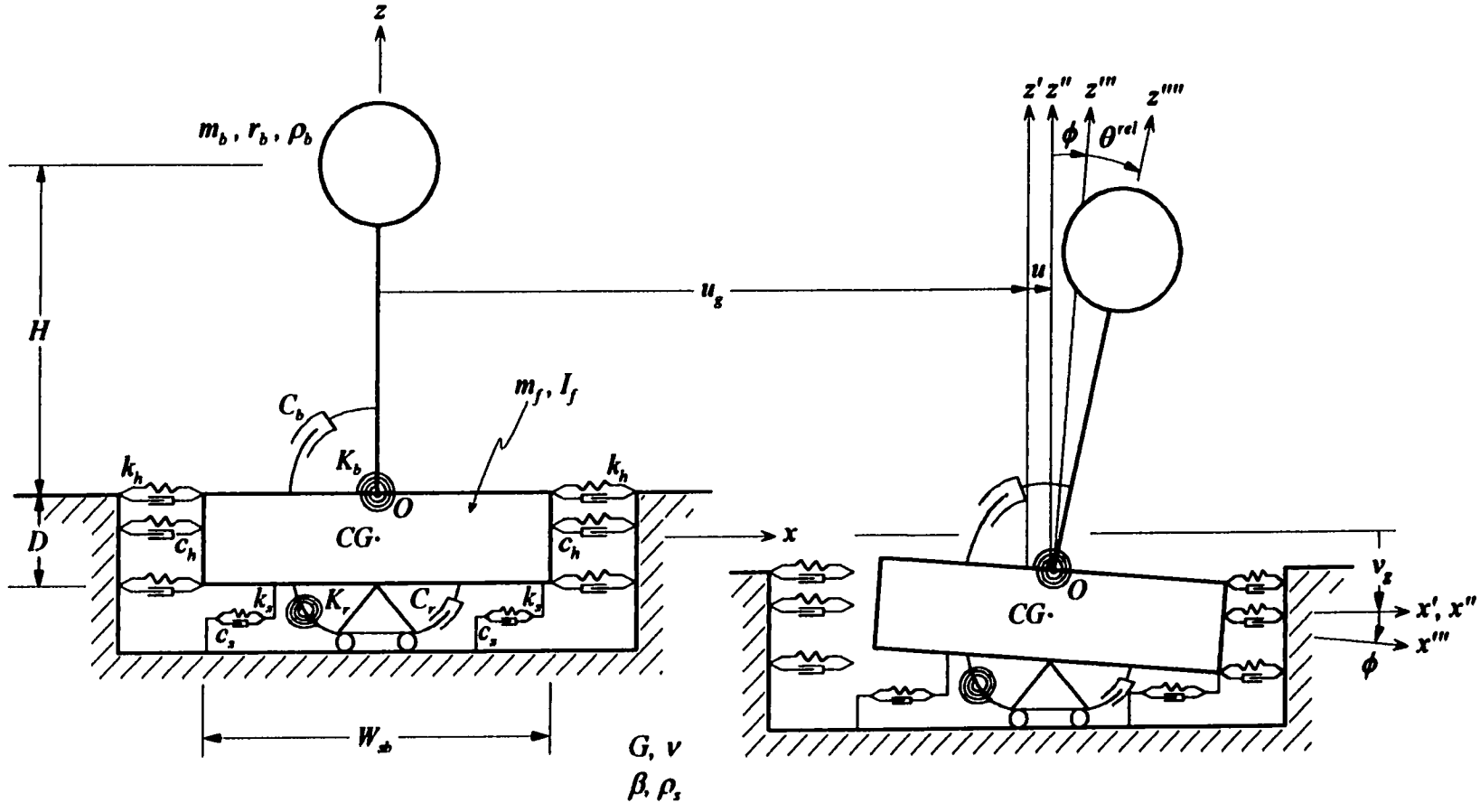

Fig. 2.1 The model of soil-foundation-building (SDOF oscillator) system in undeformed (left) and deformed (right) configurations.

to its center of gravity (point *CG*): horizontal translation, u, and rotation, ϕ. The foundation is surrounded by springs and dashpots, which model the reactive forces caused by deformation developed in the soil (Richart et al., 1970). In Fig. 2.1, k_h and c_h are the stiffness and damping constants of horizontal springs and dashpots around the foundation representing the horizontal reactive forces on the vertical faces of the foundation; k_s and c_s are the stiffness and damping constants of horizontal springs and dashpots at the base of the foundation representing the shear forces acting on the interface; and K_r and C_r are the rotational stiffness and damping constant representing the resisting moments in the half-space. Evaluation of the stiffness (k_h, k_s and K_r) and damping (c_h, c_s and C_r) constants is discussed in Trifunac et al. (2001f). This soil-foundation-oscillator system is subjected to horizontal and vertical excitations (u_g and v_g).

In our modeling, we assume the foundation is rigid, to reduce the number of degrees-of-freedom of the model (Duncan, 1952; Trifunac and Todorovska, 2001). Such models give an approximation of the system response for long wavelengths relative to the foundation dimensions (Lee, 1979). For short wavelengths, this assumption can result in nonconservative estimates of the relative deformations in the structure (Trifunac, 1997; Trifunac and Todorovska, 1997) and, in general, is expected to result in excessive estimates of scattering of the incident wave energy and in excessive radiation damping (Todorovska and Trifunac, 1990a, b, c; 1991; 1992; 1993). The extent to which this simplifying assumption is valid depends on the stiffness of the foundation system relative to that of the soil, and also on the overall

Reproduced with permission of the copyright owner. Further reproduction prohibited without permission.

rigidity of the structure (Iguchi and Luco, 1982; Liou and Huang, 1994; Hayir et al., 2001; Todorovska et al., 2001a, b, c; Trifunac et al., 1999a).

Ivanović et al. (2000) and Trifunac et al. (2001a, b, c) suggested that the soil behavior is nonlinear during most earthquakes, and that it can recover its stiffness after consolidation with time, and after small amplitude shaking from aftershocks and smaller earthquakes. The observed "softening" and "hardening" behavior of the system can be explained by a model with *gap* elements along the contact between the foundation and the soil. We assume the soil on the side of the foundation is represented by a hysteretic *slip model* (see of Fig. 2.2a) to simulate nonlinear behavior of the soil. This slip model emphasizes the pinching effects of soil with large stresses and the *gap* generated by soil compression. For the soil at the base of the foundation, the bilinear and softening characteristics are represented in Fig. 2.2b. Detailed description of these slip and bilinear hysteretic systems is presented in Trifunac et al. (2001f).

2.2 Equations of Motions

The equations of motion for the system are derived and solved including the nonlinear geometry and soil behavior, coupling of the vertical acceleration with the rocking and horizontal translation, and the effects of gravity forces ($m_b g$ and $m_f g$). The small deformation assumption is not required, and arbitrary material nonlinearity is allowed. The response of the building and of the soil can enter inelastic range during strong ground shaking. In that case, the analysis of soil-structure interaction (SSI) will be quite complicated. Consequently, at first, the building will be assumed

Reproduced with permission of the copyright owner. Further reproduction prohibited without permission.

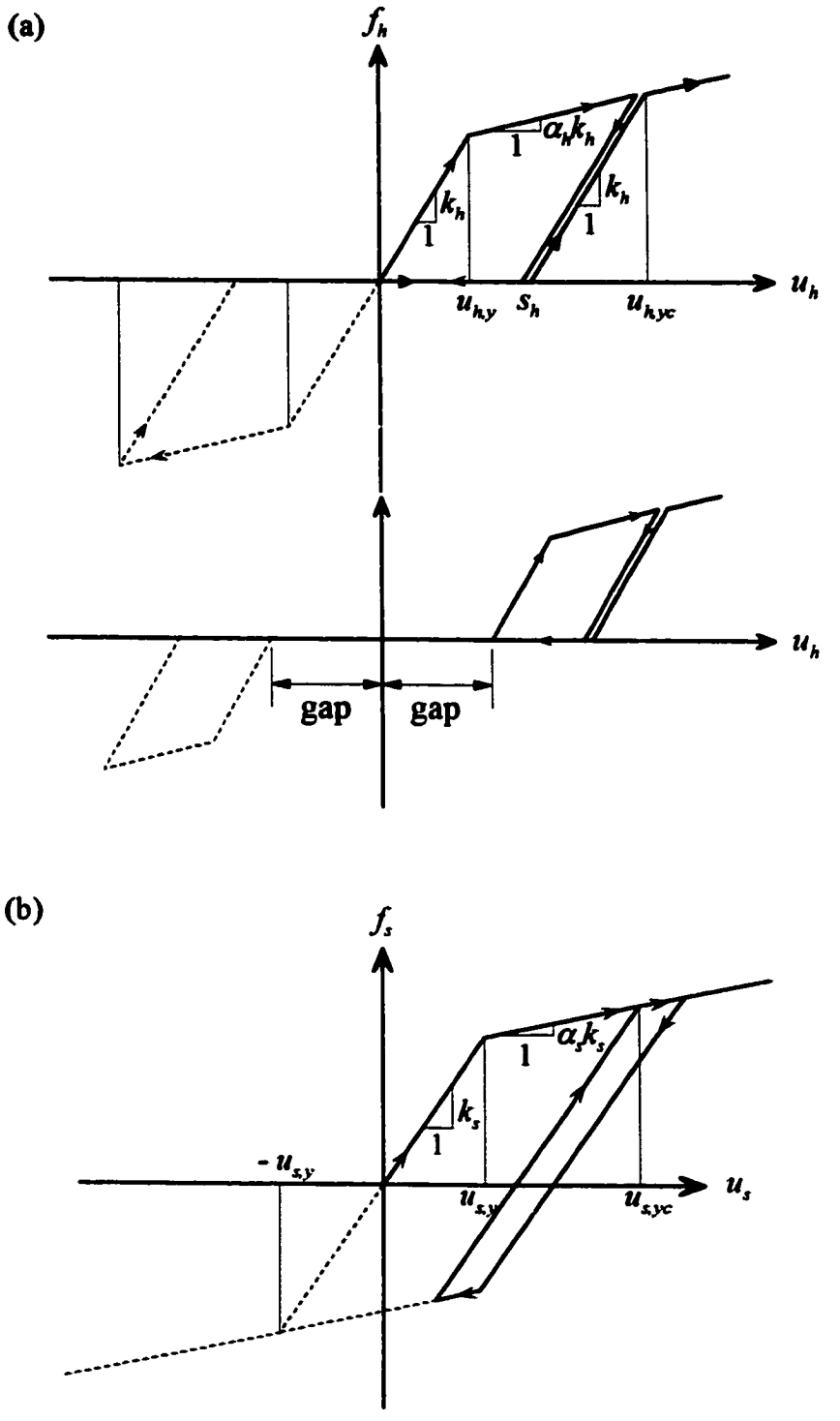

Fig. 2.2 Force-deformation relations used to represent the nonlinear behavior of soil. (a) Slip model for horizontal springs on two sides of the foundation. (b) Bilinear model for springs at the base of the foundation.

Reproduced with permission of the copyright owner. Further reproduction prohibited without permission.

to be linear, and the soil will be assumed to exhibit inelastic force-deformation relation. Later on in Chapter 4 we will briefly consider also the nonlinear response of the building.

Referring to Fig. 2.3, the total displacements due to horizontal, vertical and rocking motion of the center of mass of the foundation (point *CG*) are

$$u_{CG} = u_g + u \tag{2.2}$$

$$v_{CG} = v_g \tag{2.3}$$

$$\phi_{CG} = \phi \tag{2.4}$$

and those of point *O* are

$$u_O = u_{CG} + \frac{D}{2}\sin\phi \tag{2.5}$$

$$v_O = v_{CG} + \frac{D}{2}(1-\cos\phi) \tag{2.6}$$

$$\phi_O = \phi . \tag{2.7}$$

Similarly, the total displacements of the center of mass of the building are

$$u_b = u_{CG} + \frac{D}{2}\sin\phi + H\sin(\phi + \theta^{rel}) \tag{2.8}$$

$$v_b = v_{CG} + \frac{D}{2}(1-\cos\phi) + H[1-\cos(\phi + \theta^{rel})] \tag{2.9}$$

$$\phi_b = \phi + \theta^{rel} . \tag{2.10}$$

The equations of motion for the system then can be derived from the equilibrium of forces and moments. From the equations of dynamic equilibrium of forces in the horizontal and vertical directions, and all moments acting about

Reproduced with permission of the copyright owner. Further reproduction prohibited without permission.

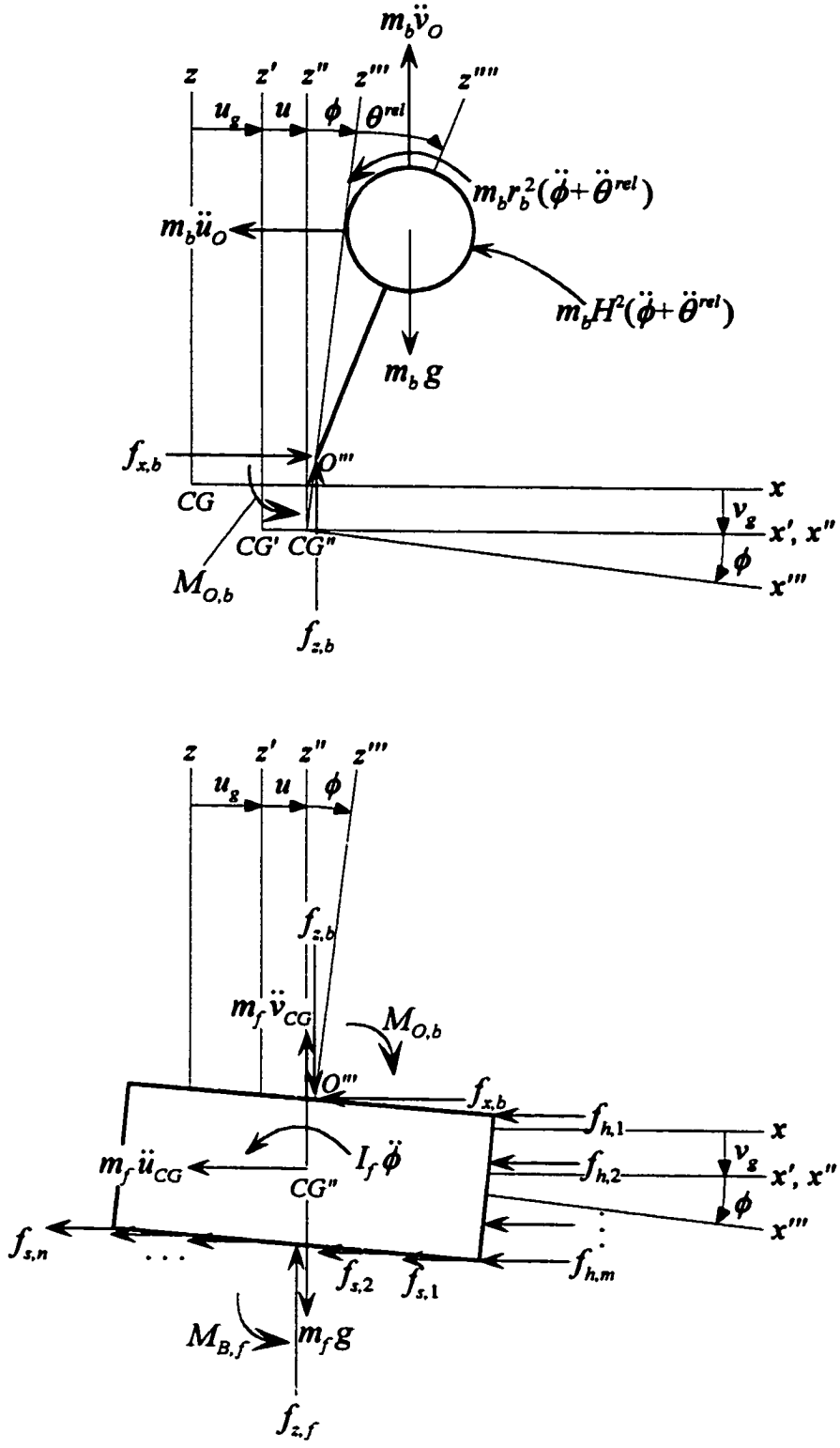

Fig. 2.3 Free-body diagrams for the deformed model in Fig. 2.1.

Reproduced with permission of the copyright owner. Further reproduction prohibited without permission.

point O, the interactive forces and the moment between the oscillator and foundation are

$$\Sigma F_x = 0 \Rightarrow f_{x,b} = m_b \ddot{u}_b \tag{2.11}$$

$$\Sigma F_z = 0 \Rightarrow f_{z,b} = -m_b(\ddot{v}_b - g) \tag{2.12}$$

$$\begin{aligned}\Sigma M_O = 0 \Rightarrow M_{O,b} = &-m_b \ddot{u}_O H \cos(\phi + \theta^{rel}) - m_b(\ddot{v}_O - g) H \sin(\phi + \theta^{rel}) \\ &-(m_b r_b^2 + m_b H^2)(\ddot{\phi} + \ddot{\theta}^{rel}).\end{aligned} \tag{2.13}$$

Since

$$M_{O,b} = K_b \theta^{rel} + C_b \dot{\theta}^{rel}, \tag{2.14}$$

the substitution of eqn (2.14) into (2.13) gives

$$I_O(\ddot{\phi} + \ddot{\theta}^{rel}) + m_b \ddot{u}_O H \cos(\phi + \theta^{rel}) + m_b(\ddot{v}_O - g) H \sin(\phi + \theta^{rel}) + K_b \theta^{rel} + C_b \dot{\theta}^{rel} = 0 \tag{2.15}$$

where $I_O = m_b r_b^2 [1 + (\frac{r_b}{H})^2]$.

From the equations of dynamic equilibrium of all forces and moments acting on the foundation about point CG, it follows that

$$\Sigma F_x = 0 \Rightarrow \sum_{i=1}^{m} f_{h,i} + \sum_{j=1}^{n} f_{s,j} = -m_f \ddot{u}_{CG} - f_{x,b} \tag{2.16}$$

$$\Sigma F_z = 0 \Rightarrow f_{z,f} = -m_f(\ddot{v}_{CG} - g) + f_{z,b} \tag{2.17}$$

$$\begin{aligned}\Sigma M_{CG} = 0 \Rightarrow M_{B,f} = &(f_{z,b} + f_{z,f})\frac{D}{2}\sin\phi - f_{x,b}\frac{D}{2}\cos\phi + M_{O,b} - I_f \ddot{\phi} \\ &-\sum_{i=1}^{m}(f_{h,i}\cos\phi)d_i + \sum_{i=1}^{m}(f_{h,i}\sin\phi)\frac{W_{sb}}{2} - \sum_{j=1}^{n}(f_{s,j}\sin\phi)l_i + \sum_{j=1}^{n}(f_{s,j}\cos\phi)\frac{D}{2}\end{aligned} \tag{2.18}$$

and

$$M_{B,f} = K_r \phi + C_r \dot{\phi}. \tag{2.19}$$

Reproduced with permission of the copyright owner. Further reproduction prohibited without permission.

In eqns (2.16), (2.17) and (2.18), $f_{h,i}$ and $f_{s,j}$, represent the spring and damping forces of the soil, and can be expressed as

$$f_{h,i} = f_{h,i}^{D} + f_{h,i}^{S} = c_{h,i}\dot{u}_i + k_{h,i}u_i \tag{2.20}$$

$$f_{s,j} = f_{s,j}^{D} + f_{s,j}^{S} = c_{s,j}\dot{u}_j + k_{s,j}u_j \tag{2.21}$$

in which

$$u_i = u + d_i \sin\phi - \frac{W_{sb}}{2}(1-\cos\phi)\,, \quad \dot{u}_i = \dot{u} + d_i \cos\phi\,\dot{\phi} - \frac{W_{sb}}{2}\sin\phi\,\dot{\phi} \tag{2.22}$$

$$u_j = u - \frac{D}{2}\sin\phi + l_j(1-\cos\phi)\,, \quad \dot{u}_j = \dot{u} - \frac{D}{2}\cos\phi\,\dot{\phi} + l_j \sin\phi\,\dot{\phi} \tag{2.23}$$

d_i is the distance from the x-axis to the point where $f_{h,i}$ is acting, and l_j is the distance from the z-axis to the point where $f_{s,j}$ is acting. It should be noted that the stiffness and damping constants are associated with yielding of soil. Hence, $c_{h,i}$, $k_{h,i}$, $c_{s,j}$ and $k_{s,j}$ are time dependent.

Next, from eqns (2.2), (2.3), (2.8) and (2.9) it follows

$$\ddot{u}_{CG} = \ddot{u}_g + \ddot{u} \tag{2.24}$$

$$\ddot{v}_{CG} = \ddot{v}_g \tag{2.25}$$

$$\begin{aligned}\ddot{u}_b = \ddot{u}_{CG} + \frac{D}{2}(-\sin\phi\ \dot{\phi}^2 + \cos\phi\ \ddot{\phi}) + H[-\sin(\phi+\theta^{rel})(\dot{\phi}+\dot{\theta}^{rel})^2 \\ + \cos(\phi+\theta)(\ddot{\phi}+\ddot{\theta}^{rel})]\end{aligned} \tag{2.26}$$

and

$$\begin{aligned}\ddot{v}_b = \ddot{v}_{CG} - \frac{D}{2}(-\cos\phi\ \dot{\phi}^2 - \sin\phi\ \ddot{\phi}) - H[-\cos(\phi+\theta^{rel})(\dot{\phi}+\dot{\theta}^{rel})^2 \\ - \sin(\phi+\theta)(\ddot{\phi}+\ddot{\theta}^{rel})].\end{aligned} \tag{2.27}$$

Reproduced with permission of the copyright owner. Further reproduction prohibited without permission.

Then, in eqns (2.11) through (2.13), $f_{x,b}$, $f_{z,b}$ and $M_{O,b}$ can be expressed in terms of θ^{rel}, u and ϕ

$$f_{x,b} = m_b(\ddot{u}_g + \ddot{u}) + m_b\frac{D}{2}(-\sin\phi\ \dot{\phi}^2 + \cos\phi\ \ddot{\phi}) + m_bH[-\sin(\phi+\theta^{rel})(\dot{\phi}+\dot{\theta}^{rel})^2 + \cos(\phi+\theta)(\ddot{\phi}+\ddot{\theta}^{rel})] \tag{2.28}$$

$$f_{z,b} = -m_b(\ddot{v}_g - g) + m_b\frac{D}{2}(-\cos\phi\,\dot{\phi}^2 - \sin\phi\,\ddot{\phi}) + m_bH[-\cos(\phi+\theta^{rel})(\dot{\phi}+\dot{\theta}^{rel})^2 - \sin(\phi+\theta)(\ddot{\phi}+\ddot{\theta}^{rel})] \tag{2.29}$$

and

$$M_{O,b} = -m_b(\ddot{u}_g + \ddot{u})H\cos(\phi+\theta^{rel}) - m_b\frac{D}{2}(-\sin\phi\,\dot{\phi}^2 + \cos\phi\,\ddot{\phi})H\cos(\phi+\theta^{rel}) - m_b(\ddot{v}_g - g)H\sin(\phi+\theta^{rel}) + m_b\frac{D}{2}(-\cos\phi\,\dot{\phi}^2 - \sin\phi\,\ddot{\phi})H\sin(\phi+\theta^{rel}) - I_O(\ddot{\phi}+\ddot{\theta}^{rel}) \tag{2.30}$$

so that, eqn (2.23) becomes

$$I_O(\ddot{\phi}+\ddot{\theta}^{rel}) + m_b(\ddot{u}_g + \ddot{u})H\cos(\phi+\theta^{rel}) + m_b\frac{D}{2}(-\sin\phi\,\dot{\phi}^2 + \cos\phi\,\ddot{\phi})H\cos(\phi+\theta^{rel}) + m_b(\ddot{v}_g - g)H\sin(\phi+\theta^{rel}) - m_b\frac{D}{2}(-\cos\phi\,\dot{\phi}^2 - \sin\phi\,\ddot{\phi})H\sin(\phi+\theta^{rel}) + K_b\theta^{rel} + C_b\dot{\theta}^{rel} = 0. \tag{2.31}$$

Now we substitute eqn (2.28) into (2.16), (2.29) into (2.17), and obtain

$$m_f(\ddot{u}_g + \ddot{u}) + m_b(\ddot{u}_g + \ddot{u}) + m_b\frac{D}{2}(-\sin\phi\,\dot{\phi}^2 + \cos\phi\,\ddot{\phi}) + m_bH[-\sin(\phi+\theta^{rel})(\dot{\phi}+\dot{\theta}^{rel})^2 + \cos(\phi+\theta^{rel})(\ddot{\phi}+\ddot{\theta}^{rel})] + \sum_{i=1}^{m} f_{h,i} + \sum_{j=1}^{n} f_{s,j} = 0 \tag{2.32}$$

and

$$f_{z,f} = -m_f(\ddot{v}_g - g) - m_b(\ddot{v}_g - g) + m_b\frac{D}{2}(-\cos\phi\,\dot{\phi}^2 - \sin\phi\,\ddot{\phi}) + m_bH[-\cos(\phi+\theta^{rel})(\dot{\phi}+\dot{\theta}^{rel})^2 - \sin(\phi+\theta)(\ddot{\phi}+\ddot{\theta}^{rel})]. \tag{2.33}$$

Reproduced with permission of the copyright owner. Further reproduction prohibited without permission.

Similarly, we substitute eqns (2.19), (2.28) through (2.30) and (2.33) into (2.18) to get

$$
\begin{aligned}
&K_r\phi + C_r\dot{\phi} + m_b(\ddot{v}_g - g)D\sin\phi - m_b\frac{D^2}{2}(-\cos\phi\dot{\phi}^2 - \sin\phi\ddot{\phi})\sin\phi \\
&\quad - m_bHD[-\cos(\phi+\theta^{rel})(\dot{\phi}+\dot{\theta}^{rel})^2 - \sin(\phi+\theta^{rel})(\dot{\phi}+\dot{\theta}^{rel})^2]\sin\phi \\
&\quad + m_f(\ddot{v}_g - g)\frac{D}{2}\sin\phi + m_b(\ddot{u}_g + \ddot{u})\frac{D}{2}\cos\phi + m_b\frac{D^2}{4}(-\sin\phi\dot{\phi}^2 + \cos\phi\ddot{\phi})\cos\phi \\
&\quad + m_bH\frac{D}{2}[-\sin(\phi+\theta^{rel})(\dot{\phi}+\dot{\theta}^{rel})^2 + \cos(\phi+\theta^{rel})(\ddot{\phi}+\ddot{\theta}^{rel})]\cos\phi \\
&\quad + m_b(\ddot{u}_g + \ddot{u})H\cos(\phi+\theta^{rel}) + m_bH\frac{D}{2}(-\sin\phi\dot{\phi}^2 + \cos\phi\ddot{\phi})\sin(\phi+\theta^{rel}) \\
&\quad + m_b(\ddot{v}_g - g)H\sin(\phi+\theta^{rel}) - m_bH\frac{D}{2}(-\cos\phi\dot{\phi}^2 - \sin\phi\ddot{\phi})\sin(\phi+\theta^{rel}) \\
&\quad + I_O(\ddot{\phi}+\ddot{\theta}^{rel}) + I_f\ddot{\phi} + \sum_{i=1}^{m} f_{h,i}(d_i\cos\phi - \frac{W_{sb}}{2}\sin\phi) + \sum_{j=1}^{n} f_{s,j}(l_j\sin\phi - \frac{D}{2}\cos\phi) = 0
\end{aligned}
\tag{2.34}
$$

The general equations of motion for the nonlinear soil-foundation-oscillator system are eqns (2.31), (2.32) and (2.34). These equations are in terms of three principal unknown displacements. The unknown displacements can be solved numerically in time domain, for example, by the Runge-Kutta method.

The response of the foundation will contribute towards dissipation of the earthquake energy. Because of this, the overall displacement of the equivalent oscillator representing the building will be decreased. Also, the dynamic stability of the system may be important. Therefore it is necessary to consider the system in which the displacements of the foundation are included explicitly in the dynamic equilibrium equations of the system. By assuming the displacements are small, the general equations of motion can be simplified, without losing the coupling terms, the gravity force effects and the vertical acceleration effects.

Reproduced with permission of the copyright owner. Further reproduction prohibited without permission.

2.3 Derivation of Energy Equations

When a system is subjected to earthquake shaking, the incident waves propagate into it. During strong ground motion, part of the incident energy is dissipated by scattering from the foundation and by the deformation of the soil, and the rest is transmitted into the building.

Referring to the free-body diagrams in Fig. 2.3, all forces and moments move through the corresponding displacements and thus do work. To evaluate this work, we integrate all six equilibrium equations of the system, eqns (2.11), (2.12), (2.15), (2.16), (2.17) and (2.18), with respect to their corresponding displacements, as follows.

$$\int_{u_b} \text{eqn (2.11)}\, du_b = \int (m_b \ddot{u}_b - f_{x,b})\, du_b = 0 \tag{2.35}$$

$$\int_{v_b} \text{eqn (2.12)}\, dv_b = \int [m_b(\ddot{v}_b - g) + f_{z,b}]\, dv_b = 0 \tag{2.36}$$

$$\begin{aligned}\int_{\phi_b} \text{eqn (2.15)}\, d\phi_b = \int [&m_b \ddot{u}_O H \cos\phi_b + m_b(\ddot{v}_O - g) H \sin\phi_b \\ &+ I_O \ddot{\phi}_b + K_b \theta^{rel} + C_b \dot{\theta}^{rel}]\, d\phi_b = 0\end{aligned} \tag{2.37}$$

$$\int_{u_{CG}} \text{eqn (2.16)}\, du_{CG} = \int (m_f \ddot{u}_{CG} + f_{x,b} + \sum_{i=1}^{m} f_{h,i} + \sum_{j=1}^{n} f_{s,j})\, du_{CG} = 0 \tag{2.38}$$

$$\int_{v_{CG}} \text{eqn (2.17)}\, dv_{CG} = \int [m_f(\ddot{v}_{CG} - g) - f_{z,b} + f_{z,f}]\, dv_{CG} = 0 \tag{2.39}$$

and

$$\begin{aligned}\int_{\phi_{CG}} \text{eqn (2.18)}\, d\phi_{CG} = \int (&K_r \phi + C_r \dot{\phi} - f_{z,b} \frac{D}{2} \sin\phi - f_{z,f} \frac{D}{2} \sin\phi + f_{x,b} \frac{D}{2} \cos\phi \\ &- K_b \theta^{rel} - C_b \dot{\theta}^{rel} + I_f \ddot{\phi} + \sum_{i=1}^{m} f_{h,i} \cos\phi\, d_i - \sum_{i=1}^{m} f_{h,i} \sin\phi \frac{W_{sb}}{2} \\ &+ \sum_{j=1}^{n} f_{s,j} \sin\phi\, l_j - \sum_{j=1}^{n} f_{s,j} \cos\phi \frac{D}{2}]\, d\phi_{CG} = 0\end{aligned} \tag{2.40}$$

Reproduced with permission of the copyright owner. Further reproduction prohibited without permission.

The total work done in the system is then computed by superposition of eqns (2.35) through (2.40).

These contributions to the system energy can be evaluated by rewriting the integrals with respect to time. Thus

$$\text{eqn (2.35)} \Rightarrow \int (m_b \ddot{u}_b - f_{x,b})\, \dot{u}_b \, dt = 0 \tag{2.41}$$

$$\text{eqn (2.36)} \Rightarrow \int [m_b (\ddot{v}_b - g) + f_{z,b}]\, \dot{v}_b \, dt = 0 \tag{2.42}$$

$$\begin{aligned}\text{eqn (2.37)} \Rightarrow \int [&m_b \ddot{u}_O H \cos\phi_b + m_b (\ddot{v}_O - g) H \sin\phi_b \\ &+ I_O \ddot{\phi}_b + K_b \theta^{rel} + C_b \dot{\theta}^{rel}]\, \dot{\phi}_b \, dt = 0\end{aligned} \tag{2.43}$$

$$\text{eqn (2.38)} \Rightarrow \int (m_f \ddot{u}_{CG} + f_{x,b} + \sum_{i=1}^{m} f_{h,i} + \sum_{j=1}^{n} f_{s,j})\, \dot{u}_{CG} \, dt = 0 \tag{2.44}$$

$$\text{eqn (2.39)} \Rightarrow \int [m_f (\ddot{v}_{CG} - g) - f_{z,b} + f_{z,f}]\, \dot{v}_{CG} \, dt = 0 \tag{2.45}$$

and

$$\begin{aligned}\text{eqn (2.40)} \Rightarrow \int (&K_r \phi + C_r \dot{\phi} - f_{z,b} \frac{D}{2} \sin\phi - f_{z,f} \frac{D}{2} \sin\phi + f_{x,b} \frac{D}{2} \cos\phi \\ &- K_b \theta^{rel} - C_b \dot{\theta}^{rel} + I_f \ddot{\phi} + \sum_{i=1}^{m} f_{h,i} \cos\phi\, d_i - \sum_{i=1}^{m} f_{h,i} \sin\phi \frac{W_{sb}}{2} \\ &+ \sum_{j=1}^{n} f_{s,j} \sin\phi\, l_j - \sum_{j=1}^{n} f_{s,j} \cos\phi \frac{D}{2}]\, \dot{\phi}_{CG} \, dt = 0\end{aligned} \tag{2.46}$$

Recalling eqns (2.2) through (2.10), the above equations can be expressed in terms of θ^{rel}, u and ϕ.

To simplify these energy formulae, we keep only the first order terms of the Taylor series expansions of the sine and cosine functions of the angles θ^{rel} and ϕ (and

Reproduced with permission of the copyright owner. Further reproduction prohibited without permission.

their linear combination), and eliminate the products of small angles and of their derivatives. Then, the above six equations give

$$\int \{m_b[\ddot{u} + \frac{D}{2}\ddot{\phi} + H(\ddot{\phi} + \ddot{\theta}^{rel})] - f_{x,b}\}\, \dot{u}_b\, dt = -\int m_b \ddot{u}_g \dot{u}_b dt \tag{2.47}$$

$$\int (-m_b g + f_{z,b})\, \dot{v}_b\, dt = -\int m_b \ddot{v}_g \dot{v}_b\, dt \tag{2.48}$$

$$\int [m_b(\ddot{u}_O + \frac{D}{2}\ddot{\phi})H - m_b g H \phi_b + I_O \ddot{\phi}_b + K_b \theta^{rel} + C_b \dot{\theta}^{rel}]\, \dot{\phi}_b\, dt = -\int (m_b \ddot{u}_g H + m_b \ddot{v}_g H \phi_b)\, \dot{\phi}_b\, dt \tag{2.49}$$

$$\int (m_f \ddot{u} + f_{x,b})\, \dot{u}_{CG}\, dt + \int (\sum_{i=1}^{m} f_{h,i} + \sum_{j=1}^{n} f_{s,j})\, \dot{u}\, dt = -\int m_f \ddot{u}_g \dot{u}_{CG}\, dt \tag{2.50}$$

$$\int (-m_f g - f_{z,b} + f_{z,f})\, \dot{v}_{CG}\, dt = -\int m_f \ddot{v}_g \dot{v}_{CG}\, dt \tag{2.51}$$

and

$$\int (K_r \phi + C_r \dot{\phi} - f_{z,b}\frac{D}{2}\phi - f_{z,f}\frac{D}{2}\phi + f_{x,b}\frac{D}{2} - K_b \theta^{rel} - C_b \dot{\theta}^{rel} + I_f \ddot{\phi} + \sum_{i=1}^{m} f_{h,i} d_i - \sum_{i=1}^{m} f_{h,i}\phi \frac{W_{sb}}{2} + \sum_{j=1}^{n} f_{s,j}\phi l_j - \sum_{j=1}^{n} f_{s,j}\frac{D}{2})\, \dot{\phi}_{CG}\, dt = 0 \tag{2.52}$$

Next, we group the energy terms, according to their physical nature, into the following categories:

$E_K(t)$ = kinetic energy

$E_P(t)$ = potential energy of gravity forces

$E_D^{bldg}(t)$ = damping energy dissipated in the building

$E_S^{bldg}(t)$ = recoverable elastic strain energy in the building

$E_D^{soil}(t)$ = energy dissipated by "dashpots" of the soil

Reproduced with permission of the copyright owner. Further reproduction prohibited without permission.

$E_S^{soil}(t)$ = elastic strain energy in the soil

$E_Y^{soil}(t)$ = irrecoverable hysteretic energy in the soil

$E_{S+Y}^{soil}(t) = E_S^{soil}(t) + E_Y^{soil}(t)$

$E_I(t)$ = total earthquake input energy.

First, based on eqns (2.47) through (2.52), the earthquake input energy is the sum of all right side terms

$$E_I(t) = -\int [m_b \ddot{u}_g \dot{u}_b + m_b \ddot{v}_g \dot{v}_b + (m_b \ddot{u}_g H + m_b \ddot{v}_g H \phi_b)\dot{\phi}_b + m_f \ddot{u}_g \dot{u}_{CG} + m_f \ddot{v}_g \dot{v}_{CG}]\, dt \qquad (2.53)$$

The kinetic energy associated with absolute motion of the two masses is

$$E_K(t) = \int \{m_b(\ddot{u} + \frac{D}{2}\ddot{\phi} + H\ddot{\phi}_b)\dot{u}_b + [m_b(\ddot{u} + \frac{D}{2}\ddot{\phi})H + I_O\ddot{\phi}_b]\dot{\phi}_b + m_f \ddot{u}\dot{u}_{CG} + I_f \ddot{\phi}\,\dot{\phi}_{CG}\}dt \qquad (2.54)$$

It can be seen that $E_K(t)$ is equal to the integrals of the inertial forces with respect to their absolute velocities. The potential energy associated with the gravity forces is

$$E_P(t) = -\int (m_b g \dot{v}_b + m_b g H \phi_b \dot{\phi}_b + m_f g \dot{v}_{CG})\, dt \qquad (2.55)$$

The energy dissipated by viscous damping in the building can be calculated from

$$E_D^{bldg}(t) = \int C_b (\dot{\theta}^{rel})^2 dt \qquad (2.56)$$

The recoverable strain energy of the building (for linear response) is

$$E_S^{bldg}(t) = \frac{1}{2} K_b (\theta^{rel})^2 \qquad (2.57)$$

For this illustration the building is assumed to deform in linear manner only, the irrecoverable hysteretic energy in the building will be zero. Then, the energy dissipated by the dashpots in the soil is

Reproduced with permission of the copyright owner. Further reproduction prohibited without permission.

$$E_D^{soil}(t) = \int (\sum_{i=1}^{m} f_{h,i}^D + \sum_{j=1}^{n} f_{s,j}^D)\, \dot{u}\, dt + \int C_r \dot{\phi}^2\, dt + \int \{\sum_{i=1}^{m} f_{h,i}^D (d_i - \frac{W_{sb}}{2}\phi) + \sum_{j=1}^{n} f_{s,j}^D (l_j \phi - \frac{D}{2})\}\, \dot{\phi}\, dt \tag{2.58}$$

The energy dissipated by the yielding and the recoverable strain energy of the soil can be obtained from

$$E_{S+Y}^{soil}(t) = \int (\sum_{i=1}^{m} f_{h,i}^S + \sum_{j=1}^{n} f_{s,j}^S)\, \dot{u}\, dt + \int K_r \phi\, \dot{\phi}\, dt + \int \{\sum_{i=1}^{m} f_{h,i}^S (d_i - \frac{W_{sb}}{2}\phi) + \sum_{j=1}^{n} f_{s,j}^S (l_j \phi - \frac{D}{2})\}\, \dot{\phi}\, dt \tag{2.59}$$

in which

$$E_S^{soil}(t) = \sum_{i=1}^{m} \frac{(f_{h,i}^S)^2}{2k_{h,i}} + \sum_{j=1}^{n} \frac{(f_{s,j}^S)^2}{2k_{s,j}} + \frac{K_r \phi^2}{2} \tag{2.60}$$

where $k_{h,i}$ and $k_{s,j}$ are the initial stiffnesses of the inelastic soil.

Based on these energy "components," the statement of energy balance of the system is then expressed as

$$E_K(t) + E_P(t) + E_D^{bldg}(t) + E_S^{bldg}(t) + E_D^{soil}(t) + E_{S+Y}^{soil}(t) = E_I(t) \tag{2.61}$$

The foregoing analysis of the nonlinear system models the energy components of the simple nonlinear SSI system in Fig. 2.1, rather than that of the fixed-base system (e.g. Akiyama, 1985, 1988, 1997; Anderson and Bertero, 1969; Uang and Bertero, 1988, 1990). Comparing eqn (2.61) with eqn (1.1), the simplifications and omissions in eqn (1.1) become clear.

Reproduced with permission of the copyright owner. Further reproduction prohibited without permission.

3. CASE STUDIES OF FIVE BUILDINGS

To illustrate the behavior of the model shown in Fig. 2.1, for energy partitioning in a soil-structure system, the Hollywood Storage building (HSB), the Van Nuys seven story hotel (VN7SH), the Sherman Oaks Bank of California building (BOC), the Pasadena (Caltech) Millikan Library (MLK), and the Santa Susana ETEC Bldg. #462 (ETEC) are selected. These five buildings have been studied previously by many investigators (see references in Trifunac et al., 2001f; Trifunac et al., 2001a, b; and Trifunac and Todorovska, 2001). There are multiple recordings in these buildings of weak, intermediate and strong earthquake responses, and three of these buildings were tested using ambient vibration methods. All, except the Santa Susana ETEC building, are reinforced concrete structures and the sites lie on recent alluvium. The ETEC building is a steel structure, and its site lies on sandstone bedrock, which make the response of this building different from others.

3.1 Building Descriptions and Earthquake Recordings

HSB The Hollywood Storage Building is located at 1025 North Highland Ave., about 300 feet south of Santa Monica Blvd., in Los Angeles, California (Trifunac et al., 2001e). It is a reinforced concrete frame structure, supported by reinforced concrete footings on Raymond concrete piles (Duke et al, 1970; Papageorgiou and Lin, 1991). The building has fourteen stories and a partial basement with plan dimensions of 217½ feet east to west by 51 feet south to north (shown in Fig. 3.1a). The roof low point is 148¾ feet above the first floor, and the typical story height is 10½ feet. The first full-scale tests of HSB appear to have been carried out in 1934,

Reproduced with permission of the copyright owner. Further reproduction prohibited without permission.

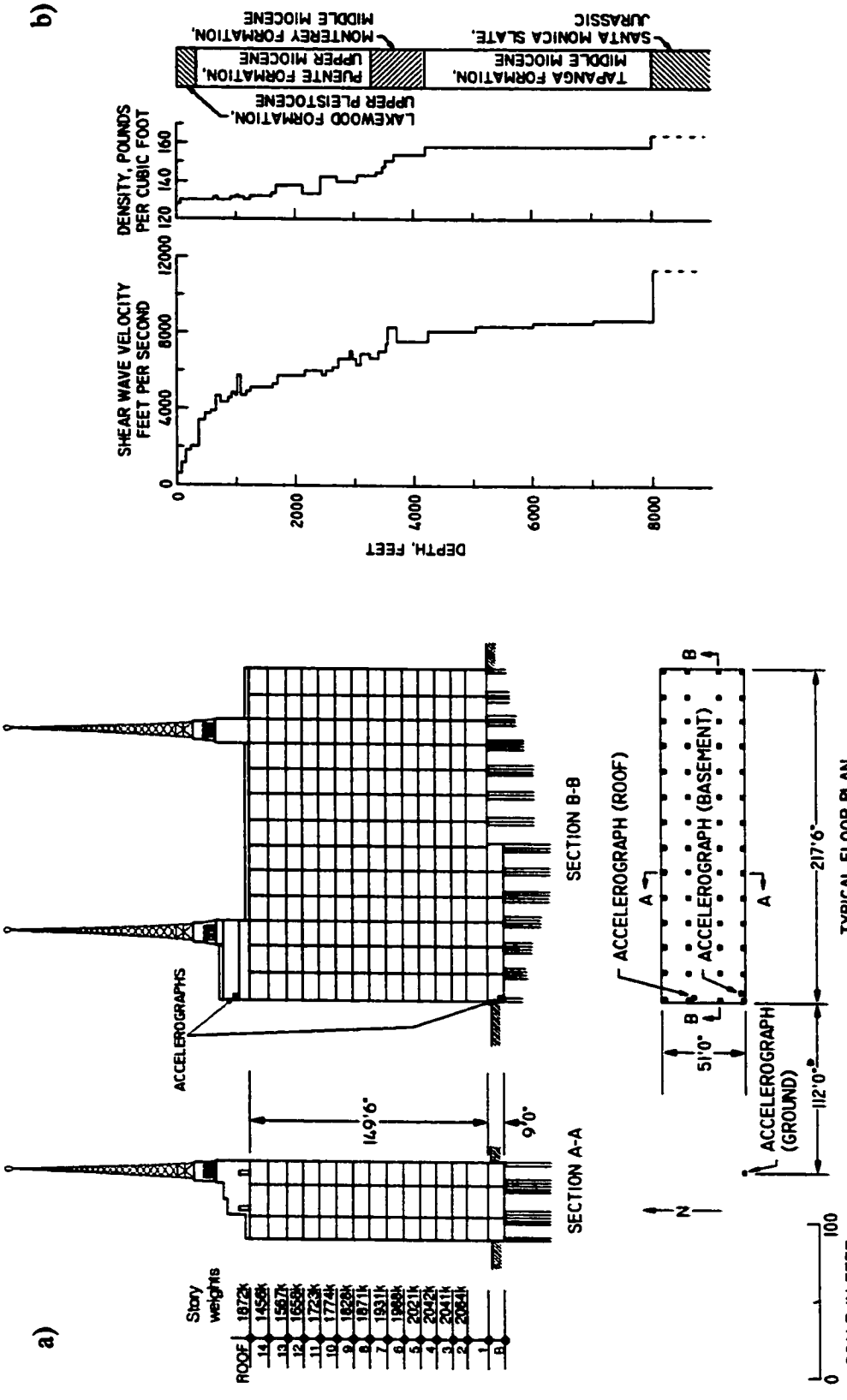

Fig. 3.1 (a) A sketch of the Hollywood Storage Building in the early 1950's. The location of the strong motion accelerographs is indicated, one in the basement, one on the roof and one at a free-field site, 112 feet west of the south-west corner of the building (after Duke et al., 1970). (b) Profiles of shear wave velocity and material density and type at the site of HSB (after Duke et al., 1970).

Reproduced with permission of the copyright owner. Further reproduction prohibited without permission.

Reproduced with permission of the copyright owner. Further reproduction prohibited without permission.

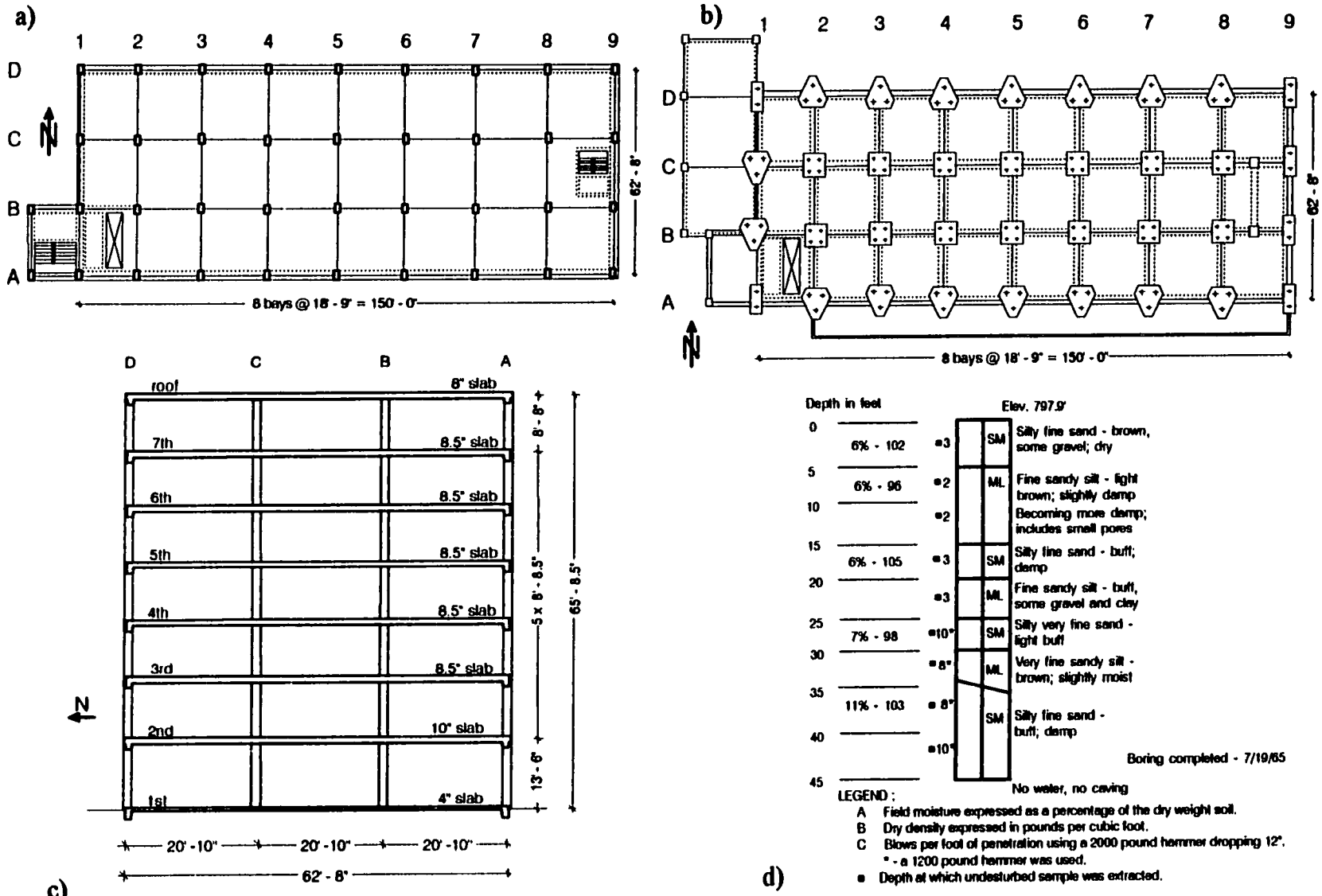

Fig. 3.2 (a) Typical floor plan, (b) Foundation plan, (c) Typical transverse section, and (d) Log of typical soil boring of the VN7SH.

BOC The Bank of California building, designed in 1969 and completed in 1970 (Blume et al., 1973), is a 12-story moment-resisting reinforced concrete structure located in the Sherman Oaks district of Los Angeles. Plan dimensions of the floors are 60 by 161 feet, except at the first story where plan dimensions are 90 by 161 feet. Story heights are typically 13 feet, except at the first story where a 16-foot height is used. The main roof stands 159 feet above the ground floor (see Fig. 3.3a, b, c). Soil conditions at the site are primarily silt and silty sand with lesser deposits of clay and sand, with 300 m/s average shear wave velocity in the top 30 meters. A typical soil boring log is shown in Fig. 3.3d. Because the upper soils at the site are only moderately firm and would tend to become weaker and more compressible when wet, pile foundations were provided.

MLK The Millikan Library building is a nine-story, reinforced concrete structure built in 1966. The library is 69 by 75 feet in plan and is 158 feet high above the basement level (Fig. 3.4a, b). Reinforced concrete shear walls located at the east and west ends of the structure resist lateral loads in the north-south direction. The reinforced concrete central core, which houses the elevators, provides partial resistance to the east-west loads. The foundation system consists of a 32 feet wide concrete pad below the central core, extending through the east-west length of the building, and of 10 feet wide beams positioned below the columns on the north and south sides of the structure. The foundation is built on alluvium composed of medium to dense sands, 900 feet (275 meters) above the bedrock. The average shear wave velocity in the top 30 meters is 450 m/s. Summary log from the site is shown in

Reproduced with permission of the copyright owner. Further reproduction prohibited without permission.

Reproduced with permission of the copyright owner. Further reproduction prohibited without permission.

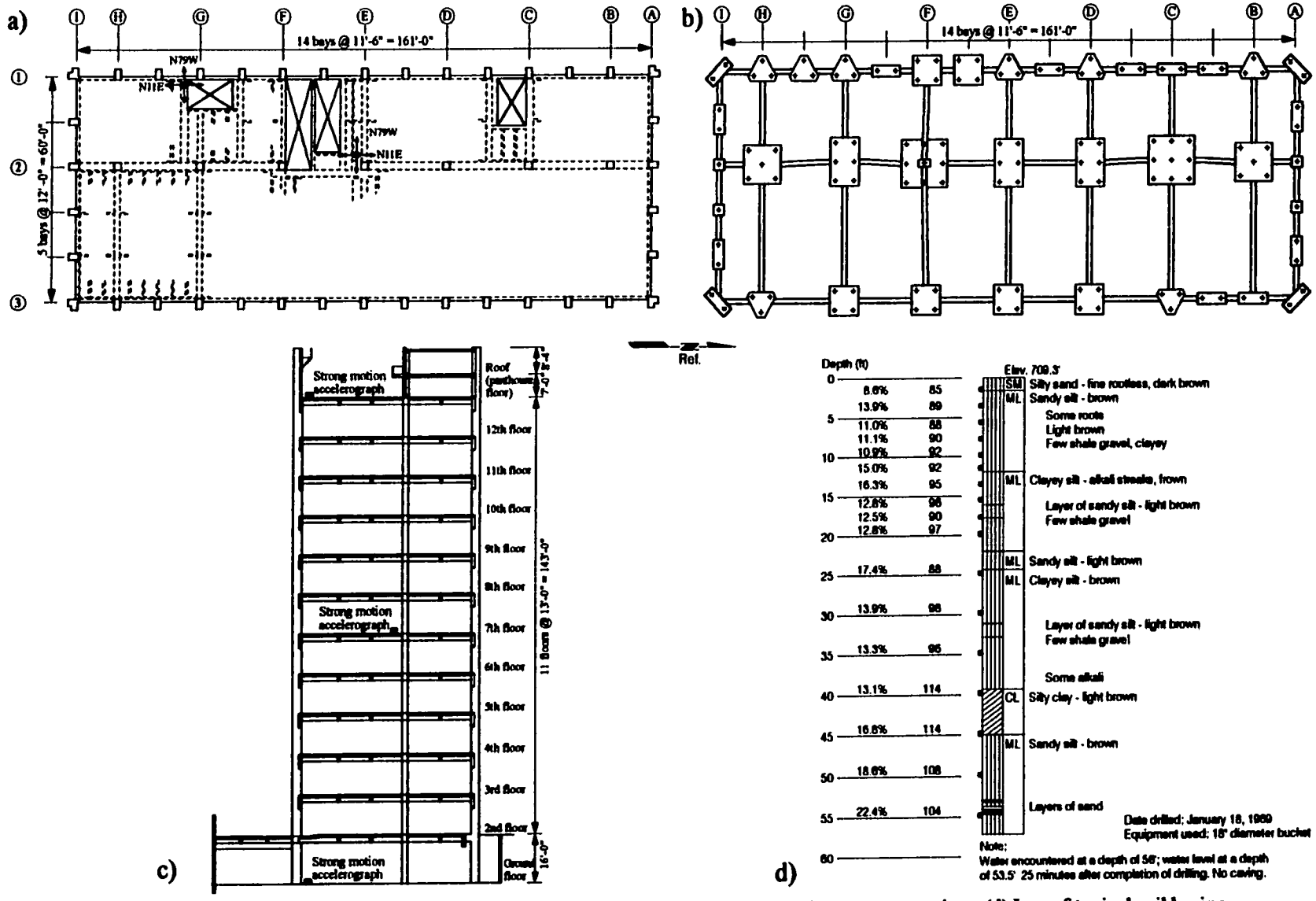

Fig. 3.3 Bank of California. (a) Typical floor plan, (b) Foundation plan, (c) Typical transverse section, (d) Log of typical soil boring.

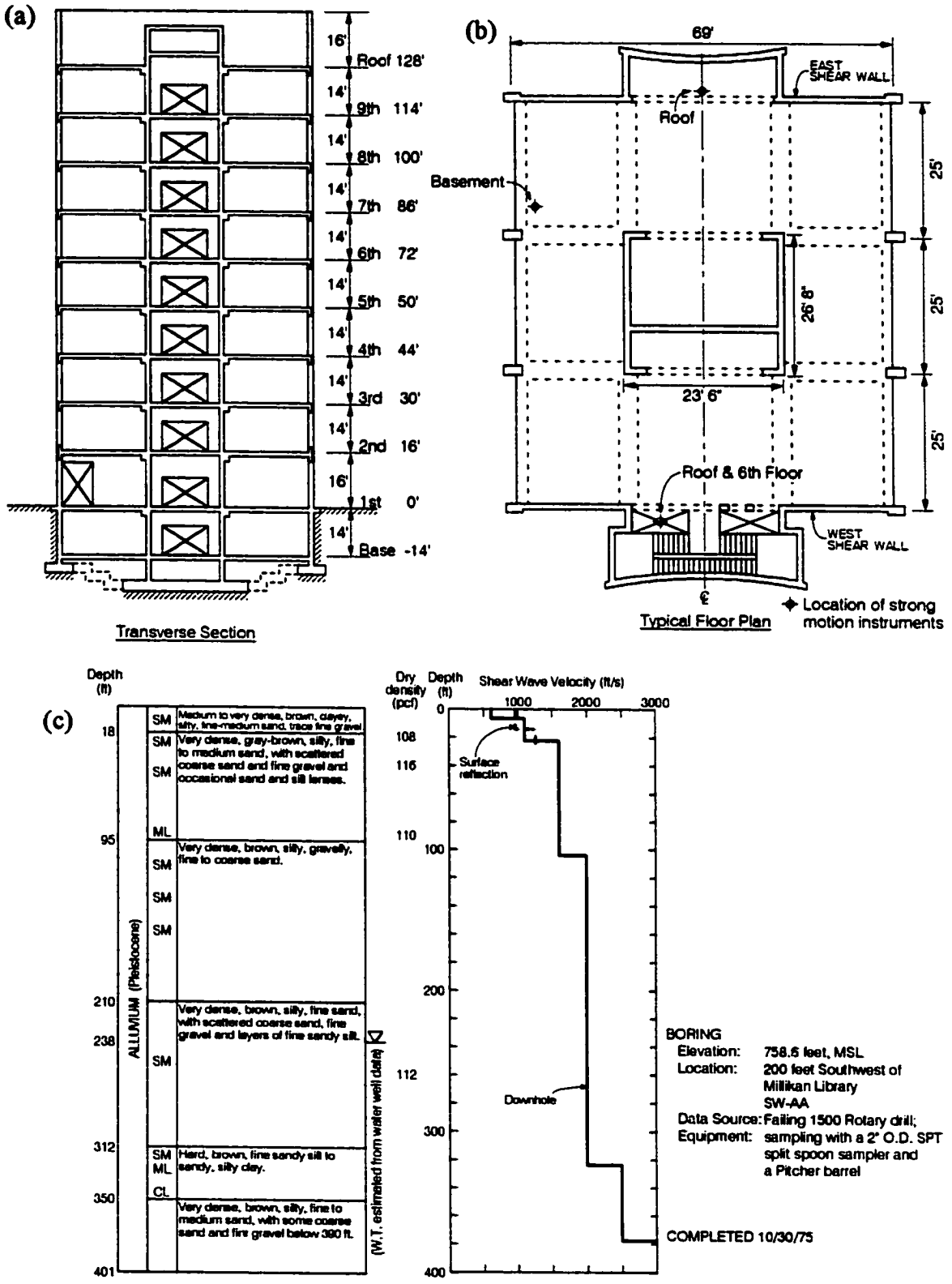

Fig. 3.4 Millikan Library structural system: (a) Transverse section, (b) typical floor plan, and (c) log of typical soil boring.

Reproduced with permission of the copyright owner. Further reproduction prohibited without permission.

Fig. 3.4c (Shannon et al., 1980). It experienced both small amplitude, ambient vibration tests and strong-motion earthquakes. Preceding and following the San Fernando event, 1971, the response of MLK had been extensively studied, and many pre- and post-earthquake forced vibration tests had been performed (Kuroiwa, 1967; Luco et al., 1986). It did not suffer any structural damage during the Whittier-Narrows earthquake or its major aftershock.

ETEC The instrumented section of Santa Susana ETEC Building 462 is an eight-level, 114-foot high rectangular structure with plan dimensions of 25 by 50 feet. Foundations of ETEC building consist of 2-foot deep continuous footings which extend between columns in both directions. Mass in the structure is concentrated at the ground and 6th levels where liquid storage tanks and pumps are located. The 6th level has a concrete floor, while other floors consist of open-grid steel decking and have little permanent equipment. The lateral force resisting system consists of inverted chevron-type braced steel frames in both directions. As shown in Fig. 3.5, accelerographs are located on the ground and 6th levels. The free-field instrument is in an open area about 160 feet north of the structure. The geologic conditions consist of very firm to hard sandstone bedrock, beneath a shallow mantle of surficial soil. No shear wave velocity measurements are available at the site at the time of this writing. The best approximation available appears to be the downhole measurements in gneiss bedrock of similar age near Pacoima Dam (Fig. 3.5).

The epicenters of major Southern California earthquakes and the above described five buildings are shown in Fig. 3.6. Table 3.1 summarizes the data that has

Reproduced with permission of the copyright owner. Further reproduction prohibited without permission.

Reproduced with permission of the copyright owner. Further reproduction prohibited without permission.

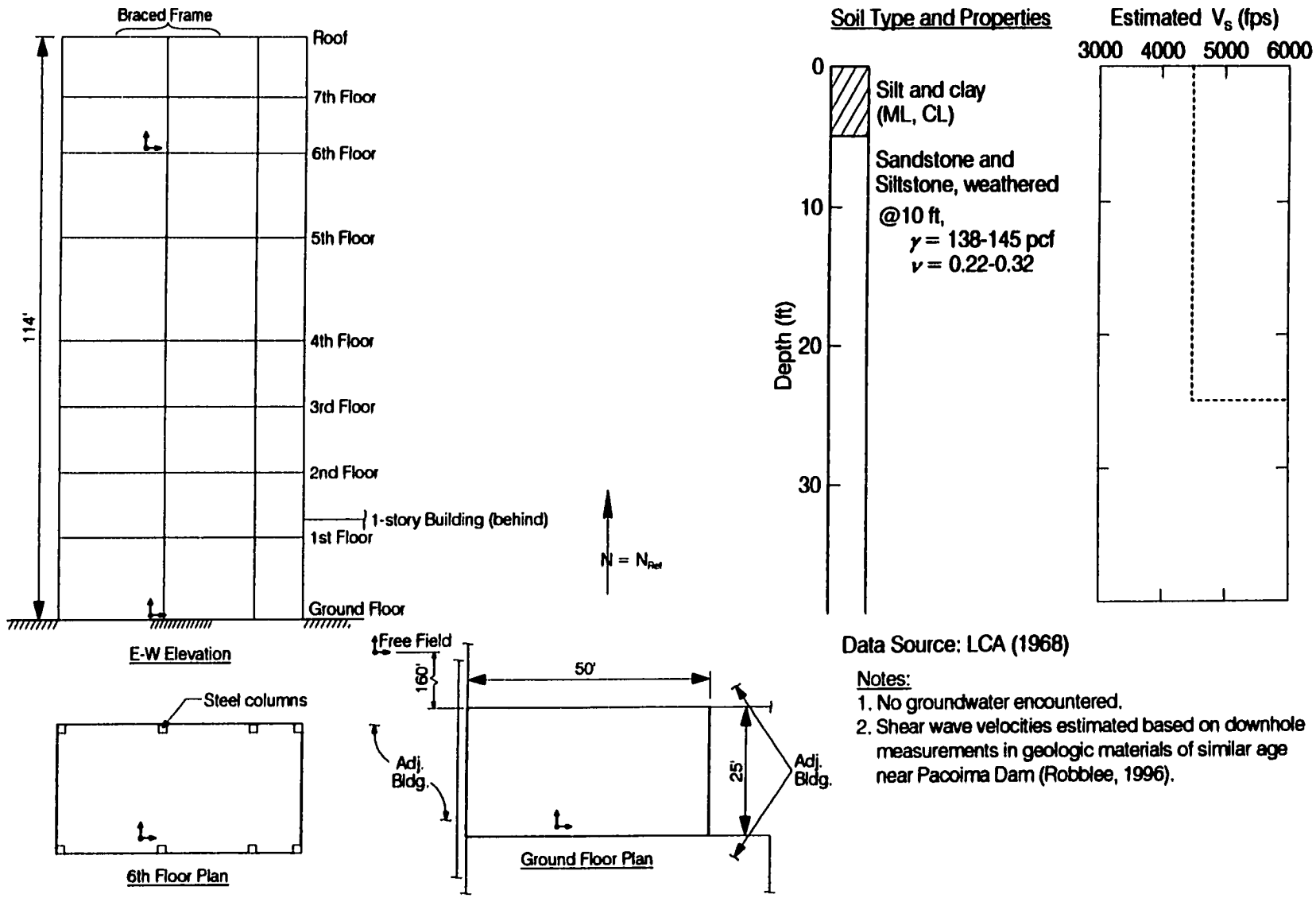

Fig. 3.5 Sensor locations and generalized soil profile of the ETEC building (after Stewart and Stewart, 1997).

Reproduced with permission of the copyright owner. Further reproduction prohibited without permission.

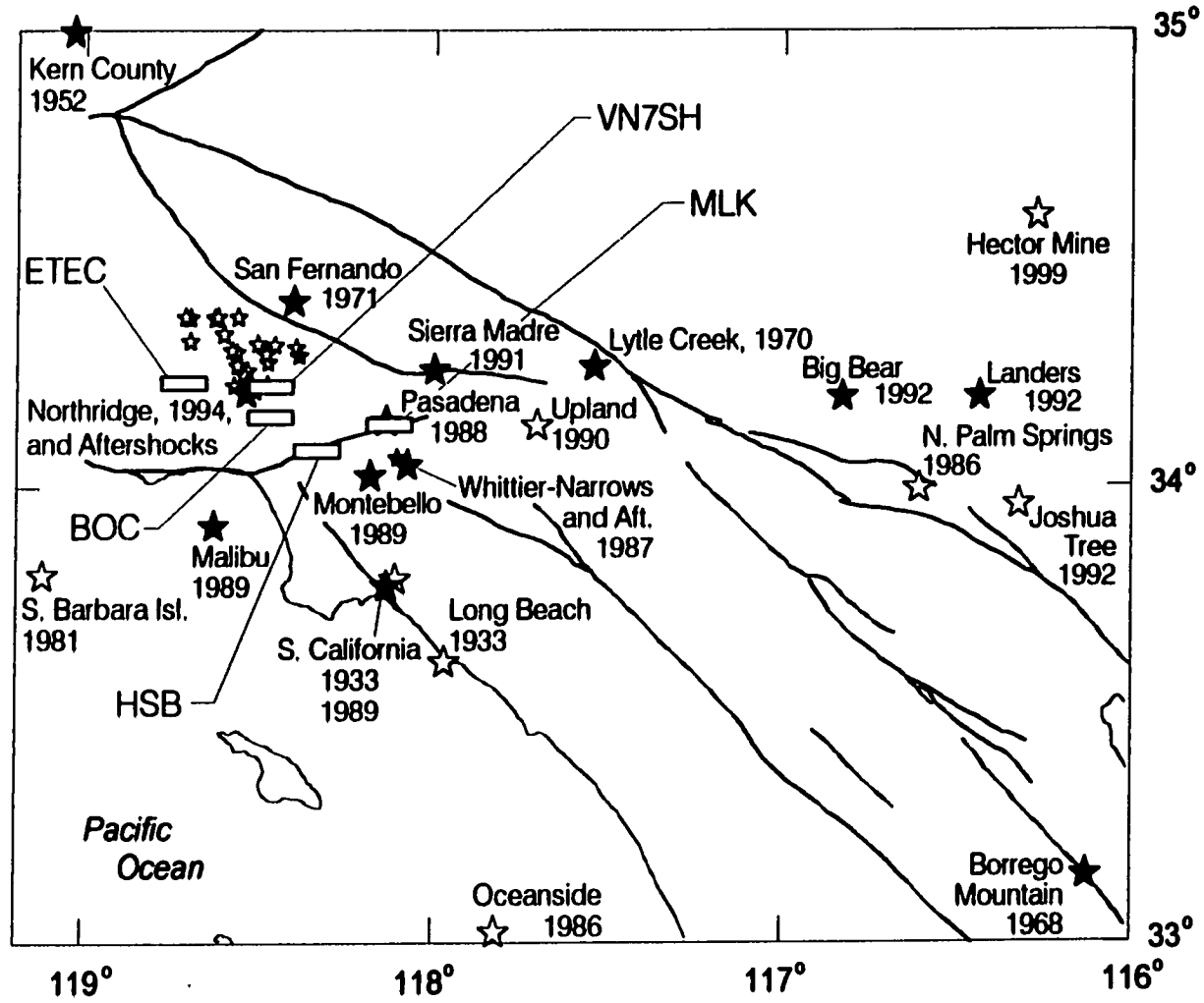

Fig. 3.6 Earthquakes in Southern California large enough to trigger the strong motion accelerographs in HSB, VN7SH, BOC, MLK and ETEC. The rectangles indicate five studied buildings. The events for which strong motion data was recorded and is available in digitized form are listed in Table 3.1.

Table 3.1 The peak ground velocity ($v_{G,max}$), and peak instantaneous difference between velocity recorded on roof and at ground level ($\dot{\theta}_{max}$), during earthquakes recorded at five selected buildings.

Hollywood Storage Building

				$NS_{West\ Wall}$ velocities		NS_{Center} velocities		EW velocities	
Earthquake	Date	M	R (km)	$v_{G,max}$ (cm/s)	$\dot{\theta}_{max}$ ($\times 10^{-3}$ rad/s)	$v_{G,max}$ (cm/s)	$\dot{\theta}_{max}$ ($\times 10^{-3}$ rad/s)	$v_{G,max}$ (cm/s)	$\dot{\theta}_{max}$ ($\times 10^{-3}$ rad/s)
Southern California[1]	10/02/1933	5.4	38	2.47	0.79630	--	--	2.24	1.61330
Kern County[1]	07/21/1952	7.7	120	6.72	3.39614	--	--	8.85	3.52799
Borrego Mountain[1]	04/08/1968	6.4	225	2.14	2.12623	--	--	3.03	0.75532
Lytle Creek[1]	09/12/1970	5.4	74	0.67	--	--	--	0.66	--
San Fernando[1]	02/09/1971	6.4	38	16.96	--	--	--	19.44	--
Whittier Narrows*	10/01/1987	5.9	24	9.23	4.26965	9.00	4.98646	6.42	3.00368
Landers*	06/28/1992	7.5	171	5.93	4.42882	6.14	5.78173	7.93	2.10864
Big Bear*	06/28/1992	6.5	135	3.68	1.58888	3.83	2.89211	4.03	1.20905
Northridge	01/17/1994	6.4	23	22.44	10.3298	22.03	9.65747	18.88	8.81063

--: record is not available.

1 : see Hudson 1976; Trifunac and Lee 1978.

* : digitized by Trifunac from Xerox copies of CDMG reports.

Van Nuys 7-Story Hotel

				NS velocities		EW velocities	
Earthquake	Date	M	R (km)	$v_{G,max}$ (cm/s)	$\dot{\theta}_{max}$ ($\times 10^{-3}$ rad/s)	$v_{G,max}$ (cm/s)	$\dot{\theta}_{max}$ ($\times 10^{-3}$ rad/s)
San Fernando	02/09/1971	6.6	10*	29.28	17.5245	23.72	9.8280
Whittier Narrows	10/01/1987	5.9	41	8.14	2.8390	--	--
Whittier 12th Aft.	10/04/1987	5.3	41	1.33	0.7675	2.18	1.7240
Pasadena	12/03/1988	4.9	32	1.46	0.4040	0.94	0.6495
Malibu	01/19/1989	5.0	35	0.93	1.0210	0.96	0.3785
Montebello	06/12/1989	4.6	34	0.45	0.2115	0.85	0.1055
Sierra Madre	06/28/1991	5.8	44	4.40	3.8190	2.78	3.0230
Landers	06/28/1992	7.5	186	10.42	13.8710	10.64	5.3720
Big Bear	06/28/1992	6.5	149	3.87	2.9480	3.58	3.1885
Northridge	01/17/1994	6.4	4*	35.32	20.9745	50.93	14.3420
Northridge Mar. Aft.	03/10/1994	5.2	1	7.61	0.7340	4.83	0.1455
Northridge Mar. Aft.	03/10/1994	5.2	1	2.58	0.3500	4.21	0.2340
Northridge Dec. Aft.	12/06/1994	4.3	11	2.67	0.7865	2.41	0.2675

--: record is not available.

*: horizontal projection of the closet distance to fault surface.

Reproduced with permission of the copyright owner. Further reproduction prohibited without permission.

Table 3.1 (Continued)

Bank of California (15250 Ventura Blvd.)

Earthquake	Date	M	R (km)	NS velocities		EW velocities	
				$v_{G,max}$ (cm/s)	$\dot{\theta}_{max}$ ($\times 10^{-3}$ rad/s)	$v_{G,max}$ (cm/s)	$\dot{\theta}_{max}$ ($\times 10^{-3}$ rad/s)
San Fernando	02/09/1971	6.6	27.8	27.73	18.6488	23.41	17.8500
EQ71	2/9~8/4/1971	?	?	0.41	0.1137	1.12	0.2117
EQ73	02/21/1973	?	?	0.81	0.7573	1.18	0.4517
Northridge	01/17/1994	6.4	9.4	--	19.4894	--	9.7059
Northridge Aft. -1	?	?	?	--	2.8248	--	1.6293
Northridge Aft. -2	?	?	?	--	0.4048	--	0.1754
Northridge Aft. -4	?	?	?	--	0.5301	--	0.3070
Northridge Aft. -5	?	?	?	--	0.7034	--	0.2515
Northridge Aft. -6	?	?	?	--	0.8181	--	0.2676
Northridge Aft. -10	?	?	?	--	0.4125	--	0.2142
Northridge Aft. -11	?	?	?	--	0.2218	--	0.4550
Northridge Aft. -17	?	?	?	--	0.3467	--	0.1692
Northridge Aft. -19	?	?	?	--	0.3485	--	0.3285
Northridge Aft. -20	?	?	?	--	0.5020	--	1.3542
Northridge Aft. -22	?	?	?	--	0.5060	--	0.0951
Northridge Aft. -24	?	?	?	--	0.3689	--	0.1288
Northridge Aft. -25	?	?	?	--	0.1882	--	0.2449
Northridge Aft. -27	?	?	?	--	0.4040	--	0.3093
Northridge Aft. -34	?	?	?	--	0.1686	--	0.3157
Northridge Aft. -38	?	?	?	--	2.6682	--	0.9739
Northridge Aft. -39	?	?	?	--	0.4191	--	0.1688
Northridge Aft. -42	?	?	?	--	0.4552	--	0.2945

--: data is not available on the base (in this case, $\dot{\theta}_{max} \approx v_{roof}/H_{sb}$ except San Fernando, EQ71 and EQ73 earthquakes).

?: absolute time, magnitude and epicenter location are not available.

Millikan Library

Earthquake	Date	M	R (km)	NS velocities		EW velocities	
				$v_{G,max}$ (cm/s)	$\dot{\theta}_{max}$ ($\times 10^{-3}$ rad/s)	$v_{G,max}$ (cm/s)	$\dot{\theta}_{max}$ ($\times 10^{-3}$ rad/s)
Lytle Creek	09/12/1970	5.4	56.1	1.40	0.9295	1.27	0.6920
San Fernando	02/09/1971	6.6	38.2	9.98	6.0666	16.44	10.5095
Whittier Narrows	10/01/1987	5.9	10.3	16.51	14.7374	10.72	7.5769
Whittier 12th Aft.	10/04/1987	5.3	7.9	16.04	7.3782	10.76	5.1156

Reproduced with permission of the copyright owner. Further reproduction prohibited without permission.

Table 3.1 (Continued)

Santa Susana ETEC Building 462

				NS velocities		EW velocities	
Earthquake	Date	M	R (km)	$v_{G,max}$ (cm/s)	$\dot{\theta}_{max}$ ($\times 10^{-3}$ rad/s)	$v_{G,max}$ (cm/s)	$\dot{\theta}_{max}$ ($\times 10^{-3}$ rad/s)
Northridge	01/17/1994	6.4	16.4	15.63	19.2561	12.39	12.9683
Northridge Aft.#7	01/17/1994	4.9	16.9	0.67	0.4254	0.96	0.6095
Northridge Aft.#9	01/17/1994	5.2	15.9	0.80	1.0650	1.00	0.9222
Northridge Aft.#83	01/17/1994	4.8	17.8	0.32	0.8134	0.19	0.3256
Northridge Aft.#100	01/17/1994	4.6	13.1	0.53	0.6867	1.30	1.0840
Northridge Aft.#129	01/17/1994	4.9	15.7	5.83	4.0145	7.05	4.9123
Northridge Aft.#142	01/17/1994	5.6	10.5	2.28	2.2442	4.42	3.7525
Northridge Aft.#151	01/18/1994	5.2	16.0	0.99	0.6942	0.35	0.5241
Northridge Aft.#253	01/19/1994	5.1	16.3	1.95	1.0873	1.59	2.7453
Northridge Aft.#254	01/19/1994	5.1	18.4	0.58	0.6124	0.66	0.8640
Northridge Aft.#336	01/29/1994	5.1	14.9	2.81	2.2639	2.94	2.3852
Northridge Aft.#253a	01/19/1994	5.1	16.2	1.08	1.2395	1.34	1.0191

Reproduced with permission of the copyright owner. Further reproduction prohibited without permission.

been digitized and processed so far for each building individually. There, columns 1, 2, 3, 4 show the earthquake name, date, magnitude, M, and epicentral distance, R, and columns 5 through 8 show the peak measured velocity, $v_{G,\max}$, either at ground level or in the basement, and an estimate of peak instantaneous rocking angular velocity, $\dot{\theta}_{\max} (=| v_{\text{roof}} - v_{\text{base}} |_{\max} / H_{sb})$.

3.2 Analysis of Recorded Motions: Time and Amplitude Dependent Response

To evaluate changes of the system frequency, f_p, during a particular earthquake motion, as function of the level of response and of the previous response history, the "instantaneous" value of system frequency, f_p, was approximated by two methods: (1) zero-crossing analysis and (2) moving window Fourier analysis. To isolate the lowest frequency mode, the data was band-pass filtered. The cutoff frequencies for the band-pass filter were chosen to include the system frequency, and were determined after analyzing the instantaneous transfer-functions between the relative horizontal motions recorded on the roof and at the base. The zero-crossing analysis consisted of determining the half periods for all approximately symmetric peaks in the relative response, assuming that the filtered relative displacements locally can be approximated by a sine wave. The time windows for the moving window Fourier analysis depended on the sampling rate of the available processed strong motion data. For the data with time step $\Delta t = 0.01$ s, 4 s windows were used (0.5 s ramp up, 3 s flat, and 0.5 s ramp down), and a sliding interval of 2 s. For the data with $\Delta t = 0.02$ s, 8 s windows were used (1 s ramp up, 6 s flat, and 1 s ramp down), and a sliding interval of 4 s.

Reproduced with permission of the copyright owner. Further reproduction prohibited without permission.

Figs. 3.7 through 3.11 show schematically the observed variations of f_p versus $v_{G,max}$ and $\dot{\theta}_{max}$. In these figures, f_p is proportional to the square root of the system stiffness, while $v_{G,max}$ and $\dot{\theta}_{max}$ can be related to the strain levels in the supporting soil. Excluding EW response of ETEC building, it appears that these soil-building systems behave like nonlinear soft spring systems. For $v_{G,max} \leq 1$ cm/s and $\dot{\theta}_{max} \leq 1\times10^{-3}$ rad/s, the system frequency of the EW response of ETEC building increases with increasing $v_{G,max}$ and $\dot{\theta}_{max}$ ("stiffer" nonlinear response). Beyond $v_{G,max} \approx 1$ cm/s and $\dot{\theta}_{max} \approx 1\times10^{-3}$ rad/s, the system frequency becomes slightly smaller.

The evaluation of the instantaneous system frequency requires complete recordings on the roof and at the base. However, during the 1994 Northridge earthquake and its aftershocks, only the motions on the roof were recorded in the Bank of California building. The possibility and accuracy of performing the approximate analysis, using motions on the roof only, are discussed in Appendix A.

Figs. 3.12 through 3.16 summarize the time dependent changes of the instantaneous system frequency, f_p, for the recorded earthquakes ordered in chronological order. Figs. 3.12, 3.13 and 3.15 also compare the variations in the system frequencies during strong-motion with the values from low amplitude testing (horizontal lines).

The amplitude dependent changes of f_p are shown in Figs. 3.17 through 3.21, by plotting f_p versus the corresponding amplitude of the envelope of the analyzed data. Based on the time- and amplitude-frequency analyses, we found that the predominant

Reproduced with permission of the copyright owner. Further reproduction prohibited without permission.

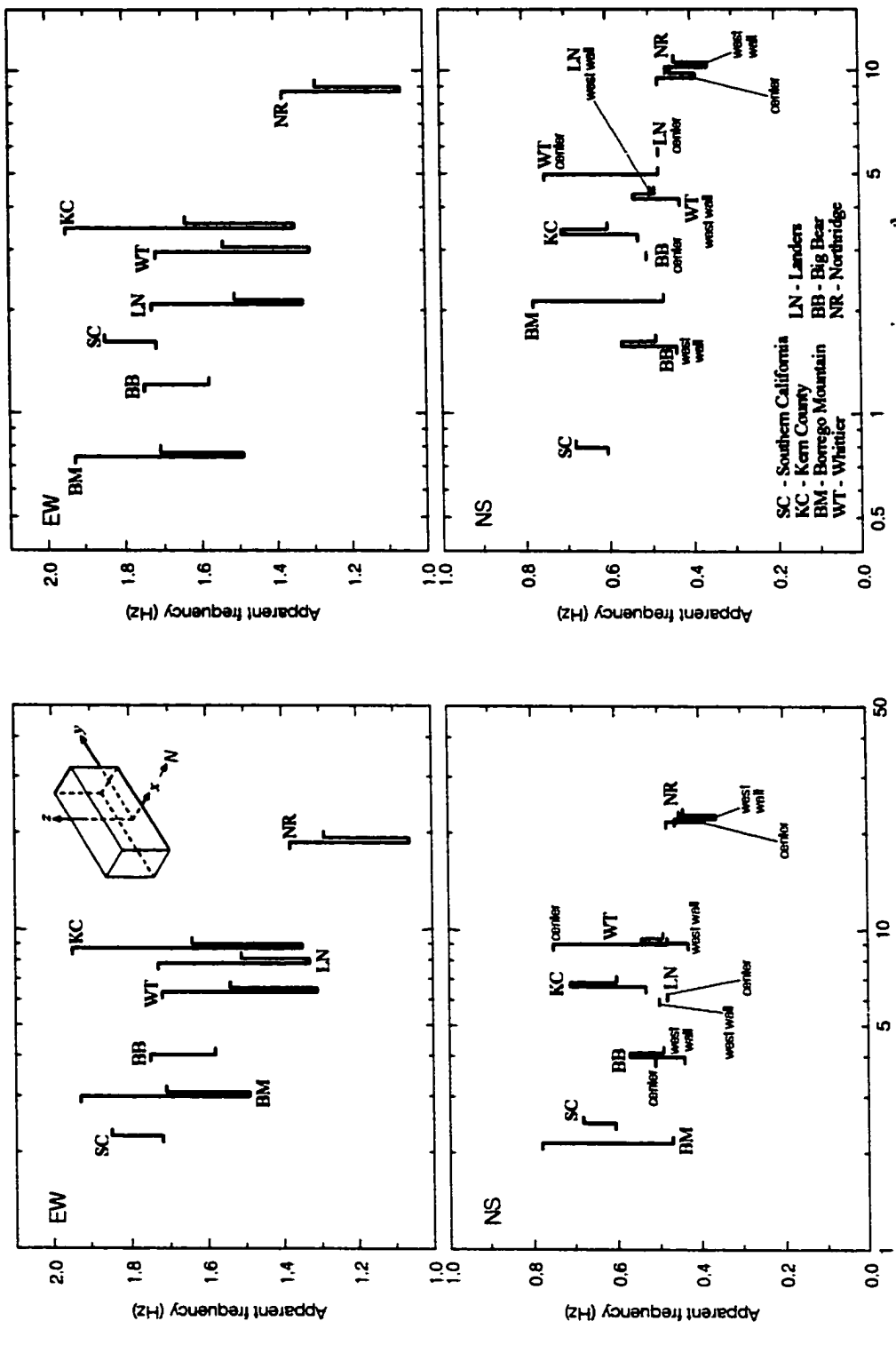

Fig. 3.7 Schematic of the observed variations of the EW (top) and NS (bottom) system frequencies, f_p, of Hollywood Storage Building versus peak measured ground velocity, $v_{G,max}$ (left), and peak instantaneous rocking angular velocity, $\dot{\theta}_{max}$ (right), during seven earthquakes. For each earthquake, the horizontal ticks represent pre and post earthquake estimates of the system frequencies.

Reproduced with permission of the copyright owner. Further reproduction prohibited without permission.

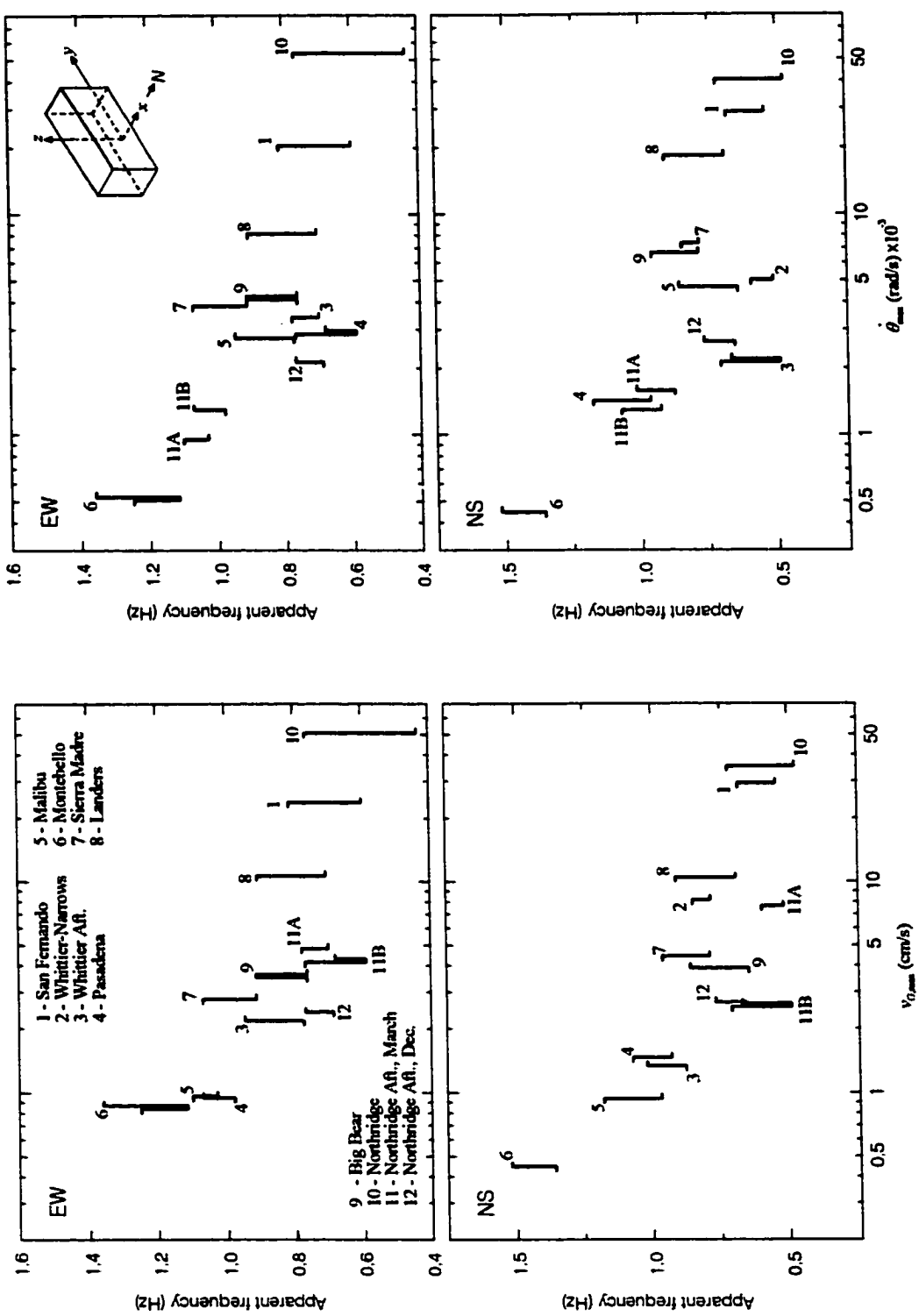

Fig. 3.8 Same as Fig. 3.7 but for the Van Nuys 7-story hotel.

Reproduced with permission of the copyright owner. Further reproduction prohibited without permission.

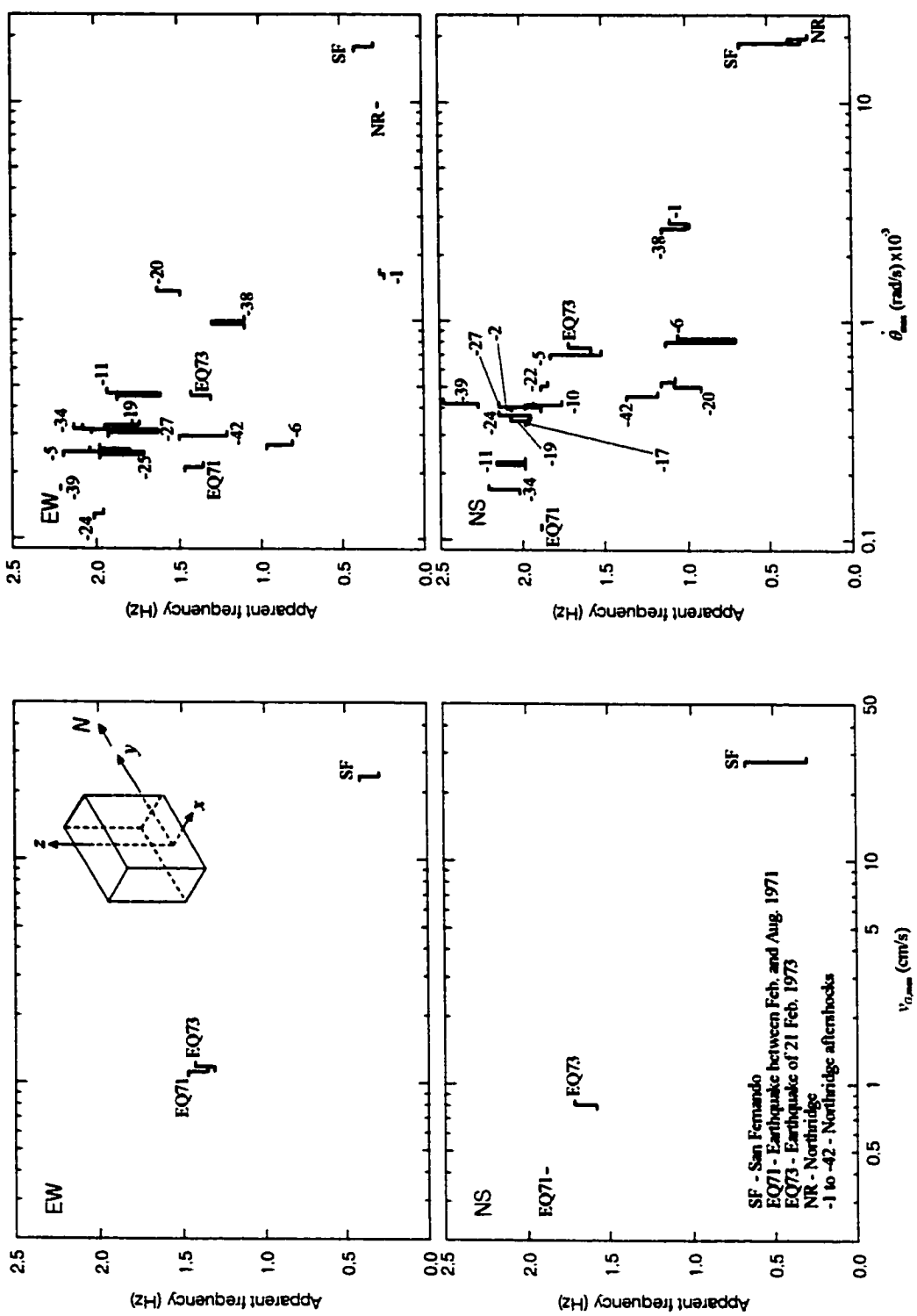

Fig. 3.9 Same as Fig. 3.7 but for the Bank of California building.

Reproduced with permission of the copyright owner. Further reproduction prohibited without permission.

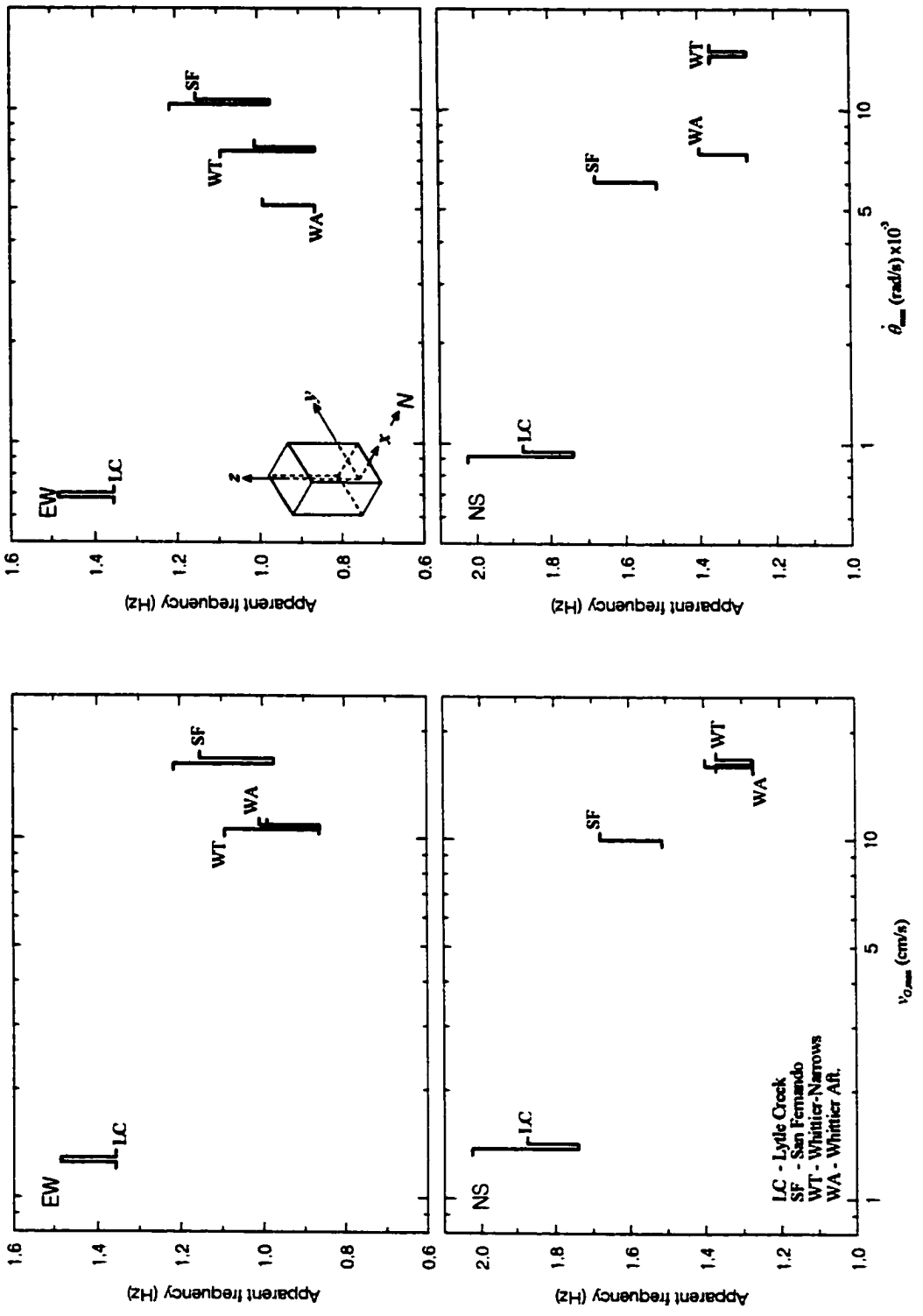

Fig. 3.10 Same as Fig. 3.7 but for the Millikan Library building.

Reproduced with permission of the copyright owner. Further reproduction prohibited without permission.

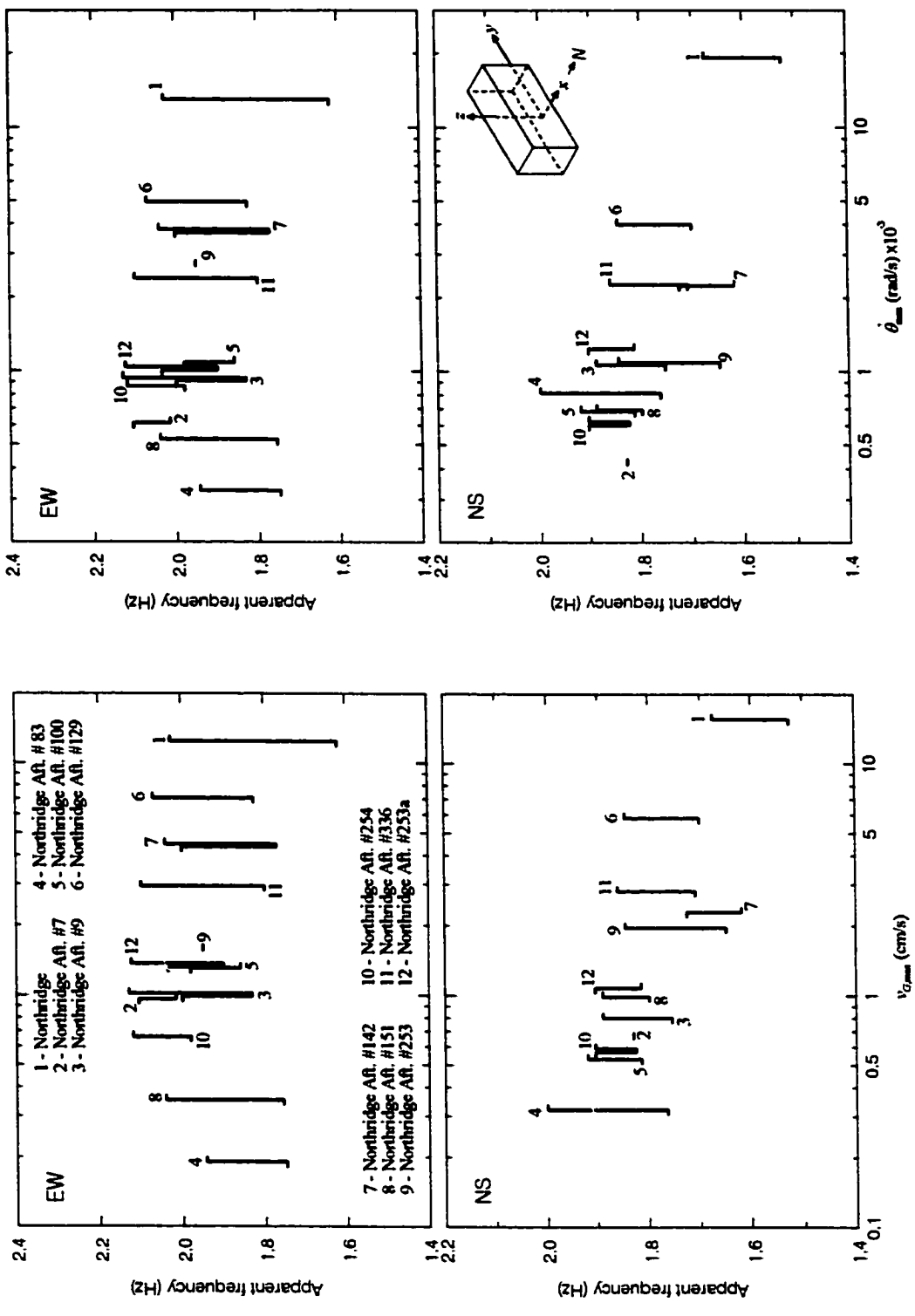

Fig. 3.11 Same as Fig. 3.7 but for the ETEC building.

Reproduced with permission of the copyright owner. Further reproduction prohibited without permission.

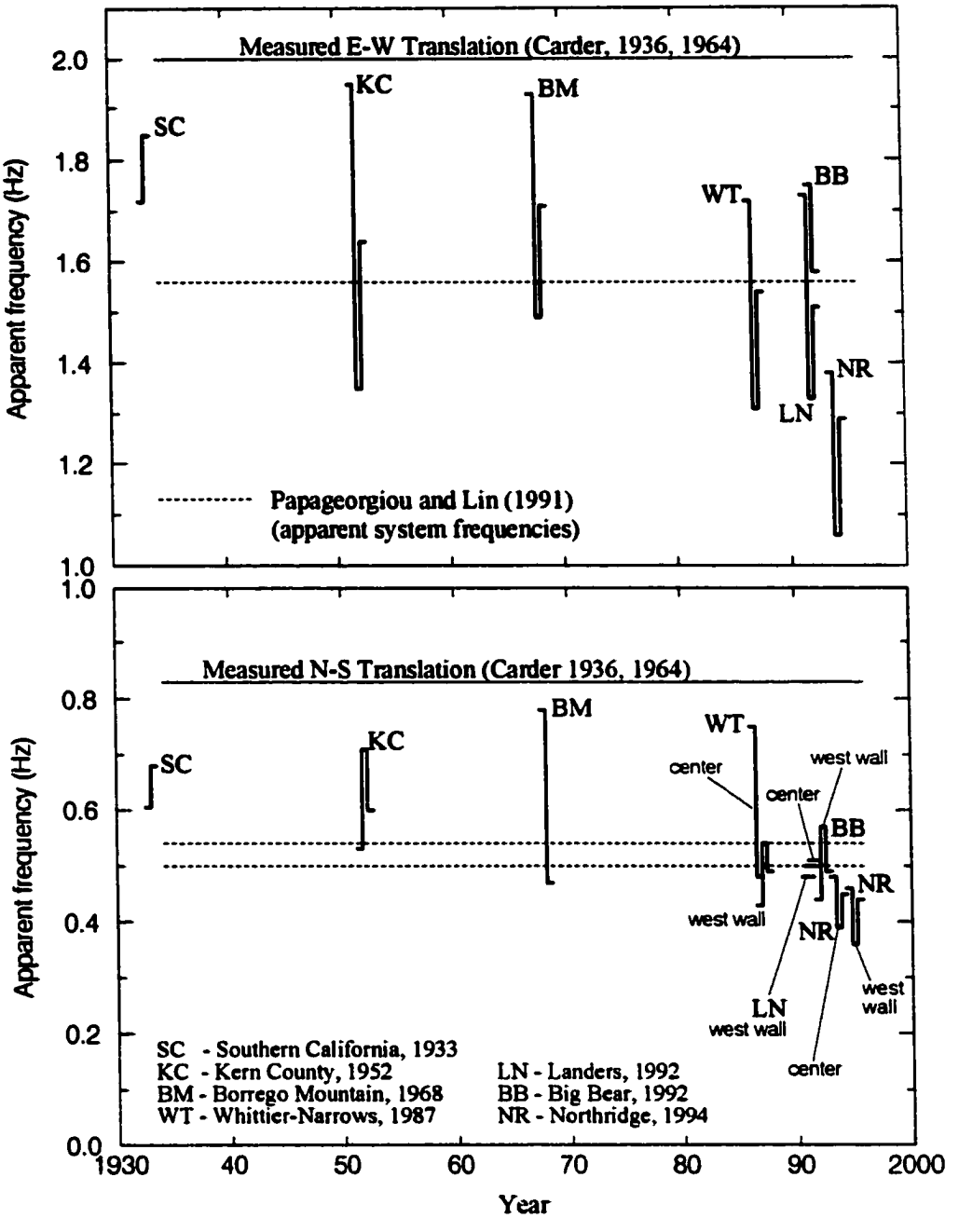

Fig. 3.12 A summary of the time dependent changes of the EW (top) and NS (bottom) system frequencies of Hollywood Storage Building during seven earthquakes between 1933 and 1994. The horizontal lines show the system frequencies determined from ambient vibration and forced vibration tests (light solid lines) (Carder, 1936; 1964), and those identified by Papageorgiou and Lin (1991) (dashed lines). For each earthquake, the horizontal ticks represent pre and post earthquake estimates of the system frequencies.

Reproduced with permission of the copyright owner. Further reproduction prohibited without permission.

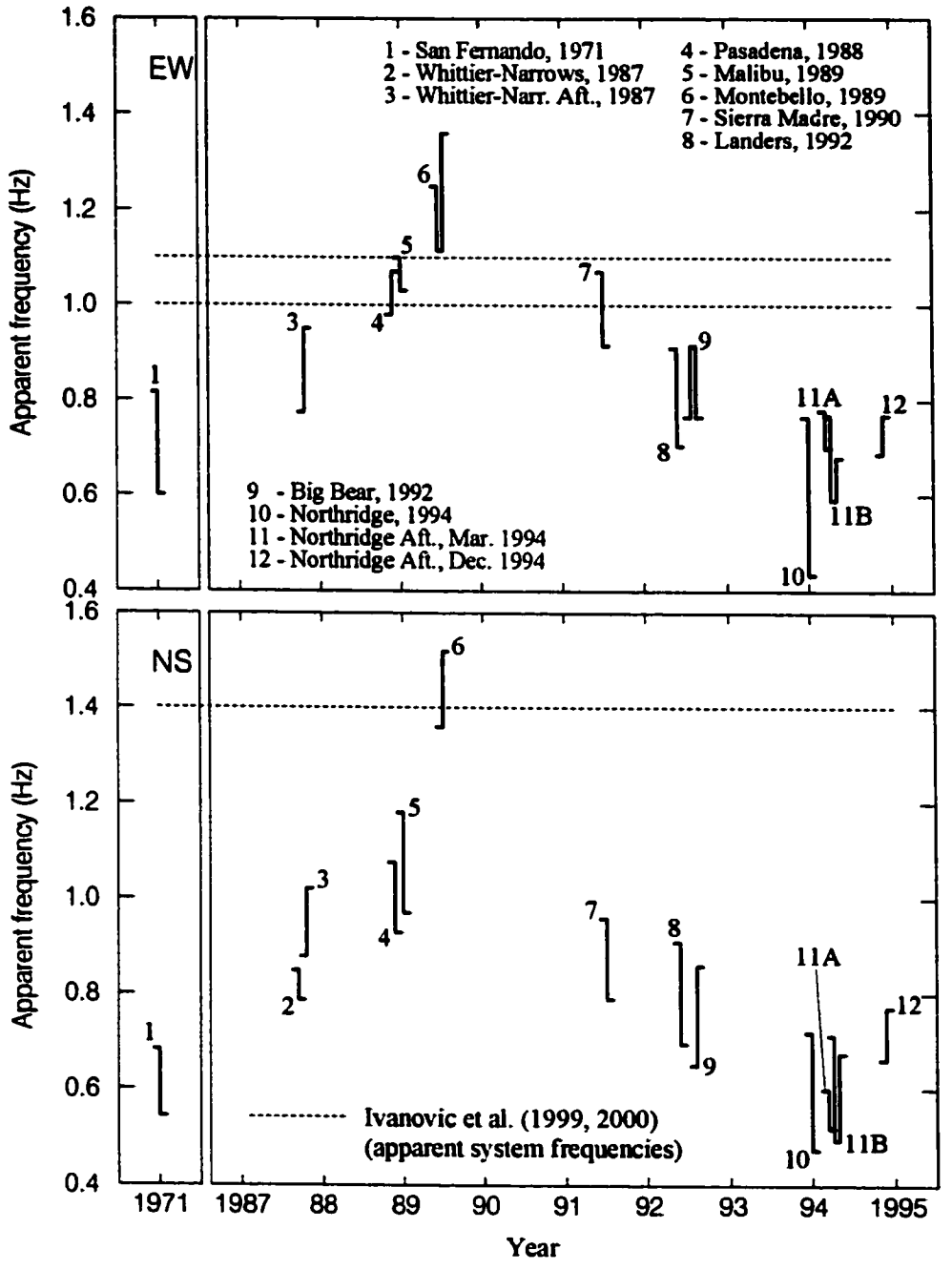

Fig. 3.13 A summary of the time dependent changes of the EW (top) and NS (bottom) system frequencies of Van Nuys 7-story hotel during twelve earthquakes between 1971 and 1994. The horizontal dashed lines show the system frequencies determined from ambient noise tests by Ivanovic et al. (1999, 2000). For each earthquake, the horizontal ticks represent pre and post earthquake estimates of the system frequencies.

Reproduced with permission of the copyright owner. Further reproduction prohibited without permission.

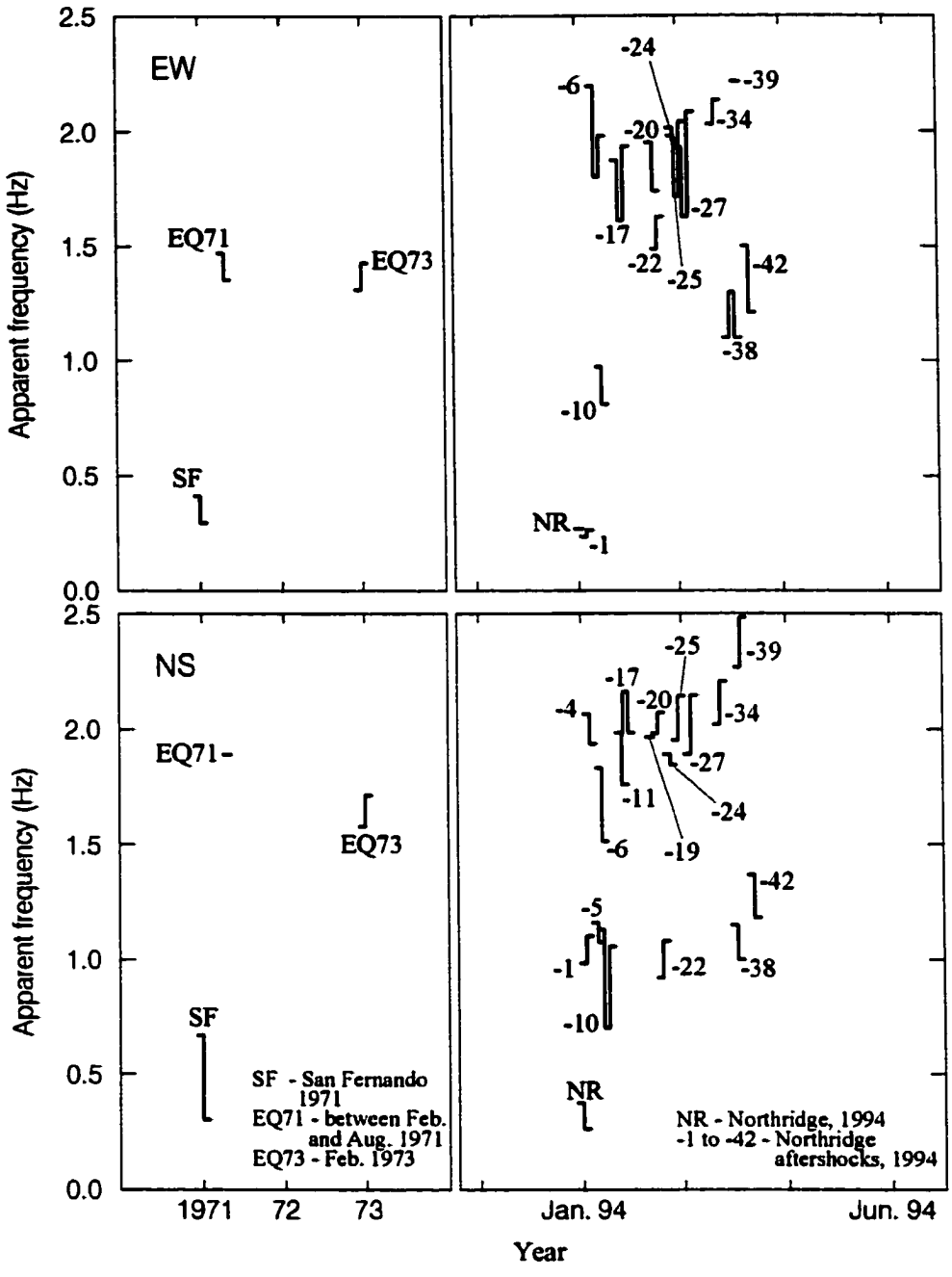

Fig. 3.14 A summary of the time dependent changes of the EW (top) and NS (bottom) system frequencies of Bank of California building following earthquakes in 1971 and 1994. For each earthquake, the horizontal ticks represent pre and post earthquake estimates of the system frequencies.

Reproduced with permission of the copyright owner. Further reproduction prohibited without permission.

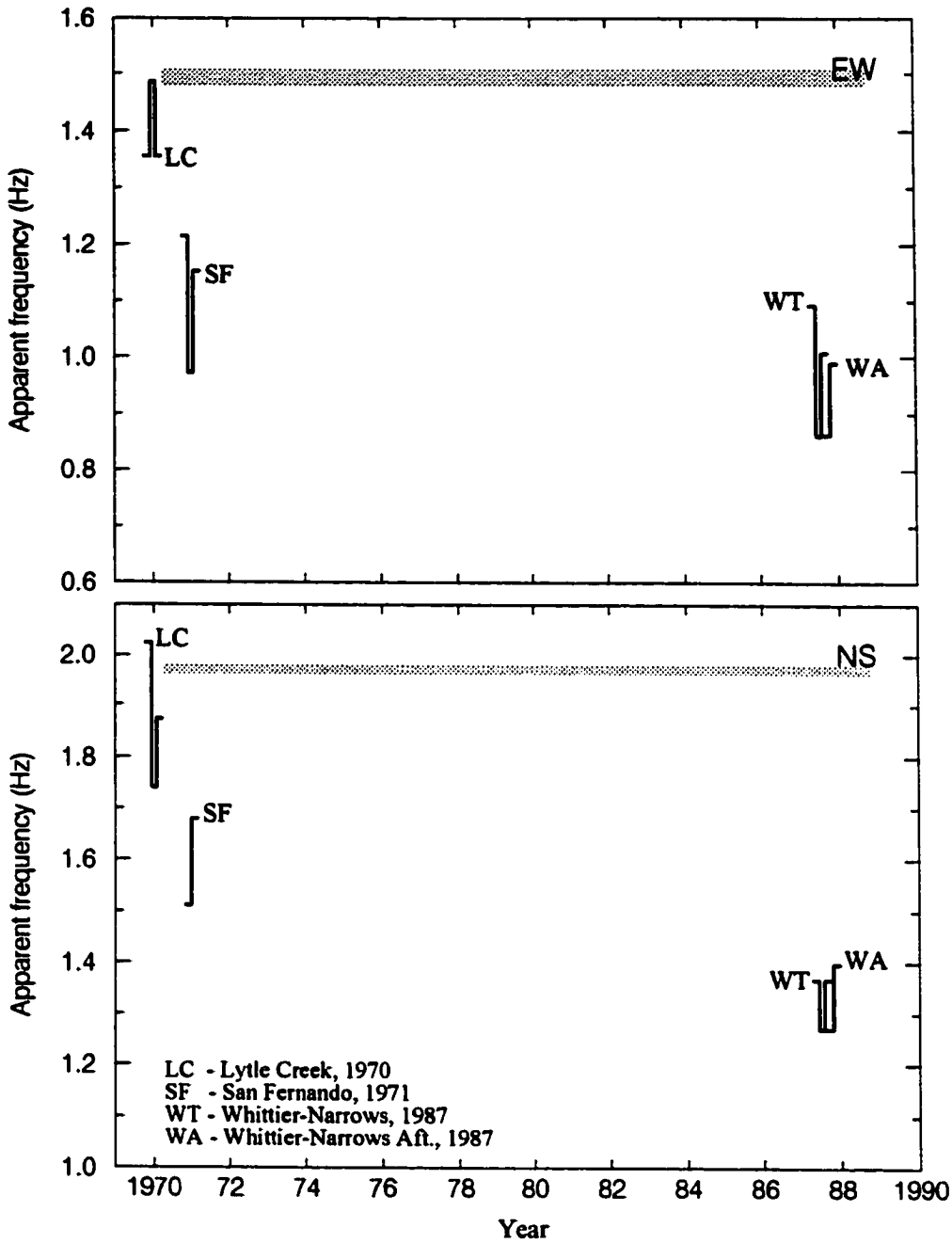

Fig. 3.15 A summary of the time dependent changes of the EW (top) and NS (bottom) system frequencies of Millikan Library building during four earthquakes between 1970 and 1987. The grey zones show the system frequencies determined from ambient vibration and forced vibration tests (Luco et al., 1986; Kuroiwa, 1967). For each earthquake, the horizontal ticks represent pre and post earthquake estimates of the system frequencies.

Reproduced with permission of the copyright owner. Further reproduction prohibited without permission.

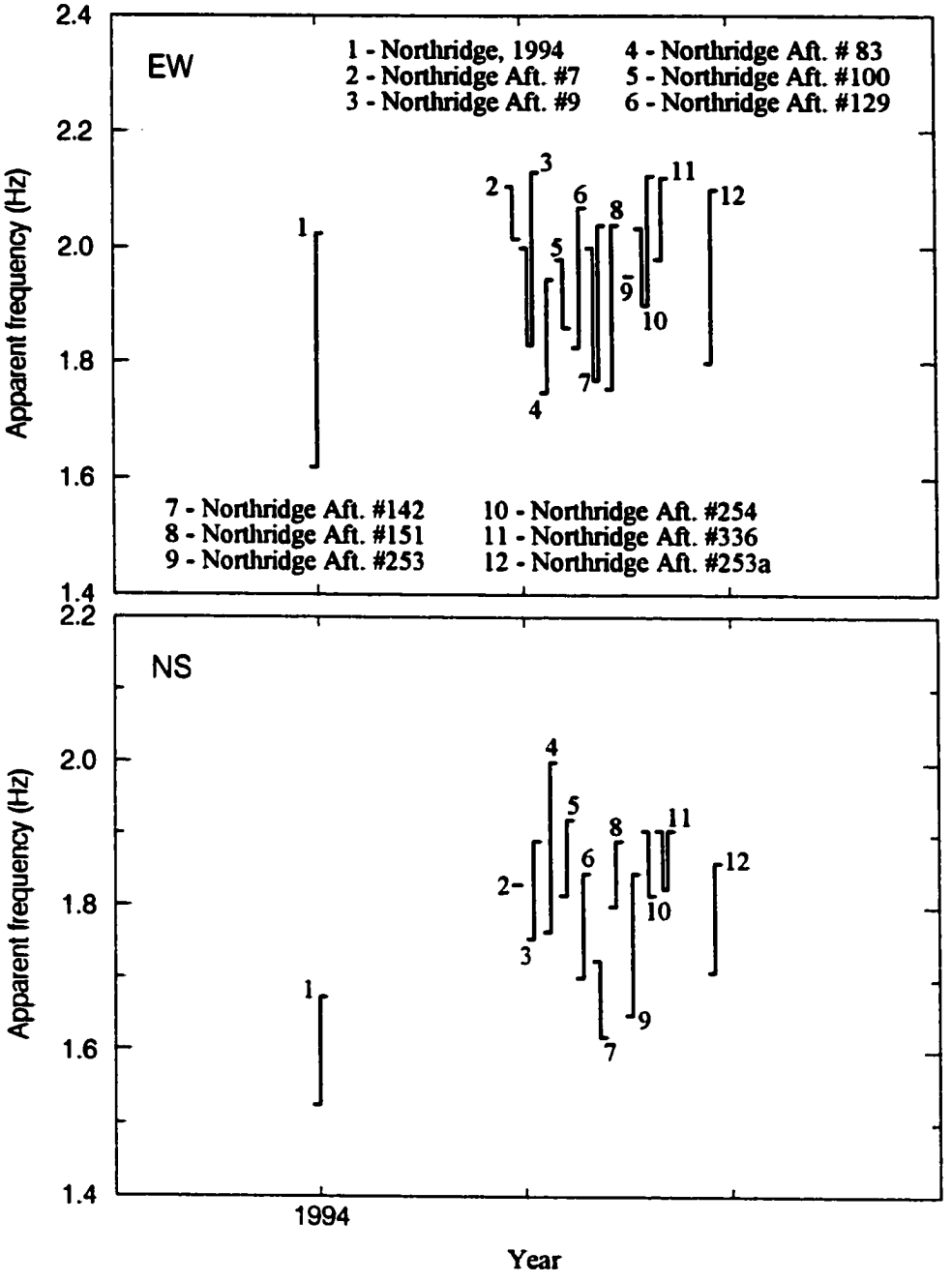

Fig. 3.16 A summary of the time dependent changes of the EW (top) and NS (bottom) system frequencies of Santa Susana ETEC Bldg. #462 during twelve earthquakes between 17 Jan. and 29 Jan. 1994. For each earthquake, the horizontal ticks represent pre and post earthquake estimates of the system frequencies.

Reproduced with permission of the copyright owner. Further reproduction prohibited without permission.

system frequencies change from one earthquake to another, and also during the response to a particular earthquake. The results also indicate that what is "loosened" by the severe strong motion shaking, appears to be "strengthened" by aftershocks and by intermediate and small earthquakes. In the response of VN7SH building (Fig. 3.13), for example, for both the 1987 Whittier-Narrows and the 1994 Northridge earthquakes, f_p during their aftershocks is larger for both the NS and EW responses.

Five backbone curves identified in the Figs. 3.17 through 3.21 were first normalized by the reference frequencies at which their corresponding relative responses (rocking angles) equal to 5×10^{-4} rad, and then plotted together in Figs. 3.22a and b, for longitudinal and transverse responses. The observed changes in f_p are as large as 1.4 to 6 times. It is seen that the nonlinear response of the supporting soil results in larger changes of the response in transverse than in the longitudinal direction, presumably due to the higher system stiffness in longitudinal direction. Furthermore, the changes of the system frequency of the ETEC building were the smallest. The ETEC building is a steel structure which is founded on hard bedrock, and which experienced no damage during 1994 Northridge earthquake. This implies that the observed changes of system frequency would be relatively small (Figs. 3.22a and b).

3.3 Numerical Response Simulation

The accelerations recorded at the base of the buildings were used as the input excitations for the idealized mathematical model. The values of model parameters corresponding to the five studied structures are presented and discussed in detail in

Reproduced with permission of the copyright owner. Further reproduction prohibited without permission.

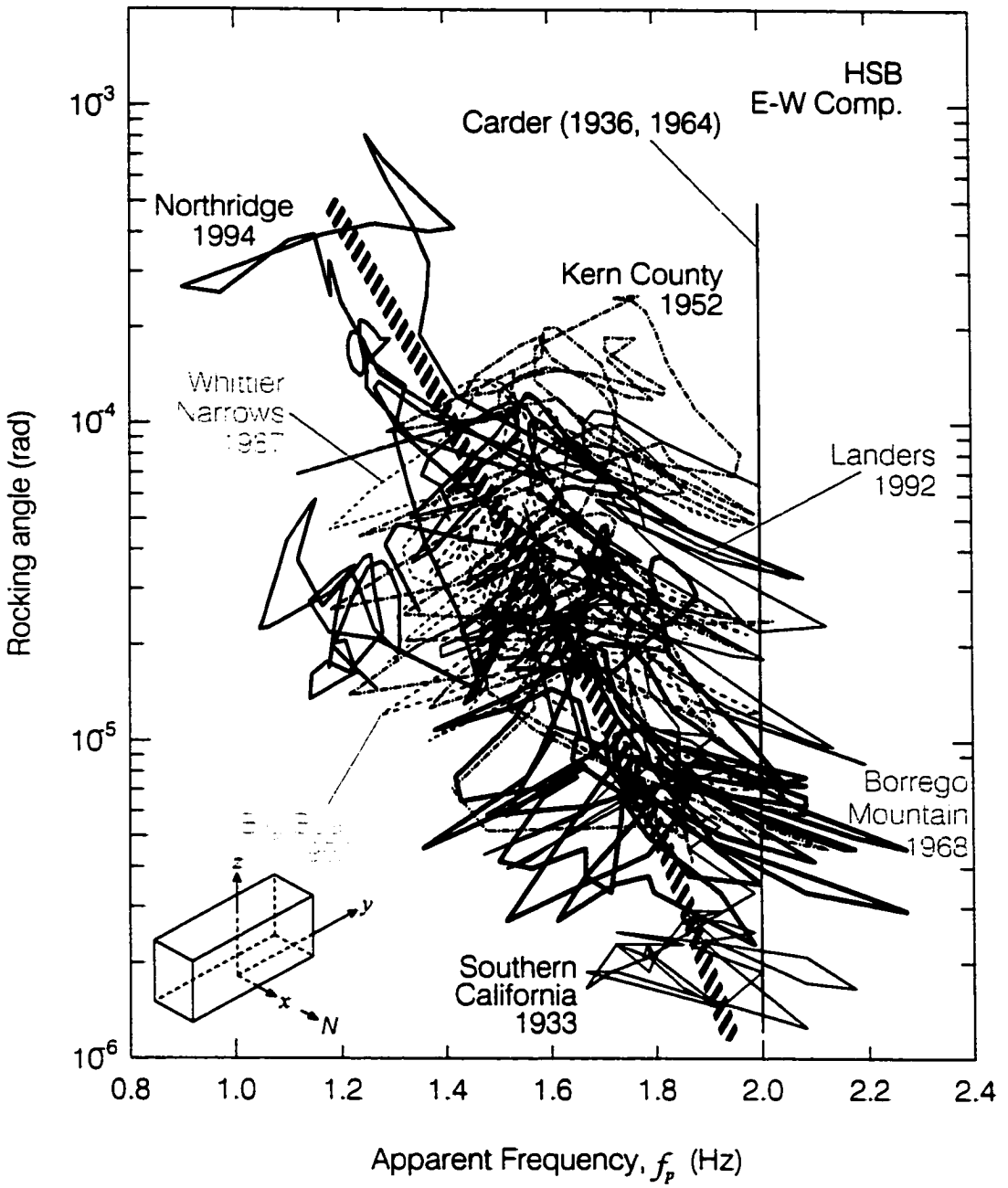

Fig. 3.17a Dependence of the apparent system frequency of Hollywood Storage Building on the peak amplitude of the EW relative response (rocking angle). The solid vertical line shows an estimate of the system frequency determined from ambient vibration and forced vibration tests by Carder (1936, 1964).

Reproduced with permission of the copyright owner. Further reproduction prohibited without permission.

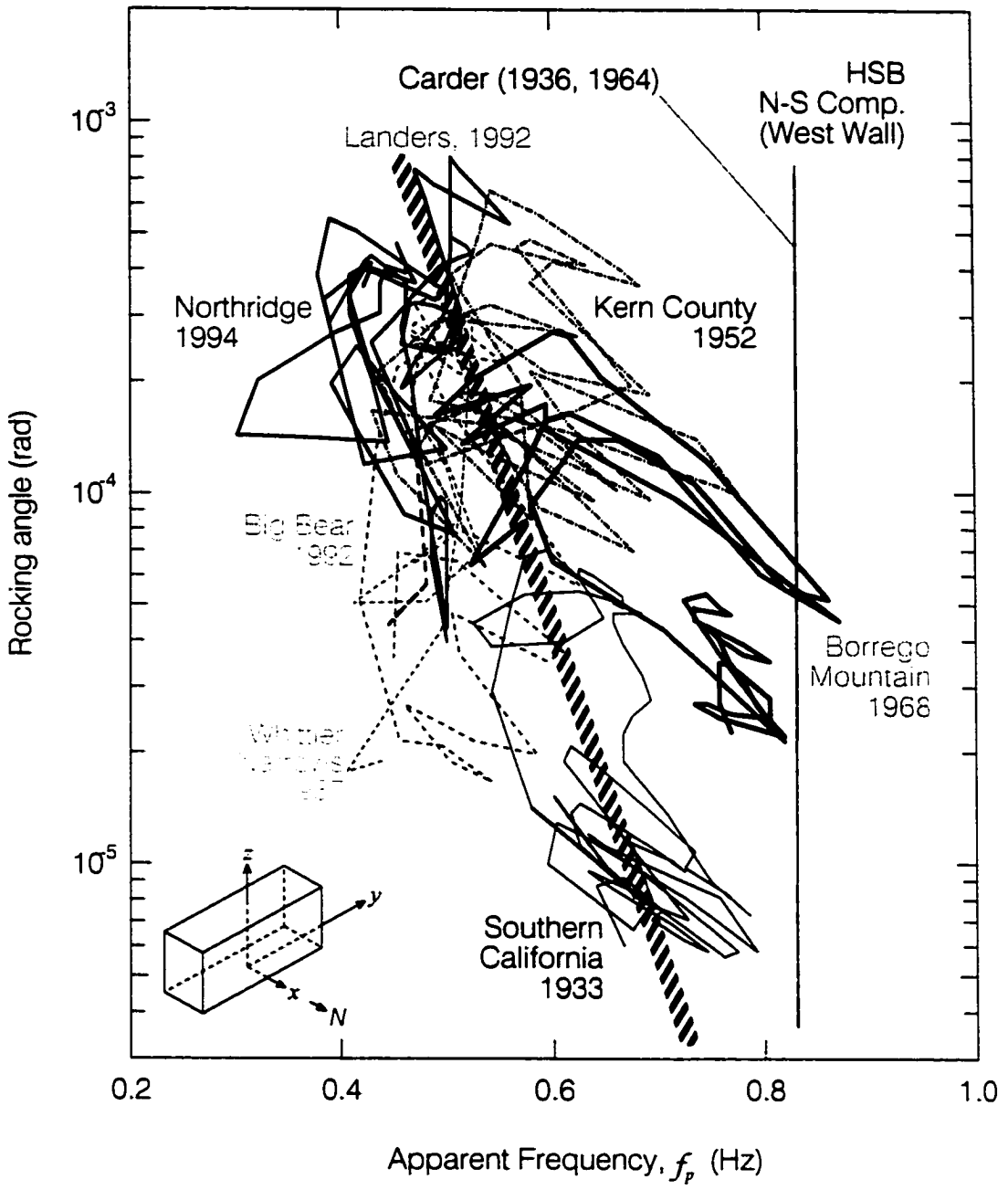

Fig. 3.17b Same as Fig. 3.17a but for the NS response.

Reproduced with permission of the copyright owner. Further reproduction prohibited without permission.

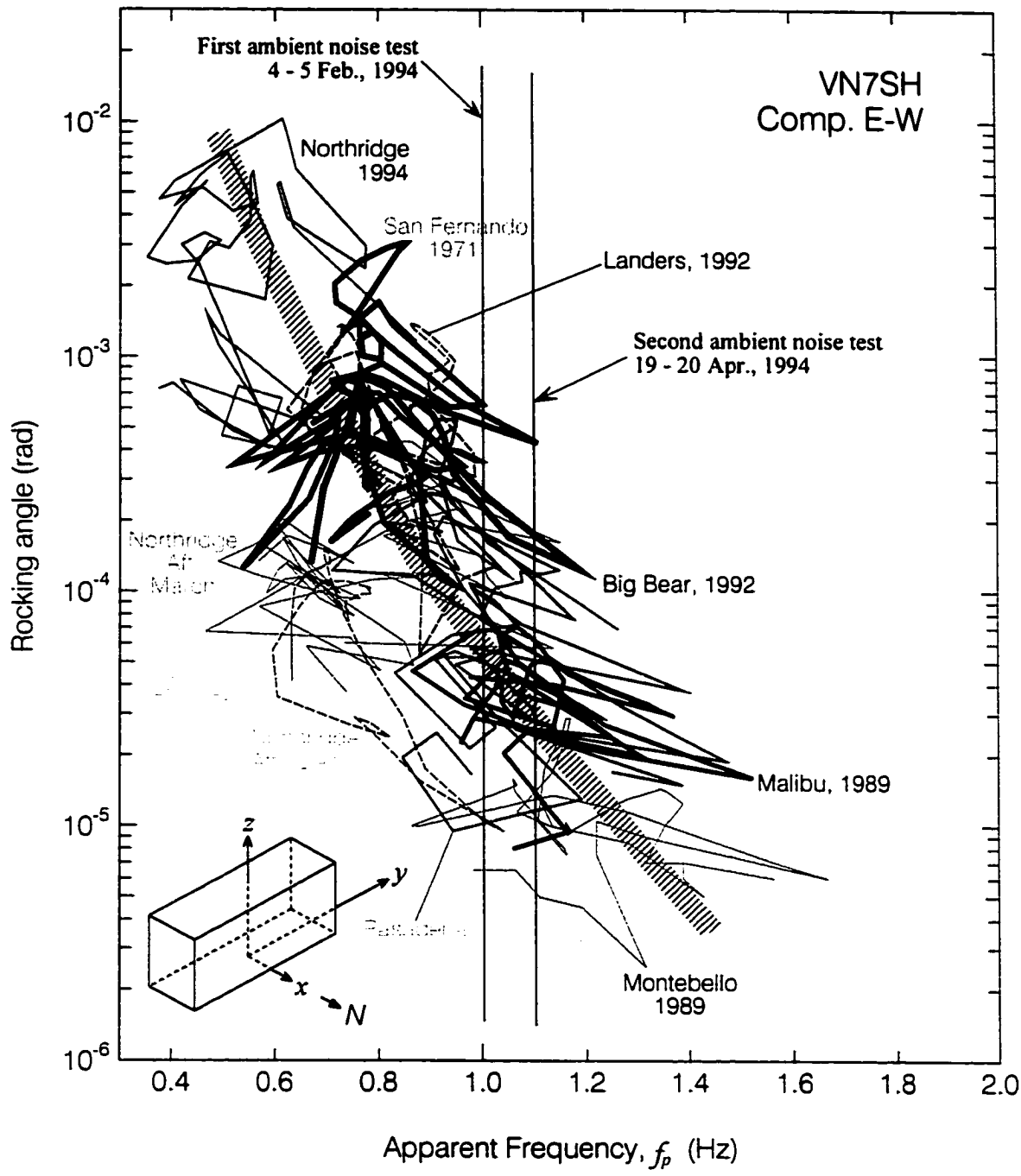

Fig. 3.18a Dependence of the apparent system frequency of Van Nuys 7-story hotel on the peak amplitude of the EW relative response (rocking angle). The solid vertical lines show estimates of the system frequencies determined from ambient vibration tests by Ivanovic et al. (1999, 2000).

Reproduced with permission of the copyright owner. Further reproduction prohibited without permission.

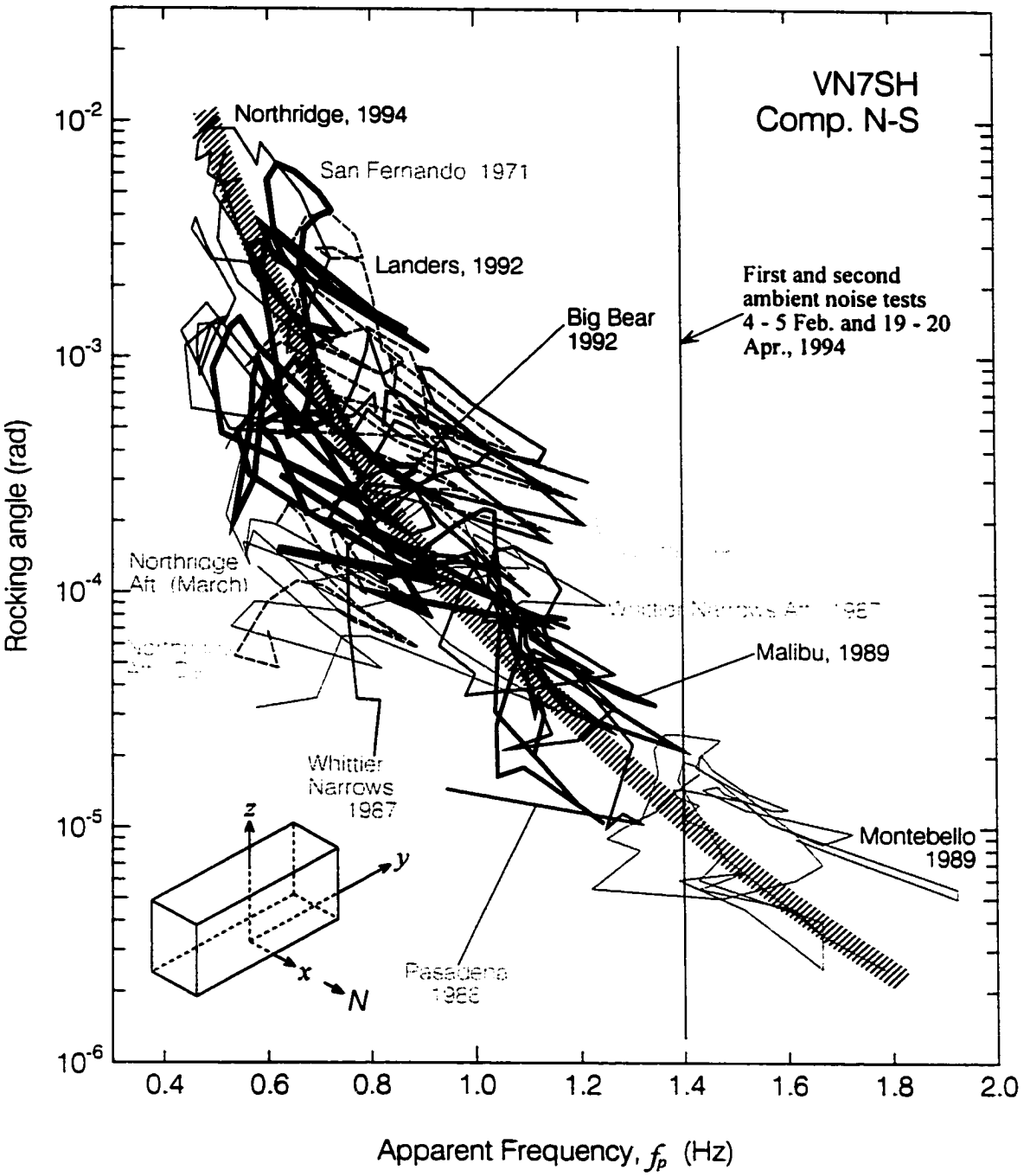

Fig. 3.18b Same as Fig. 3.18a but for the NS response.

Reproduced with permission of the copyright owner. Further reproduction prohibited without permission.

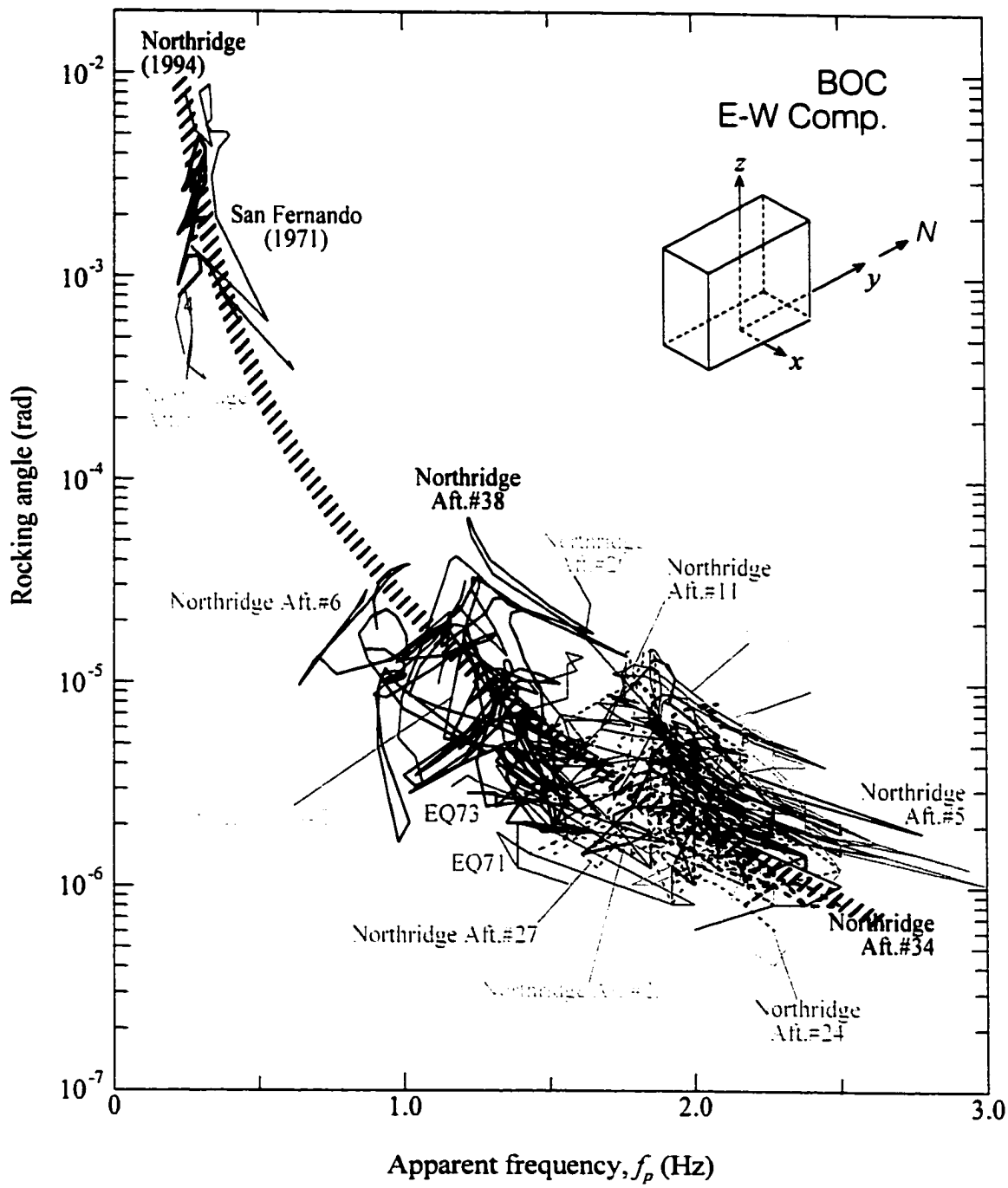

Fig. 3.19a Dependence of the apparent system frequency of Bank of California building on the peak amplitude of the EW relative response.

Reproduced with permission of the copyright owner. Further reproduction prohibited without permission.

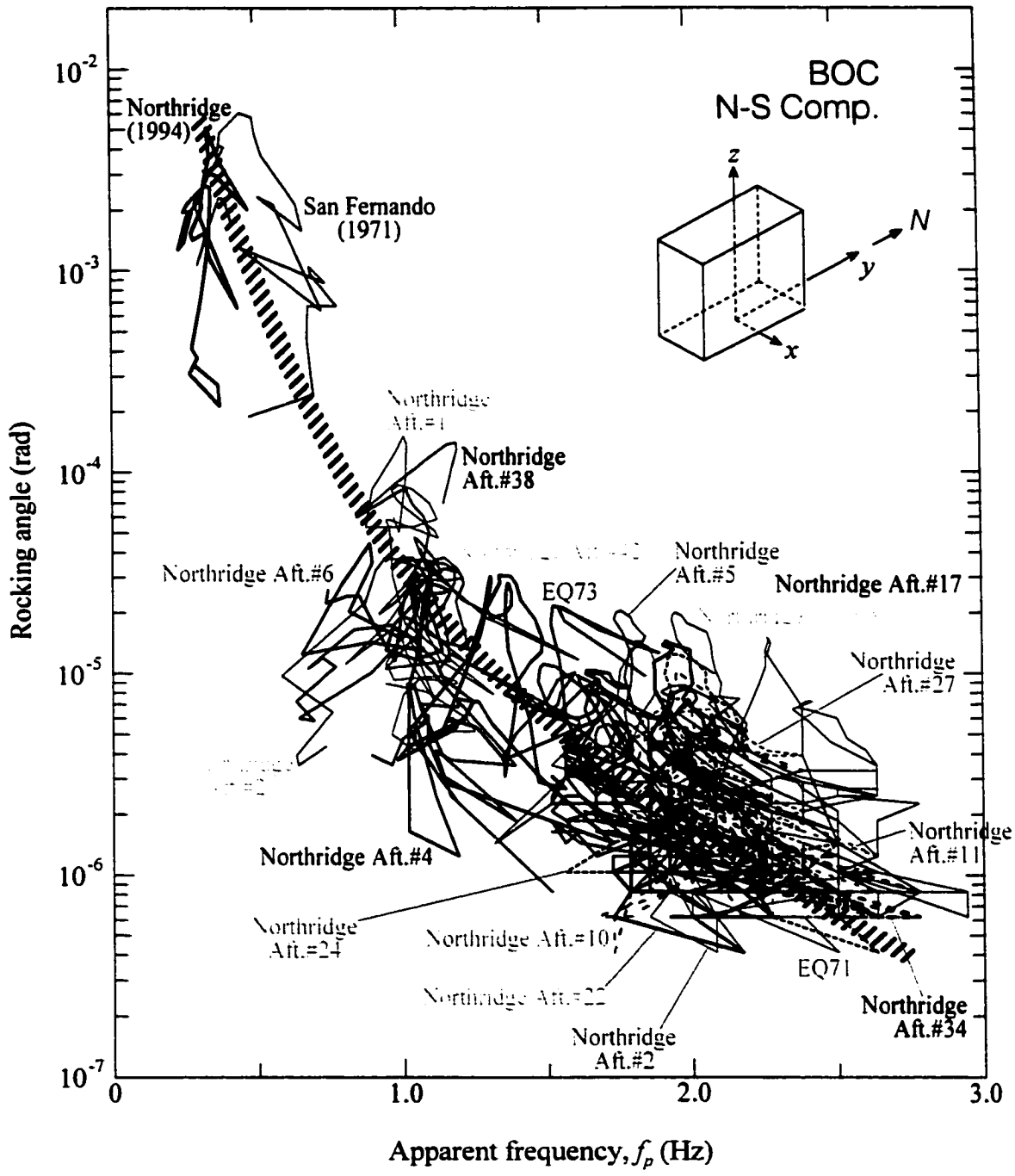

Fig. 3.19b Same as Fig. 3.19a but for the NS response.

Reproduced with permission of the copyright owner. Further reproduction prohibited without permission.

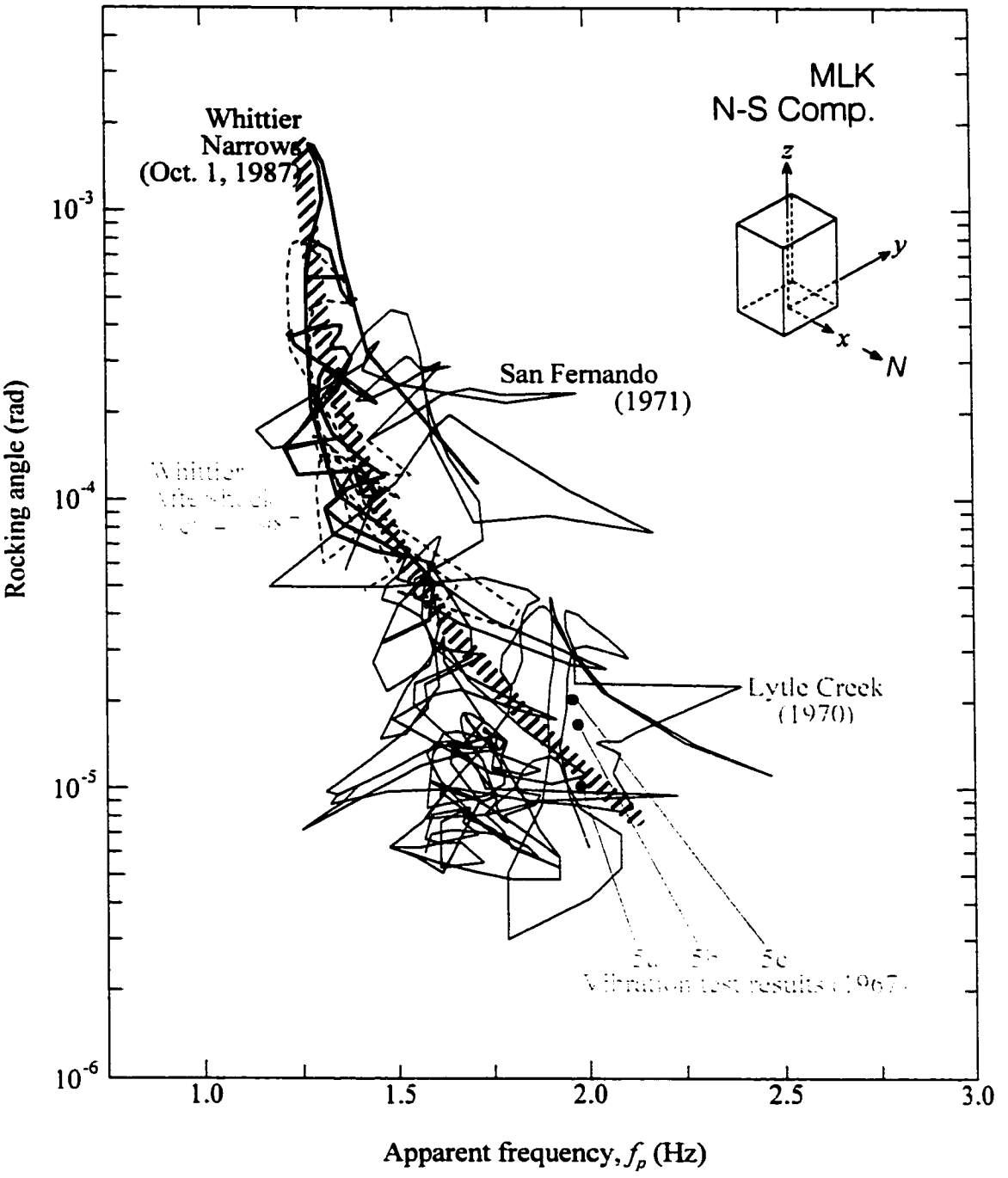

Fig. 3.20b Same as Fig. 3.20a but for the NS response.

Reproduced with permission of the copyright owner. Further reproduction prohibited without permission.

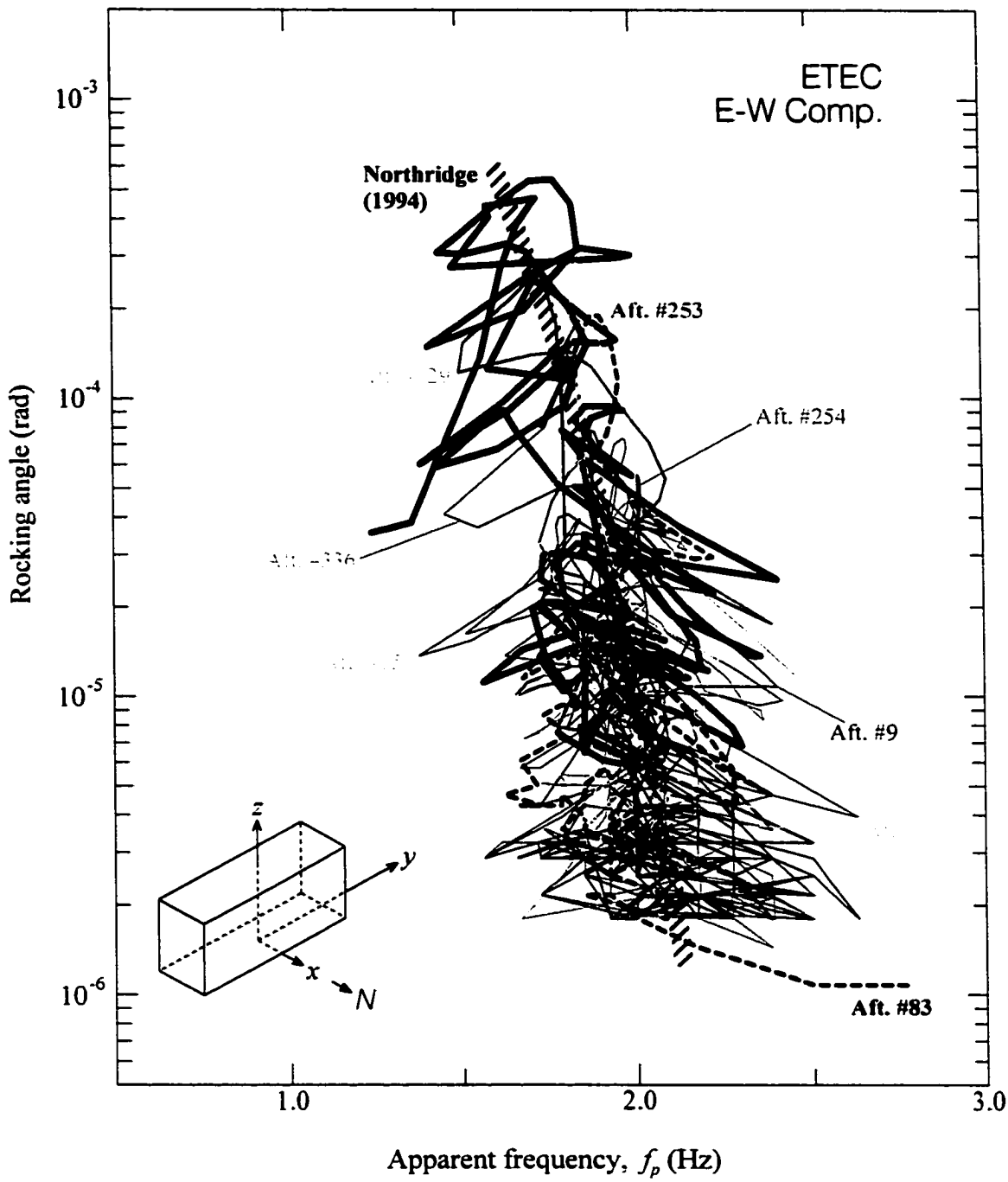

Fig. 3.21a Dependence of the apparent system frequency of Santa Susana ETEC building on the peak amplitude of the EW relative response.

Reproduced with permission of the copyright owner. Further reproduction prohibited without permission.

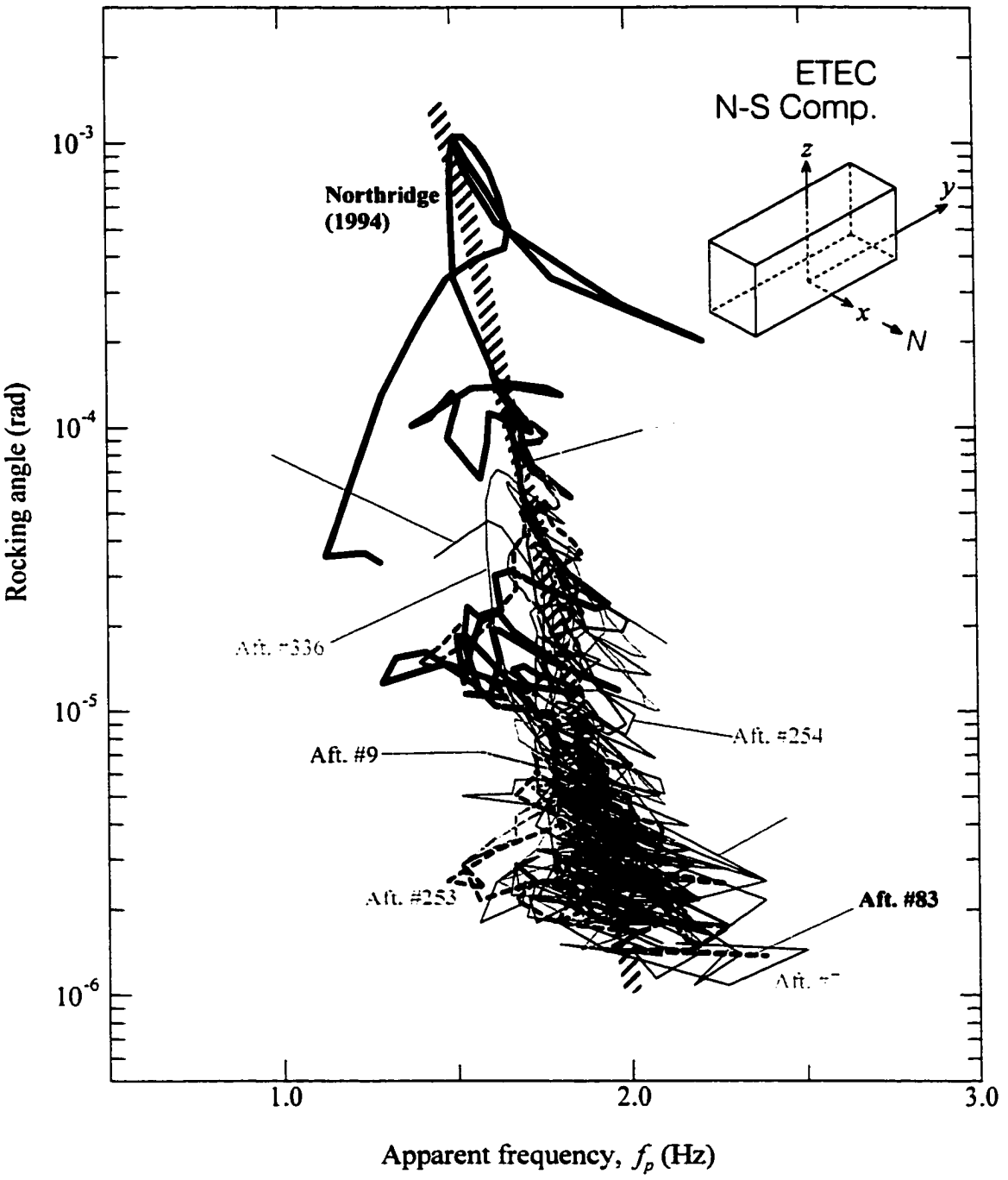

Fig. 3.21b Same as Fig.3.21a but for the NS response.

Reproduced with permission of the copyright owner. Further reproduction prohibited without permission.

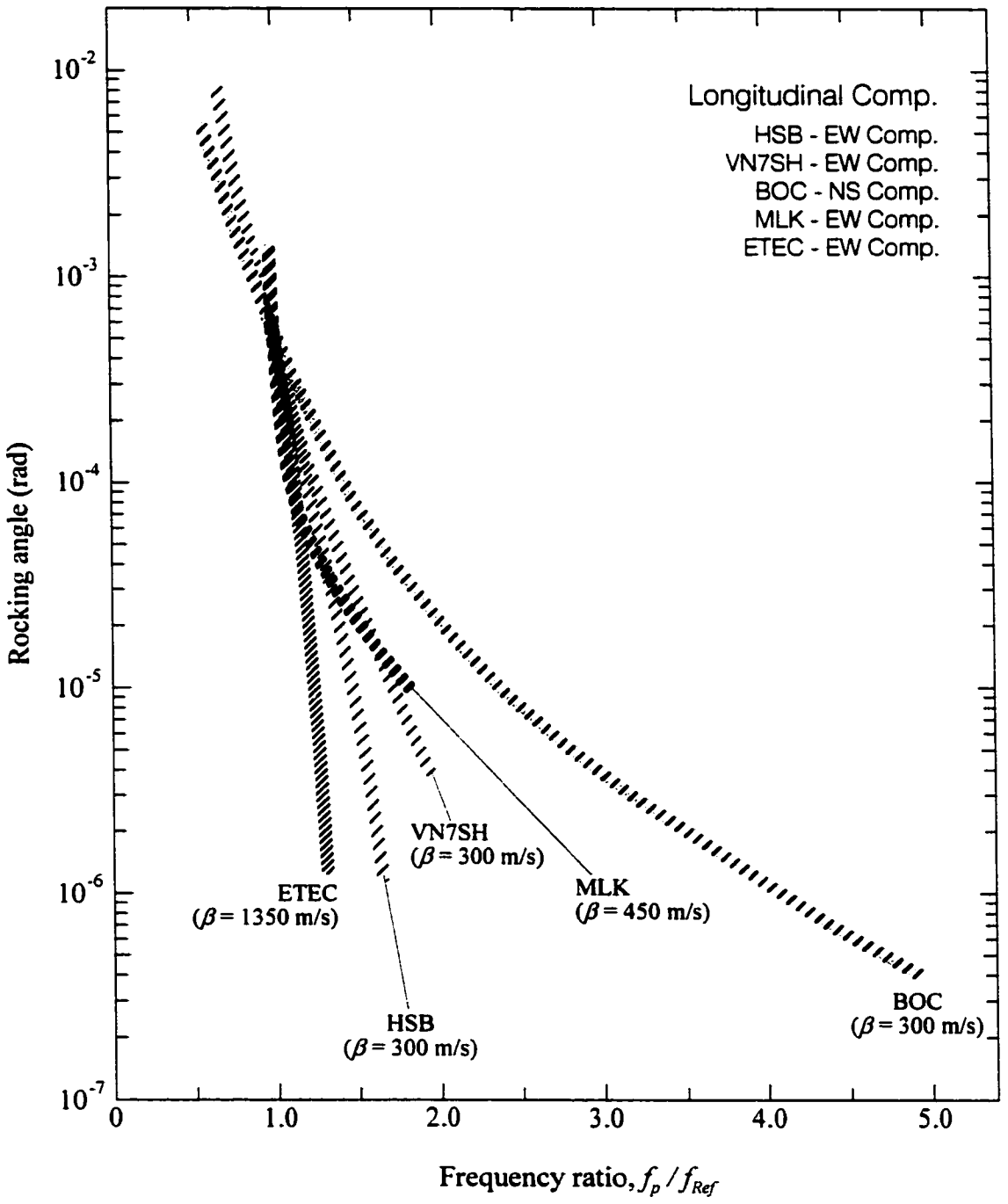

Fig. 3.22a Summary of backbone curves of the amplitude dependent changes of the longitudinal system frequencies of five studied buildings.

Reproduced with permission of the copyright owner. Further reproduction prohibited without permission.

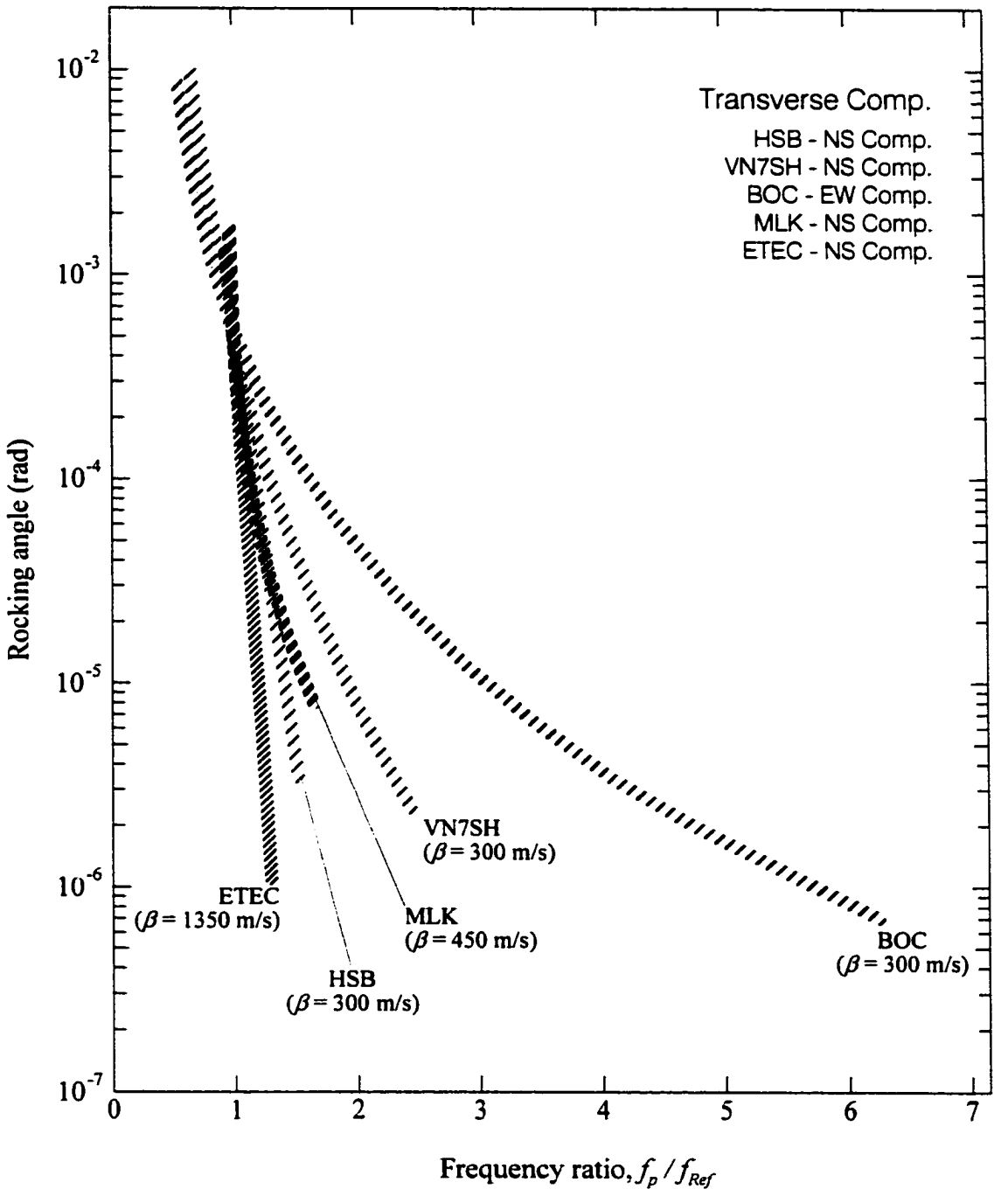

Fig. 3.22b Same as Fig. 3.22a but for the transverse response.

Reproduced with permission of the copyright owner. Further reproduction prohibited without permission.

Appendix B. From the equations of motion, the unknown displacements are solved numerically in time domain. Then the associated system energies are determined. In the following we show the results of these simulations, compare the recorded and predicted responses, and discuss the system energies.

3.3.1 Predicted Responses

Figs. 3.23 and 3.24 illustrate the results of the modeling the EW response of VN7SH building during 1992 Landers earthquake, and the NS response of MLK building during 1987 Whittier-Narrows earthquake. Parts (a) of Figs. 3.23 and 3.24 show the displacements recorded at the base of the building, which are used as input excitations for the simulation. The predicted displacements of the roof relative to the base are plotted in parts (b) of the Figs. 3.23 and 3.24. During shaking, the soil on the sides of the foundation is pushed sideways. This is shown in parts (c) of Figs. 3.23 and 3.24 (the gaps shown here represent the separations at the surface level). Parts (d) of these figures show the results of the zero-crossing (solid points) and of the moving window Fourier (solid lines) analyses of the changes of system frequency. In Section 3.2, the results of the time-frequency analysis indicate that the soil behaves nonlinearly, but can recover its stiffness during a particular earthquake. To simulate this increase in the stiffness, we can close the gaps in the soil springs, at the times when the observed frequency increases occur. In part (c) of Fig. 3.23, it is found that the separation between the foundation and the soil occurs at 3.9 seconds and keeps increasing between 3.9 to 6.0 seconds. The system is oscillating with partially contacting the soil springs on the sides and the system stiffness decreases a little.

Reproduced with permission of the copyright owner. Further reproduction prohibited without permission.

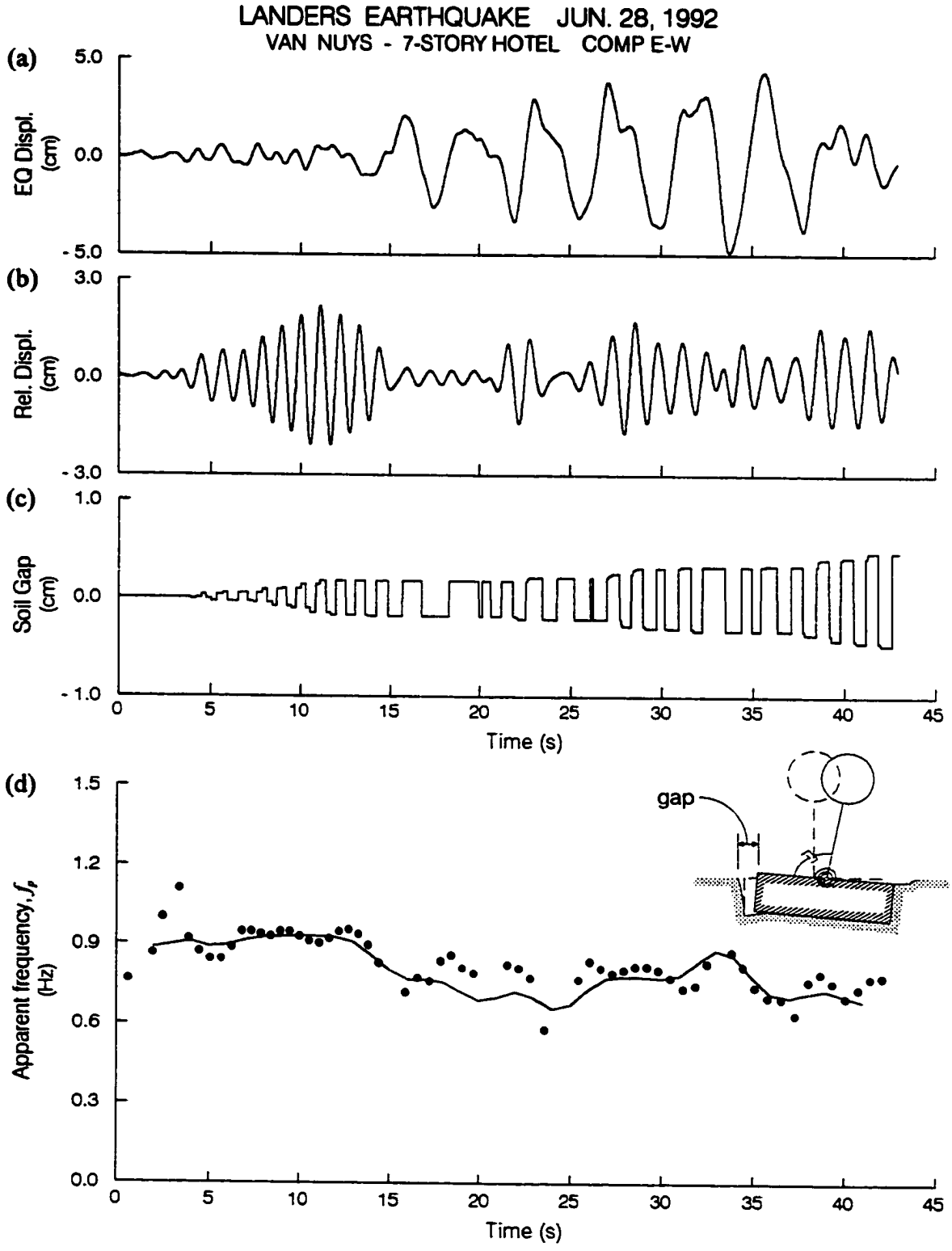

Fig. 3.23 An example of predicted EW response to the 1992 Landers earthquake of VN7SH building.

Reproduced with permission of the copyright owner. Further reproduction prohibited without permission.

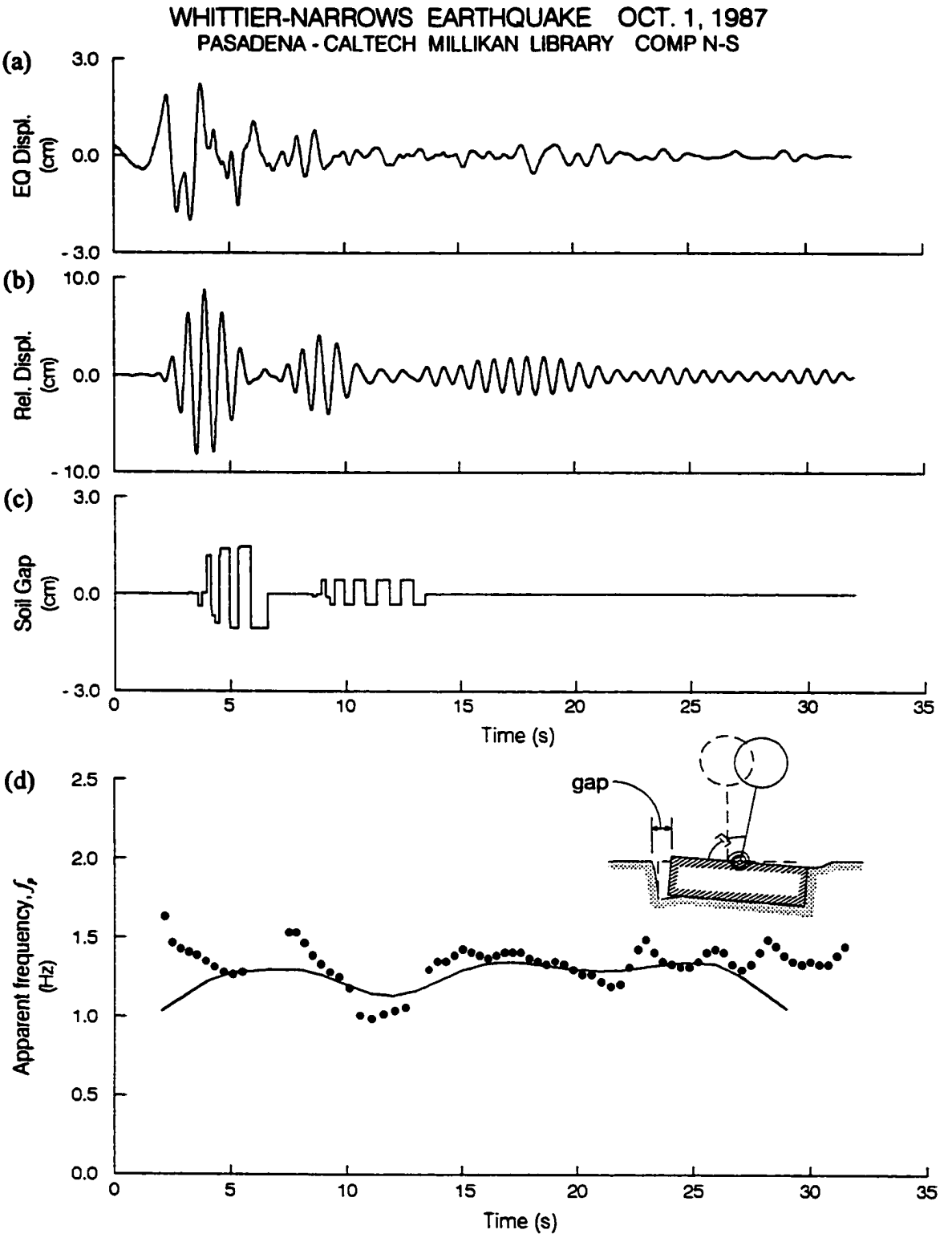

Fig. 3.24 An example of predicted NS response to the 1989 Whittier-Narrows earthquake of Millikan Library building.

Reproduced with permission of the copyright owner. Further reproduction prohibited without permission.

At about 7.35 seconds, the larger response of the foundation pushes the soil on the sides further. This increases the system stiffness (i.e. increases f_p). Again, the gap increases between 7.35 to 14.2 seconds and when the system is oscillating without contacting the soil on the sides (between 14.2 to 21.8 seconds), the system stiffness decreases. This behavior, referred to as "pinching", can also be seen at about 27.0, 30.9 and 37.7 seconds. In part (c) of Fig. 3.24, the "pinching" effect is found at 3.2 and 5.8 seconds, and the system frequency decreases while separations occur. At 6.6 and 13.4 seconds the gaps were closed, to simulate the observed stiffness recovery.

3.3.2 Comparison of the Recorded and Predicted Responses

Figs. 3.25a and b show examples of the predicted response together with recorded response of the VN7SH during 1971 San Fernando earthquake. Top parts of Figs. 3.25a and b show comparison of the band-pass filtered relative response of recorded motions (dashed lines), and the simulated motions (solid line) using the model presented in Fig. 2.1. The central parts of Figs. 3.25a and b show the time dependent changes of the system frequency, f_p. The dashed lines show the changes in f_p evaluated by moving window Fourier analysis of recorded data, and the open circles show the estimates by the zero-crossing analysis also using the recorded data. The solid line and solid points show the corresponding quantities for the predicted response. The vertical arrows show the times where the gaps in the soil springs were closed to match the observed increases in the system frequency, shown in the central parts of Figs. 3.25a and b (dashed lines and open circles). A complete set of figures showing further details of the results for HSB and VN7SH buildings, during all

Reproduced with permission of the copyright owner. Further reproduction prohibited without permission.

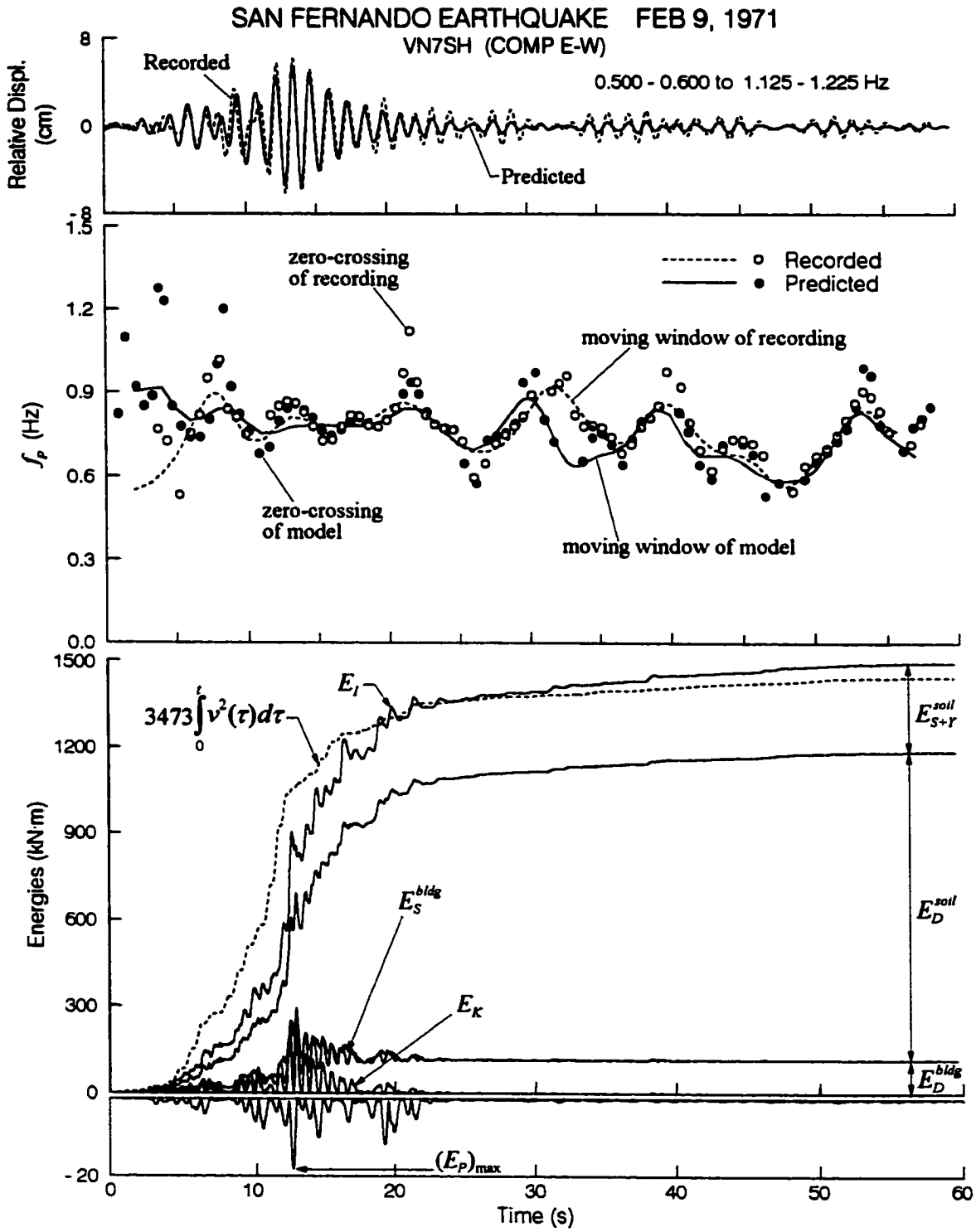

Fig. 3.25a Top: comparison of recorded (dashed lines) and predicted (solid line) EW relative displacement response at roof of VN7SH during the 1971 San Fernando earthquake. Center: time dependent changes of the system frequency f_p computed from recorded (dashed lines and open circles) and predicted (continuous line and solid dots) responses. Bottom: contributions to the system energy: E_{S+Y}^{soil}, E_D^{soil}, E_S^{bldg}, E_D^{bldg}, E_K and E_P and their sum E_I. Input wave energy $a_0\int_0^t v^2(\tau)d\tau$ is shown by dashed line.

Reproduced with permission of the copyright owner. Further reproduction prohibited without permission.

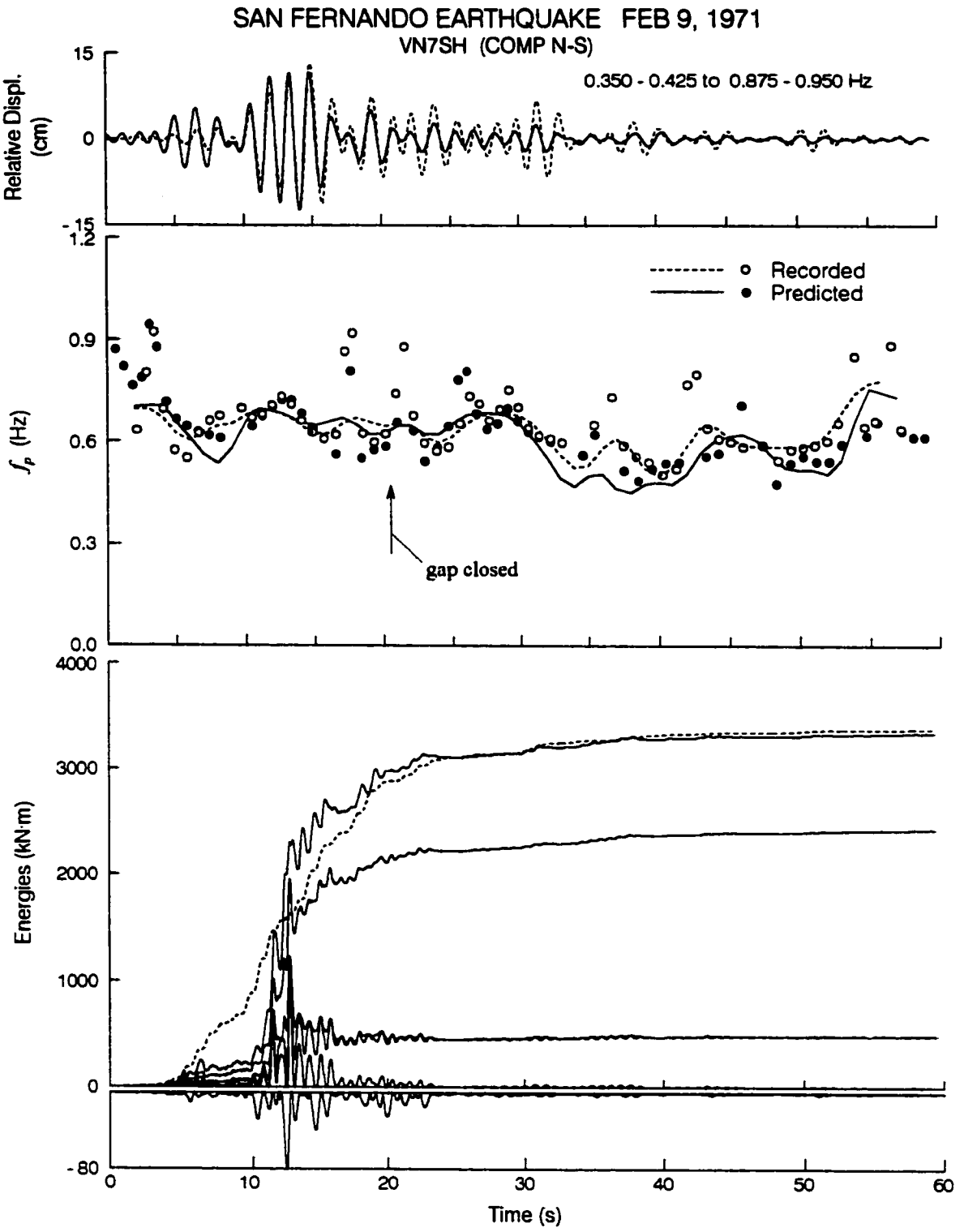

Fig. 3.25b Same as Fig. 3.25a, but for the NS response.

Reproduced with permission of the copyright owner. Further reproduction prohibited without permission.

recorded earthquakes, can be found in Trifunac et al. (2001f). The results corresponding respectively to the BOC, MLK and ETEC buildings can be found in Appendix C. These figures show that the behavior of the model is consistent with the recorded response. Thus it is seen that this "simple" model approximates the overall dynamic properties of the building systems.

The bottom parts of Figs. 3.25a and b show a comparison of the predicted total system energy with the input wave energy (further details and discussion on the "input wave energy" can be found in Trifunac et al., 2001f). The distribution of the predicted total system energy, E_I, among E_D^{bldg}, E_S^{bldg}, E_D^{soil}, E_{S+Y}^{soil}, E_K and $(E_P)_{max}$ is also illustrated in these figures.

3.3.3 Energies of System

The bottom parts of Figs. 3.25a and b show a comparison of the predicted total system energy with the input wave energy versus time. To properly compare these results, we band-pass filtered the model results and the input wave energy (the processed velocity was filtered before integration; see Trifunac et al., 2001f). In these figures, top solid line represents the sum of different parts of energy resulting in the "total" system energy, E_I. The dotted line represents $a_0 \int_0^t v^2(\tau)\, d\tau$, with a_0 determined by least squares fit of the "total" energy in terms of $\int_0^t v^2(\tau)\, d\tau$. As explained in Trifunac et al. (2001f), the integral $a_0 \int_0^t v^2(\tau)\, d\tau$ represents the cumulative energy arriving to the site in the form of seismic waves. The "total"

Reproduced with permission of the copyright owner. Further reproduction prohibited without permission.

energy represents the sum of all response energies of the soil-structure system (Fig. 2.1).

When fitting data for the total system energy in terms of the input wave energy, for different earthquake excitations, it can be assumed that the relationship is linear; that is

$$y = a_0 x \qquad \text{or} \tag{3.1a}$$

$$y = a_1 x + b_1 \tag{3.1b}$$

where x and y represent $\int_0^t v^2(\tau)\,d\tau$ and E_I, respectively; and a_0, a_1 and b_1 are constants.

Figs. 3.26 through 3.30 show the trends of computed E_I (total energy of the soil-structure system response) versus $\int_0^t v^2(\tau)\,d\tau$ (input wave energy factor) for the EW (solid circles) and NS (solid triangles) responses of five selected buildings, for all recorded earthquakes. For 1970 Lytle Creek and 1971 San Fernando earthquakes recorded in the HSB, the system energies are predicted based on assumed model parameters only, since without recorded roof motion it is not possible to find the best estimates of the system parameters. The least squares fit through the data gives $\bar{a}_0 = 1.71\times10^4$ kg/s for the HSB, $\bar{a}_0 = 0.48\times10^4$ kg/s for the VH7SH, $\bar{a}_0 = 1.55\times10^4$ kg/s for the BOC, $\bar{a}_0 = 4.11\times10^4$ kg/s for the MLK, and $\bar{a}_0 = 0.56\times10^4$ kg/s for the ETEC building. In Fig. 3.28, the earthquake motions at the ground floor in the Bank of California building were recorded only during 1971 San Fernando earthquake and its

Reproduced with permission of the copyright owner. Further reproduction prohibited without permission.

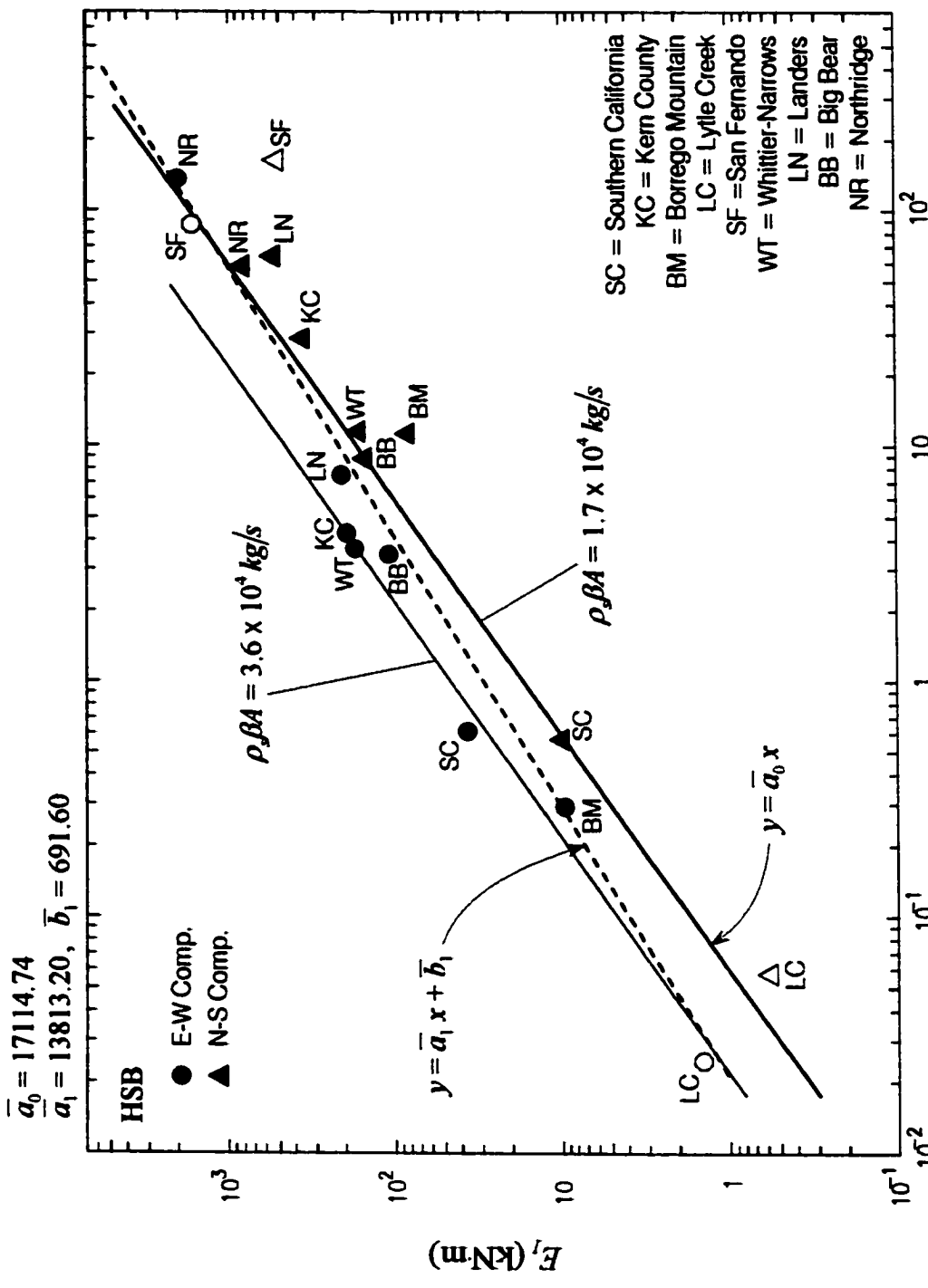

Fig. 3.26 Total computed response energy E_I (kN m) versus input energy factor, *en*, for nine earthquakes recorded in the HSB.

Reproduced with permission of the copyright owner. Further reproduction prohibited without permission.

Reproduced with permission of the copyright owner. Further reproduction prohibited without permission.

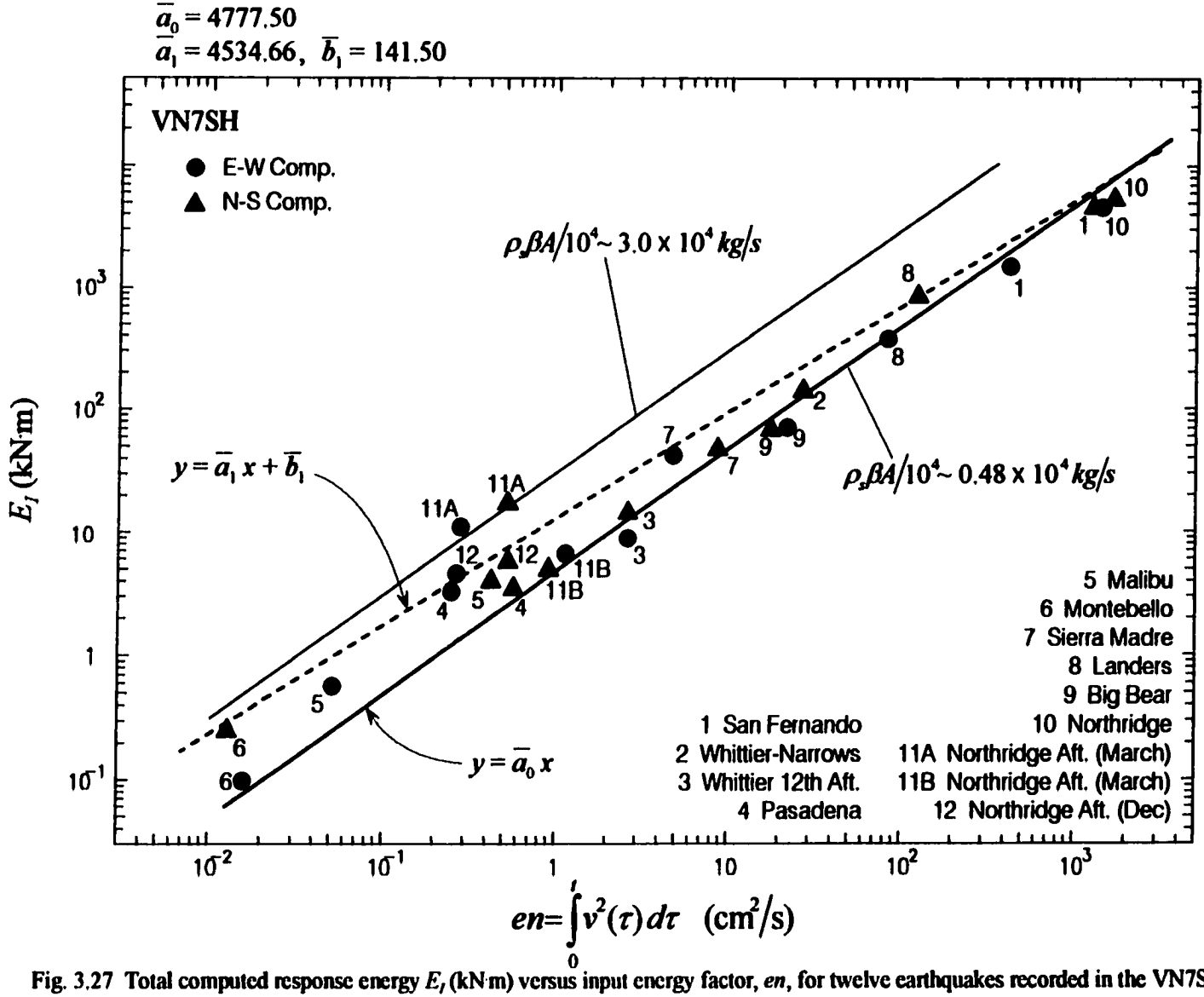

Fig. 3.27 Total computed response energy E_I (kN·m) versus input energy factor, *en*, for twelve earthquakes recorded in the VN7SH.

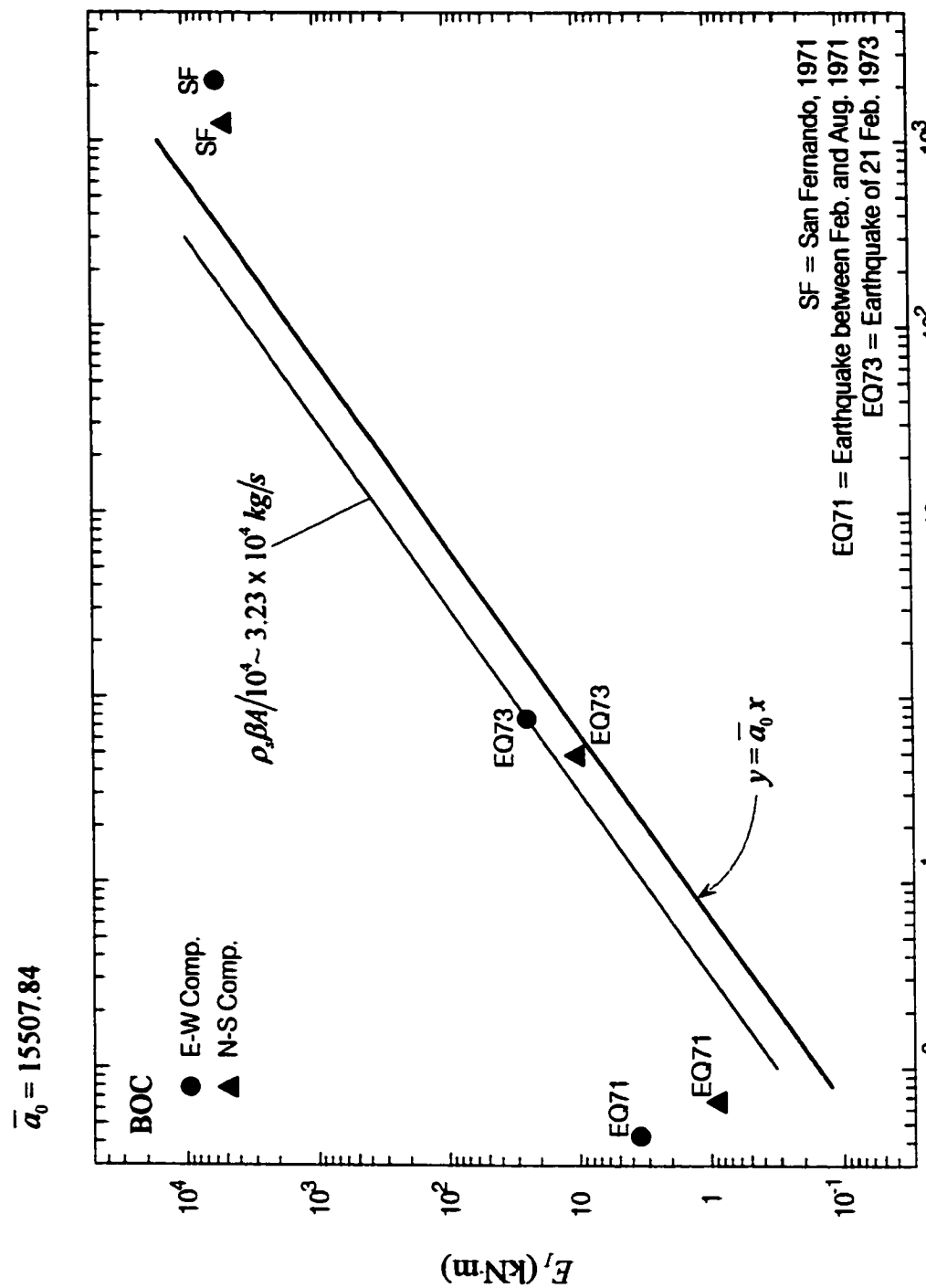

Fig. 3.28 Total computed response energy E_I (kN·m) versus input energy factor, *en*, for three earthquakes recorded in the BOC.

Reproduced with permission of the copyright owner. Further reproduction prohibited without permission.

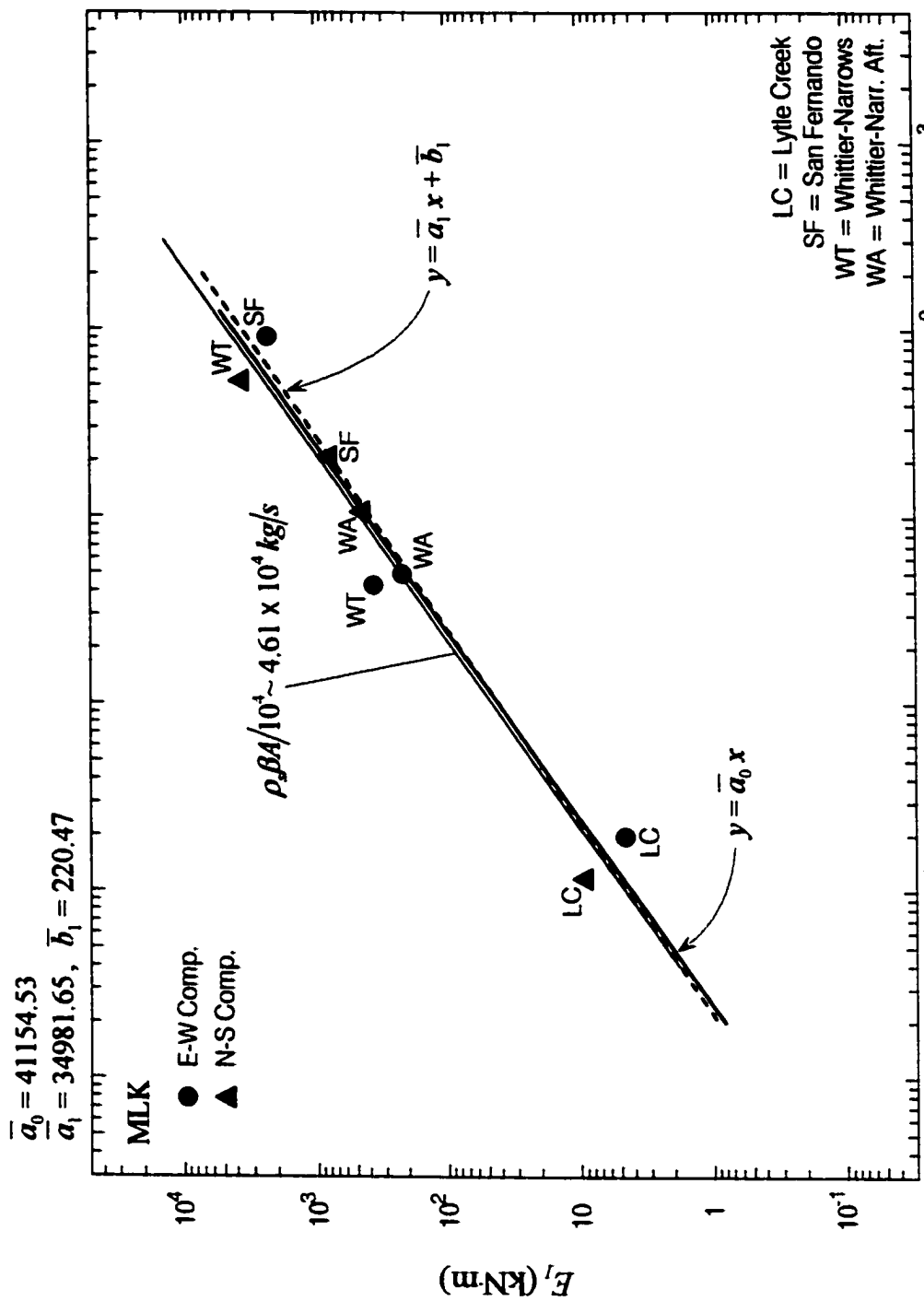

Fig. 3.29 Total computed response energy E_I (kN·m) versus input energy factor, *en*, for four earthquakes recorded in the MLK.

Reproduced with permission of the copyright owner. Further reproduction prohibited without permission.

Reproduced with permission of the copyright owner. Further reproduction prohibited without permission.

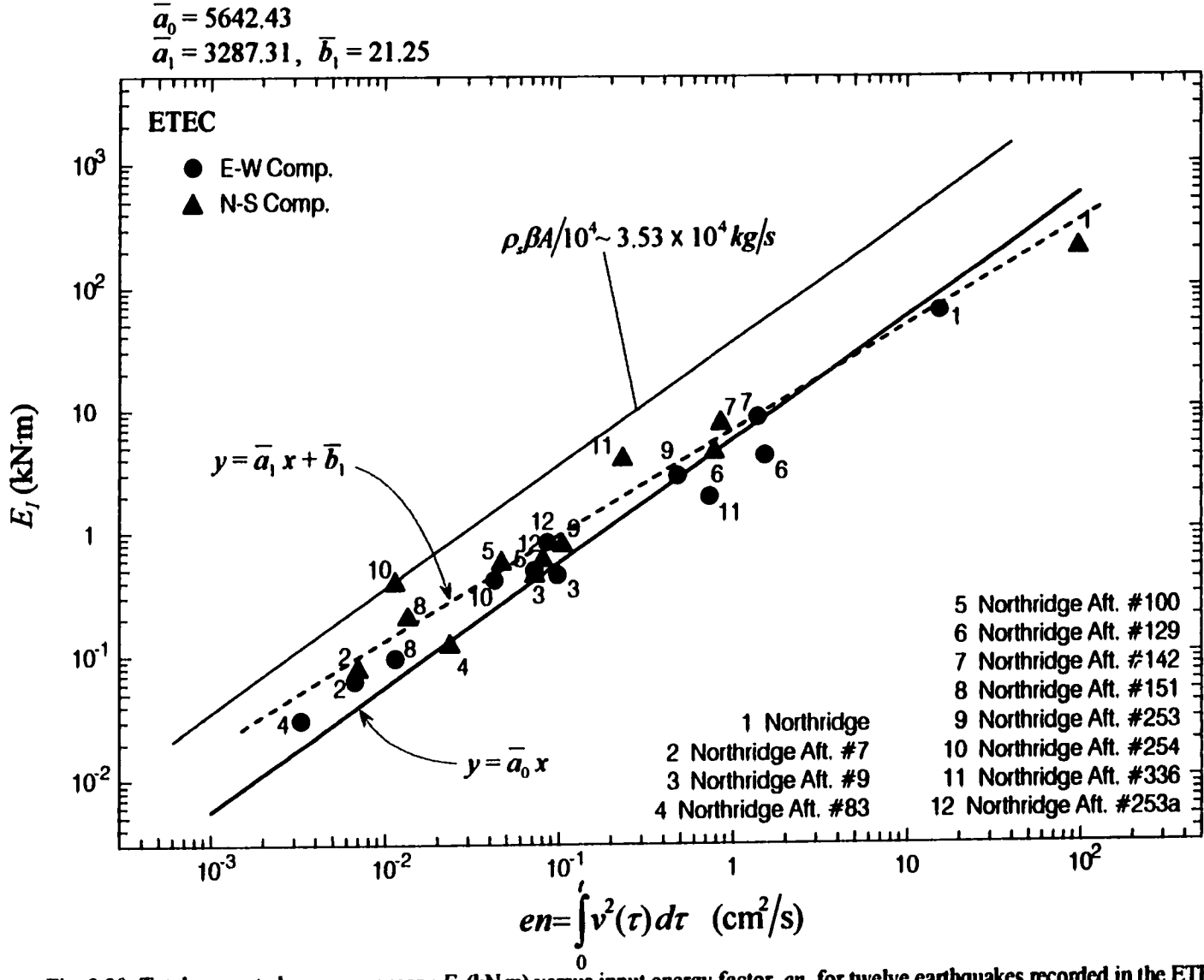

Fig. 3.30 Total computed response energy E_I (kN·m) versus input energy factor, *en*, for twelve earthquakes recorded in the ETEC.

aftershocks, between 9 Feb. and 4 Aug. 1971, and during the earthquake of 21 Feb. 1973. Since there are not enough data, $\bar{a}_1$ and $\bar{b}_1$ are not considered for this case.

For vertically incident plane shear waves, and neglecting the wave scattering from the foundation, the coefficient a_0 should be approximately equal to $\rho_s A\beta$, where ρ_s is density, β is the shear wave velocity in the soil on the top 30 meters surrounding the foundation, and A is the area of the plan of the building foundation. From Table B.1, we can find values for ρ_s, β and plan dimensions and compute $\rho_s A\beta$ for each building. After converting velocities squared from m^2/s^2 into cm^2/s^2, we obtain $a_0' = \rho_s A\beta / 10^4 = 3.6\times10^4$ kg/s for HSB, $a_0' = 3.0\times10^4$ kg/s for VN7SH, $a_0' = 3.2\times10^4$ kg/s for BOC, $a_0' = 4.6\times10^4$ kg/s for MLK and $a_0' = 3.5\times10^4$ kg/s for ETEC building. It is seen that $a_0' \log_{10} \int_0^t v^2(\tau)\, d\tau$ is an upper bound for all points shown in Figs. 3.26, 3.27 and 3.30, and for increasing amplitudes of shaking, the effective $\rho_s A\beta$ reduces. The effective factor $\rho_s A\beta$ is reduced, because the strong ground motion does not consist of plane vertically arriving S-waves, but is a complex sequence of body and surface waves whose angles of approach vary vertically and horizontally. Furthermore, coefficients a_0 and a_1 depend on the soil-structure interaction, which involves various types of foundation systems. We conclude that considering the complexities of the energy transfer from the soil into the building (Trifunac et al., 1999a; 2001b; 2001f), the agreement of the predicted E_I versus $\int_0^t v^2(\tau)\, d\tau$ is satisfactory to warrant further and more detailed studies of the energy transfer

Reproduced with permission of the copyright owner. Further reproduction prohibited without permission.

mechanisms. Therefore, if the input wave energy factor, $\int_0^t v^2(\tau)\,d\tau$, of the strong motion at a given site is known, it is possible to estimate approximately the total system energy, E_I, for an expected future earthquake.

For example, if it is expected from previous earthquake records at a certain site that $\int_0^t v^2(\tau)\,d\tau$ is 8.70×10^2 cm^2/s and the effective $\rho_s A\beta/10^4$ for a building is 1.45×10^4 kg/s, the total system energy can be approximated from

$$\begin{aligned} E_I &\approx (\rho_s A\beta)\left(\int_0^t v^2(\tau)\,d\tau\right) = (8.70\times10^2\,\text{cm}^2/\text{s})(1.45\times10^4\,\text{kg/s}) \\ &\approx 12615\ \text{kN}\cdot\text{m} \end{aligned} \tag{3.2}$$

Reproduced with permission of the copyright owner. Further reproduction prohibited without permission.

4. ENERGY-BASED DESIGN CONSIDERATIONS

For design purposes, it is important to define the meaning of "energy demand." Uang and Bertero (1990) defined the input energies E_i and E_i' (absolute and relative) in terms of the relative response of a fixed-base SDOF model subjected to horizontal ground motion only. They used these energies to convert the results to an equivalent spectral velocity and proposed the input energy equivalent velocity spectra for future design. It should be noted that the equivalent spectral velocity depends on the vibration period of the buildings and the predominant periods of the earthquake ground motions. Furthermore, the soil-structure interaction effects were not considered by Uang and Bertero (1990). Consequently, their approach is fundamentally not different from the classical Response Spectrum Method. In the following we use the model in Fig. 2.1, and energy of incident ground motion, to develop more realistic procedures for estimation of the energy demand. Then the designer has to decide how to balance this demand with all available resources, including the energy absorption capacity of soils.

4.1 Energy Demand

For a building supported by flexible soil, the soil-structure interaction will lead to horizontal and rocking deformations of the soil, and in general this will reduce the amplitude of the strong-motion pulses entering the structure. Partitioning of the incident seismic wave energy into horizontal and rocking motions of the soil-foundation-building system and scattering of incident wave from the foundation will

Reproduced with permission of the copyright owner. Further reproduction prohibited without permission.

thus reduce the energy available to cause relative deformation of the structure. This implies that the effective energy to be absorbed by structural damping and hysteretic response of structures (for nonlinear response) will be less than the traditional estimates, which consider the system as fixed-base model (the case of "rigid" soil without soil-structure interaction).

Figs. 4.1a and b though 4.5a and b illustrate the maximum kinetic energy, $(E_K + E_P)_{max}$, versus E_I^* and E_I for five studied structures, where E_I^* = the total system response energy computed at the instant when $(E_K + E_P)_{max}$ occurs, and E_I = the total system response energy at the end of excitation.

Table 4.1 summarizes the ratios of $(E_K + E_P)_{max}$ with respect to E_I^* and E_I. It is seen that $(E_K + E_P)_{max}$ is always smaller than E_I^* (it is in the range from 0.1 to $0.9E_I^*$), and mostly smaller than E_I. This implies that the amplitudes of velocity pulses entering the structure and causing the relative response have been reduced by soil-structure interaction, soil damping, and the energy absorbed by hysteretic response of soil. At the same time the average ratio observed from Table 4.1 shows that the reduction of $(E_K + E_P)_{max}$ with respect to E_I^* and E_I for the ETEC building is about 0.5, which is less than for the other buildings studied here. This structure lies on "stiffer" soil, but the structural response is still affected by soil-structure interaction and soil damping.

In the use of energy concepts for seismic-resistant design, E_I in eqn (2.61) represents the demand, and the summation of left side terms represents what should be supplied. It is important to note that this demand does not only deform the building,

Reproduced with permission of the copyright owner. Further reproduction prohibited without permission.

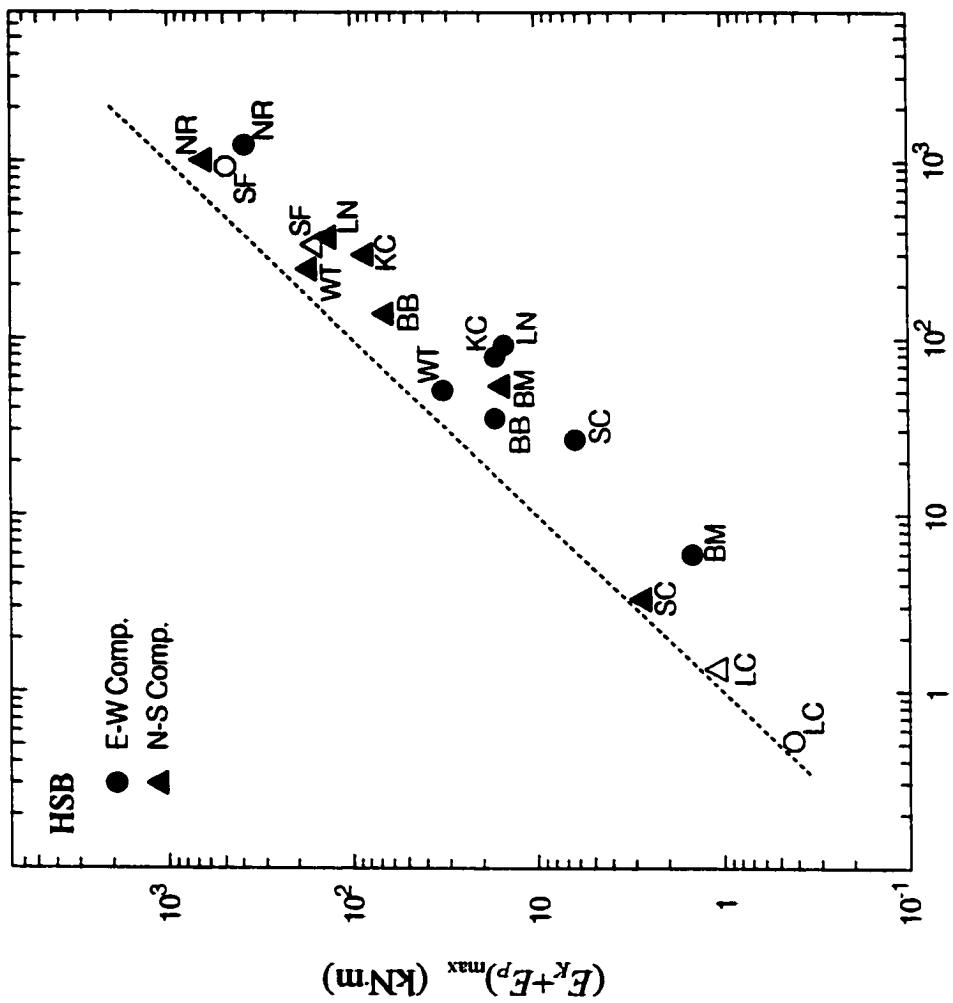

Fig. 4.1a Total computed kinetic energy $(E_K+E_P)_{max}$ versus E_I^* (kN·m), total system response energy computed at the instant when $(E_K+E_P)_{max}$ occurs, for nine earthquakes recorded in the HSB.

Reproduced with permission of the copyright owner. Further reproduction prohibited without permission.

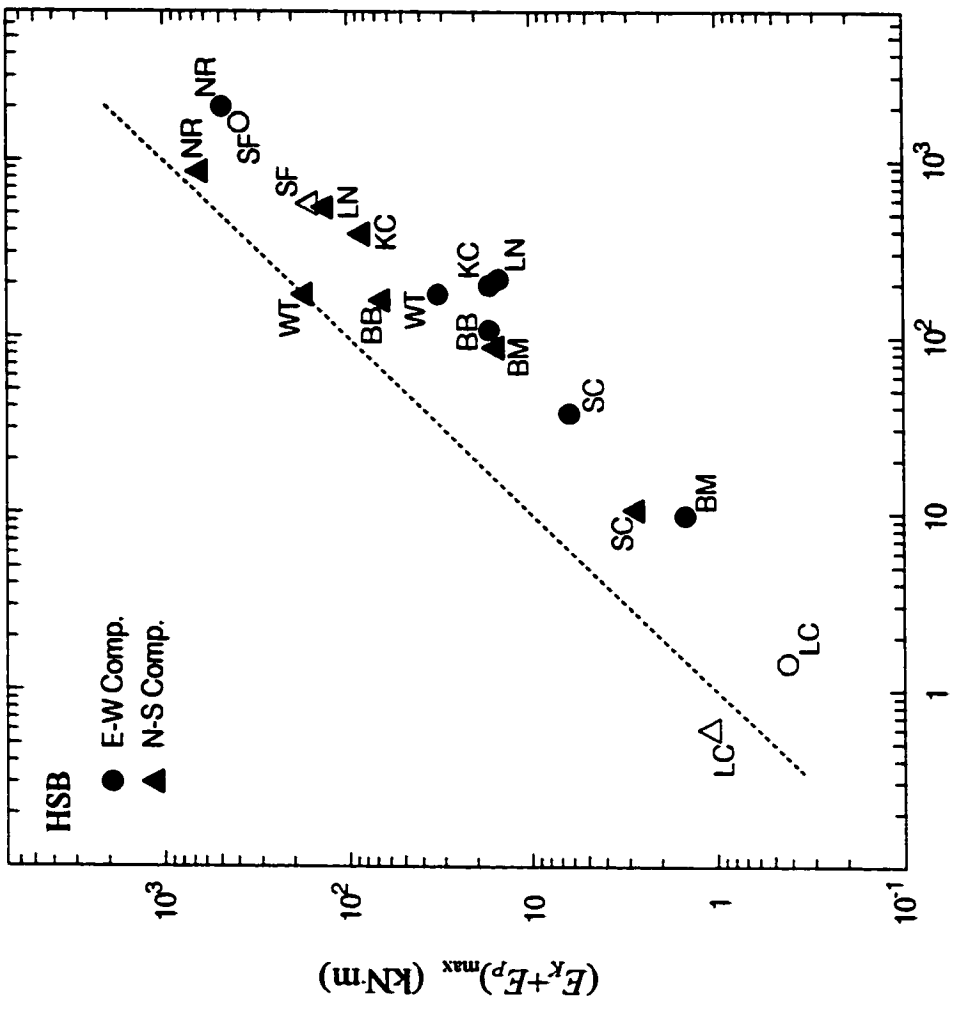

Fig. 4.1b Total computed kinetic energy $(E_K+E_P)_{max}$ versus E_I (kNm), total system response energy at the end of excitation, for nine earthquakes recorded in the HSB.

Reproduced with permission of the copyright owner. Further reproduction prohibited without permission.

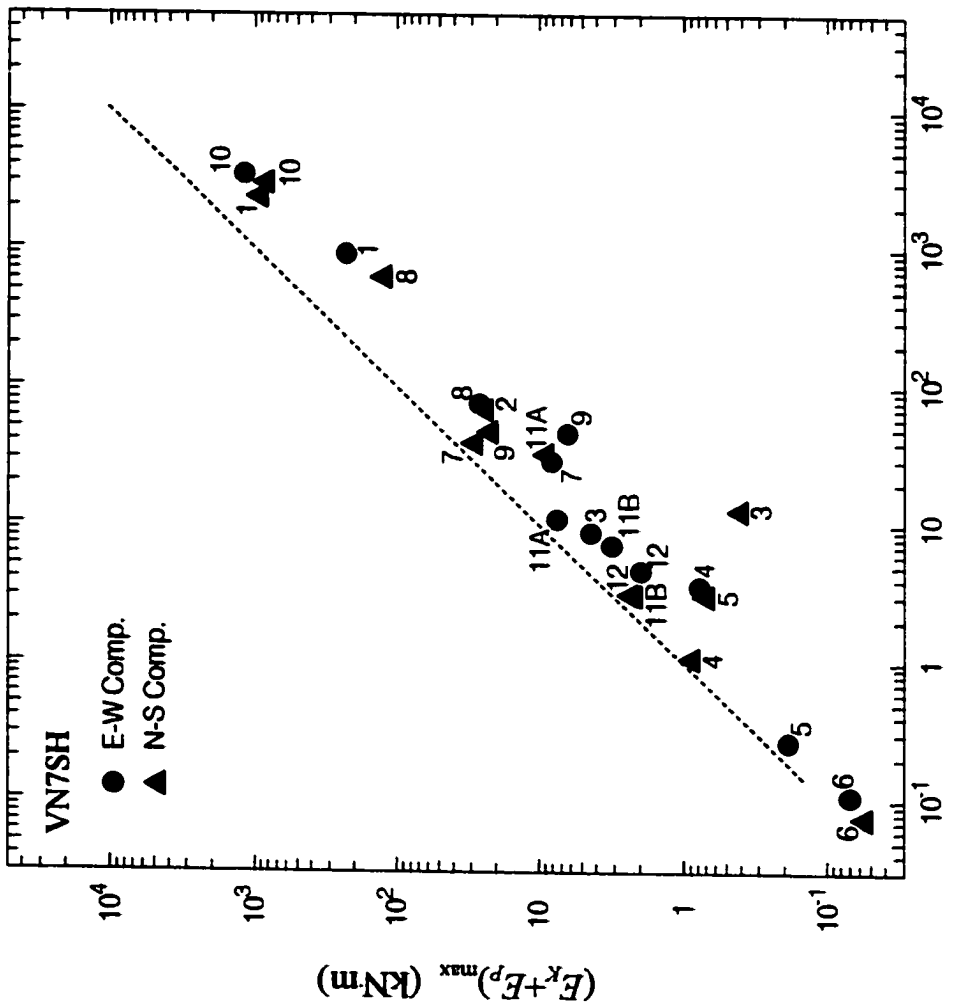

Fig. 4.2a Total computed kinetic energy $(E_K+E_P)_{max}$ versus E_I^* (kN·m), total system response energy computed at the instant when $(E_K+E_P)_{max}$ occurs, for twelve earthquakes recorded in the VN7SH.

Reproduced with permission of the copyright owner. Further reproduction prohibited without permission.

Reproduced with permission of the copyright owner. Further reproduction prohibited without permission.

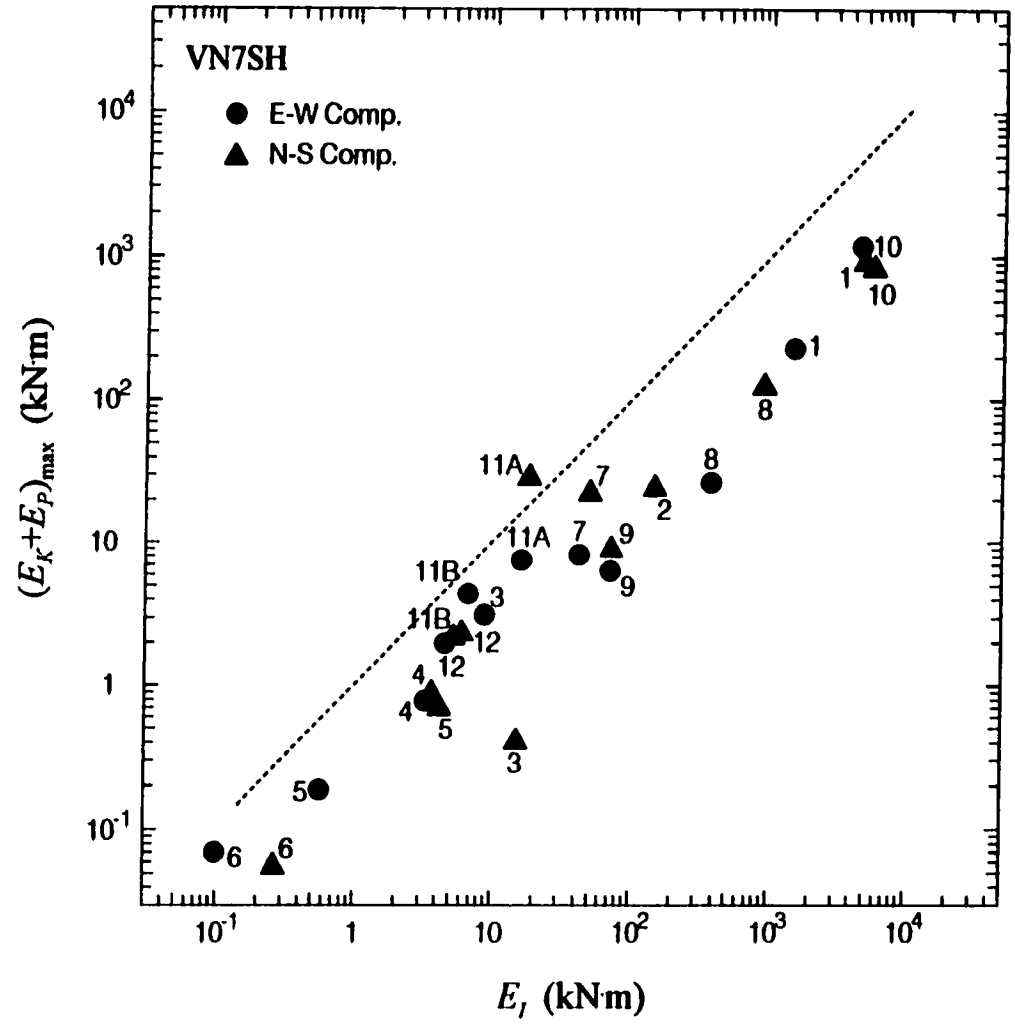

Fig. 4.2b Total computed kinetic energy $(E_K+E_P)_{max}$ versus E_I (kN·m), total system response energy at the end of excitation, for twelve earthquakes recorded in the VN7SH.

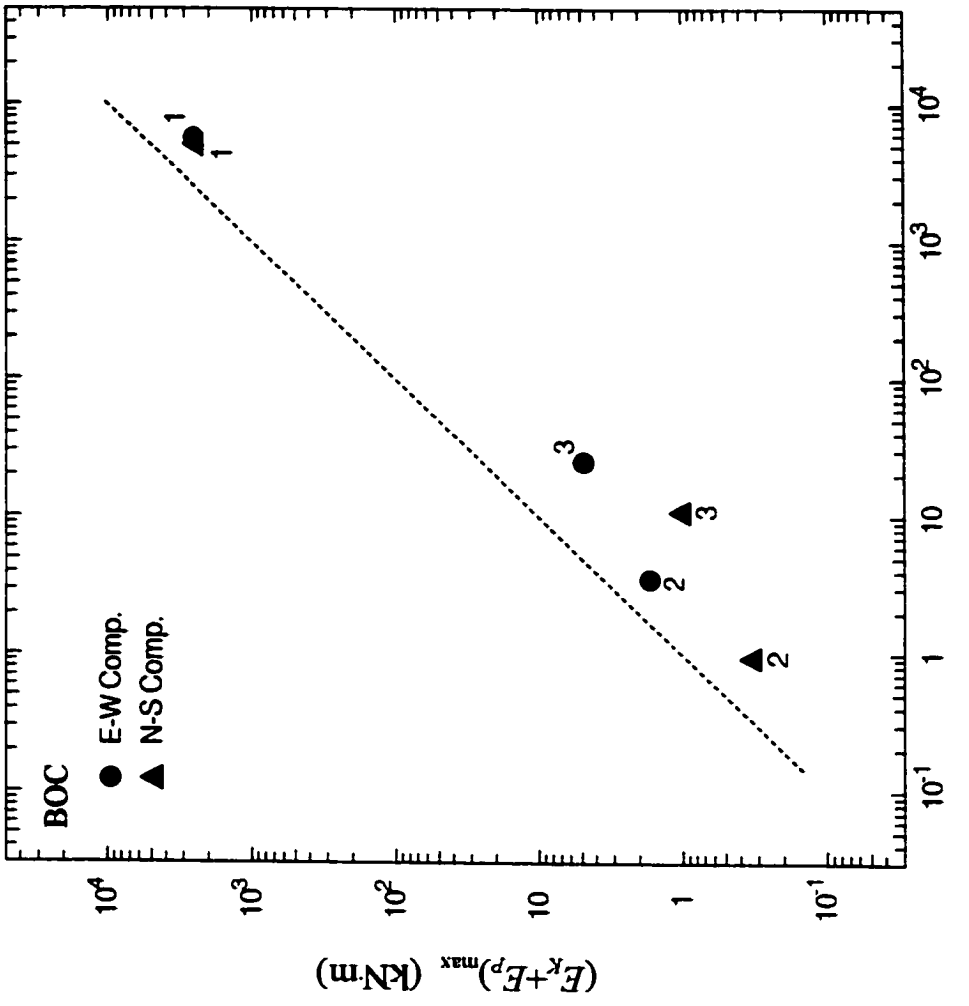

Fig. 4.3a Total computed kinetic energy $(E_K+E_P)_{max}$ versus E_I^* (kN·m), total system response energy computed at the instant when $(E_K+E_P)_{max}$ occurs, for three earthquakes recorded in the BOC building.

Reproduced with permission of the copyright owner. Further reproduction prohibited without permission.

Reproduced with permission of the copyright owner. Further reproduction prohibited without permission.

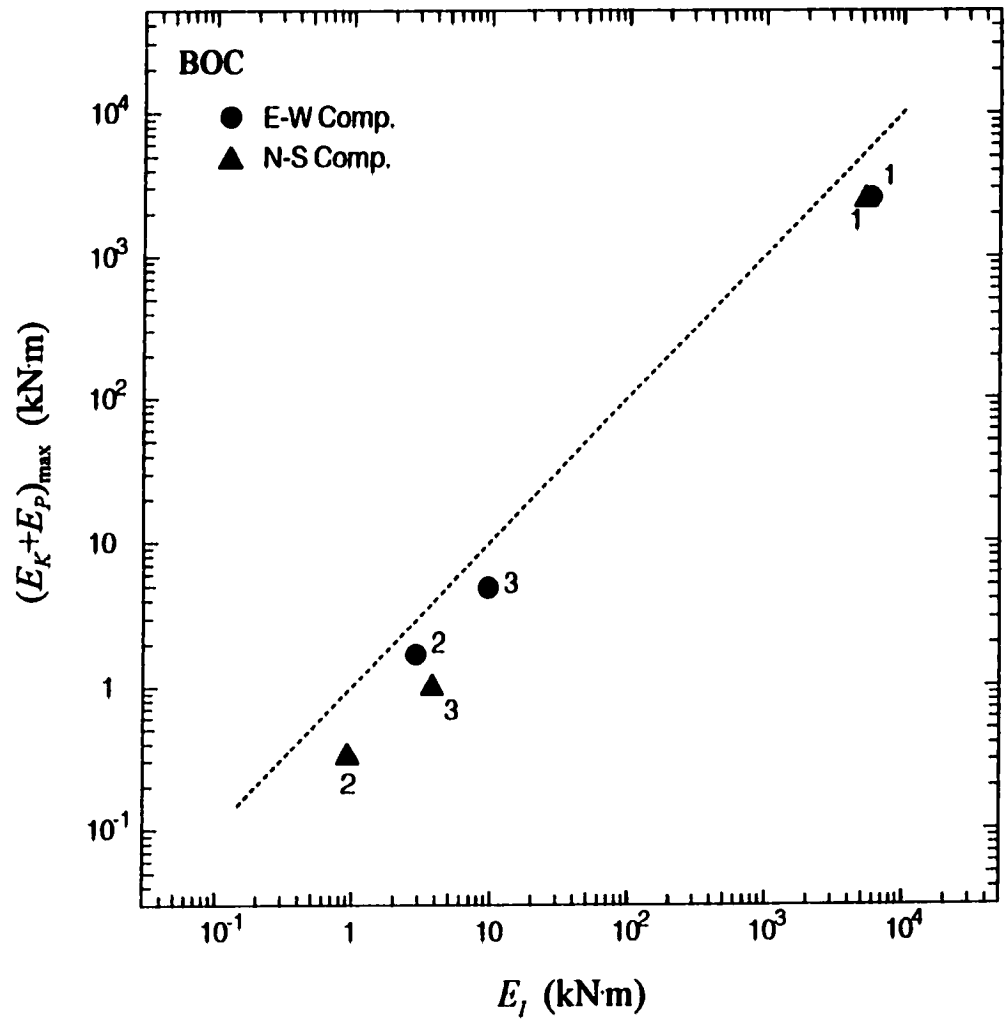

Fig. 4.3b Total computed kinetic energy $(E_K+E_P)_{max}$ versus E_I (kN·m), total system response energy at the end of excitation, for three earthquakes recorded in the BOC building.

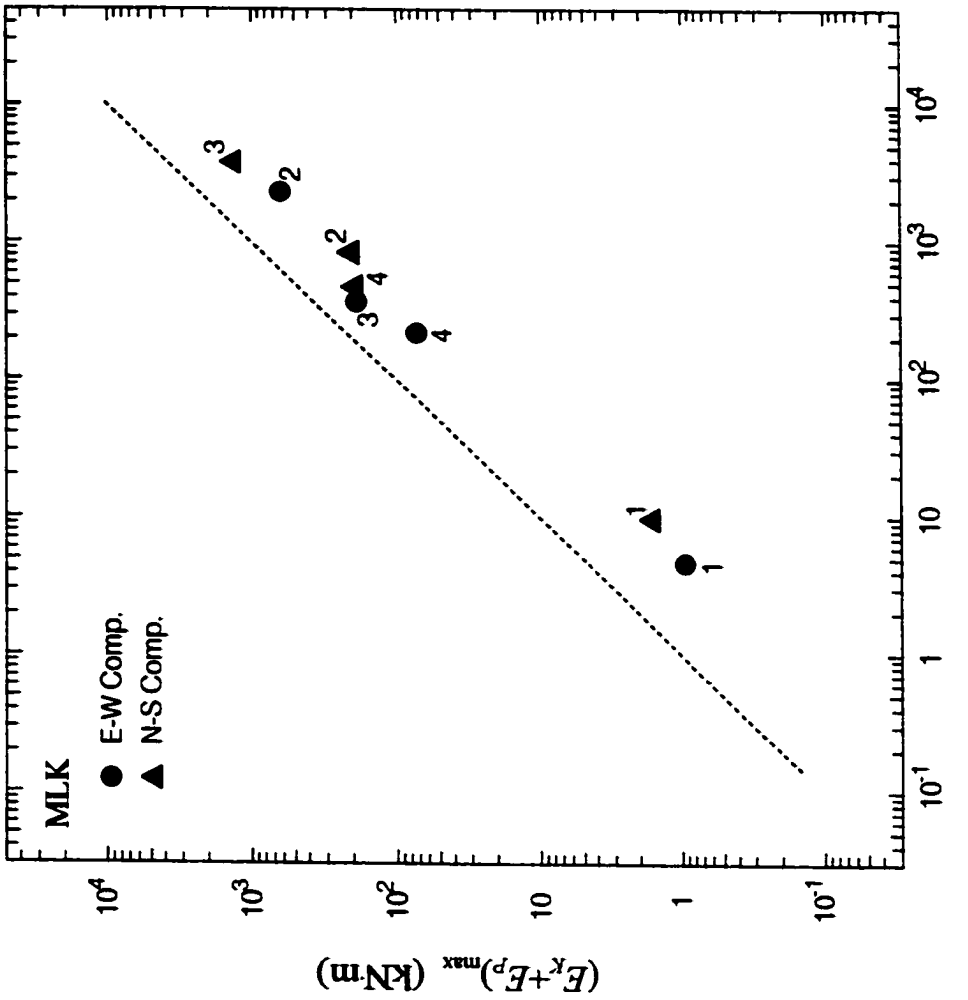

Fig. 4.4a Total computed kinetic energy $(E_K+E_P)_{max}$ versus E_I^* (kN·m), total system response energy computed at the instant when $(E_K+E_P)_{max}$ occurs, for four earthquakes recorded in the MLK building.

Reproduced with permission of the copyright owner. Further reproduction prohibited without permission.

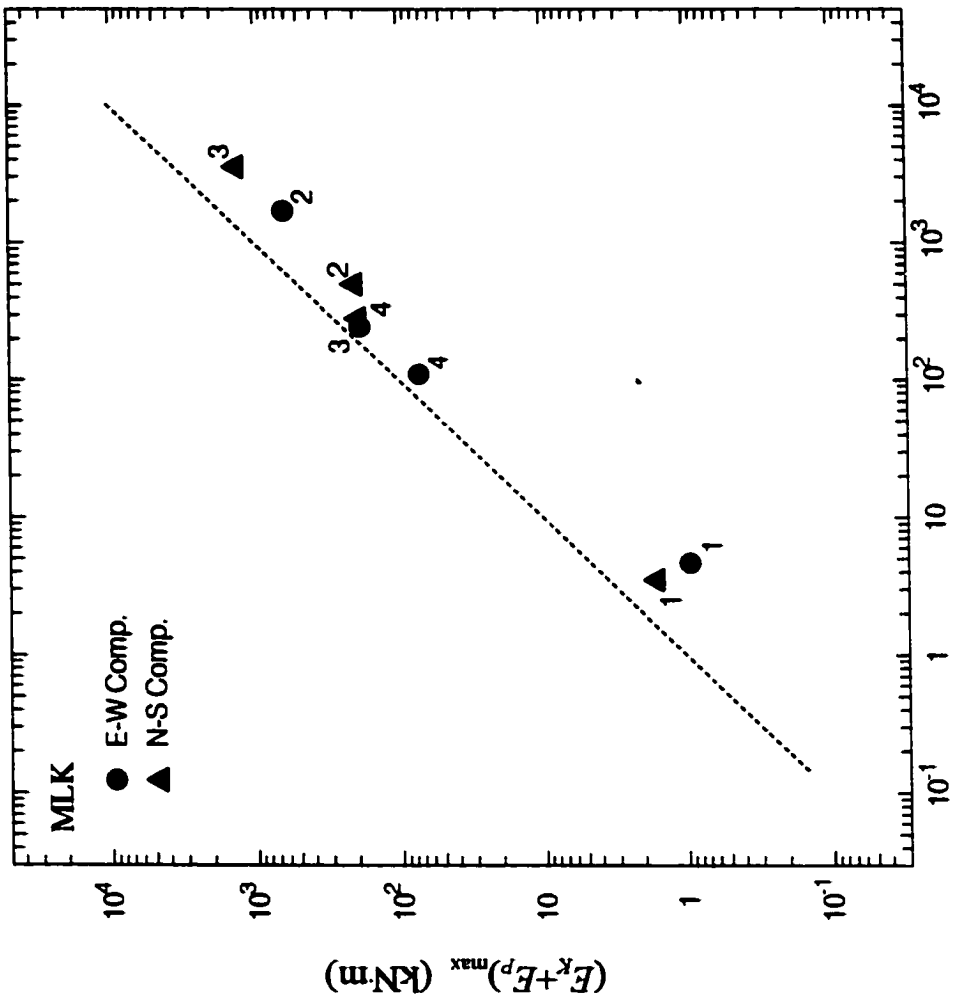

Fig. 4.4b Total computed kinetic energy $(E_K+E_P)_{max}$ versus E_I (kNm), total system response energy at the end of excitation, for four earthquakes recorded in the MLK building.

Reproduced with permission of the copyright owner. Further reproduction prohibited without permission.

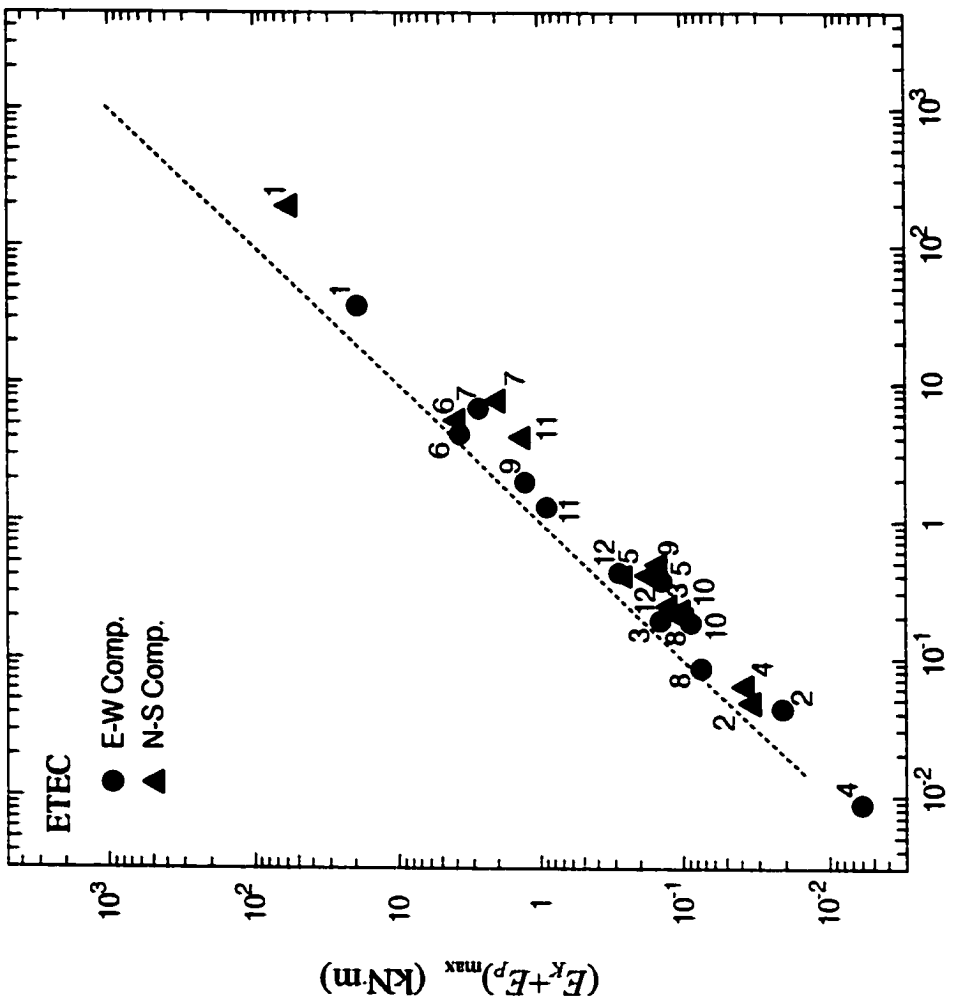

Fig. 4.5a Total computed kinetic energy $(E_K+E_P)_{max}$ versus E_I^* (kN·m), total system response energy computed at the instant when $(E_K+E_P)_{max}$ occurs, for twelve earthquakes recorded in the ETEC building.

Reproduced with permission of the copyright owner. Further reproduction prohibited without permission.

Reproduced with permission of the copyright owner. Further reproduction prohibited without permission.

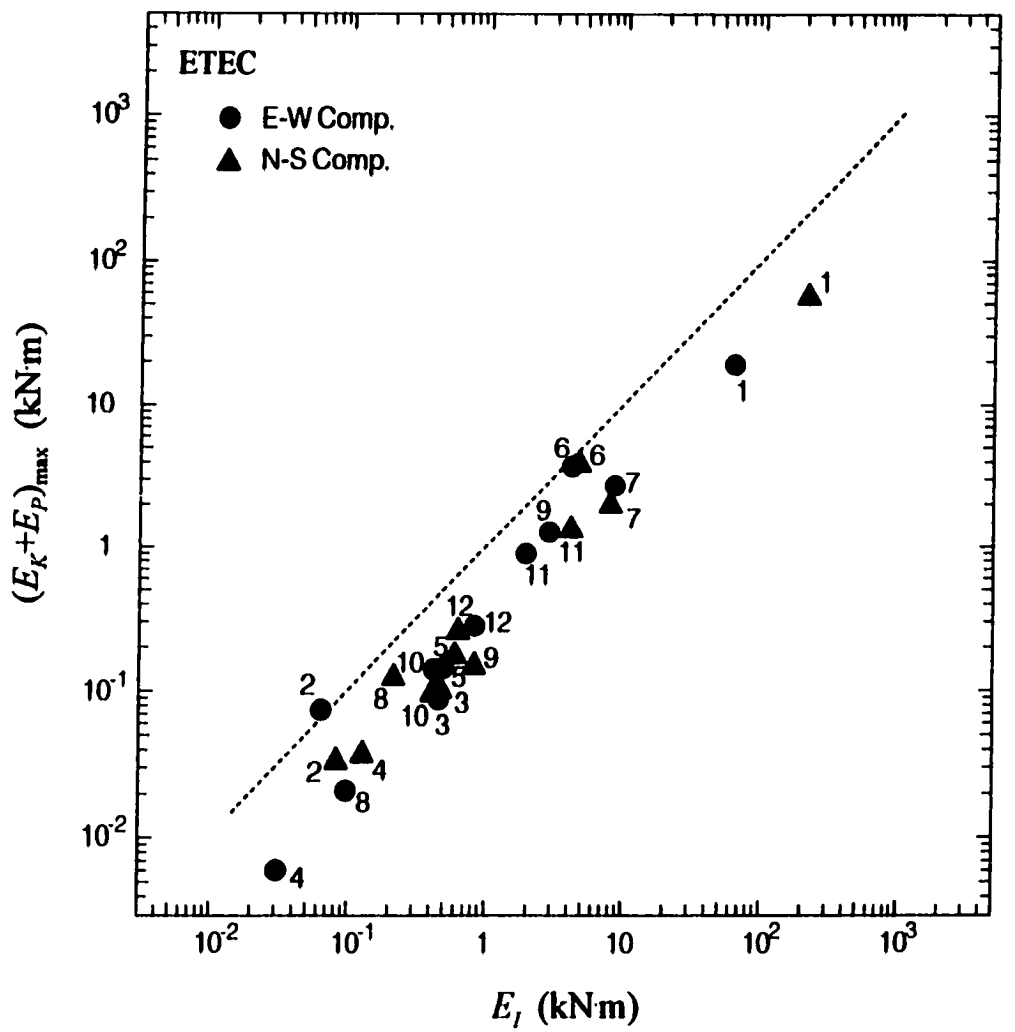

Fig. 4.5b Total computed kinetic energy $(E_K+E_P)_{max}$ versus E_I (kN m), total system response energy at the end of excitation, for twelve earthquakes recorded in the ETEC building.

Table 4.1 The ratios of maximum kinetic energy, $(E_K+E_P)_{max}$, with respect to total system energies of predicted responses, E_I^* and E_I, for studied buildings.

Hollywood Storage Building

		N-S Comp.		E-W Comp.	
Earthquake	Code	$\frac{(E_K+E_P)_{max}}{E_I^*}$	$\frac{(E_K+E_P)_{max}}{E_I}$	$\frac{(E_K+E_P)_{max}}{E_I^*}$	$\frac{(E_K+E_P)_{max}}{E_I}$
Southern California	SC	0.232	0.272	0.862	0.170
Kern County	KC	0.487	0.231	0.271	0.087
Borrego Mountain	BM	0.250	0.185	0.318	0.154
Lytle Creek	LC	0.796	1.854	0.824	0.293
San Fernando	SF	0.266	0.258	0.385	0.236
Whittier Narrows	WT	0.644	1.043	0.702	0.185
Landers	LN	0.165	0.295	0.437	0.071
Big Bear	BB	0.215	0.426	0.498	0.156
Northridge	NR	0.513	0.779	0.649	0.241

Van Nuys 7-story Hotel

		N-S Comp.		E-W Comp.	
Earthquake	Code	$\frac{(E_K+E_P)_{max}}{E_I^*}$	$\frac{(E_K+E_P)_{max}}{E_I}$	$\frac{(E_K+E_P)_{max}}{E_I^*}$	$\frac{(E_K+E_P)_{max}}{E_I}$
San Fernando	1	0.421	0.203	0.258	0.156
Whittier Narrows	2	0.380	0.174	--	--
Whittier 12th Aft.	3	0.159	0.028	0.454	0.359
Pasadena	4	0.880	0.257	0.221	0.243
Malibu	5	0.246	0.177	0.702	0.330
Montebello	6	0.791	0.222	0.655	0.718
Sierra Madre	7	0.504	0.475	0.286	0.196
Landers	8	0.212	0.147	0.356	0.071
Big Bear	9	0.292	0.133	0.140	0.091
Northridge	10	0.302	0.156	0.350	0.259
Northridge March Aft.	11A	0.786	1.693	0.610	0.463
Northridge March Aft.	11B	0.761	0.444	0.505	0.662
Northridge Dec. Aft.	12	0.805	0.411	0.435	0.438

Bank of California (15250 Ventura Blvd.)

		N-S Comp.		E-W Comp.	
Earthquake	Code	$\frac{(E_K+E_P)_{max}}{E_I^*}$	$\frac{(E_K+E_P)_{max}}{E_I}$	$\frac{(E_K+E_P)_{max}}{E_I^*}$	$\frac{(E_K+E_P)_{max}}{E_I}$
San Fernando	SF	0.526	0.501	0.458	0.444
EQ71	EQ71	0.371	0.374	0.484	0.603
EQ73	EQ73	0.098	0.281	0.196	0.512

Reproduced with permission of the copyright owner. Further reproduction prohibited without permission.

Table 4.1 (Continued)

Millikan Library

Earthquake	Code	N-S Comp.		E-W Comp.	
		$\frac{(E_K+E_P)_{max}}{E_I^*}$	$\frac{(E_K+E_P)_{max}}{E_I}$	$\frac{(E_K+E_P)_{max}}{E_I^*}$	$\frac{(E_K+E_P)_{max}}{E_I}$
Lytle Creek	LC	0.177	0.493	0.206	0.208
San Fernando	SF	0.260	0.435	0.273	0.372
Whittier Narrows	WT	0.374	0.399	0.517	0.776
Whittier 12th Aft.	WA	0.437	0.726	0.338	0.675

Santa Susana ETEC Building 462

Earthquake	Code	N-S Comp.		E-W Comp.	
		$\frac{(E_K+E_P)_{max}}{E_I^*}$	$\frac{(E_K+E_P)_{max}}{E_I}$	$\frac{(E_K+E_P)_{max}}{E_I^*}$	$\frac{(E_K+E_P)_{max}}{E_I}$
Northridge	1	0.310	0.278	0.520	0.305
Northridge Aft. #7	2	0.737	0.429	0.886	1.182
Northridge Aft. #9	3	0.482	0.228	0.485	0.195
Northridge Aft. #83	4	0.621	0.308	0.699	0.199
Northridge Aft. #100	5	0.458	0.311	0.763	0.291
Northridge Aft. #129	6	0.761	0.877	0.876	0.896
Northridge Aft. #142	7	0.280	0.261	0.414	0.319
Northridge Aft. #151	8	0.544	0.611	0.485	0.219
Northridge Aft. #253	9	0.324	0.189	0.666	0.446
Northridge Aft. #254	10	0.518	0.247	0.386	0.337
Northridge Aft. #336	11	0.348	0.343	0.709	0.467
Northridge Aft. #253a	12	0.679	0.431	0.663	0.341

Note:

- E_I^*: total energy computed at the instant when $(E_K+E_P)_{max}$ occurs.
- E_I : total energy at the end of shaking.

Reproduced with permission of the copyright owner. Further reproduction prohibited without permission.

but also causes the soil-foundation interaction effects. The advantages of not ignoring SSI are apparent. The challenge for future research is to quantify all these energies and to show how those can be estimated for use in the design.

4.2 Energy Absorption Capacity of the Structure – A Case Study (VN7SH)

In the study of Trifunac et al. (2001f), a shear beam model of a building with bilinear force-deformation relation was used to examine some elementary aspects of transient waves propagating in a structure. The results are based on dimensional analysis of the problem and represent conceptual relationships between the amplitude of peak velocity of the wave propagating up the structure, and the energy and power of the response. An application to the VN7SH building is illustrated in the following.

For the EW response of VN7SH building, the maximum accumulated energy, equal to 387 to 442 kN·m is estimated assuming the building is responding in the linear range of response. The largest power of the incident waves which the VN7SH building can take without damage is estimated to be 1932 to 2208 kN·m/s (Trifunac et al., 2001f). A larger and longer lasting incident wave would force the building to deform monotonically, entering into the nonlinear response amplitude range. The work dissipated by the hysteresis during one quarter of the vibration cycle up to the ductility of 2, was estimated to be 1240 to 1414 kN·m, and the associated power in the range from 4816 to 5492 kN·m/s. The work dissipated by the closed hysteretic loop for one complete cycle of response is estimated to be between 2480 to 2829 kN·m, and the corresponding maximum power was 2407 to 2746 kN·m/s. These estimates of the building capacity to absorb energy and power are shown by gray bands in Fig. 4.6b.

Reproduced with permission of the copyright owner. Further reproduction prohibited without permission.

The VN7SH building was damaged by the Northridge earthquake of 17 January 1994 and its aftershocks. Clearly, the inelastic action took place in the building response. In eqn (2.61) in Section 2.3, the energy equation was derived assuming the building deforms in linear manner only. In Section 3.3, the predicted energy components were calculated according to this assumption as well. To illustrate the contribution of the nonlinearity in the building to the dissipation of energy, we present a comparison of the relative responses assuming fixed-base ("w/o SSI") and flexible-base ("w/ SSI") cases, when the building and soil are linear, and nonlinear, using the model in Fig. 2.1. The considered cases are summarized in Table 4.2.

Table 4.2 The cases for comparison of relative response of the building assuming fixed-base and flexible-base cases, when the building and soil are linear and nonlinear.

	Classification					
Condition	Case I	Case II	Case III	Case IV	Case V	Case VI
Soil-structure interaction	no	no	yes	yes	yes	yes
Building property	linear	nonlinear	linear	nonlinear	linear	nonlinear
Soil property	--	--	linear	linear	nonlinear	nonlinear

The responses plotted in Fig. 4.6a and b were calculated by using the same starting parameters. The 1994 Northridge earthquake was used as input excitation to compare the predictions with the estimated energy and power demands summarized above (Trifunac et al., 2001f). Fig. 4.6a shows the relative responses of the model. Part (i) of Fig. 4.6a shows the ground velocity during 1994 Northridge earthquake. The relative responses for Cases I and II are plotted in the part (ii), Cases III and IV are plotted in the part (iii); and Cases V and VI are plotted in the part (iv). Dashed lines

Reproduced with permission of the copyright owner. Further reproduction prohibited without permission.

Reproduced with permission of the copyright owner. Further reproduction prohibited without permission.

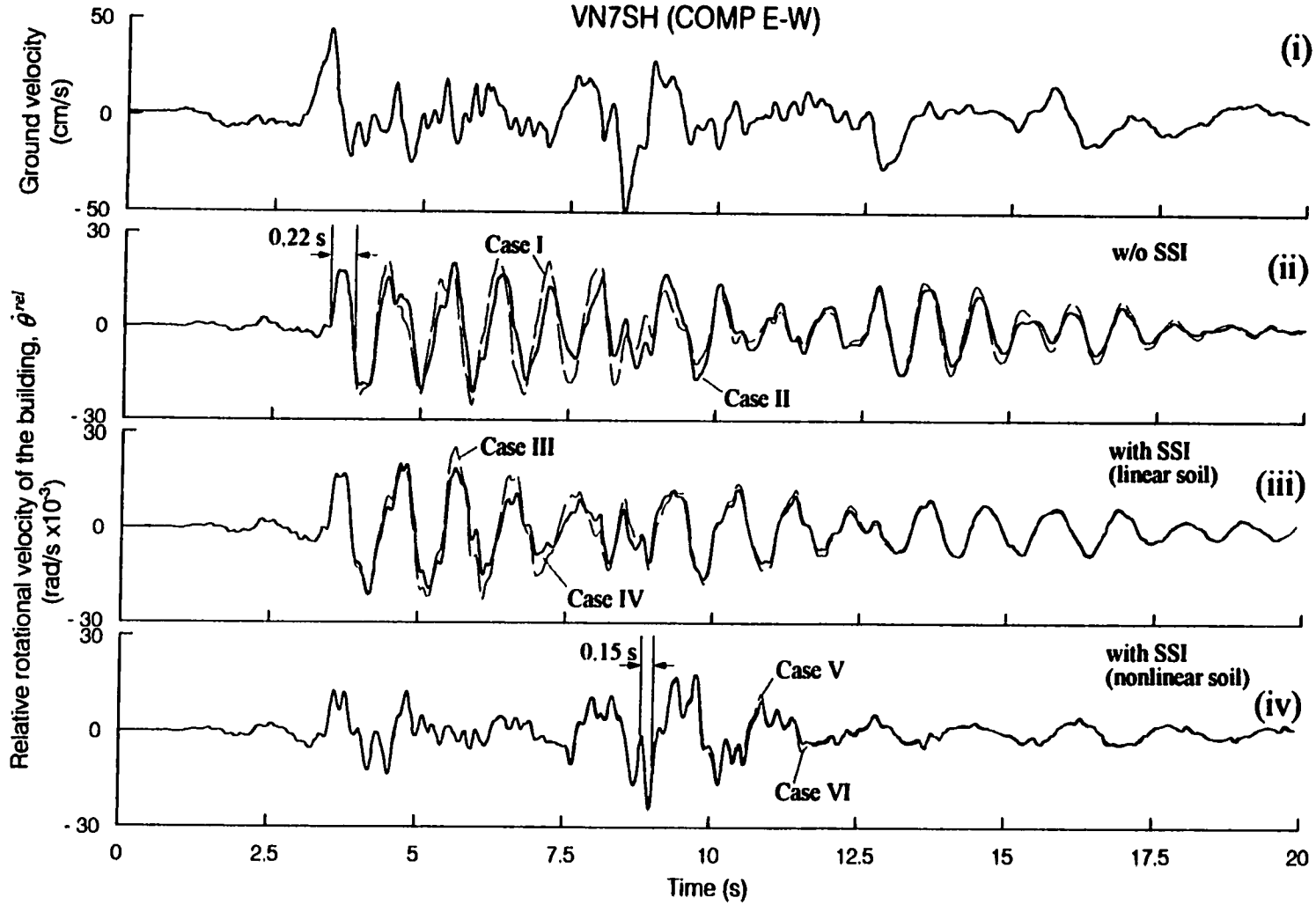

Fig. 4.6a Comparison of the EW relative velocity response of VN7SH, during 1994 Northridge earthquake, in the presence and absence of soil-structure interaction (dashed lines show the responses for linear building assumption, and solid lines show the corresponding quantities but for nonlinear building assumption). (i) Ground input velocity. (ii) Simulation without soil-structure interaction (SSI). (iii) Simulation with SSI assuming soil behaves linearly. (iv) Simulation with SSI assuming soil behaves nonlinearly.

Reproduced with permission of the copyright owner. Further reproduction prohibited without permission.

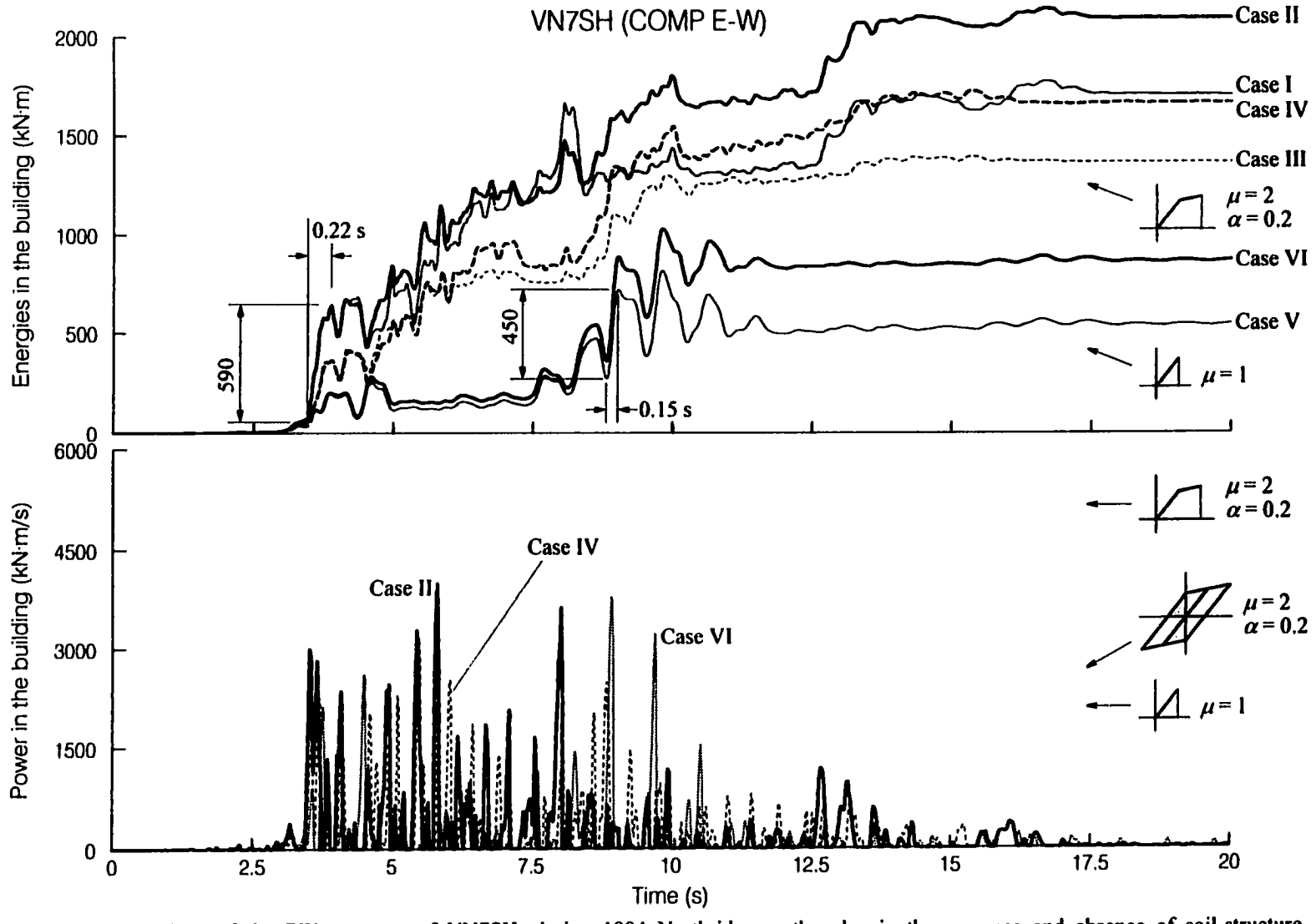

Fig. 4.6b Comparison of the EW response of VN7SH, during 1994 Northridge earthquake, in the presence and absence of soil-structure interaction, with linear and nonlinear soil considerations. Top: energies of relative response. Bottom: power of relative response.

show the relative responses for linear building, and solid lines show the corresponding quantities but for nonlinear building.

Top part of Fig. 4.6b shows the sum of all energies in the relative building response (kinetic, potential and hysteretic, when the building models are linear and nonlinear), for all of the above cases. It is seen that for the "w/o SSI" cases (Cases I and II), a large ground motion pulse starting at about 3.4 s (see part i of Fig. 4.6a) would have resulted in energy jump of about 590 kN·m, during about 0.22 s, resulting in input power approaching 3000 kN·m/s (see bottom of Fig. 4.6b). This pulse would have deformed the building beyond its linear response range, between 3.5 to 4 s into the earthquake (see also Islam, 1996). In the presence of soil-structure interaction, assuming soil is linear (Cases III and IV), the amplitude of the incident wave is slightly reduced, and the response energy in the building is reduced by a factor of about 1.25. When the soil is nonlinear (Cases V and VI), the amplitude of the incident wave is reduced considerably, and the building continues to respond in essentially a linear manner until 8.4 s into the earthquake. At about 8.9 s and 9.7 s, the SSI model with nonlinear soil (Case VI) experiences sudden jump in the energy of the relative response during short "stiff" episodes of response, for example during closure of the gaps between the foundation and the nonlinear springs representing soil. Nevertheless, the benefits of not ignoring SSI should be apparent from Fig. 4.6b (top), which shows that the response energy in the building is reduced by a factor of about 3 due to SSI and nonlinear soil response. These results lead to the conclusion that if the

Reproduced with permission of the copyright owner. Further reproduction prohibited without permission.

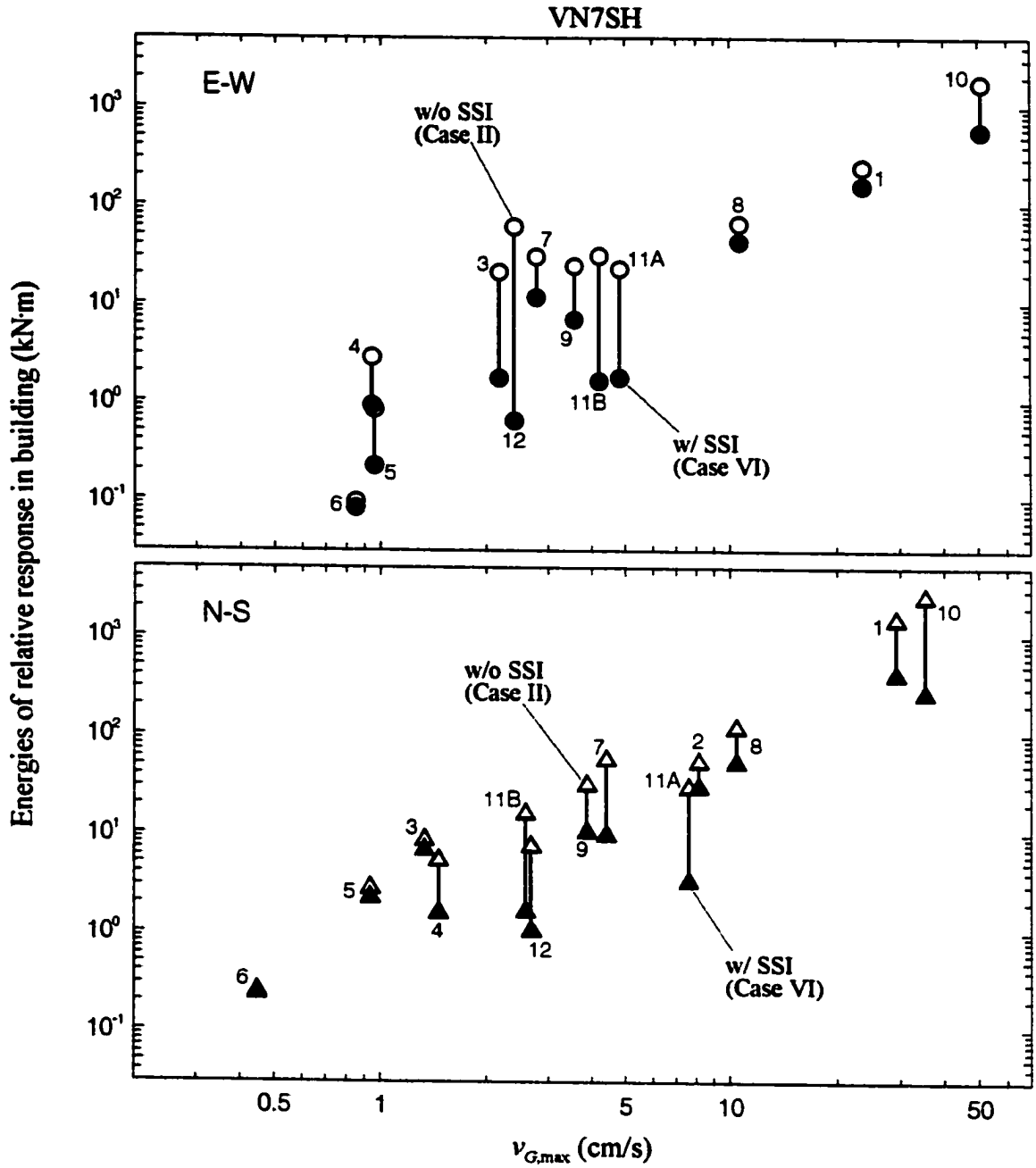

Fig. 4.7 Summary of the sum of energies of relative response (at the end of shaking) in the VN7SH building, for the response computed with and without SSI (Case VI and Case II), plotted versus peak velocity of ground level response, $v_{G,max}$.

Reproduced with permission of the copyright owner. Further reproduction prohibited without permission.

VN7SH system behaved like a "fixed-base model," the building would have collapsed during 1994 Northridge earthquake.

Fig. 4.7 shows the sum of all energies of relative response in the VN7SH building in the presence and absence of SSI (Cases VI and II), versus $v_{G,max}$ during twelve earthquakes listed in Table 3.1. Again, the contributions of nonlinear SSI reducing the energies of the building are apparent.

Next, to explore the dependence of energy absorption capacity in the soil, on the relative stiffnesses in the soil-structure system, we increased the stiffness of the building, for modeling the EW response of VN7SH (during 1994 Northridge earthquake), by factors of 1.0, 1.2, 1.5, 2.0, 3.0, 4.0 and 5.0, for Cases II, IV and VI (see Table 4.2). Parts a of Figs. 4.8 through 4.10 show the relative velocity responses for different building stiffness, K_b', and parts b of these figures show the energies of relative building responses. Figs. 4.8a and b show the results for Case II, Figs. 4.9a and b for Case IV, and Figs. 4.10a and b for Case VI. It is seen that when the system is considered as fixed-base model without SSI effects (Case II, Figs. 4.8a and b), the relative velocity responses reflect the first mode periods of the building. Fig. 4.8b shows that the energy jumps are "shifting" for different building stiffnesses.

When the system is analyzed with SSI effects (Cases IV and VI, Figs. 4.9a and b and 4.10a and b), the responses are less sensitive to the natural periods of the building and the predominant periods of the earthquake ground motions. Because of the presence of soil-structure interaction, the input energy is distributed among E_D^{bldg}, E_{S+I}^{bldg}, E_D^{soil}, E_{S+I}^{soil}, and E_{K+P}, and increasing building stiffness causes further

Reproduced with permission of the copyright owner. Further reproduction prohibited without permission.

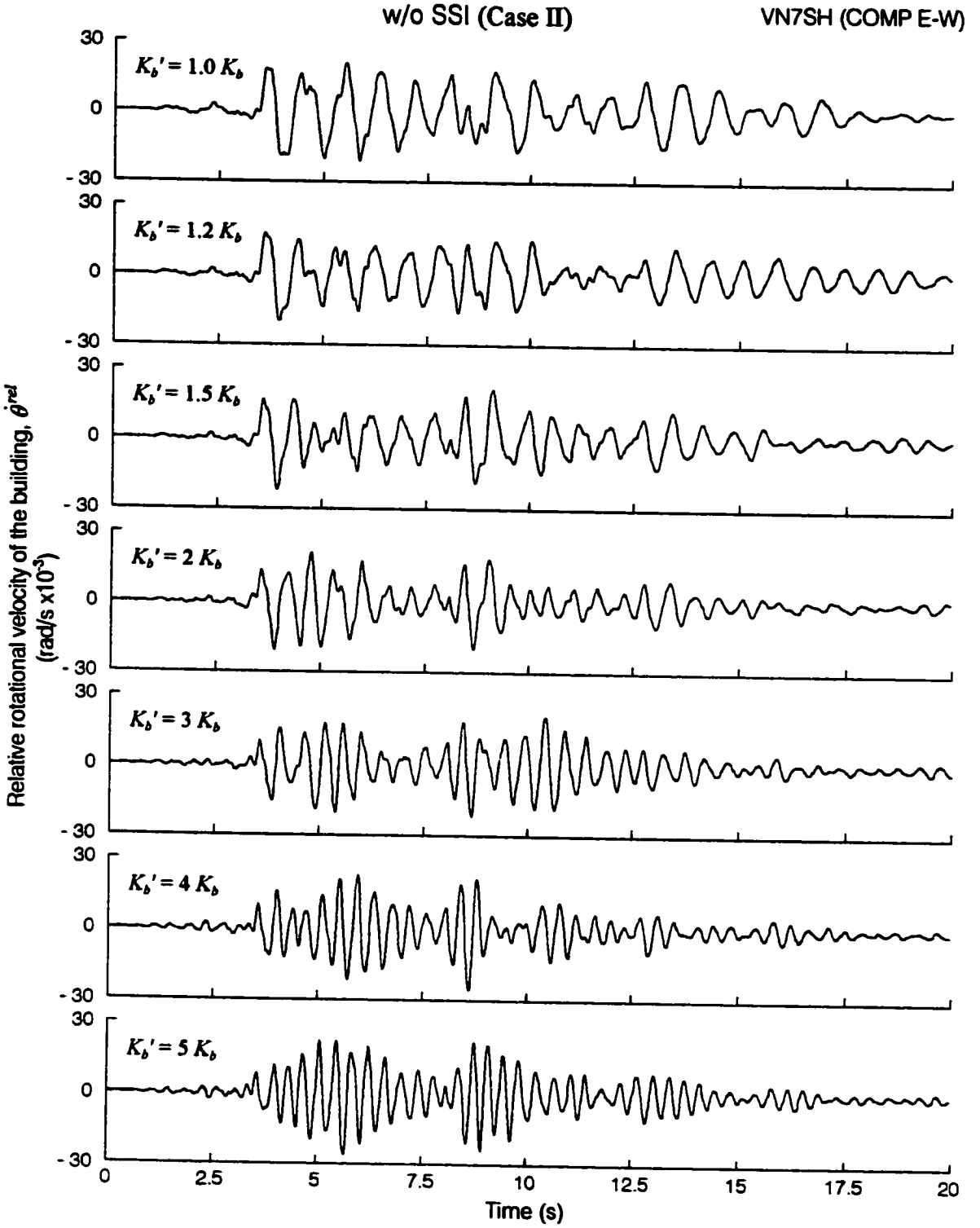

Fig. 4.8a Comparison of the EW relative velocity response of VN7SH, during 1994 Northridge earthquake, in the absence of soil-structure interaction (fixed-base model, Case II), for different building stiffness, K_b'. Simulations with $K_b' = 1.0\ K_b$, $K_b' = 1.2\ K_b$, $K_b' = 1.5\ K_b$, $K_b' = 2\ K_b$, $K_b' = 3\ K_b$, $K_b' = 4\ K_b$, and $K_b' = 5\ K_b$ (top to bottom).

Reproduced with permission of the copyright owner. Further reproduction prohibited without permission.

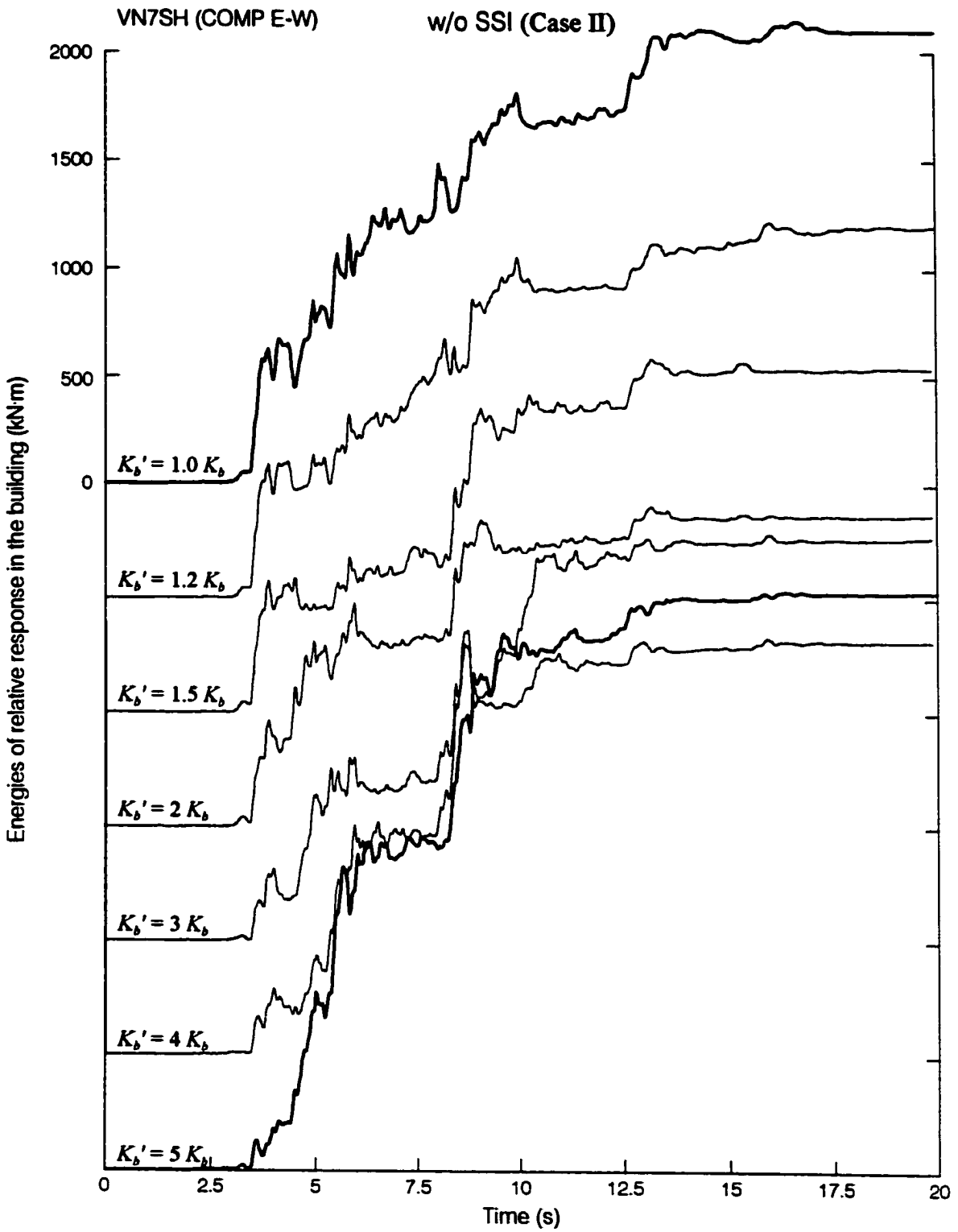

Fig. 4.8b Comparison of energies of the EW relative responses of VN7SH building, during 1994 Northridge earthquake, in the absence of soil-structure interaction (fixed-base model, Case II), for different building stiffness K_b'.

Reproduced with permission of the copyright owner. Further reproduction prohibited without permission.

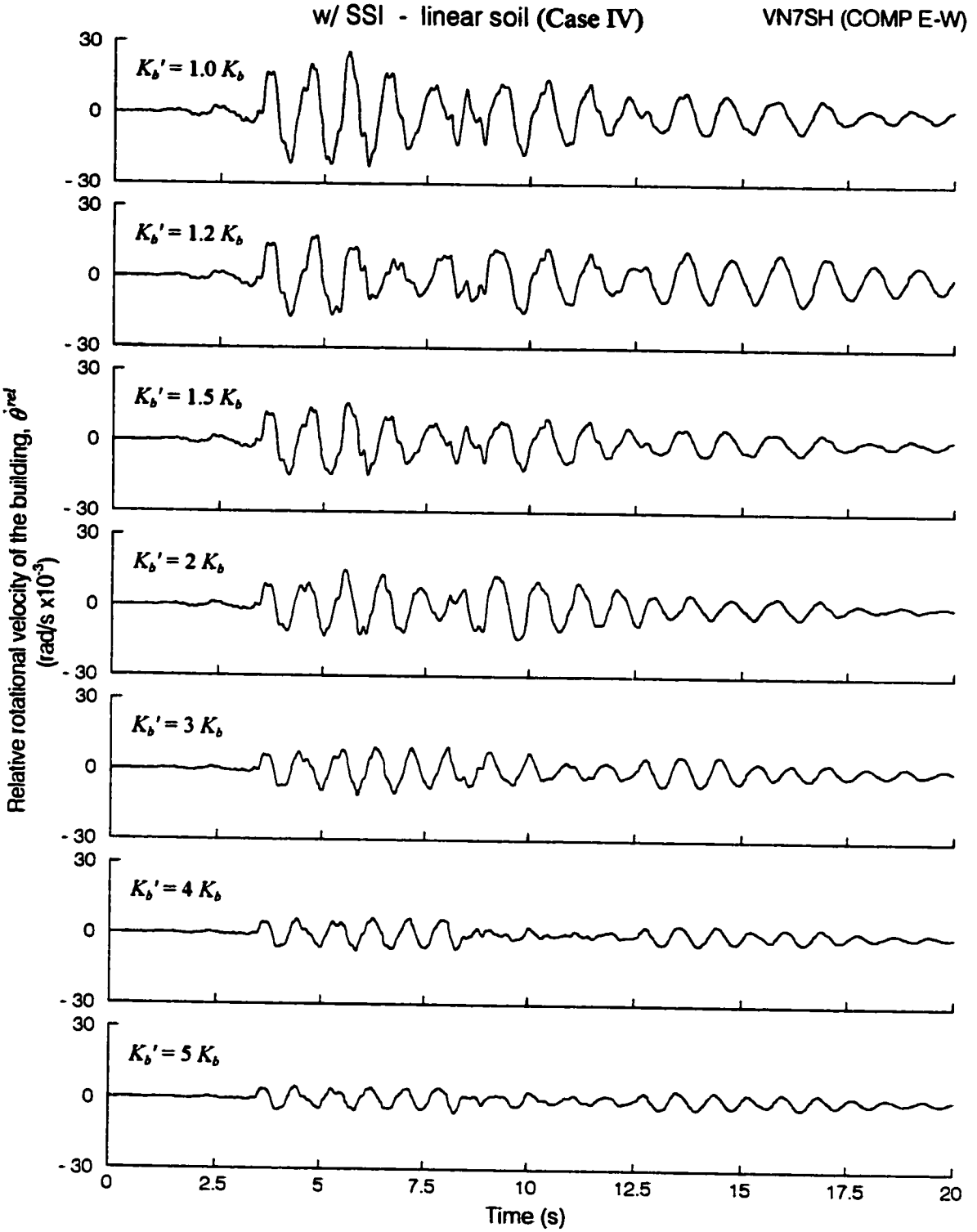

Fig. 4.9a Comparison of the EW relative velocity response of VN7SH, during 1994 Northridge earthquake, in the presence of soil-structure interaction, assuming linear soil behavior (Case IV), for different building stiffness, K_b'. Simulations with $K_b' = 1.0\ K_b$, $K_b' = 1.2\ K_b$, $K_b' = 1.5\ K_b$, $K_b' = 2\ K_b$, $K_b' = 3\ K_b$, $K_b' = 4\ K_b$, and $K_b' = 5\ K_b$ (top to bottom).

Reproduced with permission of the copyright owner. Further reproduction prohibited without permission.

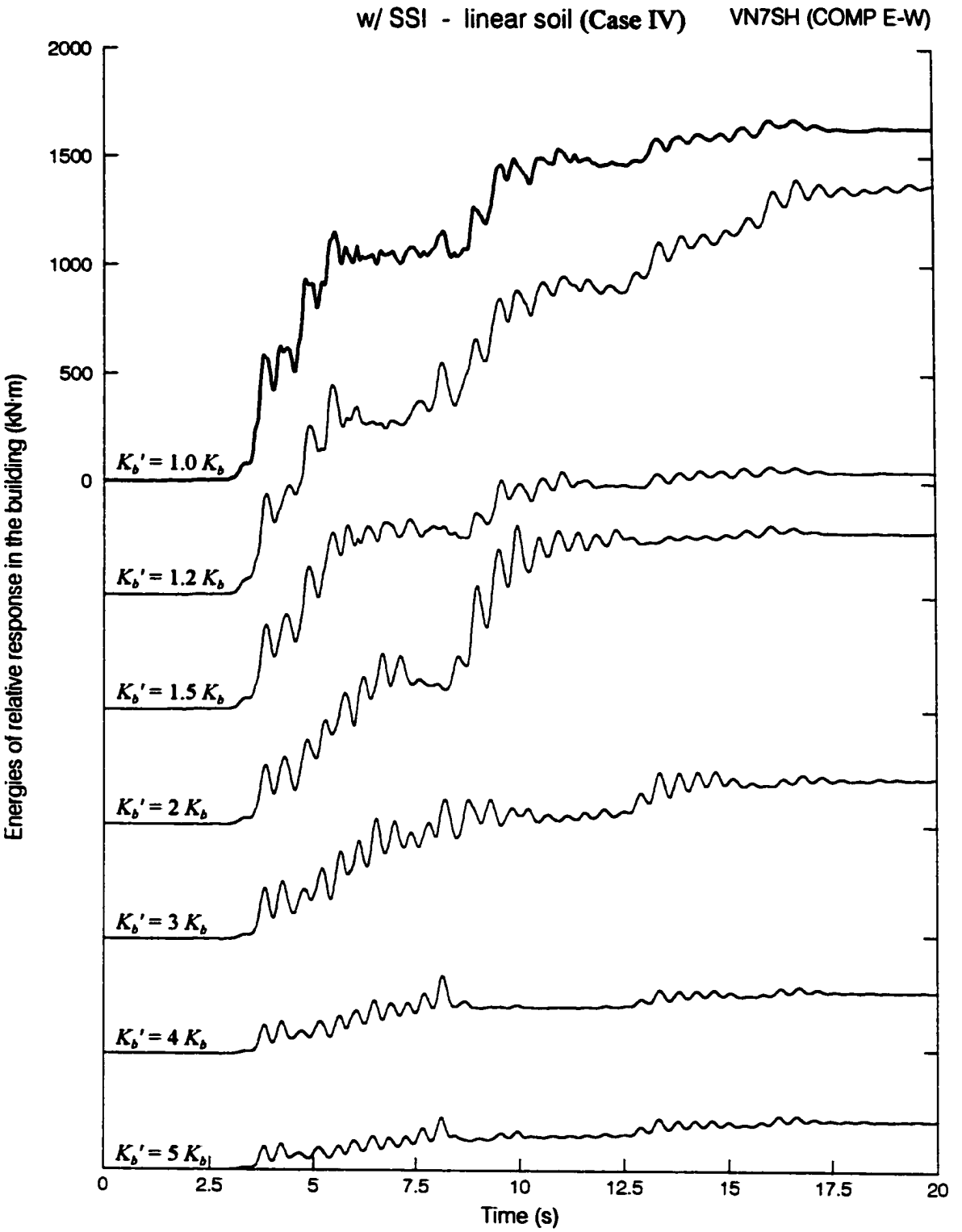

Fig. 4.9b Comparison of energies of the EW relative responses of VN7SH building, during 1994 Northridge earthquake, in the presence of soil-structure interaction, assuming linear soil behavior (Case IV), for different building stiffness K_b'.

Reproduced with permission of the copyright owner. Further reproduction prohibited without permission.

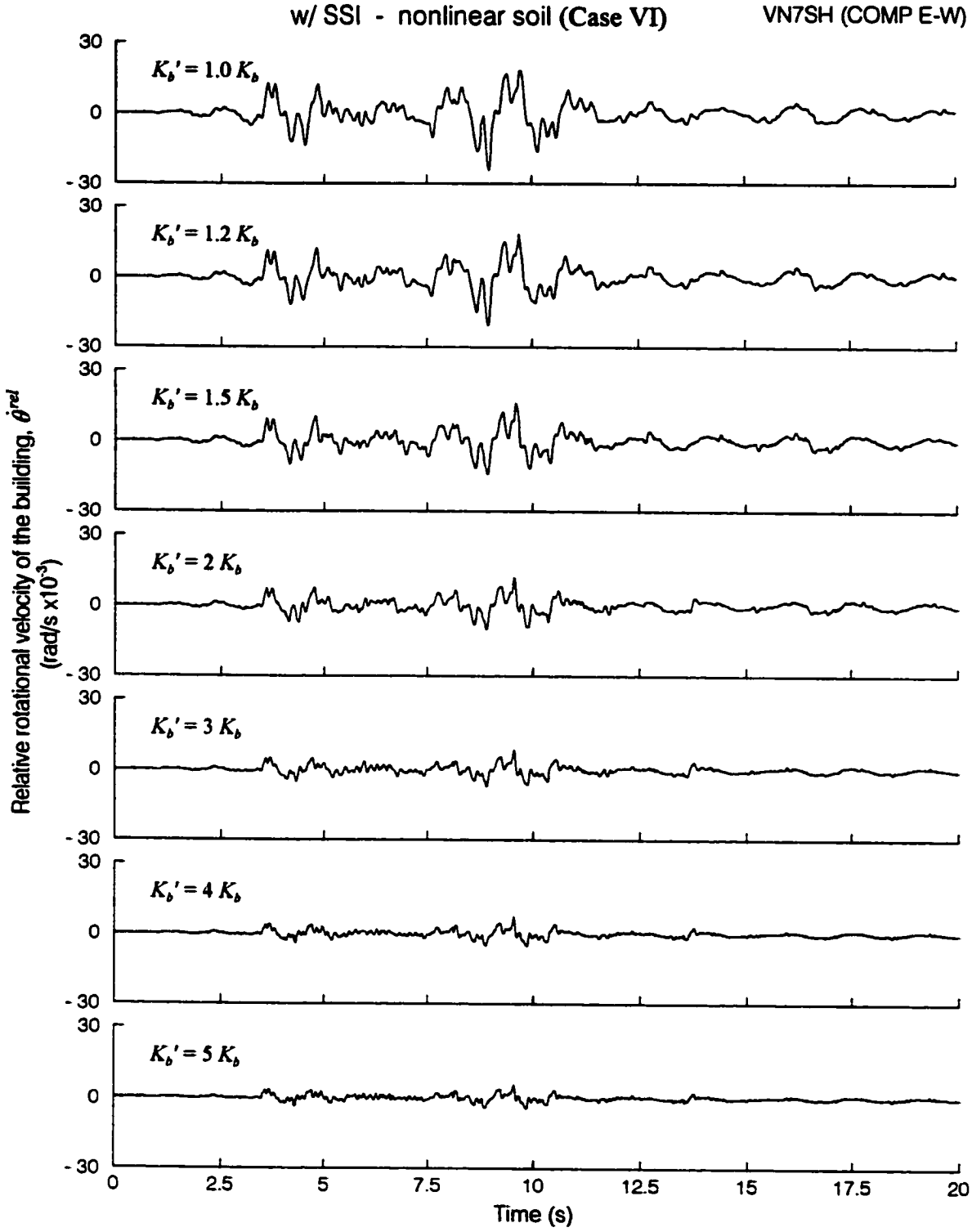

Fig. 4.10a Comparison of the EW relative velocity response of VN7SH, during 1994 Northridge earthquake, in the presence of soil-structure interaction, assuming nonlinear soil behavior (Case VI), for different building stiffness, K_b'. Simulations with $K_b' = 1.0\ K_b$, $K_b' = 1.2\ K_b$, $K_b' = 1.5\ K_b$, $K_b' = 2\ K_b$, $K_b' = 3\ K_b$, $K_b' = 4\ K_b$, and $K_b' = 5\ K_b$ (top to bottom).

Reproduced with permission of the copyright owner. Further reproduction prohibited without permission.

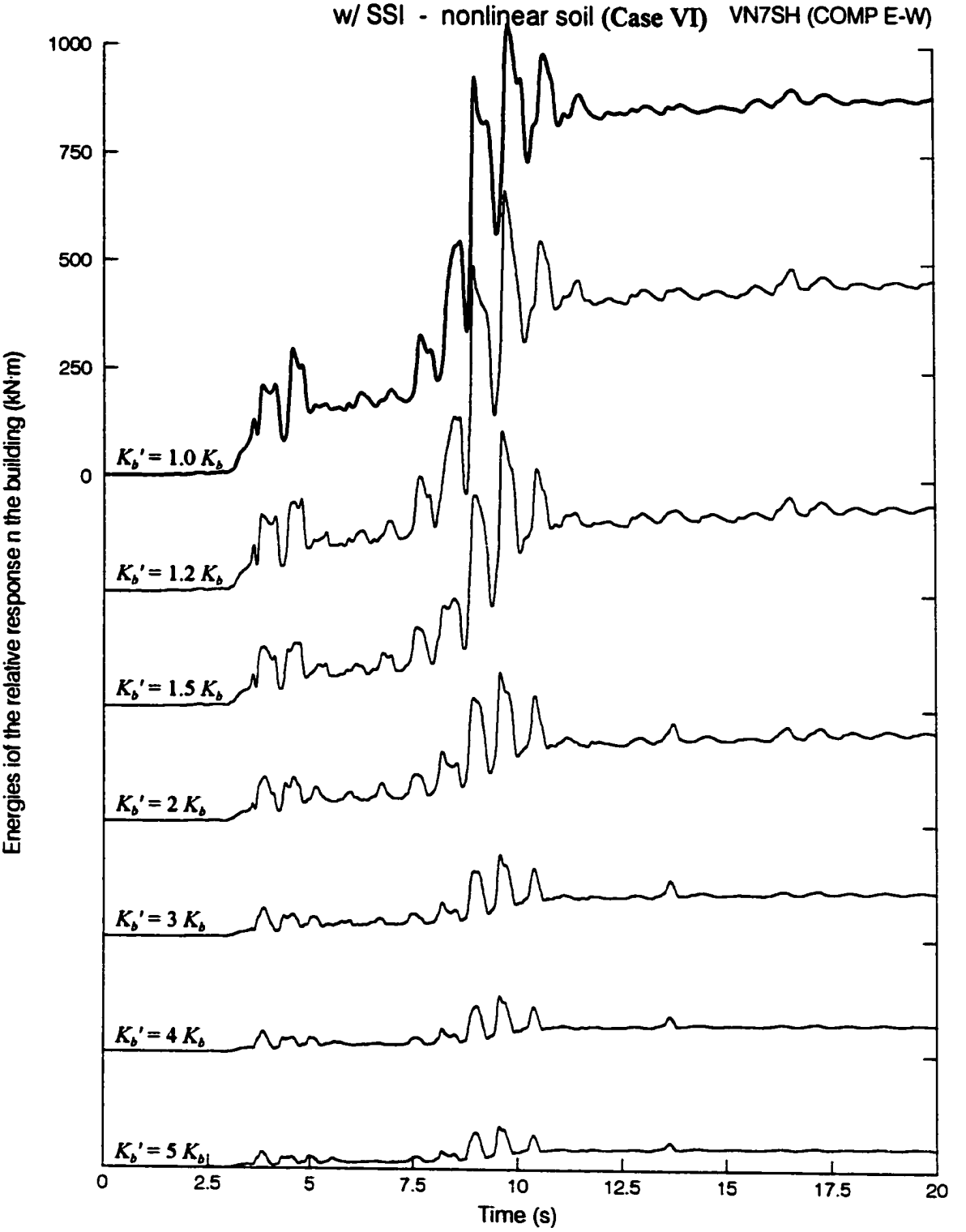

Fig. 4.10b Comparison of energies of the EW relative responses of VN7SH building, during 1994 Northridge earthquake, in the presence of soil-structure interaction, assuming nonlinear soil behavior (Case VI), for different building stiffness K_b'.

Reproduced with permission of the copyright owner. Further reproduction prohibited without permission.

re-distribution of these energies. Figs. 4.9a and b and 4.10a and b show how the relative velocity responses and the energies of relative building response decrease with increasing of the building stiffness. These can be explained qualitatively by using the fundamental concepts of wave propagation in layered media, that less energy can be propagated into a "stiffer layer" (here representing the building).

4.3 Duration of the Strong Ground Motion

One of the major shortcomings of the classical Biot's response spectrum method (Biot, 1932; 1933; 1934; 1941; 1942) has been its dependence on the peak response amplitude alone, without explicit consideration of the duration of strong shaking and of the rate of arrival of the incident strong motion energy. We use the following example to show why it is important for a realistic design method to reflect the effects of strong motion duration.

Fig. 4.11 shows the time history of two "earthquakes" that result in the same amount of the input wave "energy," $\int_0^T v^2 dt$, but different durations. The energy absorbing capacity of a hypothetical structure is shown by the wide gray line. The integral of Earthquake 1 increases rapidly and tends asymptotically towards its final value, while the integral of Earthquake 2 increases "slowly." The large average and instantaneous power produced by Earthquake 1 will cause damage and collapse of the structure, with designed capacity as shown in the figure. Thus it is important to relate the maximum and average power of incident wave energy with the capacity of structure to absorb this energy, and to choose sufficiently high energy absorbing capacity for safe earthquake-resistant design (Trifunac et al, 2001f).

Reproduced with permission of the copyright owner. Further reproduction prohibited without permission.

Reproduced with permission of the copyright owner. Further reproduction prohibited without permission.

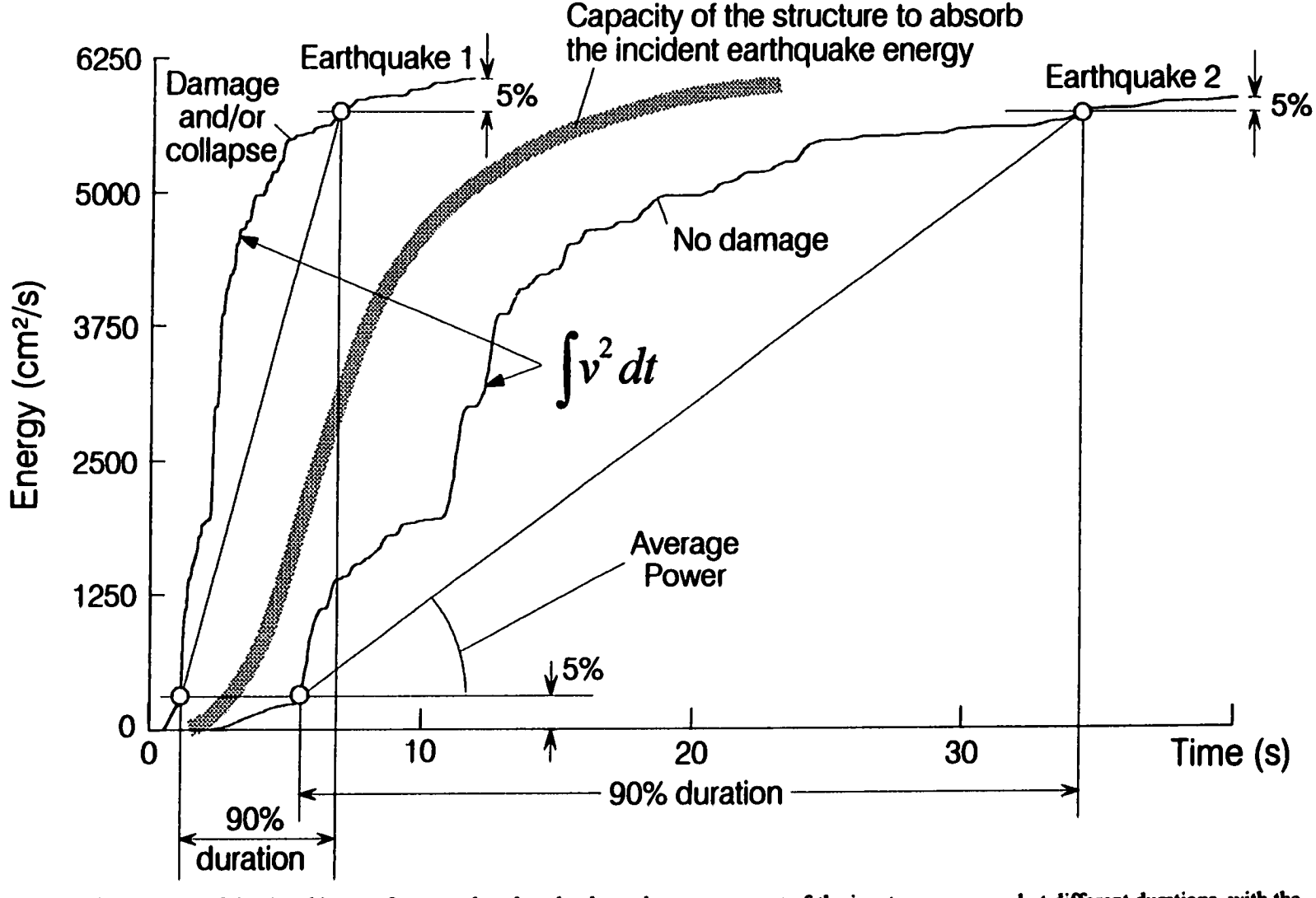

Fig. 4.11 Comparison of the time history of two earthquakes that have the same amount of the input wave energy but different durations, with the energy absorbing capacity of a hypothetical structure.

4.4 Empirical Estimation of the Energy Dissipation of Nonlinear Soil Behavior

As far as the losses of the energy through dissipation by nonlinear deformation of soil are concerned, our ability to predict and control this energy "sink" as means of reducing the seismic response of structures is essential.

In the following we explore the ad hoc system "characteristics" to estimate the energy dissipated by nonlinear soil behavior, E_{S+Y}^{soil}. With five well studied buildings for which strong motion data are available, it may just be possible to initiate the development of such empirical scaling relations.

4.4.1 Scaling Relations

In searching the "characteristics" of the SSI system, in this work, we consider three groups of scaling parameters:

Group A $v_{G,\max}$ – peak measured ground velocity at the site,

$\dot{\theta}_{\max}$ – peak instantaneous "rotation" computed from the difference between the velocity recorded on the roof and at the base, and

$(\Delta f)_{\max}$ – difference between the identified maximum and minimum apparent system frequencies during strong shaking.

Group B $\frac{v_{G,\max}}{\beta}$ – ratio of peak measured ground velocity, $v_{G,\max}$, to the average shear wave velocity, β, in the top 30 meters at the studied site,

$\frac{\text{90\% duration}}{T_e}$ – ratio of the 90% duration of strong motion to the equivalent period of the nonlinear system, and

Reproduced with permission of the copyright owner. Further reproduction prohibited without permission.

$s_{h,max}$ – peak offset of soil springs during strong shaking.

Group C $\frac{v_{G,max}}{\beta}$ – ratio of peak measured ground velocity, $v_{G,max}$, to the average shear wave velocity, β, in the top 30 meters at the studied site,

$\dot{\theta}_{max}$ – peak instantaneous rotation computed from the difference between the velocity recorded on the roof and at the base, and

Δf – the largest changes of the apparent system frequency during strong shaking,

$\frac{\text{90\% duration}}{T_e}$ – ratio of the 90% duration of strong motion to the equivalent period of the nonlinear oscillator, and

$s_{h,max}$ – peak offset of soil springs during strong shaking.

These groups have the system characteristics which might be correlated with the dissipation of energy in the soil. For example, $v_{G,max}$ measures of the severity of excitation, $\dot{\theta}_{max}$ measures the largest relative response associated with rocking, $\frac{v_{G,max}}{\beta}$ can be related to the strain levels in the supporting soil, $\frac{\text{90\% duration}}{T_e}$ can be related to the number of cycles of response during strong shaking, and $(\Delta f)_{max}$, Δf and $s_{h,max}$ can be related to the nonlinearity levels in the soil.

Using linear regression analyses, the dissipated energy E_{S+Y}^{soil} can be described in terms of the following regression equations:

Reproduced with permission of the copyright owner. Further reproduction prohibited without permission.

$$E_{S+Y}^{soil} = a_0 + a_1 v_{G,\max} + a_2 \dot{\theta}_{\max} + a_3 (\Delta f)_{\max}, \text{ for Group A} \quad (4.1a)$$

$$E_{S+Y}^{soil} = a_0 + a_1 \frac{v_{G,\max}}{\beta} + a_2 \frac{\text{90\% duration}}{T_e} + a_3 s_{h,\max}, \text{ for Group B} \quad (4.1b)$$

$$E_{S+Y}^{soil} = a_0 + a_1 \frac{v_{G,\max}}{\beta} + a_2 \dot{\theta}_{\max} + a_3 \Delta f + a_4 \frac{\text{90\% duration}}{T_e} + a_5 s_{h,\max}, \text{ for Group C} \quad (4.1c)$$

where a's are regression coefficients. For simplicity in notation, these are rewritten as

$$y = a_0 + a_1 x_1 + a_2 x_2 + a_3 x_3, \quad \text{for Groups A and B} \quad (4.2a, b)$$

$$y = a_0 + a_1 x_1 + a_2 x_2 + a_3 x_3 + a_4 x_4 + a_5 x_5, \quad \text{for Group C} \quad (4.2c)$$

Note that in the above equations there is really no physical basis to assume that E_{S+Y}^{soil} should be just a linear function of the chosen characteristics. This choice is motivated only by the simplicity of its mathematical form.

4.4.2 Regression Coefficients and Results

The regression analysis was carried out for five buildings studied in this work. The strong motion records and the computed responses were used in this database (see Table 3.1).

During the regression analysis, it was found that some of the chosen terms were not correlated to the associated energy dissipation. It is possible that these terms are insignificant and cannot reflect the nature of E_{S+Y}^{soil}. Subsequently, these terms have been deleted from the regression analysis and the final, adopted, regression coefficients are listed in Table 4.3.

Reproduced with permission of the copyright owner. Further reproduction prohibited without permission.

Table 4.3 A summary of the final regression coefficients for five studied buildings.

Group A

Bldg.	Comp.	Regression coefficients			
		a_0	a_1	a_2	a_3
HSB	EW (long.)	-59.899	14.970	--	--
	NS (trans.)	-25.989	--	43.537	--
VN7SH	EW (long.)	-66.383	40.266	-40.778	--
	NS (trans.)	-124.646	40.833	--	--
BOC	NS (long.)	-92.421	308.032	-297.104	502.632
	EW (trans.)	-484.880	292.364	-85.894	1541.776
MLK	EW (long.)	-14.733	2.595	6.988	--
	NS (trans.)	-185.013	-73.242	168.302	--
ETEC	EW (long.)	-4.993	-4.493	9.222	--
	NS (trans.)	-8.127	-11.329	20.676	--

Group B

Bldg.	Comp.	Regression coefficients			
		a_0	a_1	a_2	a_3
HSB	EW (long.)	-14.465	0.645	--	89.947
	NS (trans.)	-174.991	2.164	4.991	99.032
VN7SH	EW (long.)	-92.049	8.497	--	--
	NS (trans.)	-124.646	12.250	--	--
BOC	NS (long.)	-17.811	17.703	-0.678	150.691
	EW (trans.)	-354.398	96.209	-0.282	-88.048
MLK	EW (long.)	-0.098	4.646	-0.380	-14.810
	NS (trans.)	54.381	-10.161	--	90.769
ETEC	EW (long.)	-2.265	-5.174	--	499.645
	NS (trans.)	-19.183	-3.601	0.345	428.076

Group C

Bldg.	Comp.	Regression coefficients					
		a_0	a_1	a_2	a_3	a_4	a_5
HSB	EW (long.)	-13.949	1.014	-3.971	--	--	94.270
	NS (trans.)	-153.779	4.404	-24.073	--	4.166	120.261
VN7SH	EW (long.)	-1.542	3.701	-61.302	--	--	56.528
	NS (trans.)	-124.646	12.250	--	--	--	--
BOC	NS (long.)	93.684	104.646	-103.967	-1888.477	4.494	-46.449
	EW (trans.)	-272.421	-6.770	143.763	489.700	0.171	79.786
MLK	EW (long.)	0.373	4.216	1.208	--	-0.398	-13.905
	NS (trans.)	0.001	-10.301	20.496	-741.134	9.824	72.925
ETEC	EW (long.)	0.668	-4.014	-5.986	--	--	797.714
	NS (trans.)	-19.183	-3.601	--	--	0.345	428.076

--: quantities are deleted in the final regression analysis.

Reproduced with permission of the copyright owner. Further reproduction prohibited without permission.

Reproduced with permission of the copyright owner. Further reproduction prohibited without permission.

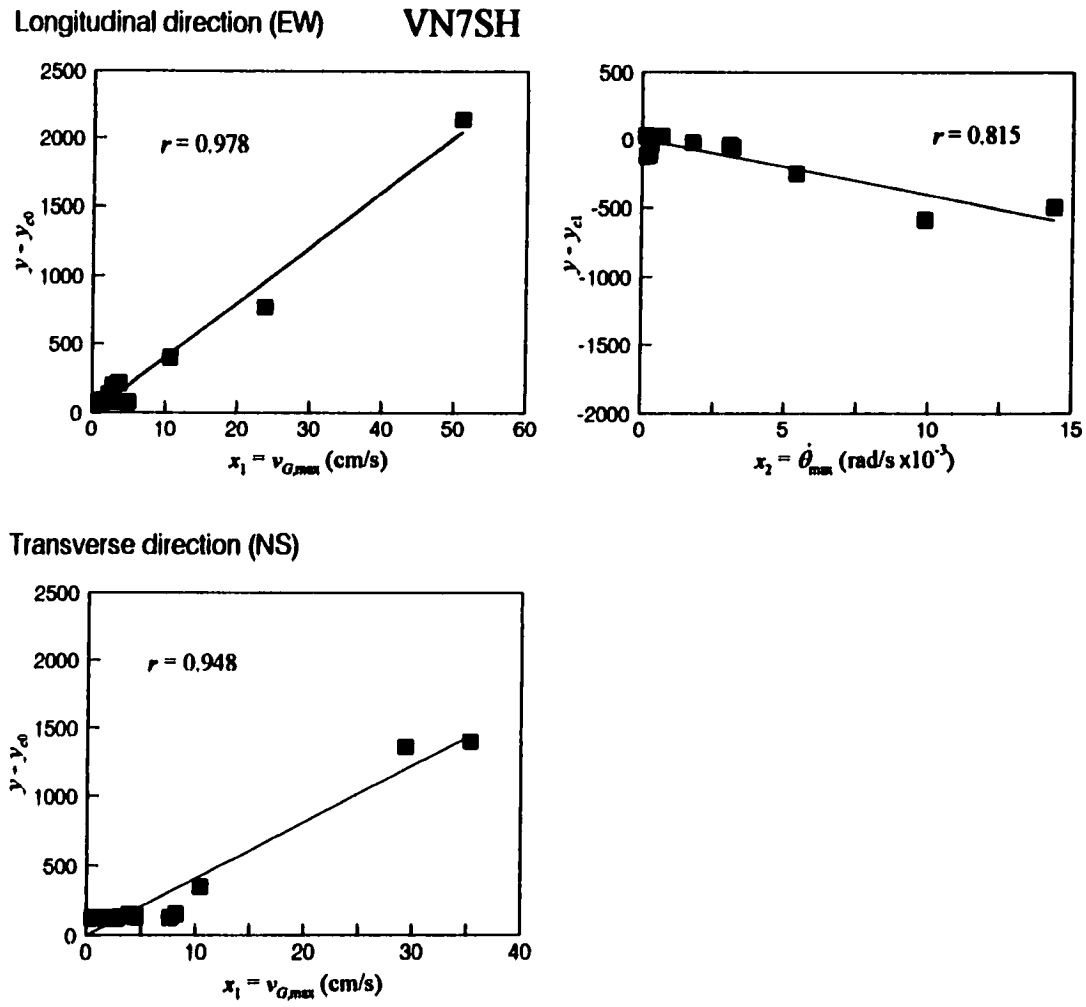

Fig. 4.13 Same as Fig. 4.12 but for Van Nuys 7-story hotel.

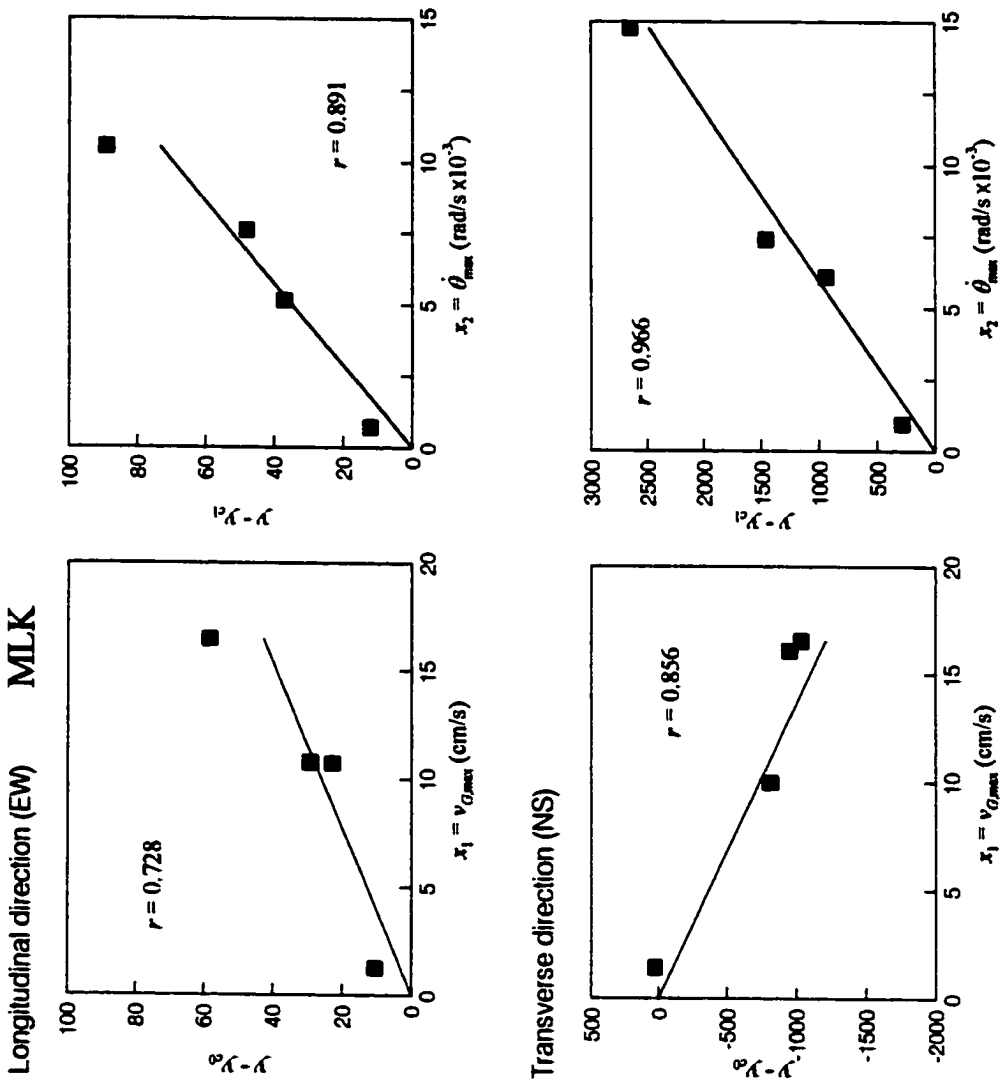

Fig. 4.14 Same as Fig. 4.12 but for Millikan Library building.

Reproduced with permission of the copyright owner. Further reproduction prohibited without permission.

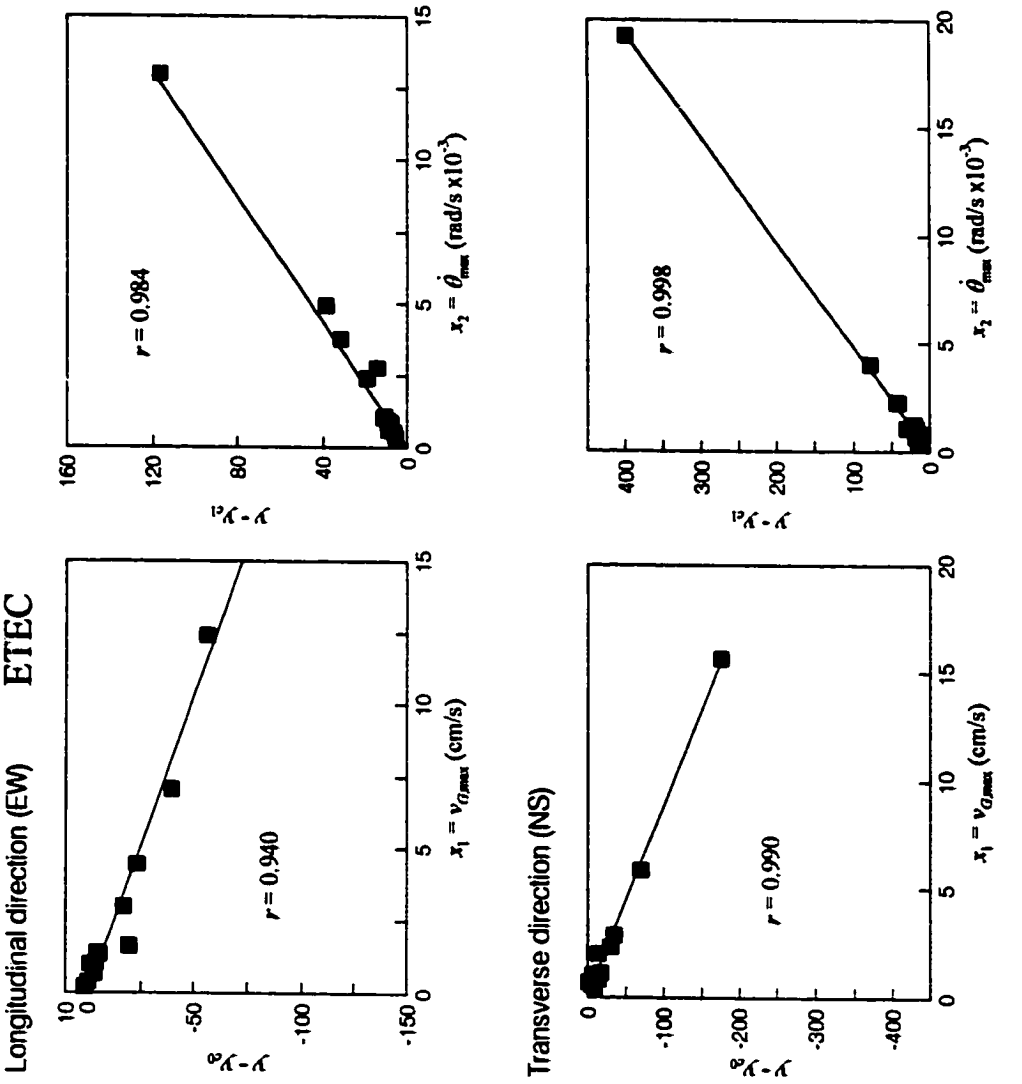

Fig. 4.15 Same as Fig. 4.12 but for Santa Susana ETEC building.

Reproduced with permission of the copyright owner. Further reproduction prohibited without permission.

Reproduced with permission of the copyright owner. Further reproduction prohibited without permission.

Table 4.4 A summary of the maximum and minimum values of the quantities used in the regression analyses (Group A) and the percentages of their contributions.

		$y = E_{S+Y}^{soil}$ (kN·m)	$x_1 = v_{G,max}$ (cm/s)		$x_2 = \dot{\theta}_{max}$ (rad/s ×10^{-3})		$x_3 = (\Delta f)_{max}$ (Hz)	
Bldg.	Comp.	y_{min}, y_{max}	$x_{1,min}, x_{1,max}$	$\frac{a_1 x_{1,max}}{\hat{y}_{max}}$	$x_{2,min}, x_{2,max}$	$\frac{a_2 x_{2,max}}{\hat{y}_{max}}$	$x_{3,min}, x_{3,max}$	$\frac{a_3 x_{3,max}}{\hat{y}_{max}}$
HSB	EW[1]	1.164, 254.686	2.24, 18.88	126.98%	--	--	--	--
	NS[2]	0.489, 379.455	--	--	0.796, 9.657	106.59%	--	--
VN7SH	EW[1]	0.007, 1495.31	0.85, 50.93	146.53%	0.146, 14.342	-41.79%	--	--
	NS[2]	0.006, 1277.71	0.45, 35.32	109.46%	--	--	--	--
BOC	NS[1]	0.034, 3094.60	0.41, 27.73	276.02%	0.114, 18.649	-179.04%	0.000, 0.370	6.01%
	EW[2]	0.107, 5005.00	1.12, 23.41	136.75%	0.212, 17.850	-30.63%	0.114, 0.116	3.75%
MLK	EW[1]	0.846, 117.23	1.24, 16.44	42.11%	0.692, 10.510	72.47%	--	--
	NS[2]	0.087, 1259.45	1.40, 16.51	-111.34%	0.930, 14.737	228.37%	--	--
ETEC	EW[1]	0.031, 62.742	0.19, 12.39	-94.48%	0.326, 12.968	202.95%	--	--
	NS[2]	0.082, 214.481	0.32, 15.63	-83.15%	0.425, 19.256	186.97%	--	--

Note:

- $\hat{y}_{max} = a_0 + a_1 x_{1,max} + a_2 x_{2,max} + a_3 x_{3,max}$
- 1: longitudinal direction.
- 2: transverse direction.
- --: deleted in the final regression analysis.

Figs. 4.12 through 4.15 show the regression results for Group A analyses for all except the BOC building. In the BOC building, motions at the base were recorded during three events only and this was not enough to show a trend. In Figs. 4.12 through 4.15, the chosen terms are plotted versus their corresponding contributions (for example, in Group A, x_1 is plotted versus $y - y_{c0}$, where $y_{c0} = a_0 + a_2 x_2 + a_3 x_3$). It is seen that E_{S+Y}^{soil} is mostly related to $v_{G,\max}$ and $\dot{\theta}_{\max}$. It is also found that $v_{G,\max}$ contributes more for longitudinal responses of the HSB and VN7SH buildings and $\dot{\theta}_{\max}$ is more important for transverse responses of the HSB, MLK and ETEC buildings. This suggests that $v_{G,\max}$ (i.e. the overall level of shaking) might be a significant measure of dissipated energy levels for longitudinal responses, while $\dot{\theta}_{\max}$ might be the best measure for energy dissipation in the transverse responses of buildings. Table 4.4 summarizes the maximum and minimum values of the quantities used in the regression analysis (read from Figs. 4.12 through 4.15) and the percentages of their contributions. The percentages of the contributions were calculated from

$$x_1 : \frac{a_1 x_{1,\max}}{\hat{y}_{\max}}\%, \text{ for example,} \tag{4.3}$$

in which $\hat{y}_{\max} = a_0 + a_1 x_{1,\max} + a_2 x_{2,\max} + a_3 x_{3,\max}$ (the a's can be found in Table 4.3).

Figs. 4.16 through 4.19 show the regression results for Group B analyses. In these figures, it is seen that E_{S+Y}^{soil} is mostly related to $\frac{v_{G,\max}}{\beta}$ and $s_{h,\max}$. Table 4.5 summarizes the maximum and minimum values of the quantities used in the

Reproduced with permission of the copyright owner. Further reproduction prohibited without permission.

Reproduced with permission of the copyright owner. Further reproduction prohibited without permission.

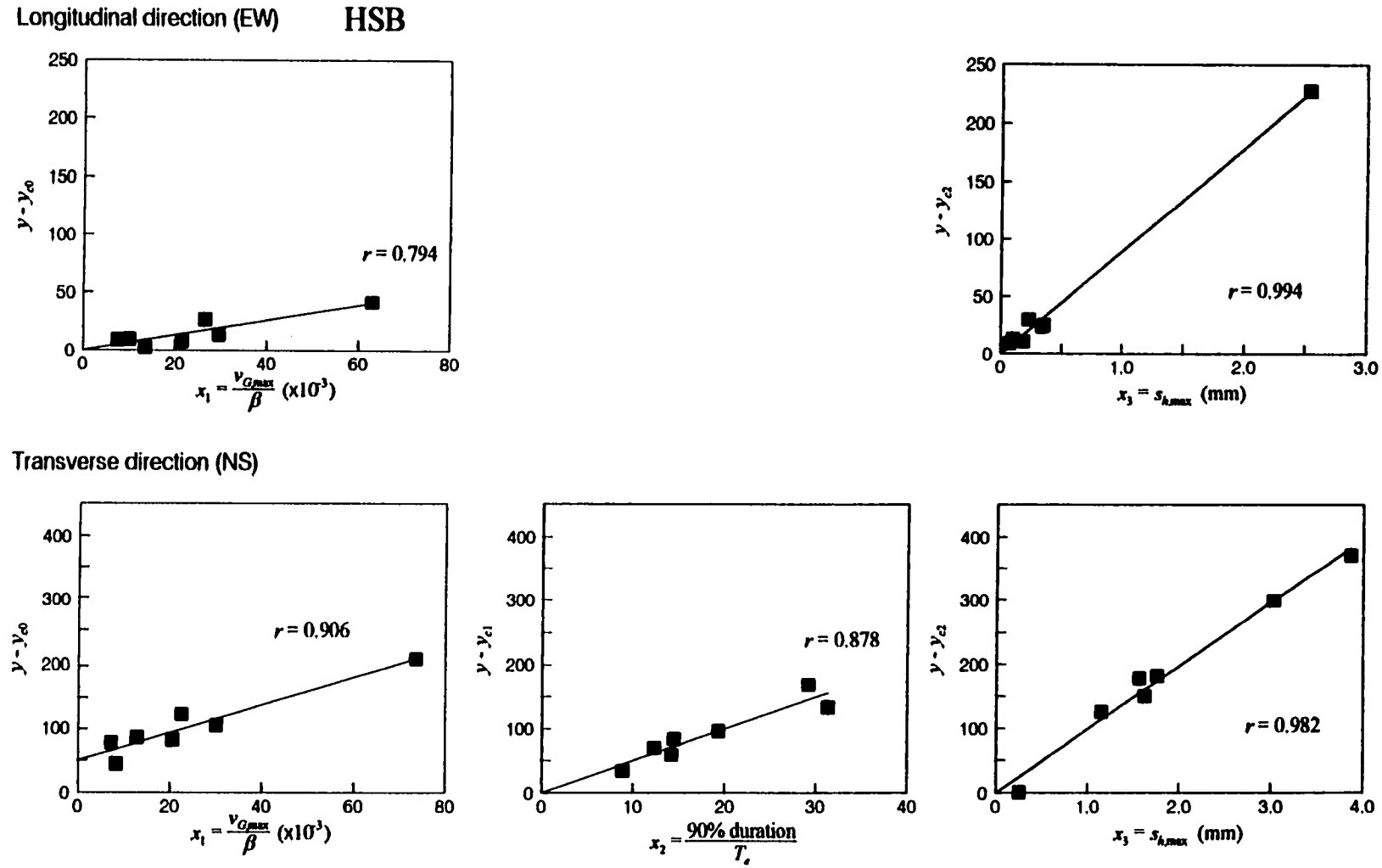

Fig. 4.16 The fianl regression analysis of E_{S+Y}^{soil} with respect to the selected scaling quantities (Group B) for Hollywood Storage building (r represents the correlation coefficient). Top: longitudinal (EW) response. Bottom: transverse (NS) response.

Reproduced with permission of the copyright owner. Further reproduction prohibited without permission.

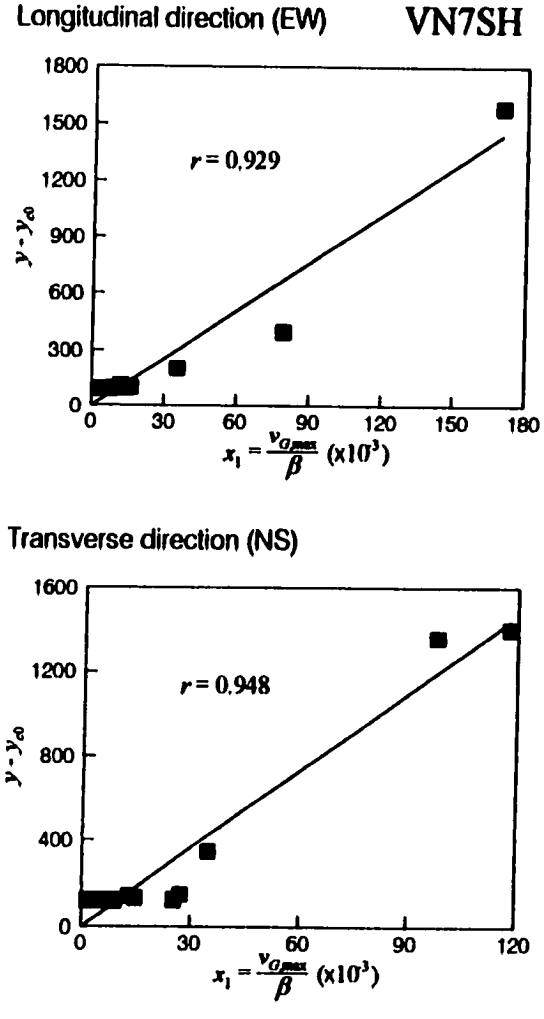

Fig. 4.17 Same as Fig. 4.16 but for Van Nuys 7-story hotel.

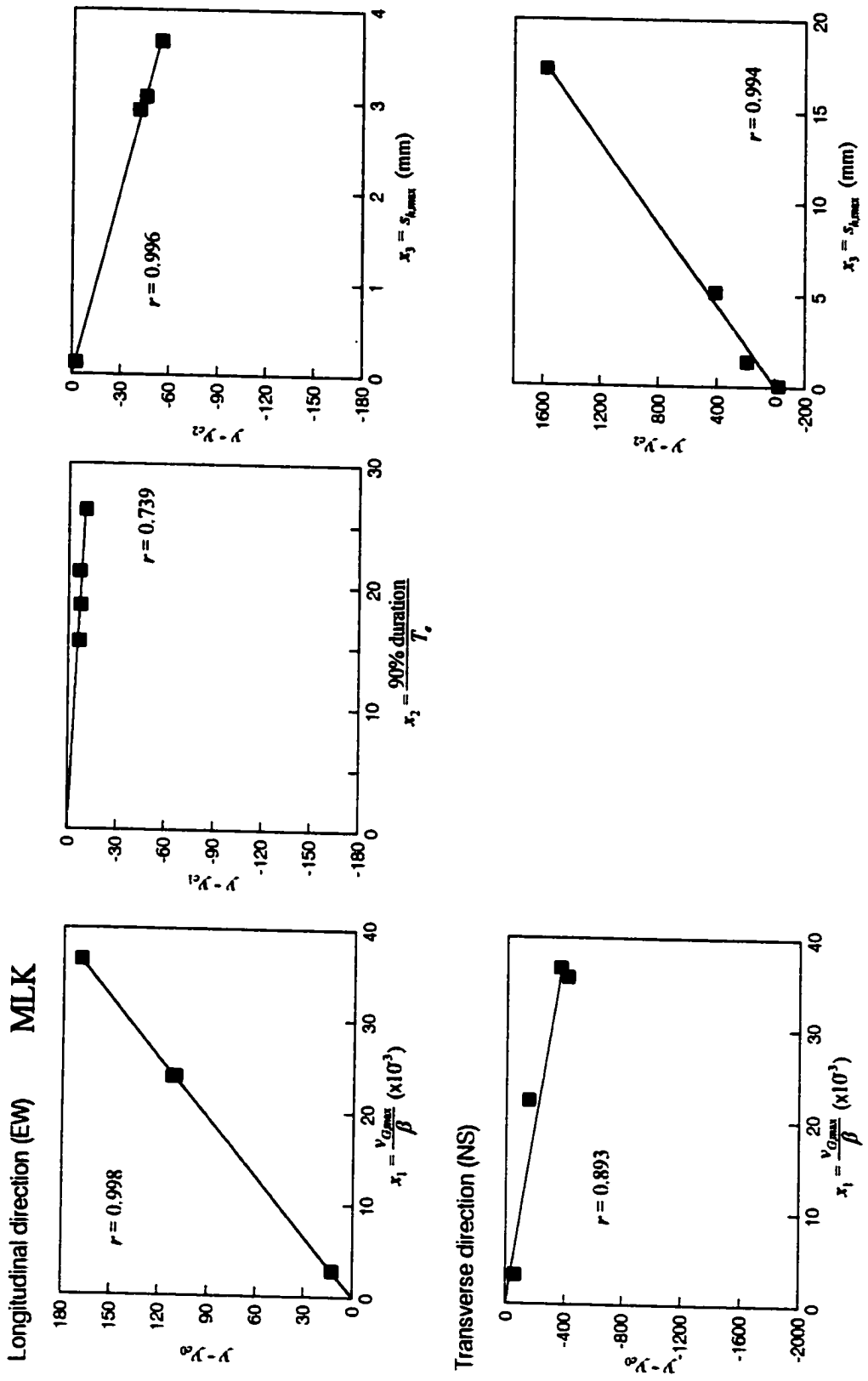

Fig. 4.18 Same as Fig. 4.16 but for Millikan Library building.

Reproduced with permission of the copyright owner. Further reproduction prohibited without permission.

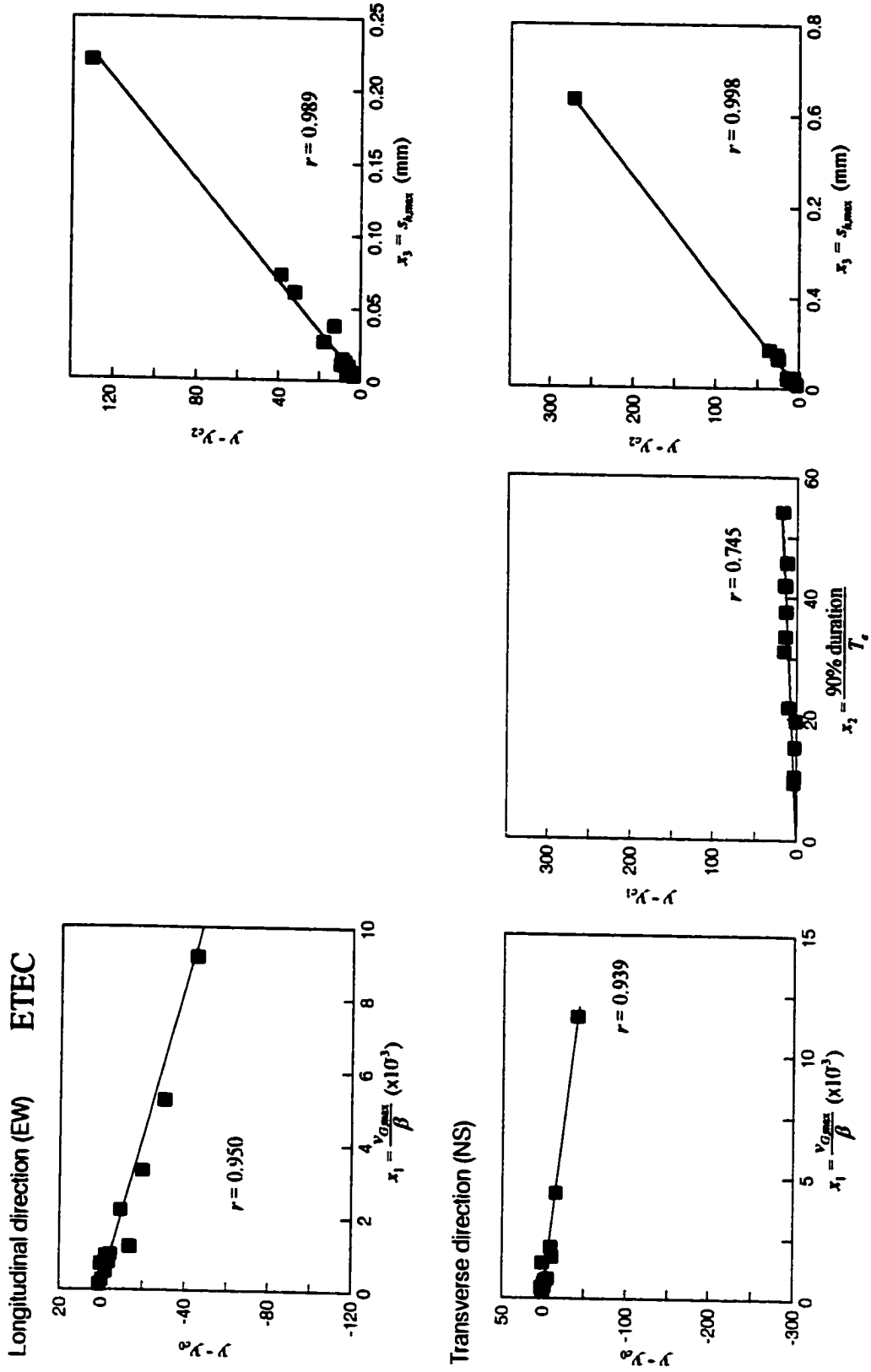

Fig. 4.19 Same as Fig.4.16 but for Santa Susana ETEC building.

Reproduced with permission of the copyright owner. Further reproduction prohibited without permission.

Reproduced with permission of the copyright owner. Further reproduction prohibited without permission.

Table 4.5 A summary of the maximum and minimum values of the quantities used in the regression analyses (Group B) and the percentages of their contributions.

		$y = E_{S+Y}^{soil}$ (kN·m)	$x_1 = \frac{v_{G,max}}{\beta}$ ($\times 10^{-3}$)		$x_2 = \frac{\text{90\% duration}}{T_e}$		$x_3 = s_{h,max}$ (mm)	
Bldg.	Comp.	y_{min}, y_{max}	$x_{1,min}, x_{1,max}$	$\frac{a_1 x_{1,max}}{\hat{y}_{max}}$	$x_{2,min}, x_{2,max}$	$\frac{a_2 x_{2,max}}{\hat{y}_{max}}$	$x_{3,min}, x_{3,max}$	$\frac{a_3 x_{3,max}}{\hat{y}_{max}}$
HSB	EW[1]	1.164, 254.686	7.467, 62.933	16.00%	--	--	0.068, 2.533	89.70%
	NS[2]	0.489, 379.455	7.133, 73.433	30.40%	8.881, 31.269	29.86%	0.248, 3.864	73.22%
VN7SH	EW[1]	0.007, 1495.31	2.833, 169.770	106.82%	--	--	--	--
	NS[2]	0.006, 1277.71	1.500, 117.730	109.46%	--	--	--	--
BOC	NS[1]	0.034, 3094.6	1.367, 92.433	53.38%	8.750, 51.344	-1.14%	0.002, 14.022	48.34%
	EW[2]	0.107, 5005.0	3.733, 78.033	150.47%	5.124, 60.644	-0.34%	0.037, 24.380	-43.02%
MLK	EW[1]	0.846, 117.23	2.822, 36.533	160.82%	15.401, 26.212	-9.44%	0.126, 3.655	-51.29%
	NS[2]	0.087, 1259.45	3.111, 36.689	-29.85%	--	--	0.061, 17.269	125.49%
ETEC	EW[1]	0.031, 62.742	0.141, 9.178	-78.93%	--	--	0.003, 0.220	182.70%
	NS[2]	0.082, 214.481	0.237, 11.578	-18.19%	9.487, 54.198	8.16%	0.007, 0.634	118.40%

Note:

- $\hat{y}_{max} = a_0 + a_1 x_{1,max} + a_2 x_{2,max} + a_3 x_{3,max}$
- 1: longitudinal direction.
- 2: transverse direction.
- --: deleted in the final regression analysis.

regression analyses (read from Figs. 4.16 through 4.19) and the percentages of their contributions.

Figs. 4.20a and b through 4.23a and b show the regression results for Group C analyses for all except the BOC building. It is seen that E_{S+Y}^{soil} is mostly related to $\frac{v_{G,max}}{\beta}$, $\dot{\theta}_{max}$ and $s_{h,max}$. Table 4.5 summarizes the maximum and minimum values of the quantities used in the regression analyses and the percentages of their contributions.

According to the above results, $\frac{v_{G,max}}{\beta}$, $\dot{\theta}_{max}$ and $s_{h,max}$ appear to be the most significant parameters for prediction of the energy dissipation associated with the nonlinear soil behavior of the SSI systems. As more strong-motion accelerograms recorded in buildings become available in digitized form and as we learn about better models for such analyses, the results presented here and the method of the analysis will be updated and improved.

Reproduced with permission of the copyright owner. Further reproduction prohibited without permission.

Reproduced with permission of the copyright owner. Further reproduction prohibited without permission.

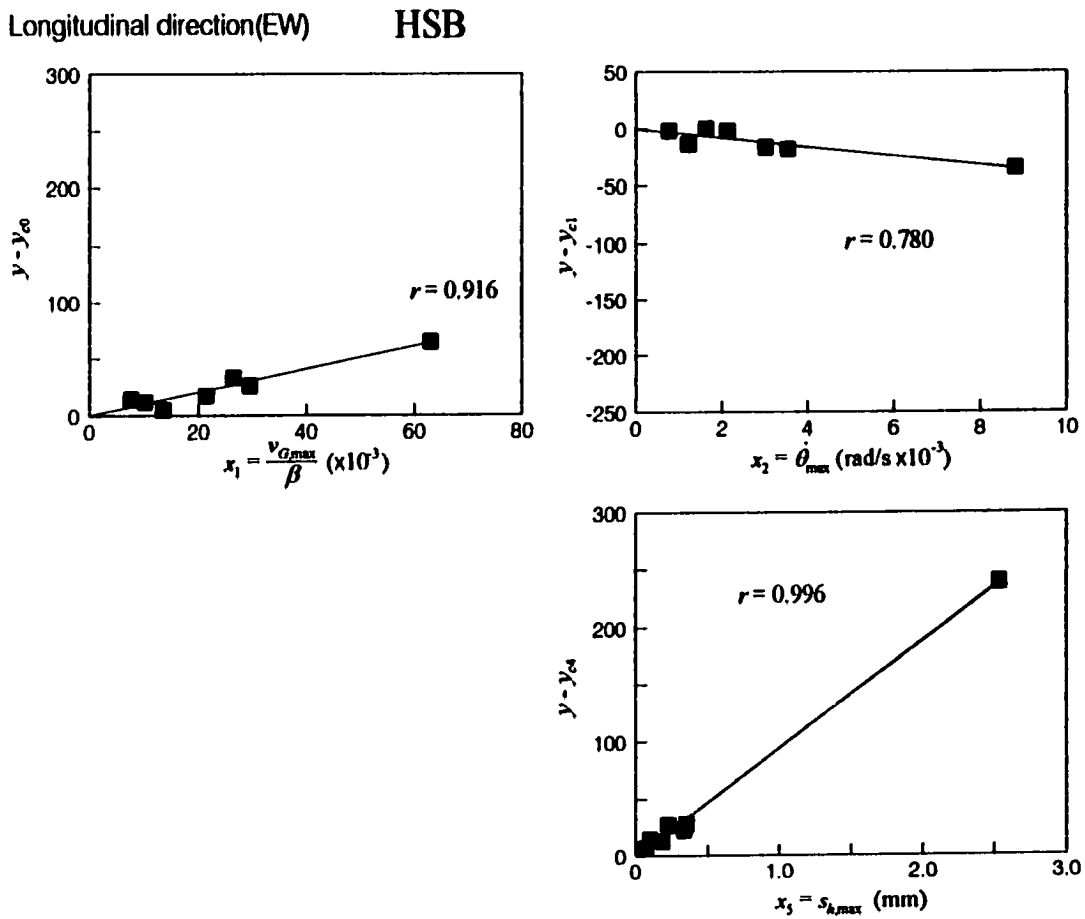

Fig. 4.20a The final regression analysis of E_{S+Y}^{soil} with respect to the selected scaling quantities (Group C) for longitudinal (EW) response of Hollywood Storage building (r represents the correlation coefficient).

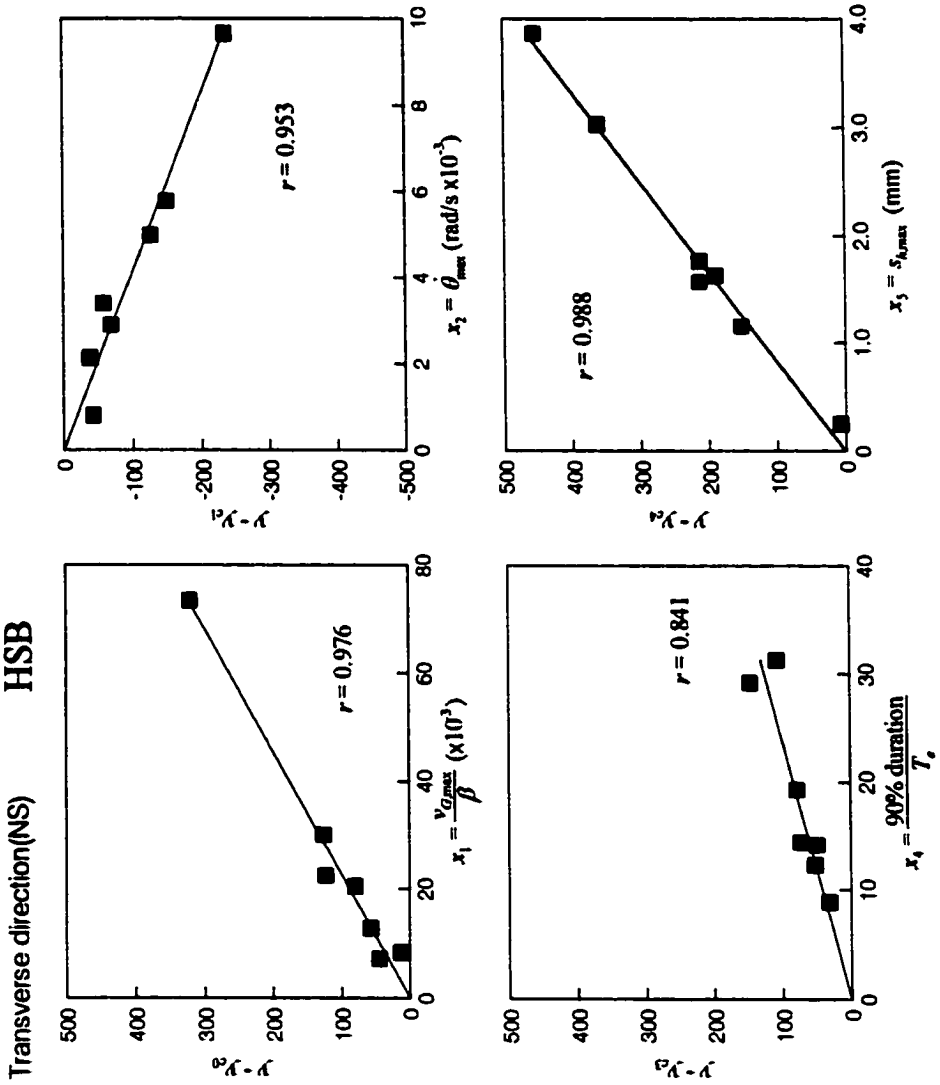

Fig. 4.20b Same as Fig. 4.20a but for the transverse (NS) response.

Reproduced with permission of the copyright owner. Further reproduction prohibited without permission.

Reproduced with permission of the copyright owner. Further reproduction prohibited without permission.

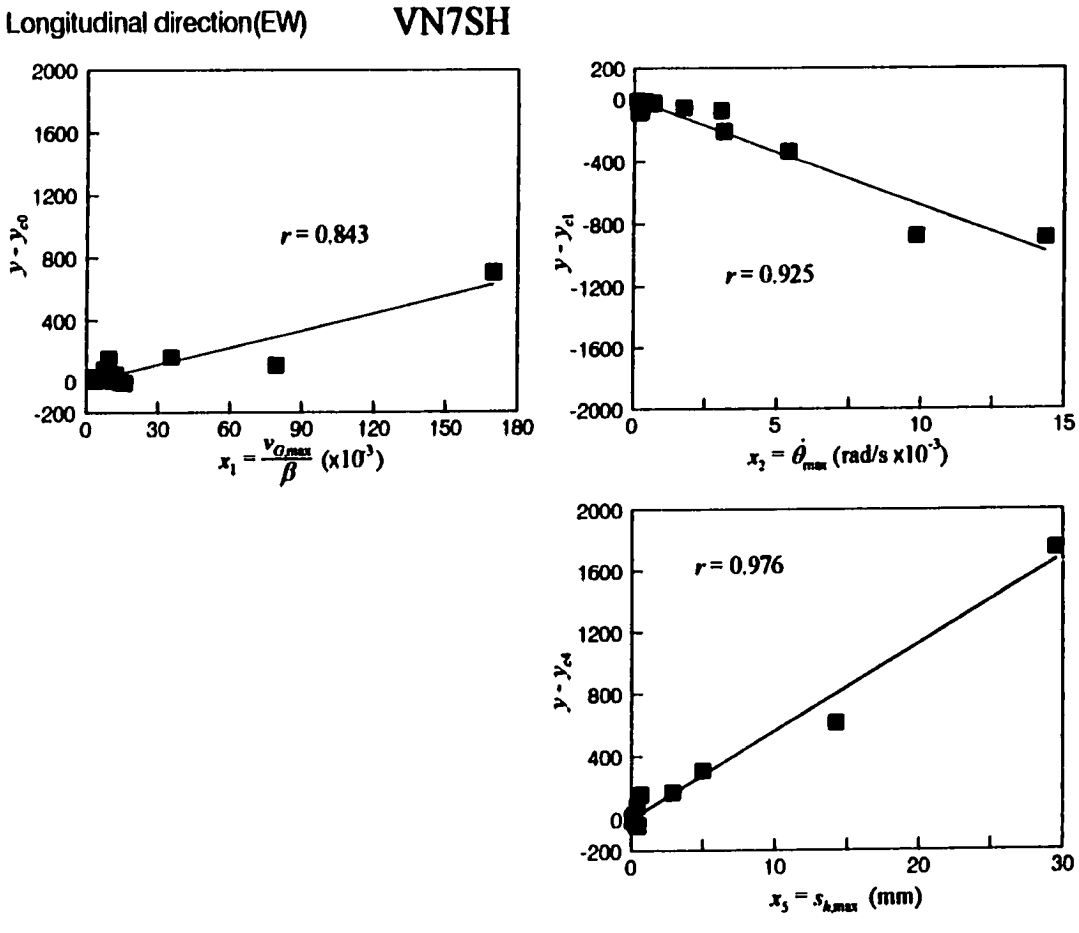

Fig. 4.21a Same as Fig. 4.20a but for Van Nuys 7-story hotel.

Reproduced with permission of the copyright owner. Further reproduction prohibited without permission.

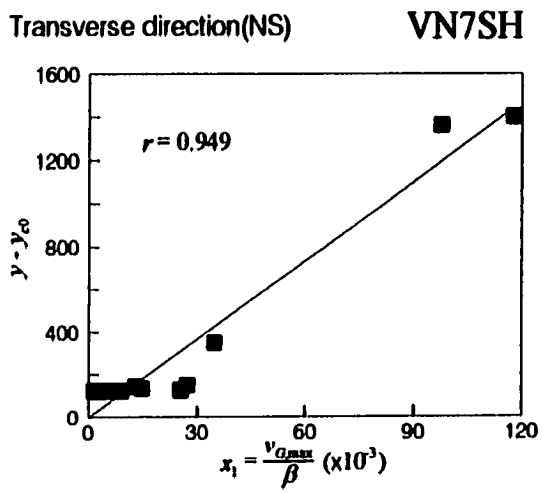

Fig. 4.21b Same as Fig. 4.21a but for the transverse (NS) response.

Reproduced with permission of the copyright owner. Further reproduction prohibited without permission.

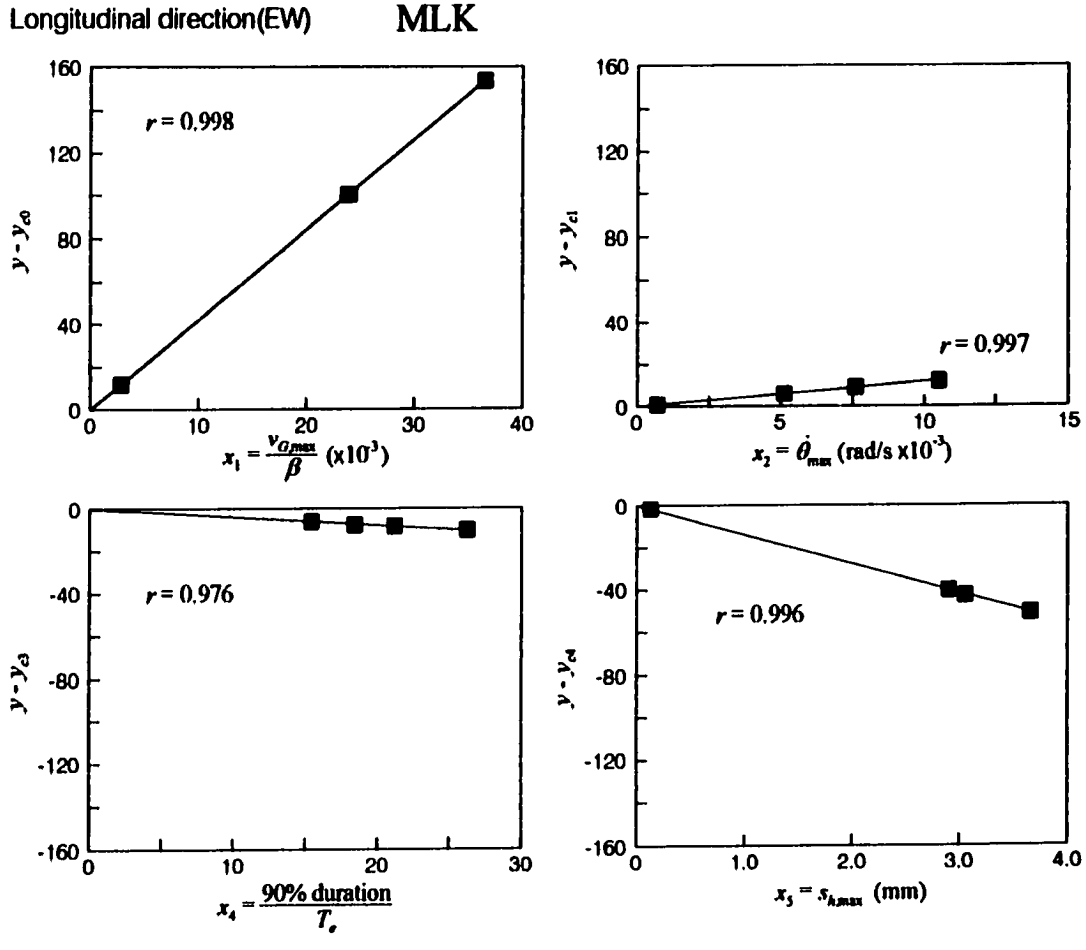

Fig. 4.22a Same as Fig. 4.20a but for Millikan Library building.

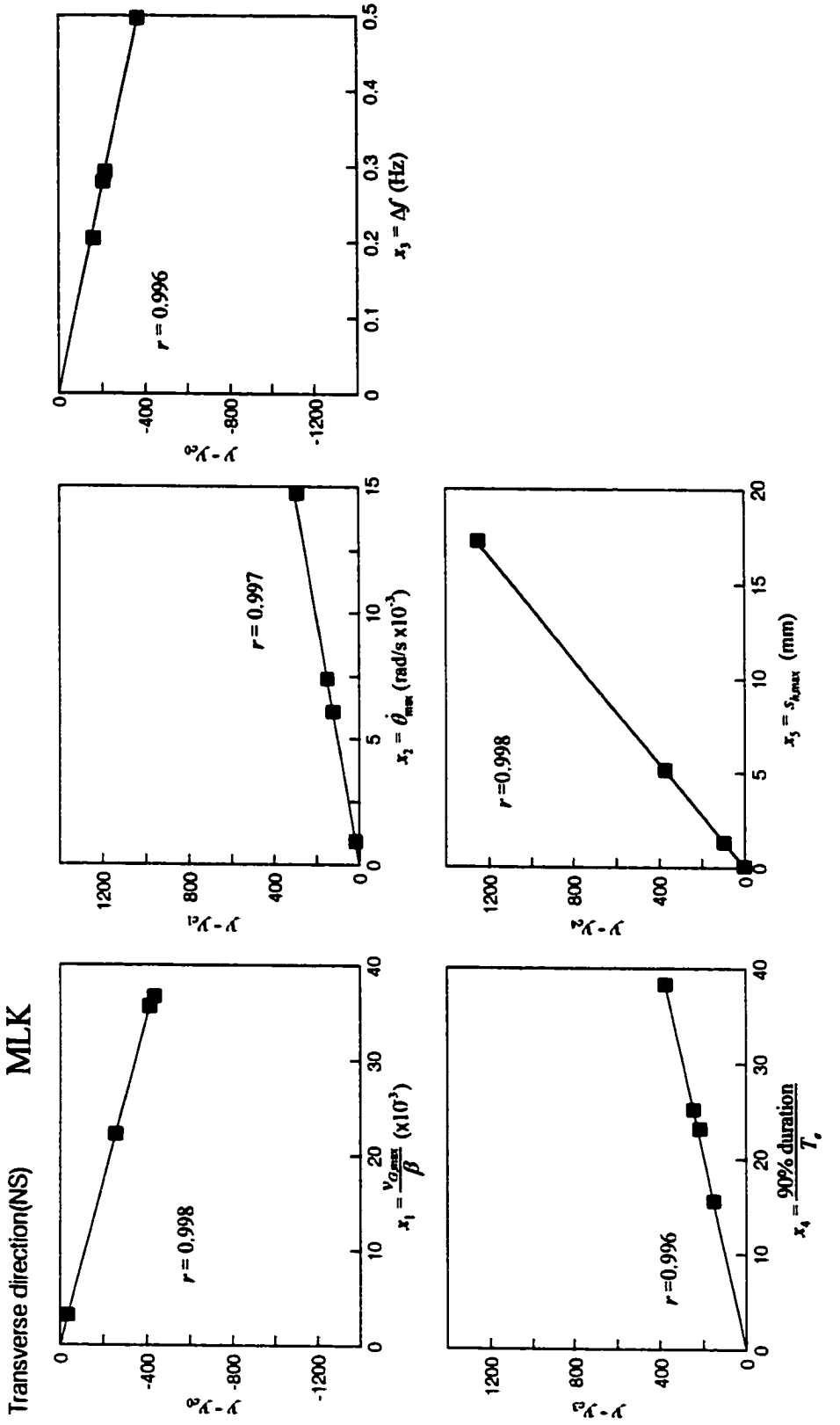

Fig. 4.22b Same as Fig. 4.22a but for the transverse (NS) response.

Reproduced with permission of the copyright owner. Further reproduction prohibited without permission.

Reproduced with permission of the copyright owner. Further reproduction prohibited without permission.

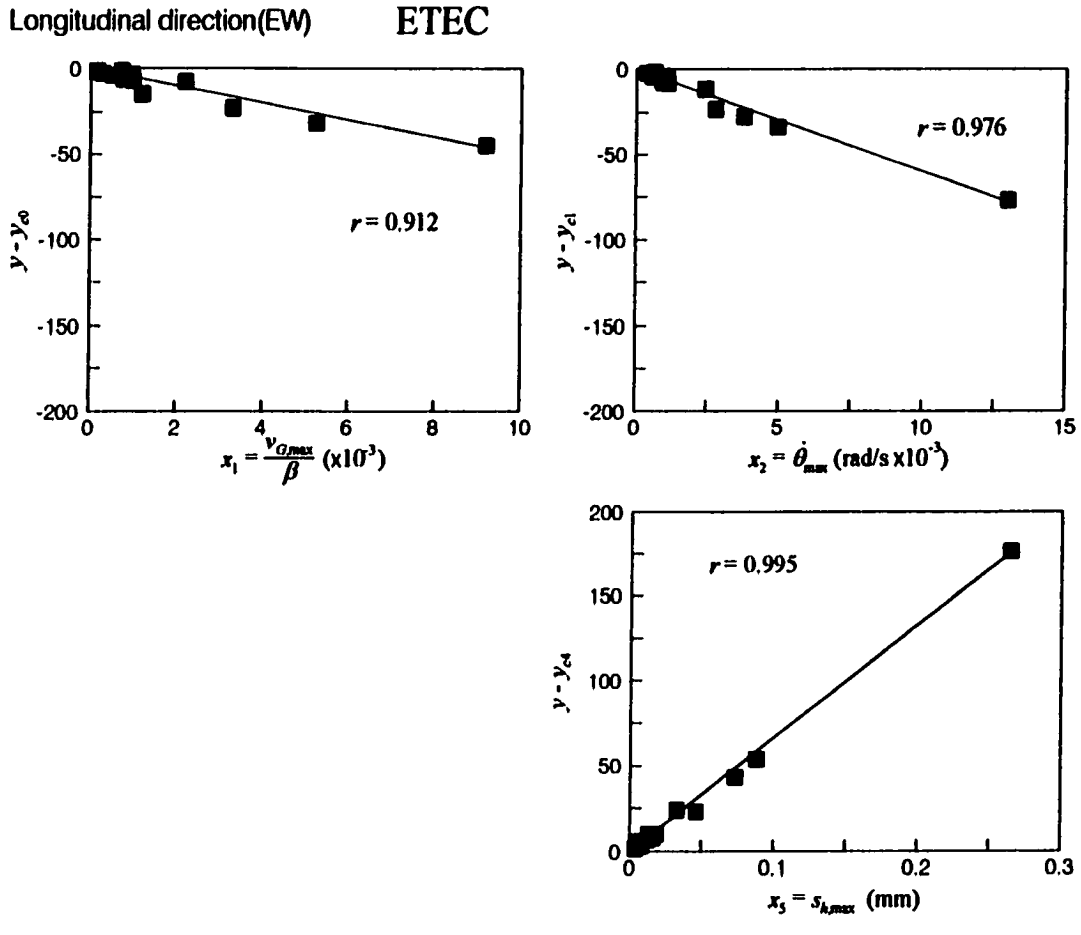

Fig. 4.23a Same as Fig. 4.20a but for Santa Susana ETEC building.

Reproduced with permission of the copyright owner. Further reproduction prohibited without permission.

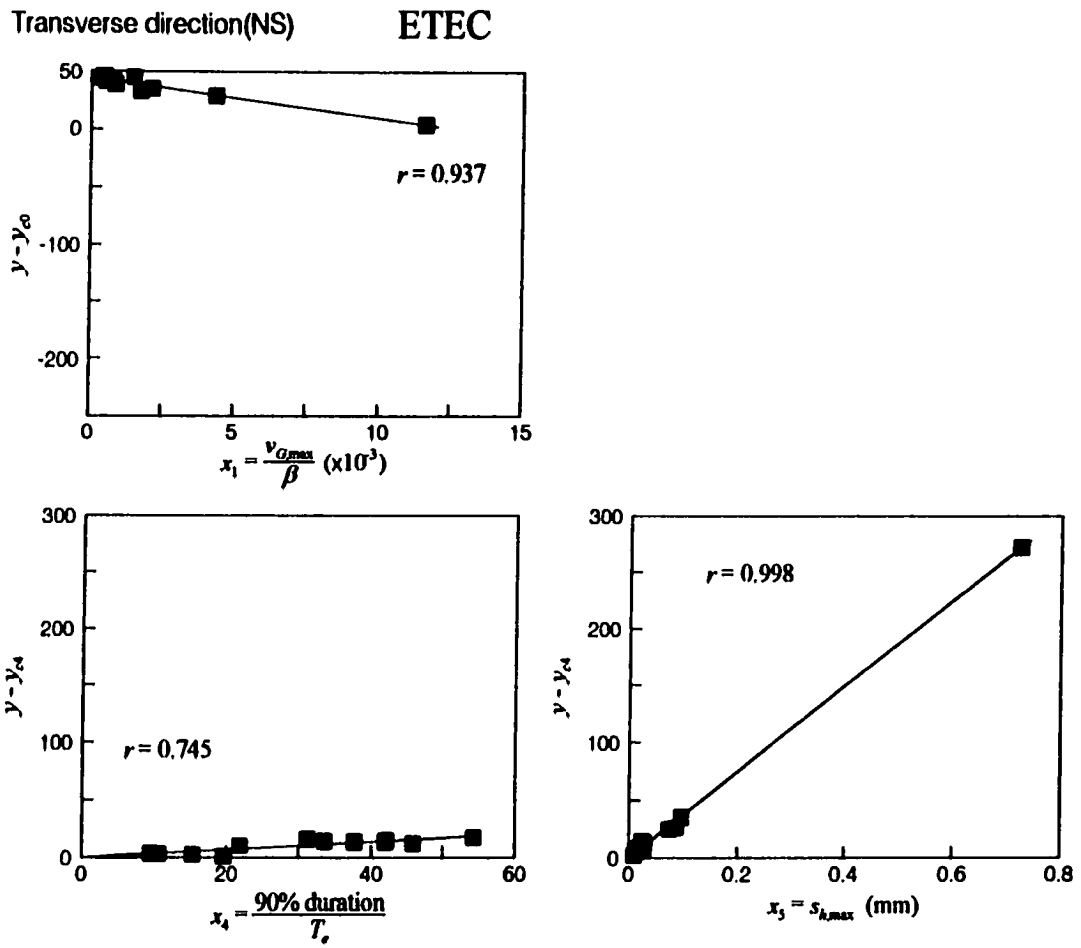

Fig. 4.23b Same as Fig. 4.23a but for the transverse (NS) response.

Reproduced with permission of the copyright owner. Further reproduction prohibited without permission.

Table 4.6 A summary of the maximum and minimum values of the quantities used in the regression analyses (Group C) and the percentages of their contributions.

		$y = E_{S+V}^{soil}$ (kN·m)	$x_1 = \frac{v_{G,max}}{\beta}$ ($\times 10^{-3}$)		$x_2 = \dot{\theta}_{max}$ (rad/s $\times 10^{-3}$)		$x_3 = \Delta f$ (Hz)		$x_4 = \frac{\text{90\% duration}}{T_e}$		$x_5 = s_{h,max}$ (mm)	
Bldg.	Comp.	y_{min}, y_{max}	$x_{1,min}, x_{1,max}$	$\frac{a_1 x_{1,max}}{\hat{y}_{max}}$	$x_{2,min}, x_{2,max}$	$\frac{a_2 x_{2,max}}{\hat{y}_{max}}$	$x_{3,min}, x_{3,max}$	$\frac{a_3 x_{3,max}}{\hat{y}_{max}}$	$x_{4,min}, x_{4,max}$	$\frac{a_4 x_{4,max}}{\hat{y}_{max}}$	$x_{5,min}, x_{5,max}$	$\frac{a_5 x_{5,max}}{\hat{y}_{max}}$
HSB	EW[1]	1.164, 254.686	7.467, 62.933	25.16%	0.755, 8.811	-13.80%	--	--	--	--	0.068, 2.533	94.14%
	NS[2]	0.489, 379.455	7.133, 73.433	60.78%	0.769, 9.657	-43.69%	--	--	8.881, 31.269	24.48%	0.248, 3.864	87.33%
VN7SH	EW[1]	0.007, 1495.31	2.833, 169.770	44.41%	0.106, 14.342	-62.14%	--	--	--	--	0.016, 29.493	117.84%
	NS[2]	0.006, 1277.71	1.500, 117.733	109.46%	--	--	--	--	--	--	--	--
BOC	NS[1]	0.034, 3094.6	1.367, 92.433	-19.72%	0.114, 18.649	84.48%	0.346, 0.538	8.30%	8.750, 51.344	0.28%	0.002, 14.022	35.25%
	EW[2]	0.107, 5005.0	3.733, 78.033	169.53%	0.212, 17.850	-38.53%	0.154, 0.385	-15.09%	5.124, 60.644	5.66%	0.037, 24.380	-23.51%
MLK	EW[1]	0.846, 117.23	2.822, 36.533	145.52%	0.692, 10.510	11.99%	--	--	15.401, 26.212	-9.85%	0.126, 3.655	-48.02%
	NS[2]	0.087, 1259.45	3.111, 36.689	-31.70%	0.930, 14.737	25.34%	0.204, 0.496	-30.84%	15.589, 38.295	31.56%	0.061, 17.269	105.64%
ETEC	EW[1]	0.031, 62.742	0.141, 9.178	-59.71%	0.326, 12.968	-125.82%	--	--	--	--	0.003, 0.220	284.46%
	NS[2]	0.082, 214.481	0.237, 11.578	-18.19%	--	--	--	--	9.487, 54.198	8.16%	0.008, 0.634	118.40%

Note:

- $\hat{y}_{max} = a_0 + a_1 x_{1,max} + a_2 x_{2,max} + a_3 x_{3,max} + a_4 x_{4,max} + a_5 x_{5,max}$
- 1: longitudinal direction.
- 2: transverse direction.
- --: deleted in the final regression analysis.

5. SUMMARY AND CONCLUSIONS

In this work, an alternative to the spectral method in earthquake resistant design is investigated, by analyzing the flow of seismic wave energy associated with strong motion, and focusing on the energy during soil-foundation-structure system response. Starting with the derivation of energy equations, we attempted to identify and to quantify the energy dissipation mechanisms. For design considerations, it is necessary first to understand and to quantify all these energies, and then to show how it is possible to incorporate maximum power demands into the design process.

To study the energy flow and dissipation through a soil-structure system, as a basic vehicle we adopted a simple model in which both the soil and structural response can be nonlinear. This model, shown in Fig. 2.1, consists of a rigid foundation supported by nonlinear soil springs, and a structure represented by a single-degree-of-freedom oscillator. For illustrative case studies using this model, we used a 14-story storage building in Hollywood, a 7-story hotel in Van Nuys, a 12-story commercial building in Sherman Oaks, a 9-story library building in Pasadena, and an 8-story research building in Santa Susana, for which processed strong motion data was available. All of the currently processed strong motion data were analyzed, and the simple model was used to quantify approximately the distribution of the incident wave energy. We were able to show that there is good correspondence between the estimates of the incident wave energy and the sum of all response energies in the soil-structure system (shown in Figs. 3.26 through 3.30). This result points to the need to research the transfer of the incident wave energy into soil-structure systems.

Reproduced with permission of the copyright owner. Further reproduction prohibited without permission.

Our results show that a typical soil-structure system is capable of reflecting large fractions of the incident strong motion energy back into the soil by means of scattering (not present for the model in Fig. 2.1) and nonlinear soil response. Clearly, the nature of these powerful energy dissipation mechanism must be carefully studied to provide reliable and verifiable estimates for use in the future earthquake-resistant design. Towards this end, we first presented a definition for the energy demand and showed that this demand does not only result in deformation of the building, but also leads to strong soil-foundation interaction effects. Then, we examined some elementary aspects of energy absorption capacity of structures, and pointed out the roles of the duration of strong shaking and of the rate of arrival of the incident strong motion energy. At the end, we presented the regression analyses to begin to characterize the energy dissipation associated with nonlinear soil behavior as means of reducing the seismic response of structures. The presented analyses are, of course, preliminary, but indicate that there exist major advantages and rational reasons for adoption of power based description of seismic demands in the design of earthquake-resistant structures.

Reproduced with permission of the copyright owner. Further reproduction prohibited without permission.

REFERENCES

1. Akiyama, H. (1985). Earthquake-Resistant Limit-State Design for Buildings, *Univ. of Tokyo Press*, Tokyo, Japan.

2. Akiyama, H. (1988). Earthquake Resistant Design Based on the Energy Concept, *Proc. of the Ninth World Conference on Earthquake Engrg.*, Tokyo, Japan, 905-910.

3. Akiyama, H. (1997). Damage-Controlled Earthquake Resistant Design Method Based on the Energy Concept, *Report No. UCB/EERC-97/05*, Earthquake Engineering Research Center, University of California, Berkeley, California, 49-56.

4. Anderson, J. C. and Bertero, V. V. (1969). Seismic Behavior of Multistory Frames by Different Philosophies, *Report No. UCB/EERC-69/11*, Earthquake Engineering Research Center, University of California, Berkeley, California.

5. Arias, A. (1970). A Measure of Earthquake Intensity, in "Seismic Design of Nuclear Power Plants," R. J. Hansen (editor), *The Mass. Inst. of Tech. Press.*

6. Benioff, H. (1934). The Physical Evaluation of Seismic Destructiveness, *Bull. Seism. Soc. Amer.*, **24**, 398-403.

7. Biot, M. A. (1932). Vibrations of Buildings During Earthquake, Chapter II in *Ph.D. Thesis* No. 259 entitled "Transient Oscillations in Elastic Systems," Aeronautics Department, Calif. Inst. of Tech., Pasadena, California.

8. Biot, M. A. (1933). Theory of Elastic Systems Vibrating Under Transient Impulse with an Application to Earthquake – Proof Buildings, *Proc. National Academy of Science*, **19(2)**, 262-268.

9. Biot, M. A. (1934). Theory of Vibration of Buildings During Earthquake, *Zeitschrift für Angewandte Matematik und Mechanik*, **14(4)**, 213-223.

10. Biot, M. A. (1941). A Mechanical Analyzer for the Prediction of Earthquake Stresses, *Bull. Seism. Soc. Amer.*, **31(2)**, 151-171.

11. Biot, M. A. (1942). Analytical and Experimental Methods in Engineering Seismology, *ASCE, Transactions*, **108**, 365-408.

12. Blume, J. A. (1960). A Reserve Energy Technique for the Earthquake Design and Rating of Structures in the Inelastic Range, *Proc. of the Second World Conference on Earthquake Engrg.*, Tokyo, Japan, 1061-1083.

13. Blume, J. A. and Assoc. (1973). Holiday Inn, Chapter 29 in "San Fernando, California Earthquake of February 9, 1971." Volume I, part A, U.S. Dept. of Commerce, National Oceanic and Atmospheric Administration, Washington, D.C.

14. Carder, D. S. (1936). Vibration Observation, Chapter 5 in "Earthquake Investigation in California 1934-1935," *Special Publication No. 201*, U.S. Dept. of Commerce, Coast and Geodetic Survey, 49-106.

15. Carder, D. S. (1964). (Editor). Earthquake Investigations in the Western United States 1931-1964, *Publication 41-2*, U.S. Dept. of Commerce, Coast and Geodetic Survey.

Reproduced with permission of the copyright owner. Further reproduction prohibited without permission.

16. Crowder, R. E. (1961). Los Angeles City Oil Field, Summary of Operation, Calif. Div. Oil and Gas, **47**, 66-77.

17. Crowder, R. E. and Johnson, R. A. (1963). Recent Developments in Jade-Buttram Area of Salt Lake Oil Field, Summary of Operation, Calif. Div. Oil and Gas, **49**, 53-58.

18. Decanini, L. D. and Mollaioli, F. (2001). An Energy-Based Methodology for the Assessment of Seismic Demand, *Soil Dynam. and Earthquake Engrg.*, **21**(2), 113-137.

19. De la Llera, J. C., Chopra, A. K. and Almazan, J. L. (2001). Three-dimensional Inelastic Response of a RC Building During the Northridge Earthquake, *J. Struct. Eng.*, ASCE, **127**(5), 482-489.

20. Duke, C. M., Luco, J. E., Carriveau, A. R., Hradilek, P. J., Lastrico, R. and Osrtrom, D. (1970). Strong Earthquake Motion and Site Conditions: Hollywood, *Bull. Seism. Soc. Amer.*, **60**(4), 1271-1289.

21. Duncan, W. J. (1952). A Critical Examination of the Representation of Massive and Elastic Bodies by Systems of Rigid Masses Elastically Connected, *Quart. J. Mech. Appl. Math.*, **5**(1), 97-108.

22. Fajfar, P. and Fischinger, M. A. (1990). A Seismic Design Procedure Including Energy Concept, *Proc. of the Ninth European Conference on Earthquake Engrg.*, Moscow.

23. Gutenberg, B. and Richter, C. F. (1956). Earthquake Magnitude, Intensity, Energy, and Acceleration, *Bull. Seism. Soc. Amer.*, **46**(2), 105-145.

24. Hayir, A., Todorovska, M. I. and Trifunac, M. D. (2001). Antiplane Response of a Dike with Flexible Soil-Structure Interaction to Incident SH-Waves, *Soil Dynam. and Earthquake Engrg.*, **21**(7), 603-613.

25. Housner, G. W. (1956). Limit Design of Structures to Resist Earthquakes, *Proc. of the First World Conference on Earthquake Engrg.*, Berkeley, California, 5.1-5.13.

26. Hudson, D. E. (1976). Strong motion Earthquake Accelerograms, Index Volume, *Report EERL 76-02*, Earthquake Eng. Res. Lab., Calif. Inst. of Tech., Pasadena, California.

27. Husid, R. (1967). Gravity Effects on the Earthquake Response of Yielding Structures, *Ph.D. Thesis*, Calif. Inst. of Tech., Pasadena, California.

28. Iguchi, M. and Luco, J. E. (1982). Vibration of Flexible Plate on Viscoelastic Medium, *J. of Engrg. Mech.*, ASCE, **108**(6), 1103-1120.

29. Ivanović, S. S., Trifunac, M. D., Novikava, E. I., Gladkov, A. A. and Todorovska, M. I. (1999). Instrumented 7-Story Reinforced Concrete Building in Van Nuys, California: Ambient Vibration Surveys Following the Damage from the 1994 Northridge Earthquake, *Rep. No. CE 99-03*, Dept. of Civil Eng., Univ. of Southern California, Los Angeles, California.

30. Ivanović, S. S., Trifunac, M. D., Novikava, E. I., Gladkov, A. A. and Todorovska, M. I. (2000). Ambient Vibration Tests of a Seven-Story Reinforced Concrete Building in Van Nuys, California, Damaged by the 1994 Northridge Earthquake, *Soil Dynam. and Earthquake Engrg.*, **19**(6), 391-411.

31. Jenkins, O. P. (1943). Geologic Formations and Economic Development of the Oil and Gas Fields of California, Calif. Div. Mines, Bull. 118, 773 pages.

Reproduced with permission of the copyright owner. Further reproduction prohibited without permission.

32. Joyner, W. B. (1975). A Method for Calculating Nonlinear Seismic Response in Two Dimensions, *Bull. Seism. Soc. Amer.*, **65**(5), 1337-1357.

33. Joyner, W. B. and Chen, A. T. F. (1975). Calculating of Nonlinear Ground Response in Earthquakes, *Bull. Seism. Soc. Amer.*, **65**(5), 1315-1336.

34. Kuroiwa, J. H. (1967). *Vibration Test of a Multiple Building,* Earthquake Eng. Res. Lab., Calif. Inst. of Tech., Pasadena, California.

35. Lee, V. W. (1979). Investigation of Three-Dimensional Soil-Structure Interaction, *Rep. No. CE 79-11*, Dept. of Civil Eng., University of Southern California, Los Angeles, California.

36. Liou, G.-S. and Huang, P. R. (1994). Effects of Flexibility on Impedance Functions for Circular Foundations, *J. of Engrg. Mech.*, ASCE, **120**(7), 1429-1446.

37. Luco, J. E., Trifunac, M. D. and Wong, H. L. (1986). Soil Structure Interaction Effects on Forced Vibration Tests, *Rep. No. 86-05*, Dept. of Civil Eng., Univ. of Southern California, Los Angeles, California.

38. McCulloh, T. H. (1960). Gravity Variations and the Geology of the Los Angeles Basin of California, U.S. Geol. Survey, *Profess. Papers 400 B*, 320.

39. Papageorgiou, A. S. and Lin, B. C. (1991). Analysis of Recorded Earthquake Response and Identification of a Multi-Story Structure Accounting for Foundation Interaction Effects, *Soil Dynam. and Earthquake Engrg.*, **10**(1), 55-64.

40. Richart, F. E., Jr., Hall, J. R., Jr. and Woods, R. D. (1970). Vibrations of Soils and Foundations, *Prentice-Hall*, Englewood Cliffs, New Jersey.

41. Sezawa, K. and Kanai, K. (1936). Improved Theory of Energy Dissipation in Seismic Vibrations on a Structure, *Bull. Earth. Res. Inst.*, XIV, Part 2, 164-168.

42. Shannon & Wilson, Inc. and Agbabian Assoc. (1980). Geotechnical Data from Accelerograph Stations Investigated During the Period 1975-1979, *NUREG/CR-1643*, R6, RA, U.S. Nuclear Regulatory Commission, Washington, D.C.

43. Stewart, J. P. and Stewart, A. F. (1997). Analysis of Soil-Structure Interaction Effects on Building Response from Earthquake Strong Motion Recordings at 58 Sites, *Report No. UCB/EERC-97/01*, Earthquake Engineering Research Center, Univ. of California, Berkeley, California.

44. Tanabashi, R. (1937). *On the Resistance of Structures to Earthquake Shocks*, Memoirs of the College of Engineering, Kyoto Imperial University.

45. Tanabashi, R. (1956). Studies of the Nonlinear Vibrations of Structures Subjected to Destructive Earthquakes, *Proc. of the First World Conference on Earthquake Engrg.*, Berkeley, California.

46. Tembulkar, J. M. and Nau, J. M. (1987). Inelastic Modeling and Seismic Energy Dissipation, *J. of Struct. Engrg.*, ASCE, **113**(6) 1373-1377.

47. Todorovska, M. I. and Trifunac, M. D. (1990a). A Note on the Propagation of Earthquake Waves in Buildings with Soft First Floor, *J. of Engrg. Mech.*, ASCE, **116**(4), 892-900.

48. Todorovska, M. I. and Trifunac, M. D. (1990b). A Note on Excitation of Long Structures by Ground Waves, *J. of Engrg Mech.*, ASCE, **116**(4), 952-964.

Reproduced with permission of the copyright owner. Further reproduction prohibited without permission.

49. Todorovska, M. I. and Trifunac, M. D. (1990c). Analytical Model for In-Plane Building-Foundation-Soil Interaction: Incident P-, SV- and Rayleight Waves, *Rep. No. 90-01*, Dept. of Civil Engrg., Univ. of Southern California, Los Angeles, California.

50. Todorovska, M. I. and Trifunac, M. D. (1991). Radiation Damping During Two-Dimensional Building-Soil Interaction, *Rep. No. 91-01*, Dept. of Civil Eng., Univ. of Southern California, Los Angeles, California.

51. Todorovska, M. I. and Trifunac, M. D. (1992). The System Damping, the System Frequency and the System Response Peak Amplitudes During In-Plane Building-Soil Interaction, *Earthquake Eng. and Struct. Dynam.*, **21**(2), 127-144.

52. Todorovska, M. I. and Trifunac, M. D. (1993). The Effects of Wave Passage on the Response of Base-Isolated Buildings on Rigid Embedded Foundations, *Rep. No. CE 93-10*, Dept of Civil Eng., Univ. of Southern California, Los Angeles, California.

53. Todorovska, M. I., Ivanović, S. S. and Trifunac, M. D. (2001a). Wave Propagation in a Seven-Story Reinforced Concrete Building, I: Theoretical Models, *Soil Dynam. and Earthquake Engrg.*, **21**(3), 211-223.

54. Todorovska, M. I., Ivanović, S. S. and Trifunac, M. D. (2001b). Wave Propagation in a Seven-Story Reinforced Concrete Building, II: Observed Wave Numbers, *Soil Dynam. and Earthquake Engrg.*, **21**(3), 225-236.

55. Todorovska, M. I., Hayir, A. and Trifunac, M. D. (2001c). Antiplane Response of a Dike on Flexible Embedded Foundation to Incident SH-Waves, *Soil Dynam. and Earthquake Engrg.*, **21**(7), 593-601.

56. Trifunac, M. D. (1994). Q and High Frequency Strong Motion Spectra, *Soil Dynam. and Earthquake Engrg.*, **13**(3), 149-161.

57. Trifunac, M. D. (1997). Differential Earthquake Motion of Building Foundation, *J. of Struct. Engrg.*, ASCE, **123**(4), 414-422.

58. Trifunac, M. D. and Brady, A. G. (1975). A Study of the Duration of Strong Earthquake Ground Motion. *Bull. Seism. Soc. Amer.*, **65**, 581-626.

59. Trifunac, M. D. and Lee, V. W. (1978). Uniformly Processed Strong Earthquake Ground Accelerations in the Western United States of America for the Period from 1933 to 1971: Corrected Acceleration, Velocity and Displacement Curves, *Rep. No. 78-01*, Dept. of Civil Eng., Univ. of Southern California, Los Angeles, California.

60. Trifunac, M. D. and Todorovska, M. I. (1996). Nonlinear Soil Response – 1994 Northridge California, Earthquake, *J. Geotechnical Engrg.*, ASCE, **122**(9), 725-735.

61. Trifunac, M. D. and Todorovska, M. I. (1997). Response Spectra for Differential Motion of Columns, *Earthquake Engrg and Struct. Dynam.*, **26**(2), 251-268.

62. Trifunac, M. D. and Todorovska, M. I. (1998). Nonlinear Soil Response as a Natural Passive Isolation Mechanism – The 1994 Northridge, California Earthquake, *Soil Dynamics and Earthquake Eng.*, **17**(1), 41-51.

Reproduced with permission of the copyright owner. Further reproduction prohibited without permission.

63. Trifunac, M. D. and Todorovska, M. I. (2001). Recording and Interpreting Earthquake Response of Full-Scale Structures, Proc. NATO Workshop on Strong Motion Instrumentation for Civil Engineering Structures, June 2-5, 1999, Istanbul, Turkey, M. Erdik et al. (eds.), *Kluwer Academic Publishers*, 131-155.

64. Trifunac, M. D., Ivanović, S. S., Todorovska, M. I., Novikova, E. I. and Gladkov, A. A. (1999a). Experimental Evidence for Flexibility of a Building Foundation Supported by Concrete Friction Piles, *Soil Dynam. and Earthquake Engrg.*, **18**(3), 169-187.

65. Trifunac, M. D., Ivanović, S. S. and Todorovska, M. I. (1999b). Seven Story Reinforced Concrete Building in Van Nuys, California: Strong Motion Data Recorded Between 7 February 1971 and 9 December 1994, and Description of Damage Following Northridge, 17 January 1994 Earthquake, *Rep. No. 99-02*, Dept. of Civil Eng., Univ. of Southern California, Los Angeles, California.

66. Trifunac, M. D., Ivanović, S. S. and Todorovska, M. I. (2001a). Apparent Periods of a Building, Part I: Fourier Analysis, *J. of Struct. Engrg.*, ASCE, **127**(5), 517-526.

67. Trifunac, M. D., Ivanović, S. S. and Todorovska, M. I. (2001b). Apparent Periods of a Building, Part II: Time-Frequency Analysis, *J. of Struct. Engrg.*, ASCE, **127**(5), 527-537.

68. Trifunac, M. D., Todorovska, M. I. and Hao, T-Y. (2001c). Full-Scale Experimental Studies of Soil-Structure Interaction – A Review, *Proc. 2nd U.S.-Japan Workshop on Soil-Structure Interaction*, March 6-8, Tsukuba City, Japan.

69. Trifunac, M. D., Ivanović, S. S. and Todorovska, M. I. (2001d). Wave Propagation in a Seven-Story Reinforced Concrete Building, III: Damage Detection Via Changes in Wave Numbers, *Soil Dynam. And Earthquake Engrg.*, (in press).

70. Trifunac, M. D., Hao, T-Y. and Todorovska, M. I. (2001e). Response of a 14-Story Reinforced Concrete Structure to Nine Earthquakes: 61 Years of Observation in the Hollywood Storage Building, *Rep. No. 01-02*, Dept. of Civil Eng., Univ. of Southern California, Los Angeles, California.

71. Trifunac, M. D., Hao, T-Y. and Todorovska, M. I. (2001f). On Energy Flow in Earthquake Response, *Rep. No. 01-03*, Dept. of Civil Eng., Univ. of Southern California, Los Angeles, California.

72. Uang, C. M. and Bertero, V. V. (1988). Use of Energy as a Design Criterion in Earthquake-Resistant Design, *Report No. UCB/EERC-88/18*, Earthquake Engineering Research Center, Univ. of California, Berkeley, California.

73. Uang, C. M. and Bertero, V. V. (1990). Evaluation of Seismic Energy in Structures, *Earthquake Engrg. and Struct. Dynam.*, **19**(1), 77-90.

74. Wolf, J. P. (1988). Soil-Structure-Interaction Analysis in Time Domain, *Prentice Hall*, Englewood Cliffs, New Jersey.

75. Zahrah, T. F. and Hall, W. J. (1984). Earthquake Energy Absorption in SDOF Structures, *J. of Struct. Engrg.*, **110**(8), 1757-1772.

Reproduced with permission of the copyright owner. Further reproduction prohibited without permission.

APPENDIX A
APPROXIMATE FREQUENCY CHANGES ANALYSIS

To evaluate changes of system frequency, f_p, during particular earthquake shaking, as a function of the level of response and the previous response history, the "instantaneous" value of f_p was approximated by two methods: (1) zero-crossing analysis and (2) moving window Fourier analysis. To isolate the lowest frequency mode, the response was band-pass filtered. The band-pass frequencies were chosen to include the system frequency, and were determined after analyzing the instantaneous transfer-function between the relative horizontal motions recorded on the roof and at the base. For the Bank of California, earthquake motions were recorded by SMA-1 strong-motion accelerographs, located on the roof, seventh floor and ground floor, during 1971 San Fernando earthquake, its aftershock between 9 Feb. and 4 Aug. 1971, and the earthquake of 21 Feb. 1973. These accelerograms provided the data for analyzing the instantaneous transfer-function of the building. Unfortunately, during the 1994 Northridge earthquake and its aftershocks, the earthquake motions were recorded only on the roof. To take advantages of every available record, we studied the possibility and accuracy of performing the analysis without the recorded motions at the base (ground). We first used the data of 1971 San Fernando earthquake, its aftershocks between 9 Feb. and 4 Aug. 1971 (EQ71), and earthquake of 21 Feb. 1973 (EQ73) and evaluated the changes of the system frequency. Then, we used only the roof motions of these three events, assuming the ground motions were broad band, and repeated the evaluation.

Reproduced with permission of the copyright owner. Further reproduction prohibited without permission.

Fig. A.1 shows the Fourier amplitudes of base and roof motions, and the corresponding transfer-functions for three earthquakes. Based on these transfer-functions, the band-pass cut off frequencies were chosen (0.20 to 1.00 Hz for San Fernando earthquake, 1.35 to 2.00 Hz for EQ71, and 1.10 to 1.95 Hz for EQ73) and the data were filtered. Top parts of Figs. A.2, A.3 and A.4 show the filtered relative displacements of the building displacement response. The instantaneous system frequencies, f_p, were plotted versus time and shown in bottom parts (dashed lines and open circles) of Figs. A.2, A.3 and A.4.

In the case when the ground motions are not available, we assume the ground motions have broad band nature. This implies that the Fourier amplitude of the roof and the transfer-function are approximately equal. Based on the Fourier amplitudes of the roof motions, the band-pass frequencies can be chosen (0.20 to 1.00 Hz for San Fernando earthquake, 1.65 to 2.10 Hz for EQ71, and 1.075 to 1.975 Hz for EQ73) and the changes of f_p can be evaluated. Center parts of Figs. A.2, A.3 and A.4 show the relative displacements of the building, assuming there is no recording of base motion. Solid lines and dots in bottom parts of these figures represent the corresponding instantaneous system frequencies.

The amplitude dependent changes are shown in Fig. A.5, by plotting f_p versus the corresponding amplitude of the envelope of the analyzed data (relative rocking angle $\theta(t) = (u_{roof} - u_{base})/H_{sb}$) for two cases ("complete roof and base data" and "base data not available").

Reproduced with permission of the copyright owner. Further reproduction prohibited without permission.

Reproduced with permission of the copyright owner. Further reproduction prohibited without permission.

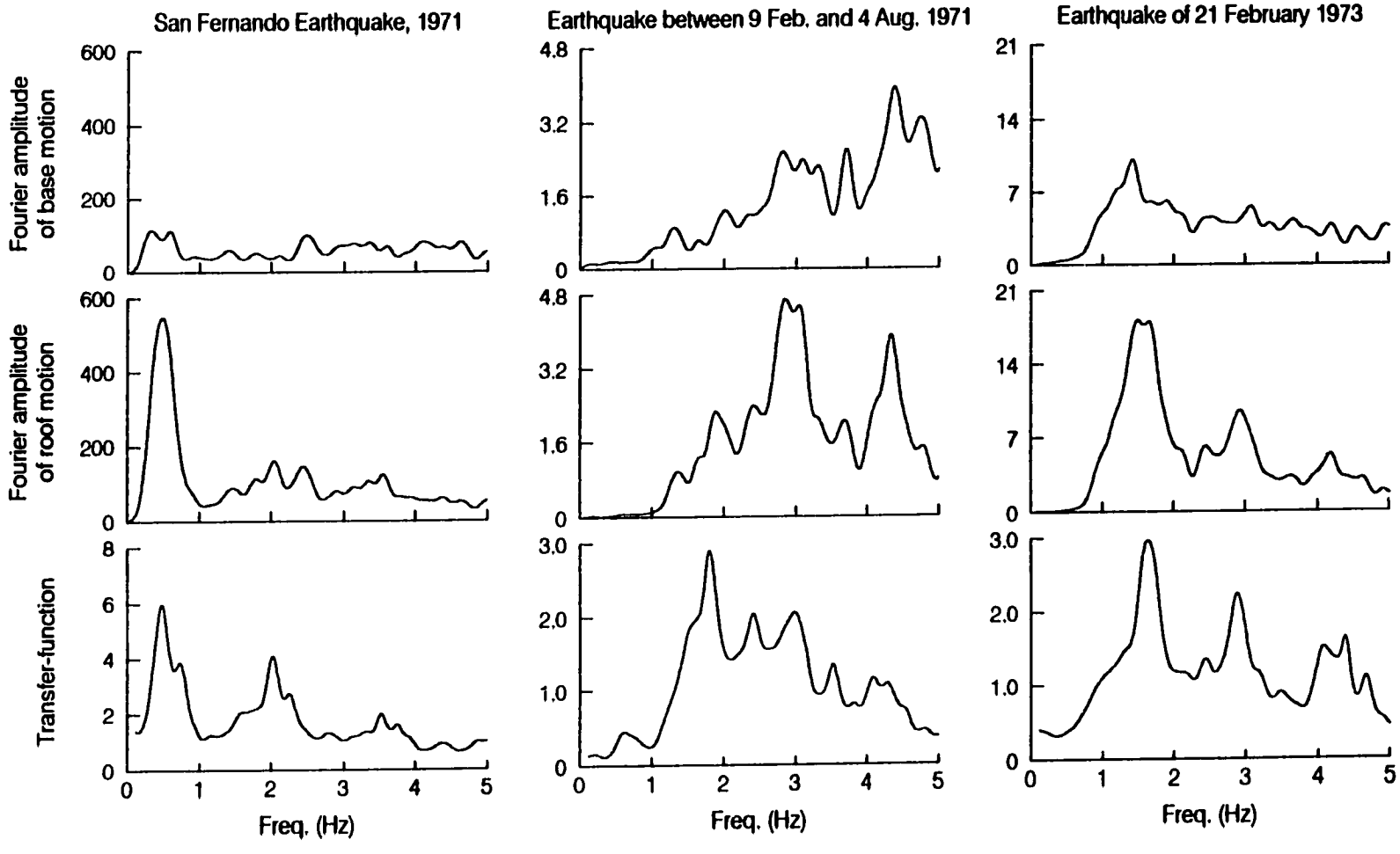

Fig. A.1 Fourier amplitudes of base and roof motions and transfer-functions of the system during 1971 San Fernando (left), EQ71 (center) and EQ73 (right) earthquakes.

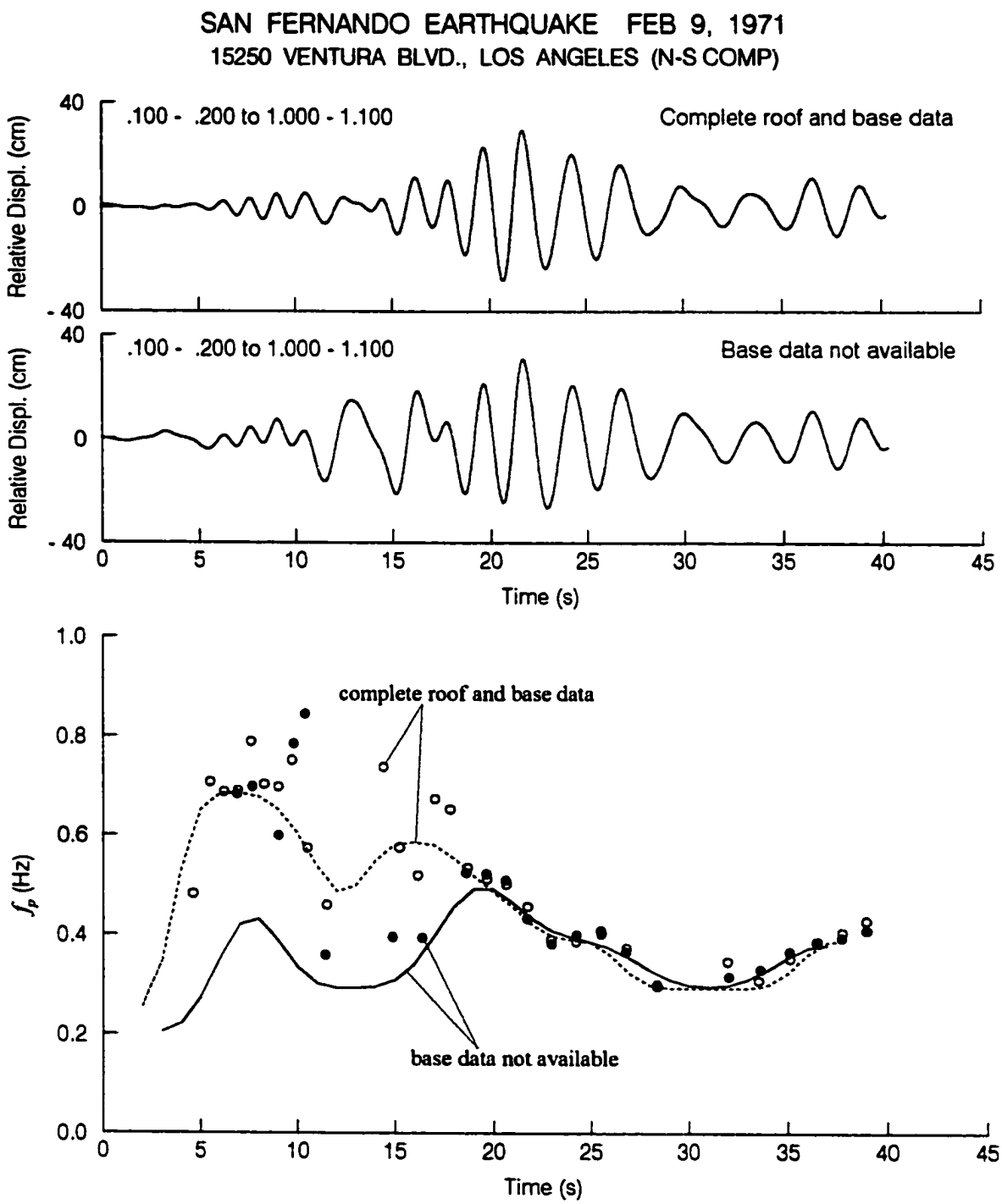

Fig. A.2 Top: the filtered relative displacement of the building with its band-pass frequencies for the case of "complete roof and base data." Center: the filtered relative displacement of the builduing with its band-pass frequencies for the case of "base data not available." Bottom: time dependet changes of the instantaneous system frequency, f_p, computed from "complete roof and base data" (dashed line and open circles) and "base data not available" (continuous line and solid dots) NS responses during the 1971 San Fernando earthquake.

Reproduced with permission of the copyright owner. Further reproduction prohibited without permission.

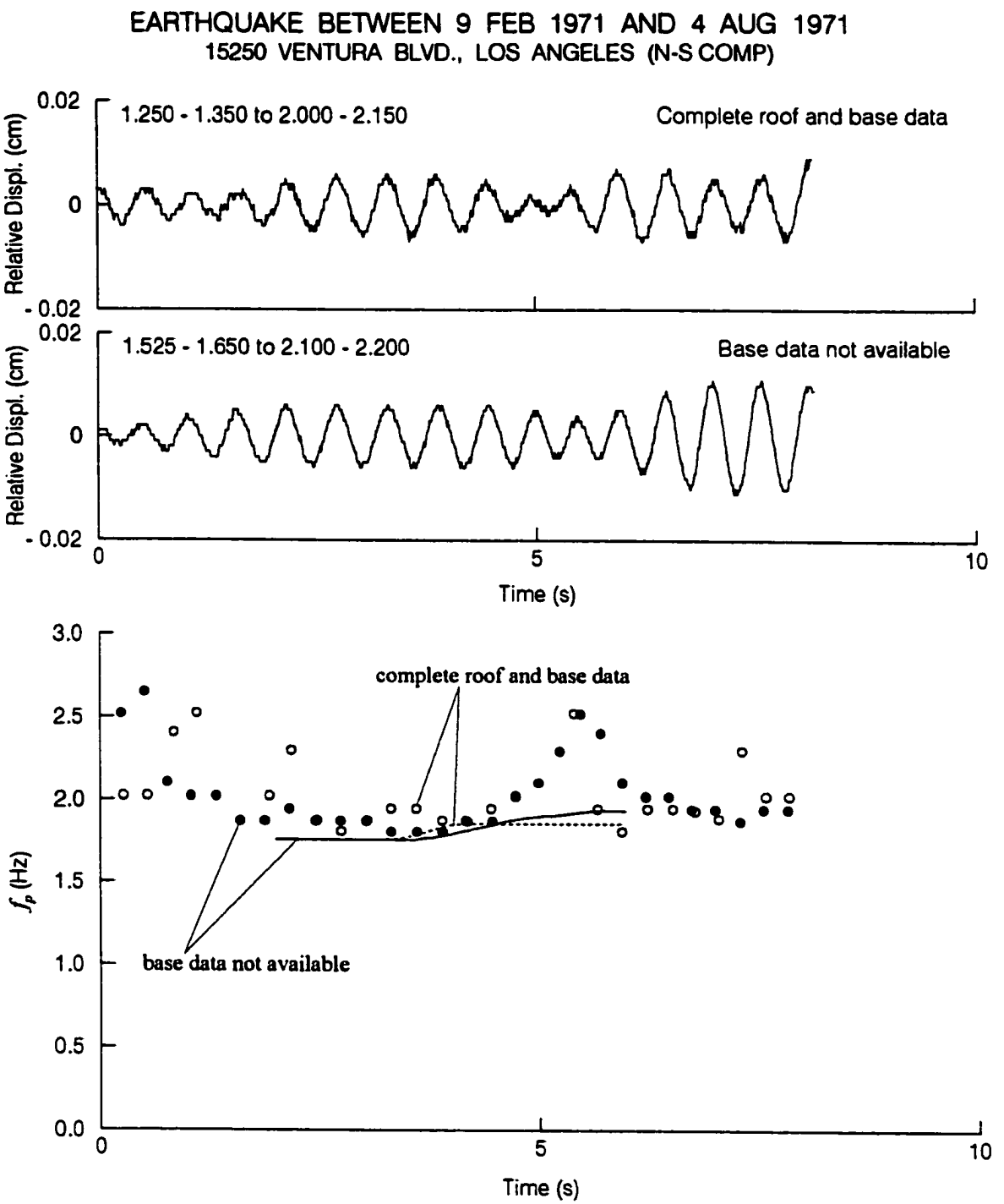

Fig. A.3 Same as Fig. A.2 but for the San Fernando aftershock between 9 Feb. and 4 Aug. 1971.

Reproduced with permission of the copyright owner. Further reproduction prohibited without permission.

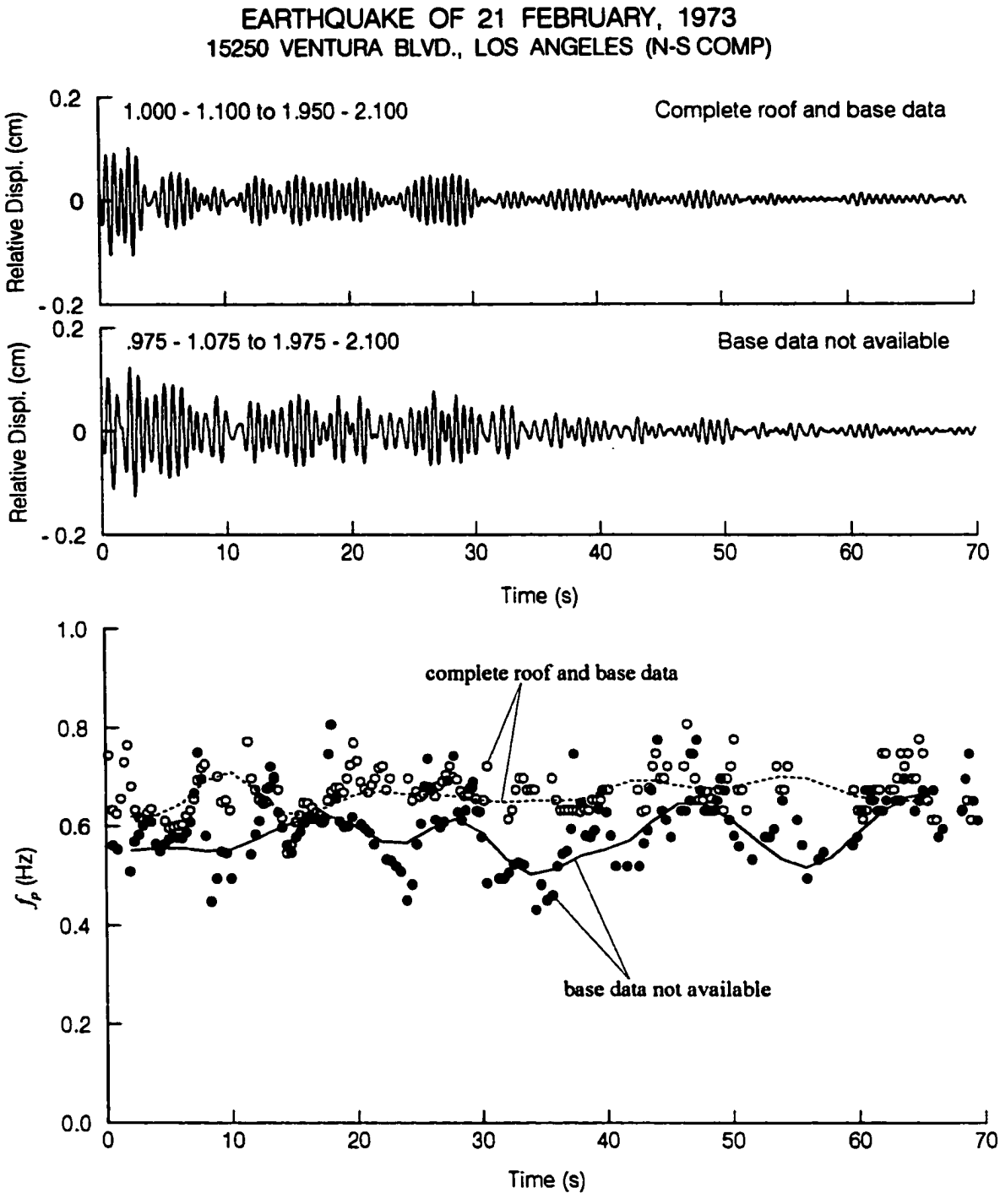

Fig. A.4 Same as Fig. A.2 but for the earthquake of 21 Feb. 1973.

Reproduced with permission of the copyright owner. Further reproduction prohibited without permission.

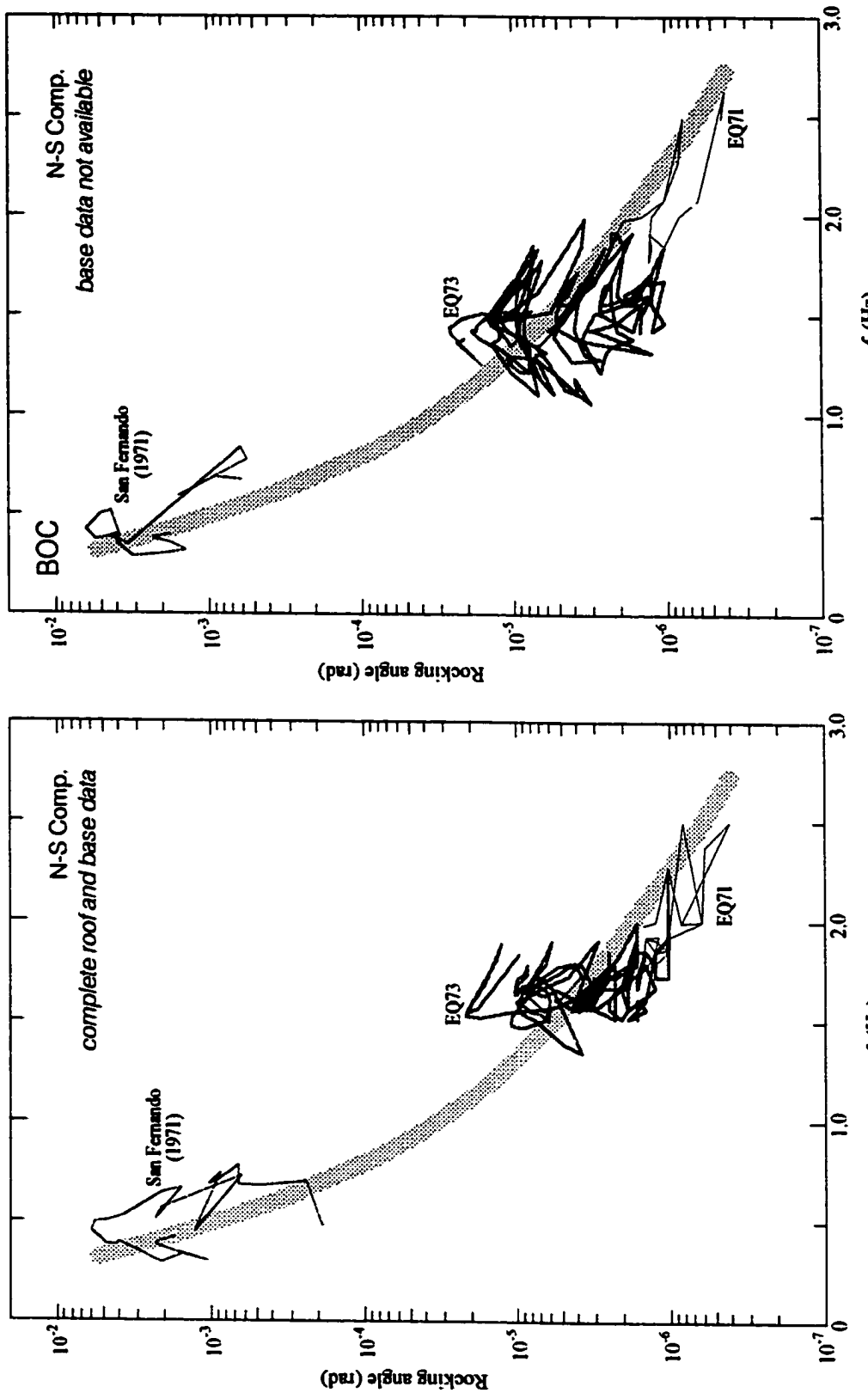

Fig. A.5 Dependence of the apparent system frequency of BOC on the peak amplitude of the NS relative responses (rocking angle). Right: response analysis with complete roof and base data. Left: response analysis without base data.

Reproduced with permission of the copyright owner. Further reproduction prohibited without permission.

It is clear that the results for the two cases are not the same. Nevertheless, the overall system responses are similar and the trends of the changes of system frequency are similar. This implies that events recorded during 1994 Northridge earthquake (roof motions only) could be used for this study. The results are approximate and valid for the overall system behavior only.

Reproduced with permission of the copyright owner. Further reproduction prohibited without permission.

APPENDIX B
EQUATION PARAMETERS

The adopted properties of the "buildings" are listed in Table B.1. There, H_{sb} and W_{sb} are the height and the width of the building. The equivalent SDOF system (shown in Fig. 2.1) is such that m_b equals the actual mass of the building (above ground level), and H and r_b are such that the moment of inertia of lumped mass about the base (point O in Fig. 2.1) equals the moment of inertia about the base of a shear-beam building model (see eqn (2.1)). Because the study was limited to planar analyses, each model was two-dimensional, and the buildings were assumed to be symmetrical, with no eccentricity between the center of mass and the center of rigidity. This assumption is considered to be reasonable because the selected buildings are essentially symmetrical geometrically with center of mass essentially coincident with the center of rigidity. The period of the equivalent SDOF oscillator was chosen to correspond to the estimate of the building first fixed-base mode, T_1. Because the building and the soil respond as a system, the period of the system, $\tilde{T}$, will be different from T_1. The period T_1 also can be estimated using the empirical formulae related to the building height, or calculated considering the mechanical properties of the modeled structure. Table B.1 also lists the properties of the equivalent rectangular foundation. There, D is the equivalent depth of the rigid foundation. In our modeling, the foundation is chosen to have the same plan dimensions as the building. It has been assumed that the density of the equivalent rectangular foundation, ρ_f, is approximately equal to the density of the building, ρ_b.

Reproduced with permission of the copyright owner. Further reproduction prohibited without permission.

Reproduced with permission of the copyright owner. Further reproduction prohibited without permission.

Table B.1 Properties of the idealized SDOF model and the idealized rectangular rigid foundation model of studied buildings.

		Longitudinal modeling				Transverse modeling				Foundation modeling				
Bldg.	m_b (kips·s^2/ft)	T_1 (s)	H_{sb} (ft)	W_{sb} (ft)	ζ_b (%)	T_1 (s)	H_{sb} (ft)	W_{sb} (ft)	ζ_b (%)	D (m)	ρ_f/ρ_b	ρ_s (kg/m^3)	β (m/s)	ν
HSB	751.64	0.500	150	215	5	1.200	150	51	5	5.50	1.00	1200	300	0.333
VN7SH	327.31	0.625	66	150	5	0.750	66	62.5	5	4.25	1.15	1200	300	0.333
BOC	595.95	0.600	160	161	5	0.625	160	60	5	5.00	1.00	1200	300	0.333
MLK	729.80	0.610	144	75	5	0.500	144	69	5	4.25	1.15	1750	450	0.333
ETEC	75.37	0.470	91.5	50	3	0.425	91.5	25	3	1.25	0.85	2250	1350	0.275

Note:

- $H = \frac{H_{sb}}{\sqrt{3}}$, $r_b = \frac{W_{sb}}{\sqrt{3}}$.
- $K_b = \frac{m_b}{T_1^2}(2\pi)^2$, $C_b = 2\zeta_b \frac{m_b}{T_1}(2\pi)$.
- the shear modulus is $G = \rho_s \times \beta^2$ for the soil medium.
- 1 kips·s^2/ft = 14.59×10^3 kg, 1 ft = 0.3048 m.

Last three columns in Table B.1 list ρ_s, β and ν, which represent the density, and shear wave velocity in the top 30 meters, and Poisson's ratio of the supporting soil.

In this work, the initial estimates of the soil spring and damping constants depend on the plan dimensions of the foundation, and on the supporting soil density and Poisson's ratio, but this is not reviewed here for brevity (classical text-book formulae can be found e.g. in Richart et al., 1970, and Wolf, 1988). Using these as initial trial values, if the predicted model response was "similar" to the recorded response in both the time and frequency domains, these constants were accepted for further use. If it was not similar to the recorded response, the estimates were modified until the predictions became similar to the recordings. Details on the adopted values of the initial soil spring constants and the associated second stiffness ratios, yielding levels and gap closure times of studied structures are listed in Table B.2. The associated damping ratios were approximated by the frequency independent formulae which can be found in Trifunac et al. (2001f).

An example of the force-deformation relations of top surface soil spring in one side of the VN7SH building, modeling EW response, for twelve recorded earthquakes is shown in Fig. B.1 (using parameters listed in Tables B.1 and B.2). The force-deformation relations are arranged in order of smallest to largest measured ground velocity, $v_{G,max}$, and plotted in log-log scale. Fig. B.2 shows how we determined the yielding levels and second stiffness ratios. Based on dynamic soil properties, the nonlinear stress-strain behavior of soils can be represented by cyclic nonlinear models that follow the actual laboratory stress-strain path during cyclic loading. A variety of

Reproduced with permission of the copyright owner. Further reproduction prohibited without permission.

Table B.2 Equation parameters of the initial soil spring constants and associated second stiffness ratios, yielding levels and gap closure times of studied structures.

Hollywood Storage building

Longitudinal modeling (EW)								
Code	Σk_h (N/m)	α_h	$u_{h,y}$ (cm)	Σk_s (N/m)	α_s	$u_{s,y}$ (cm)	K_r (N·m/rad)	Gap closure times (s)
SC	2.044×10^{12}	0.01	0.00325	2.555×10^{10}	0.10	0.00325	2.484×10^{12}	6.12, 21.98, 37.00
KC	1.067×10^{12}	0.08	0.00375	1.663×10^{11}	0.08	0.00375	5.294×10^{12}	14.75
BM	2.044×10^{12}	0.65	0.00150	2.555×10^{10}	0.65	0.00150	2.484×10^{12}	28.56, 37.25
LC	2.044×10^{12}	0.01	0.00085	2.555×10^{10}	0.05	0.00085	2.484×10^{12}	10.00
SF	1.445×10^{12}	0.00	0.00475	1.806×10^{10}	0.00	0.00475	1.242×10^{12}	
WT	1.057×10^{12}	0.00	0.00325	1.900×10^{11}	0.00	0.00325	3.971×10^{12}	11.83
LN	1.388×10^{12}	0.00	0.00325	2.494×10^{11}	0.00	0.00325	3.530×10^{12}	20.75
BB	2.044×10^{12}	0..02	0.00075	2.555×10^{10}	0.08	0.00075	2.484×10^{12}	12.12, 17.55, 22.68, 40.25
NR	1.277×10^{12}	0.00	0.00475	1.597×10^{10}	0.00	0.00475	1.552×10^{12}	18.37, 23.33

Transverse modeling (NS)								
Code	Σk_h (N/m)	α_h	$u_{h,y}$ (cm)	Σk_s (N/m)	α_s	$u_{s,y}$ (cm)	K_r (N·m/rad)	Gap closure times (s)
SC	8.479×10^{10}	0.01	0.01375	9.814×10^{8}	0.90	0.01375	2.747×10^{10}	8.65, 16.88, 40.50
KC	3.512×10^{11}	0.00	0.01625	3.990×10^{9}	0.00	0.01625	2.747×10^{10}	22.70, 36.30
BM	3.512×10^{11}	0.10	0.00682	3.990×10^{9}	0.90	0.01375	2.747×10^{10}	27.50, 32.50, 39.20
LC	1.886×10^{11}	0.75	0.00325	2.143×10^{9}	0.90	0.01375	2.747×10^{10}	9.20, 16.45
SF	2.634×10^{11}	0.20	0.01875	2.993×10^{9}	0.90	0.01375	2.747×10^{10}	16.50, 32.65
WT	3.512×10^{11}	0.20	0.0300	3.990×10^{9}	0.90	0.01375	2.747×10^{10}	9.45, 16.15
LN	3.512×10^{11}	0.25	0.00150	3.990×10^{9}	0.90	0.01375	2.747×10^{10}	13.75, 21.60, 25.40, 34.25, 39.10
BB	1.137×10^{11}	0.05	0.00625	1.663×10^{10}	0.05	0.00625	2.976×10^{10}	15.00, 21.75, 39.10
NR	3.512×10^{11}	0.02	0.01625	3.990×10^{9}	0.90	0.01375	2.747×10^{10}	19.80, 27.50, 38.50, 49.10

Reproduced with permission of the copyright owner. Further reproduction prohibited without permission.

Table B.2 (Continued)

Van Nuys 7-story hotel

Longitudinal modeling (EW)								
Code	Σk_h (N/m)	α_h	$u_{h,y}$ (cm)	Σk_s (N/m)	α_s	$u_{s,y}$ (cm)	K_r (N·m/rad)	Gap closure times (s)
1	4.020×10^{10}	0.02	0.008250	2.513×10^{9}	0.05	0.008250	1.182×10^{11}	
2	--	--	--	--	--	--	--	--
3	4.020×10^{10}	0.00	0.012375	2.513×10^{9}	0.00	0.012375	1.182×10^{11}	18.05
4	5.025×10^{10}	0.05	0.002750	3.141×10^{9}	0.10	0.002750	2.702×10^{11}	6.35, 14.60
5	4.020×10^{10}	0.15	0.003285	2.513×10^{9}	0.30	0.003285	1.182×10^{11}	14.80, 22.95
6	7.968×10^{11}	0.10	0.000175	1.901×10^{10}	0.10	0.000175	5.104×10^{11}	11.35, 15.75
7	4.020×10^{10}	0.30	0.016500	2.513×10^{9}	0.50	0.016500	1.351×10^{11}	16.90
8	4.804×10^{10}	0.05	0.006806	3.002×10^{9}	0.05	0.006808	1.701×10^{11}	
9	4.020×10^{10}	0.00	0.005156	2.513×10^{9}	0.00	0.005156	1.351×10^{11}	7.00, 15.35
10	5.976×10^{10}	0.08	0.042875	1.901×10^{9}	0.08	0.042875	3.828×10^{10}	11.20, 30.05
11A	7.968×10^{10}	0.08	0.009298	9.507×10^{9}	0.08	0.009298	1.021×10^{10}	
11B	7.968×10^{10}	0.08	0.009298	2.377×10^{9}	0.08	0.009298	1.028×10^{10}	9.25, 14.25
12	5.817×10^{10}	0.08	0.006431	3.740×10^{8}	0.08	0.006431	3.509×10^{10}	7.65, 11.35, 22.80

Transverse modeling (NS)								
Code	Σk_h (N/m)	α_h	$u_{h,y}$ (cm)	Σk_s (N/m)	α_s	$u_{s,y}$ (cm)	K_r (N·m/rad)	Gap closure times (s)
1	3.518×10^{10}	0.01	0.031875	1.205×10^{10}	0.02	0.031875	4.923×10^{10}	20.50
2	2.892×10^{10}	0.03	0.023756	3.769×10^{9}	0.03	0.0023756	5.504×10^{10}	
3	7.805×10^{10}	0.01	0.004050	3.803×10^{10}	0.01	0.004050	9.516×10^{10}	11.50, 19.25
4	3.484×10^{10}	0.20	0.004147	3.769×10^{9}	0.35	0.004147	9.561×10^{10}	21.25
5	5.025×10^{10}	0.02	0.006736	3.769×10^{9}	0.02	0.006736	9.127×10^{10}	
6	9.756×10^{10}	0.05	0.000675	9.507×10^{10}	0.05	0.000675	2.284×10^{11}	
7	3.811×10^{10}	0.02	0.009282	2.513×10^{9}	0.05	0.009282	7.771×10^{10}	
8	1.525×10^{10}	0.02	0.033408	1.884×10^{9}	0.02	0.0033408	4.195×10^{10}	
9	2.189×10^{10}	0.00	0.005336	1.368×10^{9}	0.00	0.005336	5.628×10^{10}	8.35
10	1.506×10^{10}	0.02	0.049500	7.336×10^{9}	0.05	0.049500	1.702×10^{10}	37.30
11A	8.781×10^{9}	0.25	0.041302	4.753×10^{9}	0.25	0.041302	8.029×10^{9}	
11B	1.561×10^{10}	0.01	0.015188	9.507×10^{9}	0.01	0.015188	8.029×10^{9}	3.80, 8.75, 15.45
12	1.238×10^{10}	0.01	0.011240	2.848×10^{9}	0.01	0.012240	2.808×10^{9}	6.70, 10.60

Reproduced with permission of the copyright owner. Further reproduction prohibited without permission.

Table B.2 (Continued)

Bank of California

Longitudinal modeling (NS)								
Code	Σk_h (N/m)	α_h	$u_{h,y}$ (cm)	Σk_s (N/m)	α_s	$u_{s,y}$ (cm)	K_r (N·m/rad)	Gap closure times (s)
SF	7.057×10^{10}	0.08	0.38750	1.230×10^{8}	0.08	0.38750	1.268×10^{12}	23.42, 32.51
EQ71	1.129×10^{12}	0.43	0.00015	1.968×10^{10}	0.43	0.00015	6.339×10^{13}	
EQ73	1.411×10^{11}	0.43	0.00125	2.460×10^{9}	0.43	0.00125	1.268×10^{13}	14.00, 37.50

Transverse modeling (EW)								
Code	Σk_h (N/m)	α_h	$u_{h,y}$ (cm)	Σk_s (N/m)	α_s	$u_{s,y}$ (cm)	K_r (N·m/rad)	Gap closure times (s)
SF	4.705×10^{10}	0.18	0.37500	8.201×10^{8}	0.18	0.37500	6.339×10^{8}	
EQ71	2.306×10^{11}	0.04	0.00060	3.937×10^{10}	0.20	0.00060	6.339×10^{12}	
EQ73	2.823×10^{11}	0.43	0.00375	4.921×10^{9}	0.43	0.00375	5.388×10^{12}	20.00, 37.50

Millikan Library

Longitudinal modeling (EW)								
Code	Σk_h (N/m)	α_h	$u_{h,y}$ (cm)	Σk_s (N/m)	α_s	$u_{s,y}$ (cm)	K_r (N·m/rad)	Gap closure times (s)
LC	6.010×10^{10}	0.04	0.00165	1.203×10^{10}	0.20	0.00125	5.939×10^{12}	
SF	3.803×10^{10}	0.10	0.05878	7.613×10^{8}	0.35	0.05878	2.506×10^{12}	32.11
WT	1.864×10^{10}	0.04	0.05124	8.253×10^{7}	0.20	0.02562	1.233×10^{12}	17.22, 27.23
WA	1.864×10^{10}	0.01	0.03725	8.253×10^{7}	0.10	0.01242	1.233×10^{12}	8.91

Transverse modeling (NS)								
Code	Σk_h (N/m)	α_h	$u_{h,y}$ (cm)	Σk_s (N/m)	α_s	$u_{s,y}$ (cm)	K_r (N·m/rad)	Gap closure times (s)
LC	5.487×10^{10}	0.20	0.00325	6.015×10^{9}	0.43	0.00225	9.563×10^{12}	3.85
SF	3.803×10^{10}	0.20	0.03725	7.613×10^{8}	0.65	0.03725	6.488×10^{12}	13.83, 27.37
WT	1.902×10^{10}	0.04	0.18750	3.331×10^{8}	0.20	0.18750	3.083×10^{12}	5.48, 12.52
WA	1.864×10^{10}	0.04	0.08725	8.253×10^{7}	0.20	0.08725	2.467×10^{12}	4.71

Reproduced with permission of the copyright owner. Further reproduction prohibited without permission.

Table B.2 (Continued)

Santa Susana ETEC building

Longitudinal modeling (EW)								
Code	Σk_h (N/m)	α_h	$u_{h,y}$ (cm)	Σk_s (N/m)	α_s	$u_{s,y}$ (cm)	K_r (N·m/rad)	Gap closure times (s)
1	5.883×10^{11}	0.05	0.00625	4.073×10^{9}	0.50	0.00625	1.069×10^{11}	30.00
2	7.354×10^{11}	0.90	0.00025	4.073×10^{9}	0.90	0.00025	1.778×10^{11}	
3	7.354×10^{11}	0.01	0.00035	4.073×10^{9}	0.02	0.00035	8.891×10^{10}	11.50
4	5.883×10^{11}	0.90	0.00025	4.073×10^{9}	0.90	0.00025	8.891×10^{10}	
5	5.883×10^{11}	0.80	0.00065	4.073×10^{9}	0.80	0.00065	8.891×10^{10}	11.25
6	5.883×10^{11}	0.80	0.00325	4.073×10^{9}	0.80	0.00325	8.891×10^{10}	12.50
7	5.883×10^{11}	0.40	0.00425	4.073×10^{9}	0.40	0.00425	1.069×10^{11}	7.75, 15.75
8	5.883×10^{11}	0.40	0.00025	4.073×10^{9}	0.40	0.00025	1.069×10^{11}	10.00
9	5.883×10^{11}	0.90	0.00025	4.073×10^{9}	0.90	0.00025	1.069×10^{11}	
10	7.354×10^{11}	0.04	0.00055	6.109×10^{9}	0.20	0.00055	1.778×10^{11}	12.50
11	5.883×10^{11}	0.04	0.00112	4.073×10^{9}	0.40	0.00112	1.778×10^{11}	5.00, 20.75
12	7.354×10^{11}	0.40	0.00055	6.109×10^{9}	0.40	0.00055	1.778×10^{11}	

Transverse modeling (NS)								
Code	Σk_h (N/m)	α_h	$u_{h,y}$ (cm)	Σk_s (N/m)	α_s	$u_{s,y}$ (cm)	K_r (N·m/rad)	Gap closure times (s)
1	2.358×10^{11}	0.00	0.01575	4.073×10^{9}	0.04	0.03150	8.891×10^{11}	17.50
2	4.716×10^{11}	0.90	0.00060	4.073×10^{9}	0.90	0.00060	8.891×10^{11}	
3	4.716×10^{11}	0.04	0.00085	4.073×10^{9}	0.20	0.00125	7.113×10^{11}	25.00
4	4.716×10^{11}	0.20	0.00060	4.073×10^{9}	0.40	0.00060	7.113×10^{11}	
5	4.716×10^{11}	0.20	0.00115	4.073×10^{9}	0.40	0.00115	5.344×10^{11}	7.25
6	4.716×10^{11}	0.40	0.00375	4.073×10^{9}	0.65	0.00375	8.891×10^{11}	
7	4.716×10^{11}	0.40	0.00215	4.073×10^{9}	0.65	0.00425	8.891×10^{11}	
8	4.716×10^{11}	0.20	0.00100	4.073×10^{9}	0.40	0.00100	8.063×10^{11}	
9	4.716×10^{11}	0.40	0.00085	4.073×10^{9}	0.65	0.00085	7.113×10^{11}	15.60
10	4.716×10^{11}	0.20	0.00100	4.073×10^{9}	0.40	0.00100	7.113×10^{11}	
11	4.716×10^{11}	0.20	0.00375	4.073×10^{9}	0.40	0.00375	7.113×10^{11}	20.00
12	4.716×10^{11}	0.25	0.00085	4.073×10^{9}	0.65	0.00100	6.891×10^{11}	

Note:

* the soil damping constants were calculated using formulae found in Richart et al. (1970).

Reproduced with permission of the copyright owner. Further reproduction prohibited without permission.

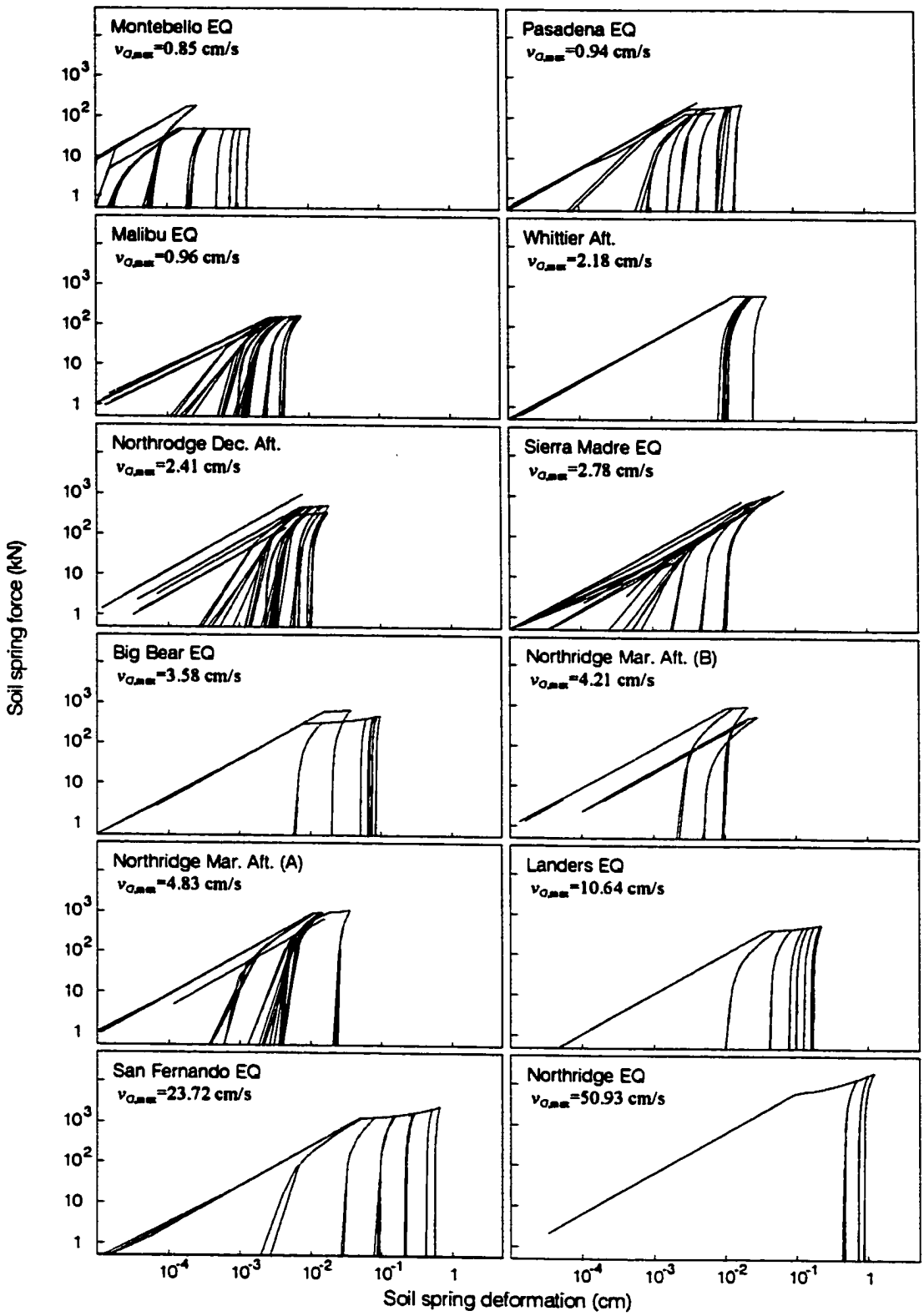

Fig. B.1 Schematical representation of the force-deformation relation of soil spring on the top surface of the VN7SH building, modeling EW response, for twelve earthquakes.

Reproduced with permission of the copyright owner. Further reproduction prohibited without permission.

Reproduced with permission of the copyright owner. Further reproduction prohibited without permission.

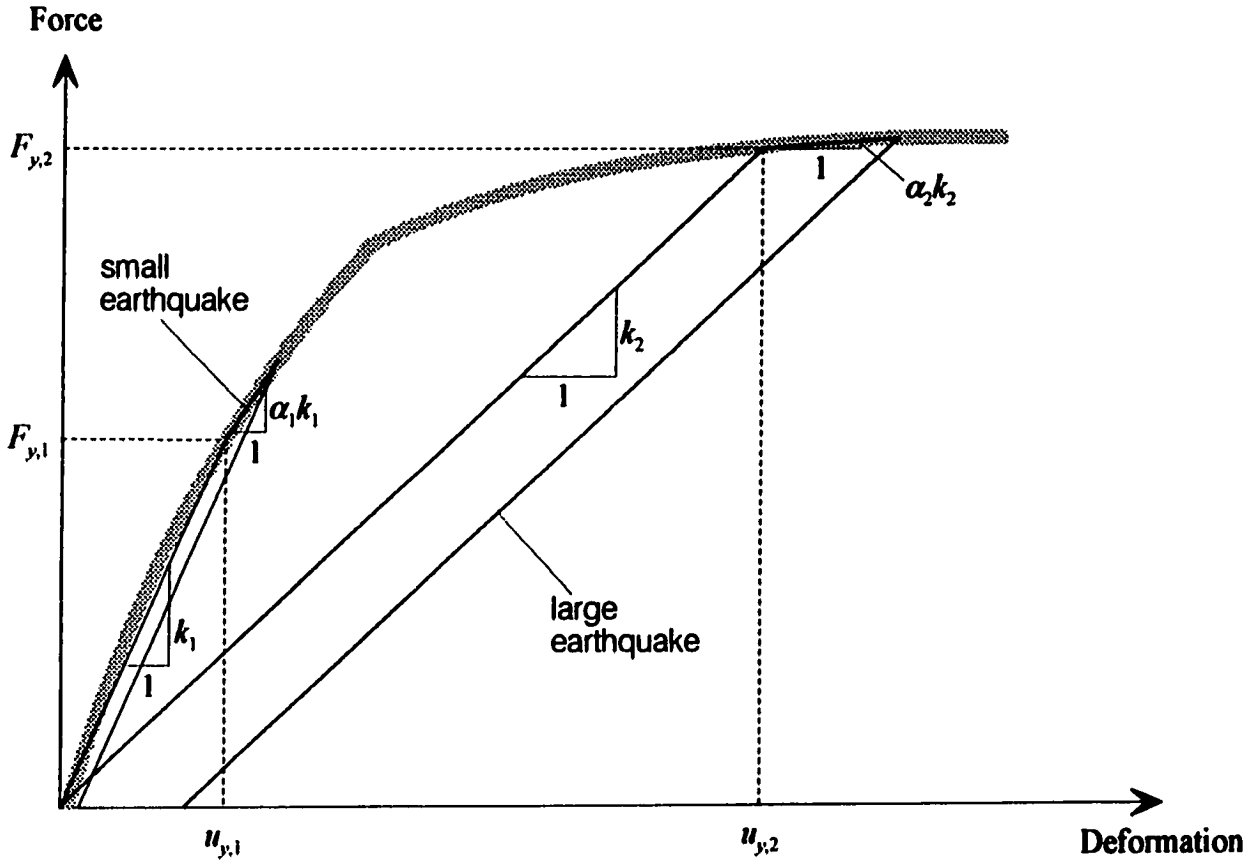

Fig. B.2 Representation of backbone curve (wide gray line) of the force-deformation behavior of cyclically loaded soils and ideal mathematical slip hysteretic loops, for small and large earthquakes respectively.

cyclic nonlinear models have been developed and can be characterized by (1) a backbone curve and (2) a series of "rules" that govern unloading-reloading behavior, stiffness degradation, and other effects. In Fig B.2, the wide gray line represents an assumed stress-strain backbone curve and two hysteretic slip loops represent the force-deformation relations for small and large earthquakes respectively.

Reproduced with permission of the copyright owner. Further reproduction prohibited without permission.

APPENDIX C
COMPARISON OF THE RECORDED AND PREDICTED RESPONSES OF THE BOC, MLK AND ETEC BUILDINGS

This appendix presents the results of simulated EW and NS responses of the BOC, MLK and ETEC buildings, using the model in Fig. 2.1 and the equation parameters listed in Tables B.1 and B.2, for earthquakes listed in Table 3.1. The top parts show comparison of the band-pass filtered relative response of recorded motions (dashed lines), and the simulated motions (solid lines). The central parts show the time dependent changes of the system frequency, f_p. The dashed line shows the changes in f_p evaluated by moving window Fourier analysis of recorded data, and the open circles show the estimates by the zero-crossing analysis also using the recorded data. The solid line and solid points show the corresponding quantities for the predicted response. The vertical arrows show the times where the gaps in the soil springs were closed. The bottom parts show comparison of the predicted total energy with the input wave energy, and the distribution of the predicted total system energy.

Reproduced with permission of the copyright owner. Further reproduction prohibited without permission.

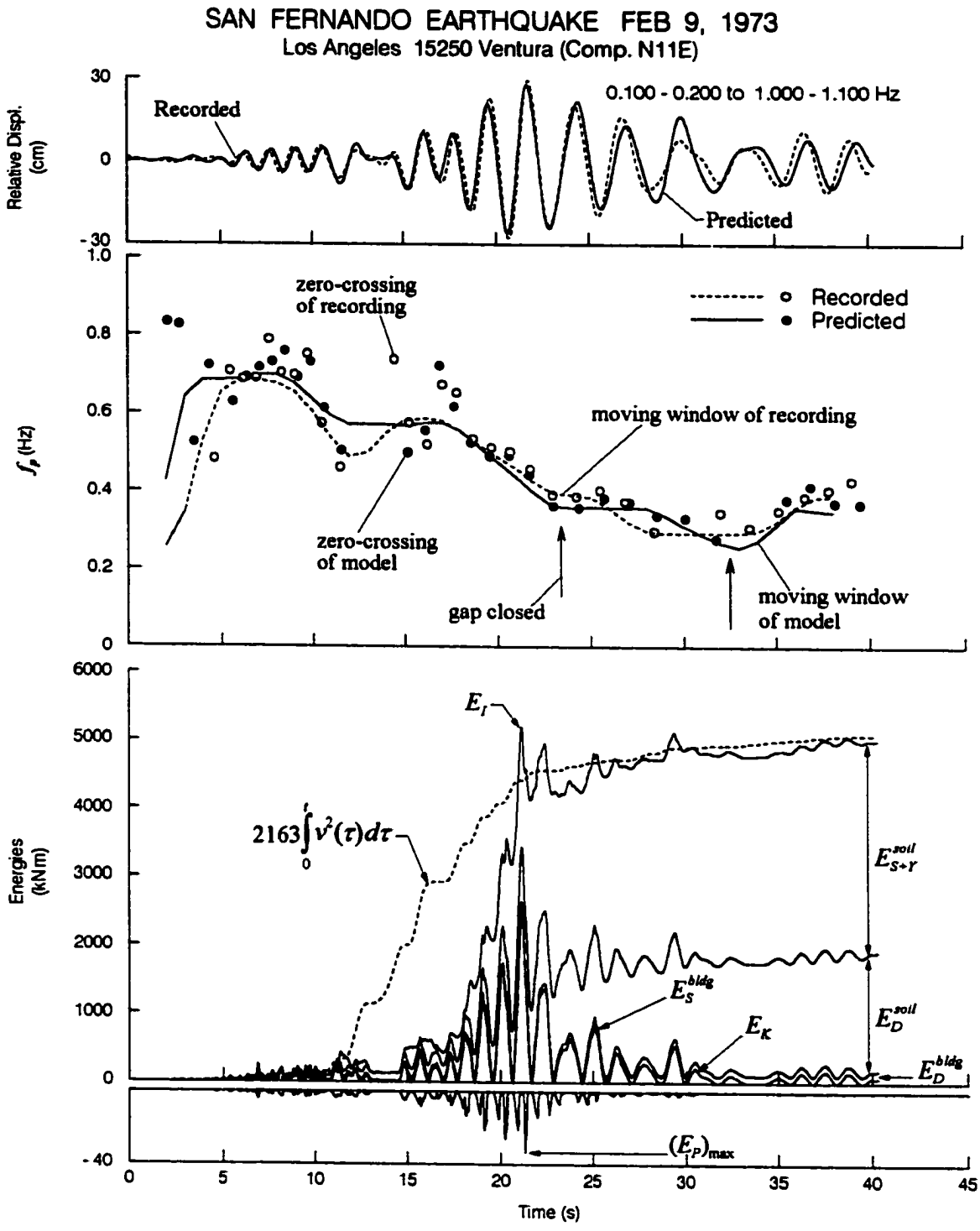

Fig. C.1a Top: comparison of recorded (dashed line) and predicted (solid line) NS relative displacement response at roof of Bank of California building during the 1971 San Fernando earthquake. Center: time dependent changes of the system frequency f_p computed from recorded (dashed line and open circles) and predicted (continuous line and solid dots) responses. Bottom: contributions to the system energy: $E_{S+\gamma}^{soil}$, E_D^{soil}, E_S^{bldg}, E_D^{bldg}, E_K and E_P and their sum E_I. Input wave energy $a_0\int_0^t v^2(\tau)d\tau$ is shown by dashed line.

Reproduced with permission of the copyright owner. Further reproduction prohibited without permission.

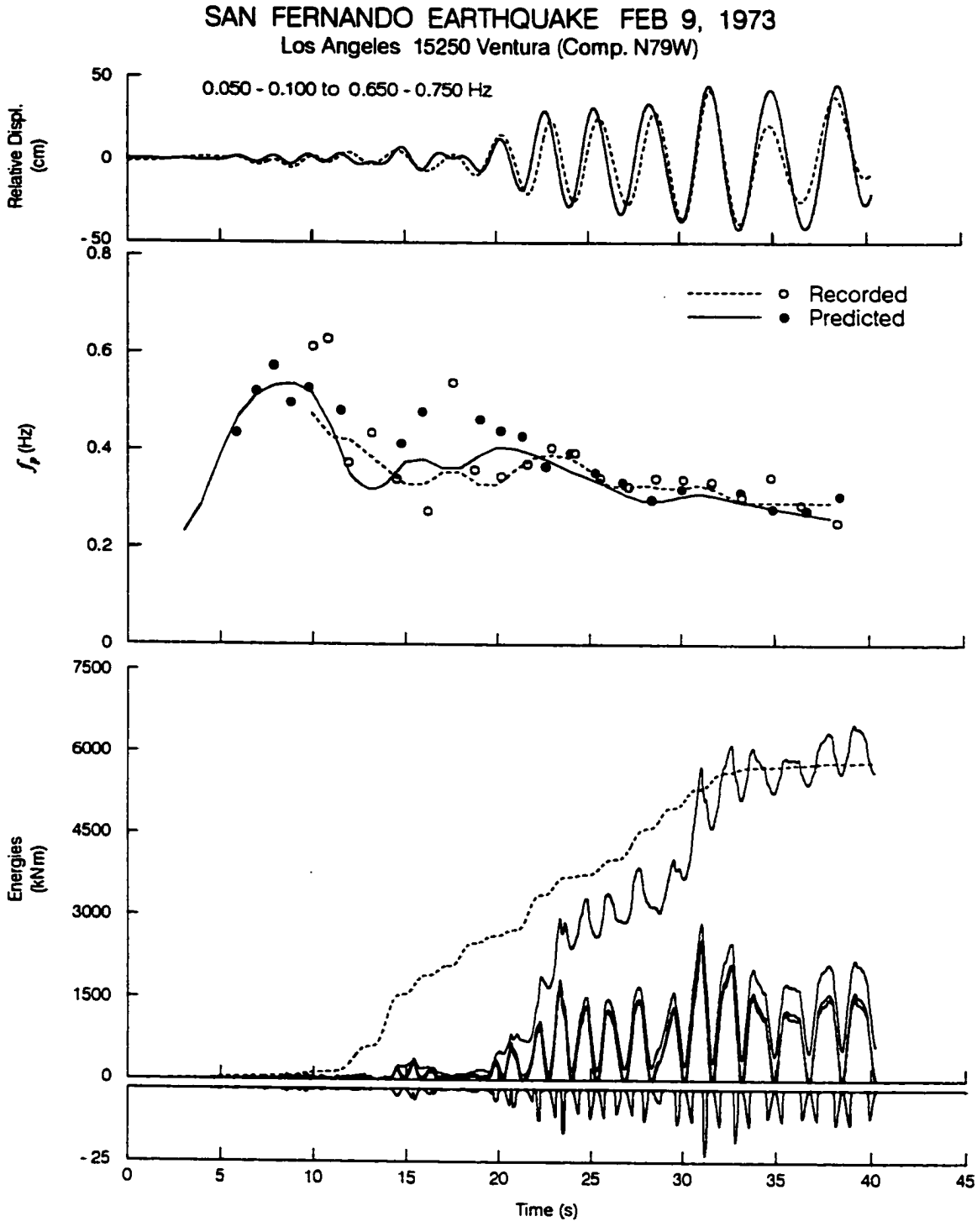

Fig. C.1b Same as Fig. C.1a, but for EW response.

Reproduced with permission of the copyright owner. Further reproduction prohibited without permission.

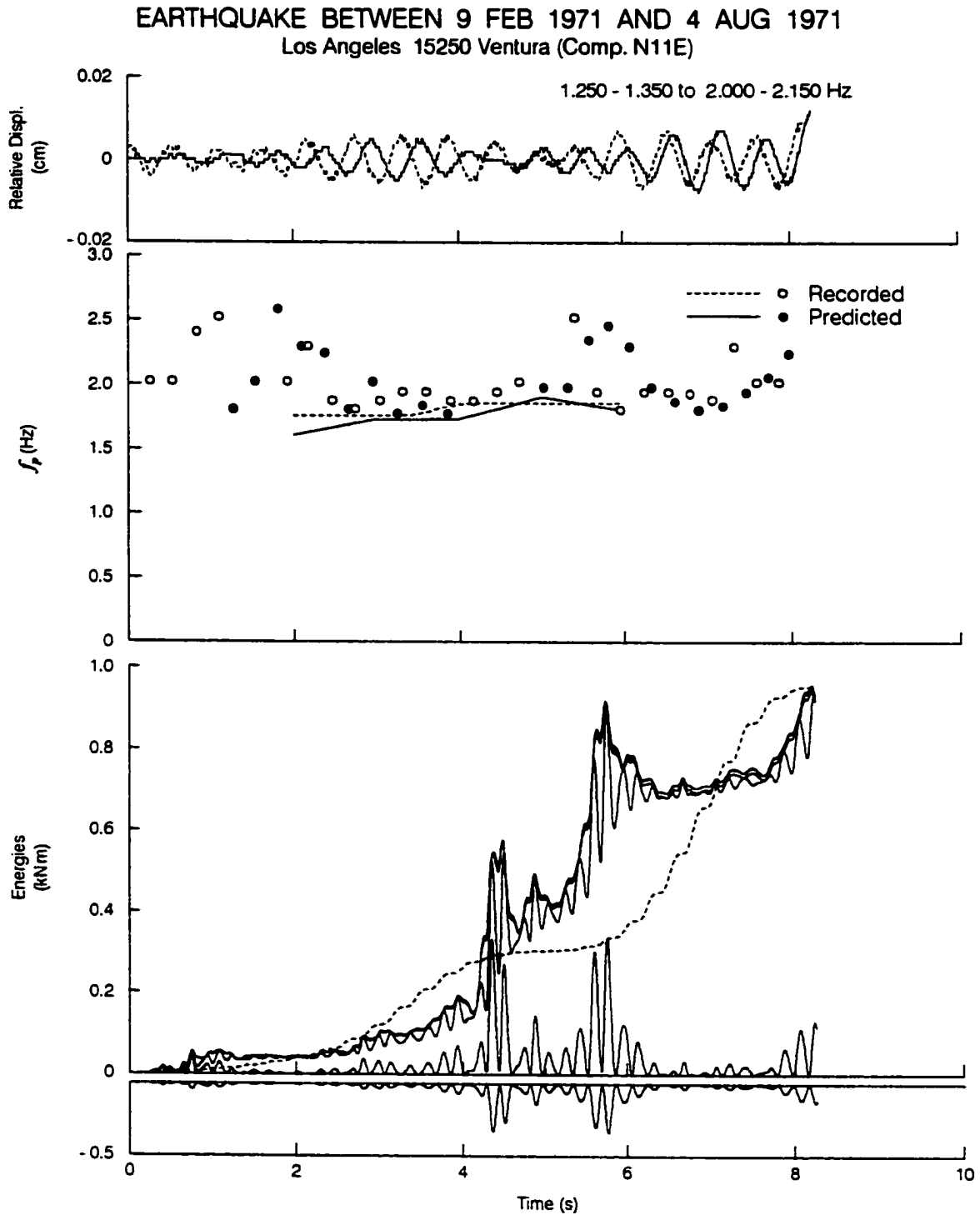

Fig. C.2a Same as Fig. C.1a, but for the San Fernando aftershock between Feb. 9 and Aug. 4, 1971.

Reproduced with permission of the copyright owner. Further reproduction prohibited without permission.

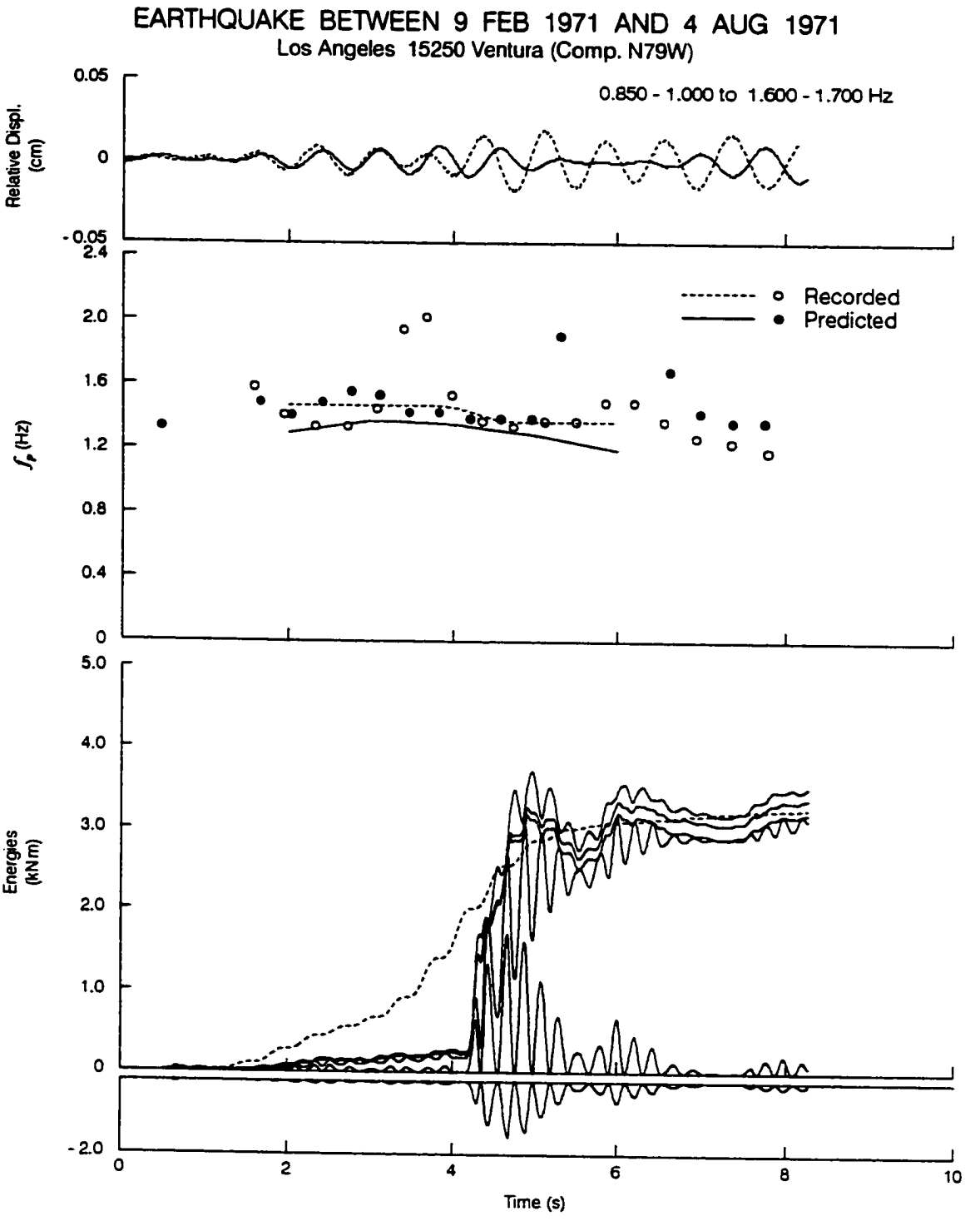

Fig. C.2b Same as Fig. C.2a, but for EW response.

Reproduced with permission of the copyright owner. Further reproduction prohibited without permission.

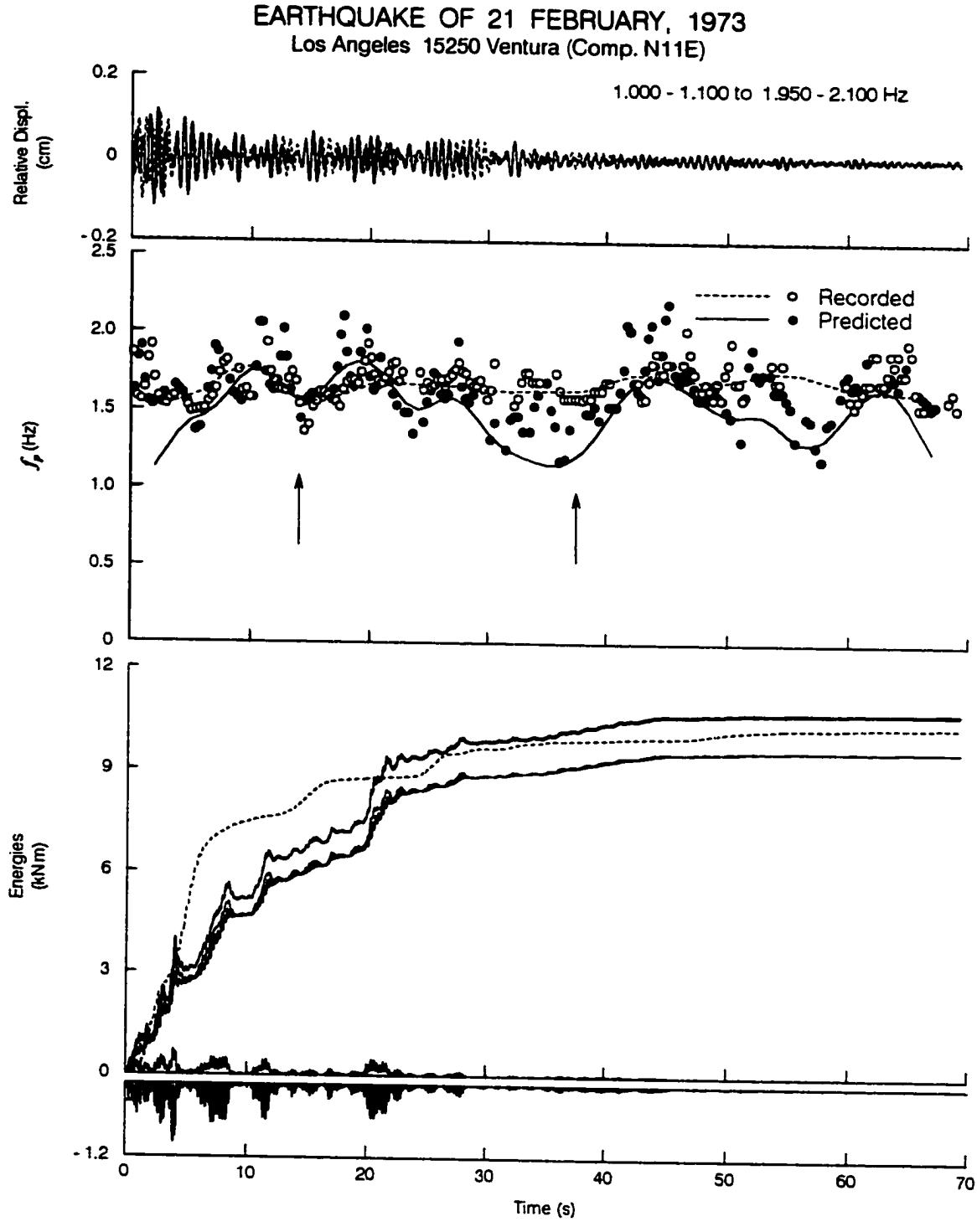

Fig. C.3a Same as Fig. C.1a, but for earthquake of 21 February, 1973.

Reproduced with permission of the copyright owner. Further reproduction prohibited without permission.

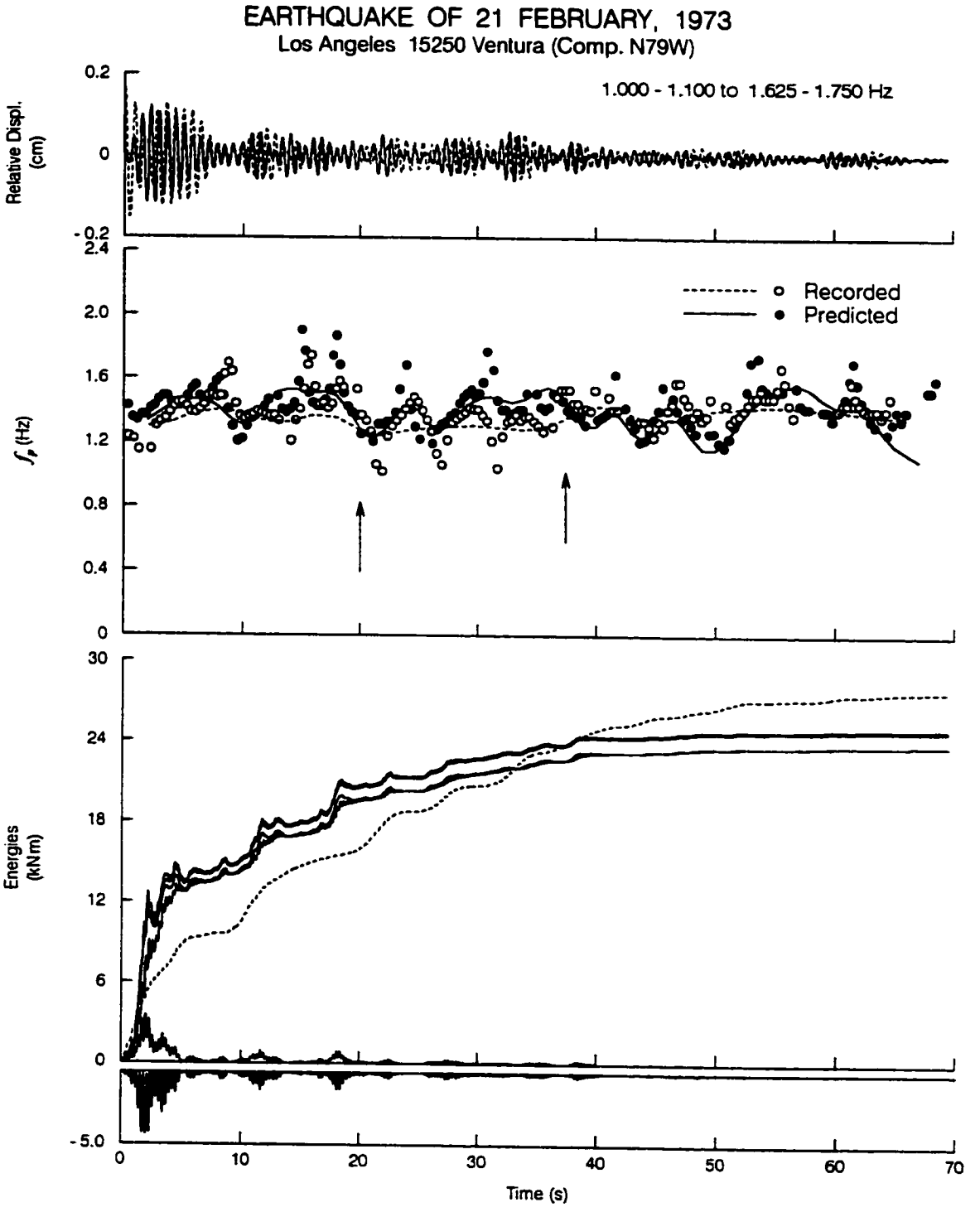

Fig. C.3b Same as Fig. C.3a, but for EW response.

Reproduced with permission of the copyright owner. Further reproduction prohibited without permission.

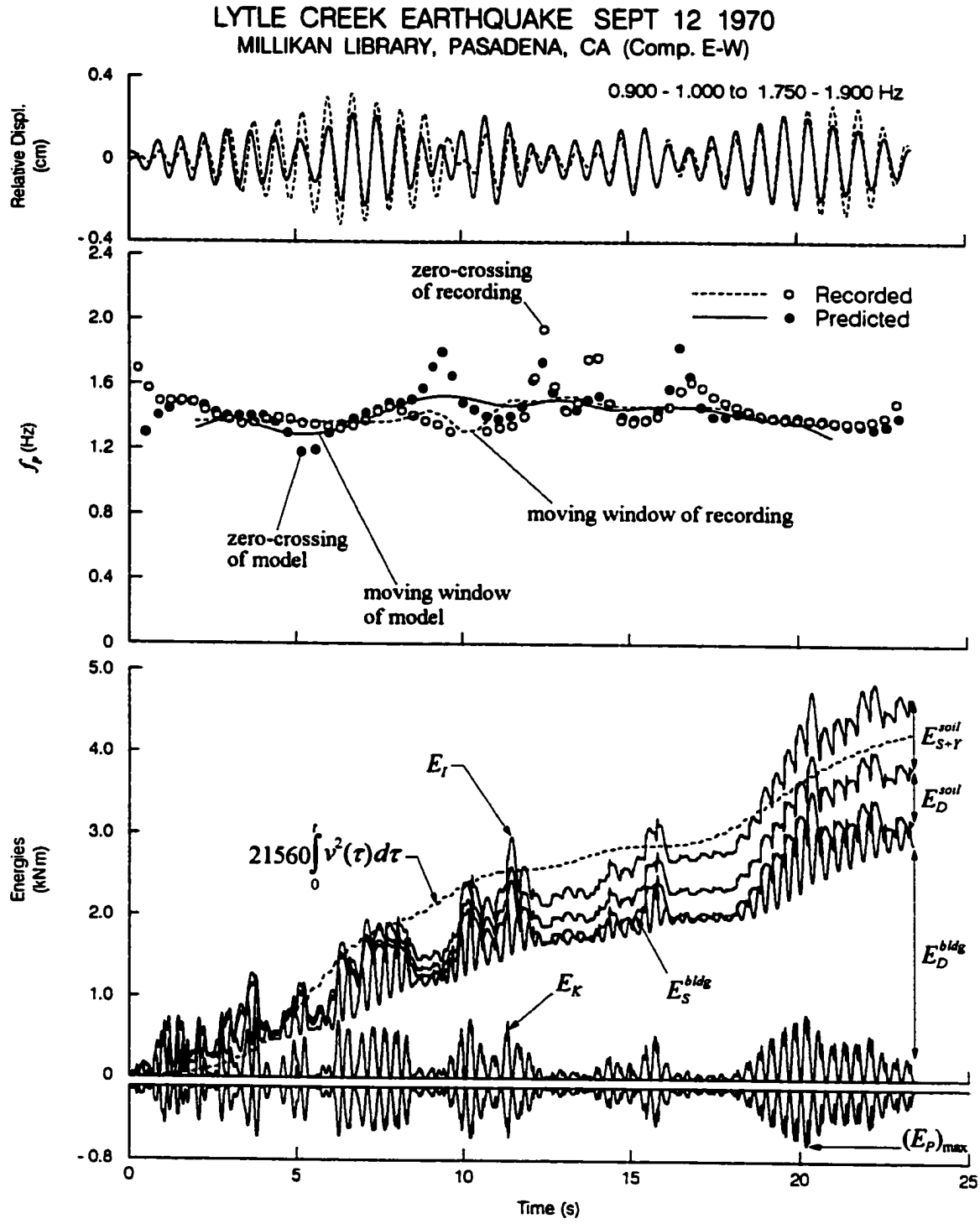

Fig. C.4a Top: comparison of recorded (dashed line) and predicted (solid line) EW relative displacement response at roof of Millikan Library building during the 1970 Lytle Creek earthquake. Center: time dependent changes of the system frequency f_p computed from recorded (dashed line and open circles) and predicted (continuous line and solid dots) responses. Bottom: contributions to the system energy: $E_{S+\gamma}^{soil}$, E_D^{soil}, E_S^{bldg}, E_D^{bldg}, E_K and E_P and their sum E_I. Input wave energy $a_0\int_0^t v^2(\tau)d\tau$ is shown by dashed line.

Reproduced with permission of the copyright owner. Further reproduction prohibited without permission.

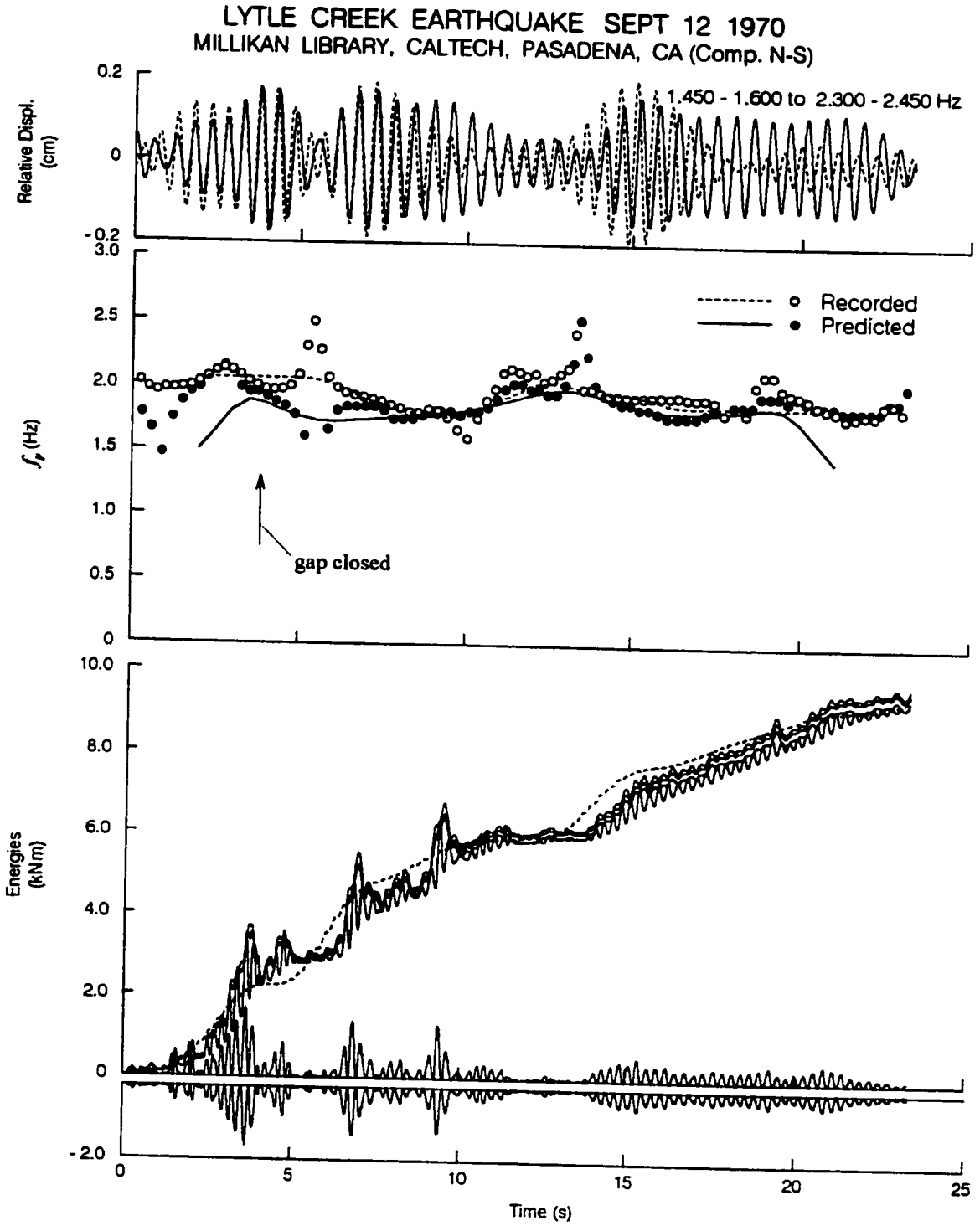

Fig. C.4b Same as Fig. C.4a, but for NS response.

Reproduced with permission of the copyright owner. Further reproduction prohibited without permission.

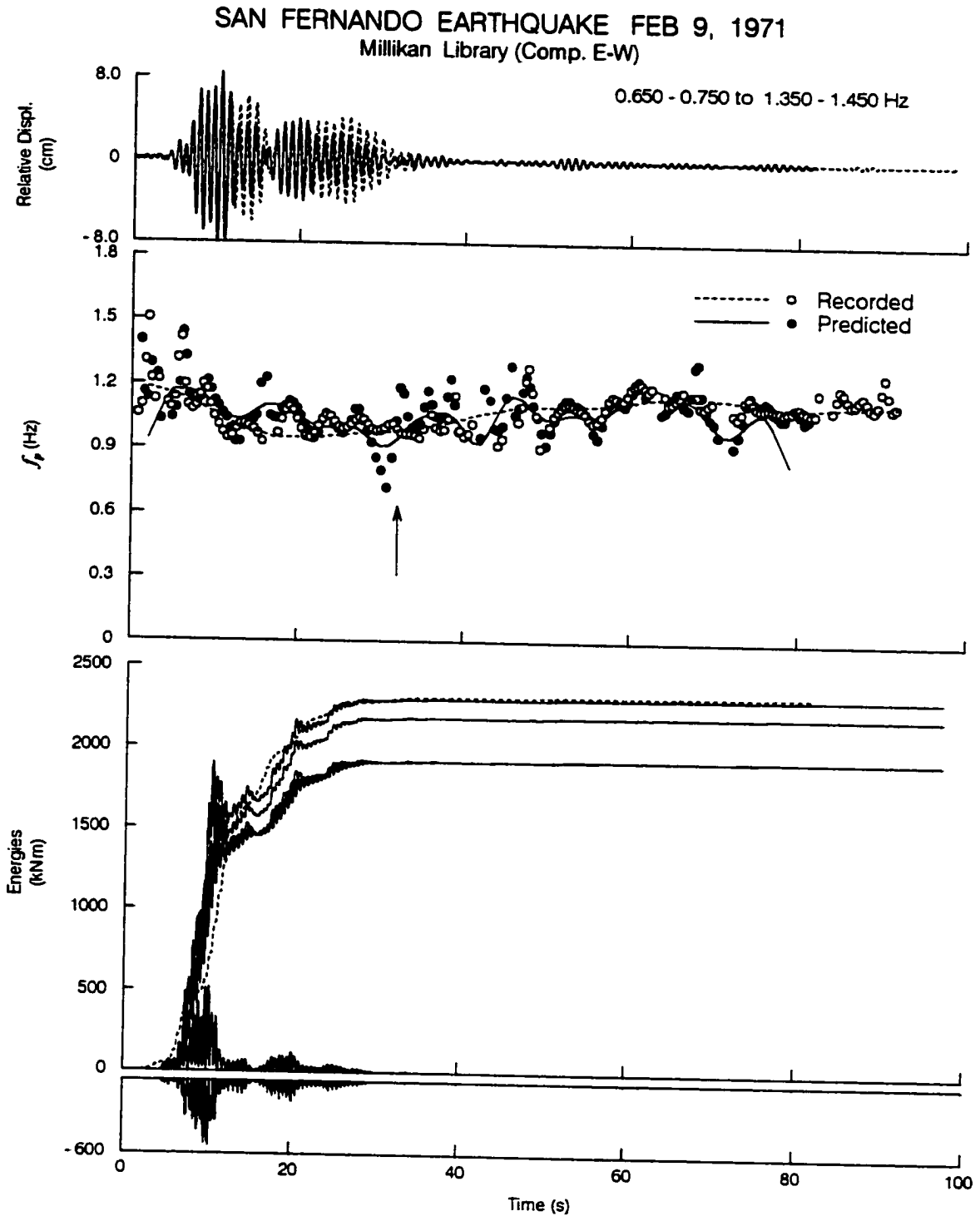

Fig. C.5a Same as Fig. C.4a, but for the 1971 San Fernando earthquake.

Reproduced with permission of the copyright owner. Further reproduction prohibited without permission.

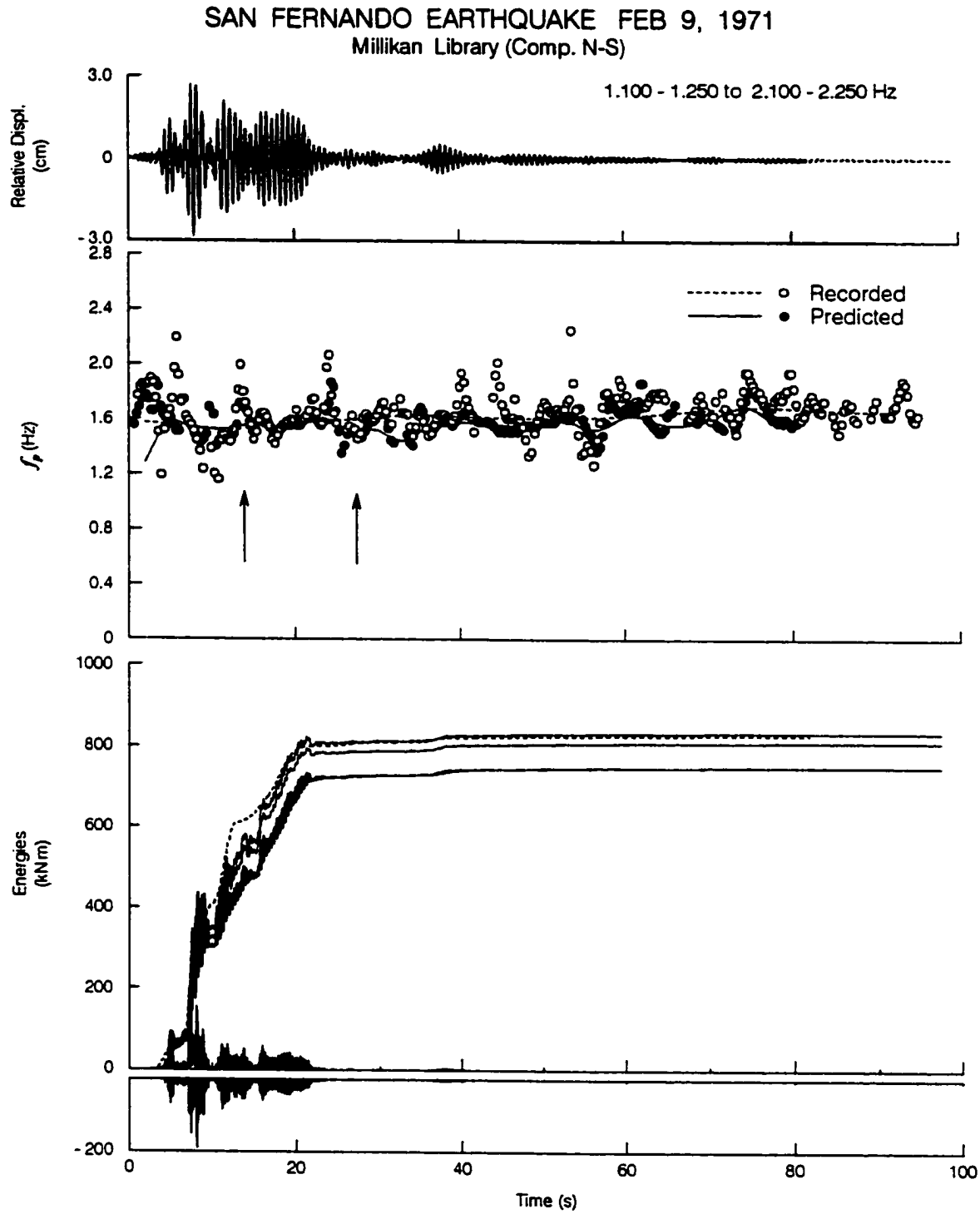

Fig. C.5b Same as Fig. C.5a, but for NS response.

Reproduced with permission of the copyright owner. Further reproduction prohibited without permission.

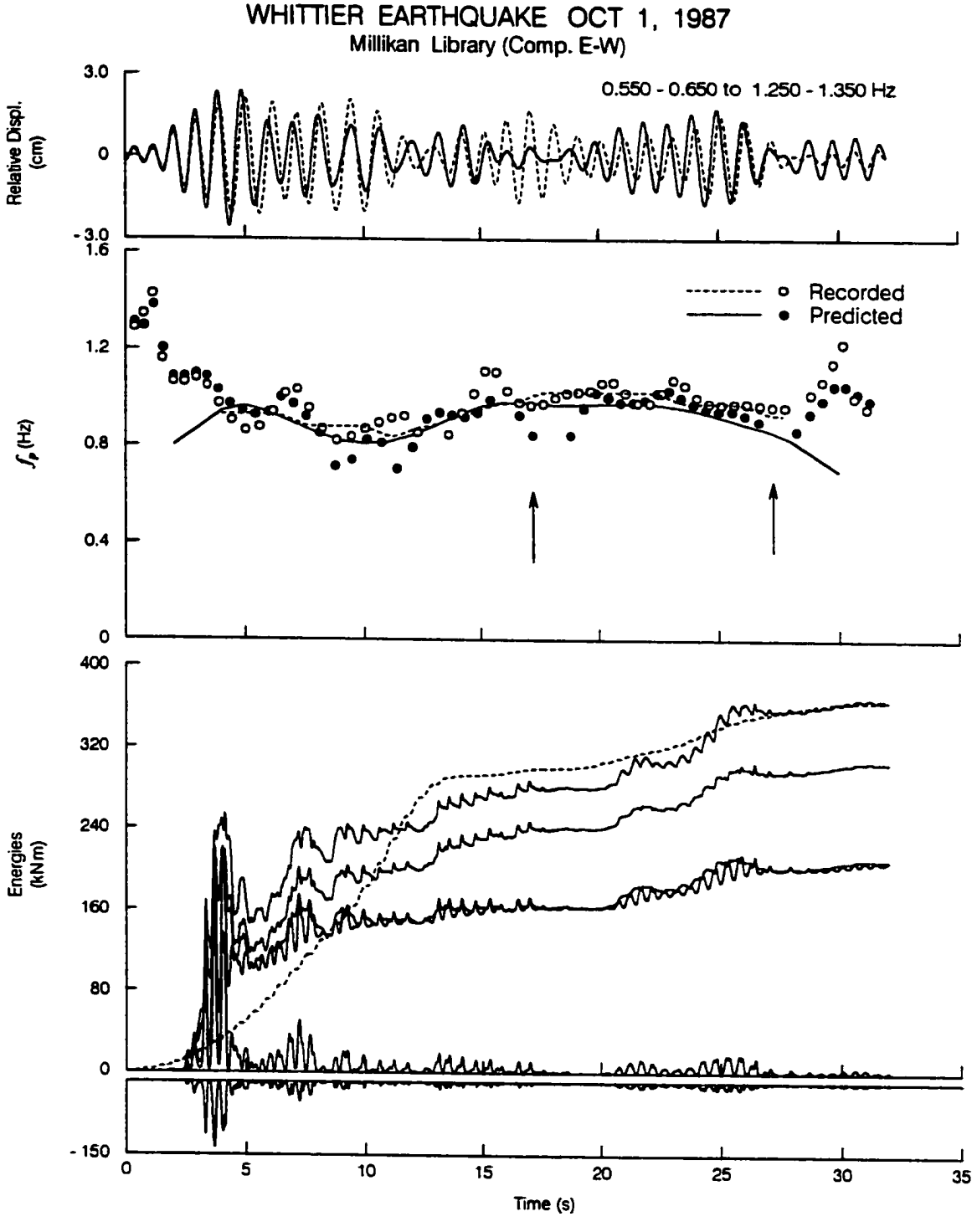

Fig. C.6a Same as Fig. C.4a, but for the 1987 Whittier-Narrows earthquake.

Reproduced with permission of the copyright owner. Further reproduction prohibited without permission.

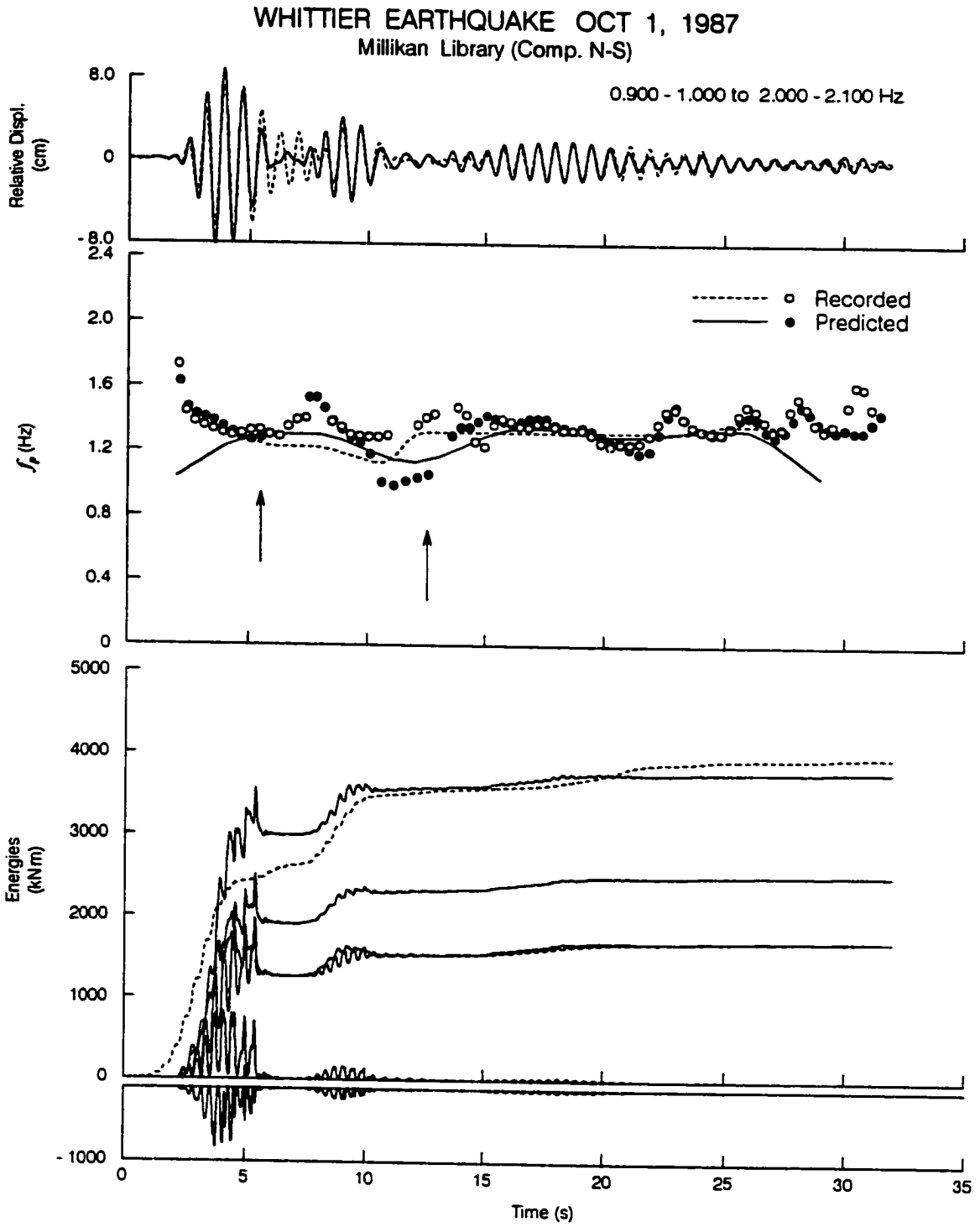

Fig. C.6b Same as Fig. C.6a, but for NS response.

Reproduced with permission of the copyright owner. Further reproduction prohibited without permission.

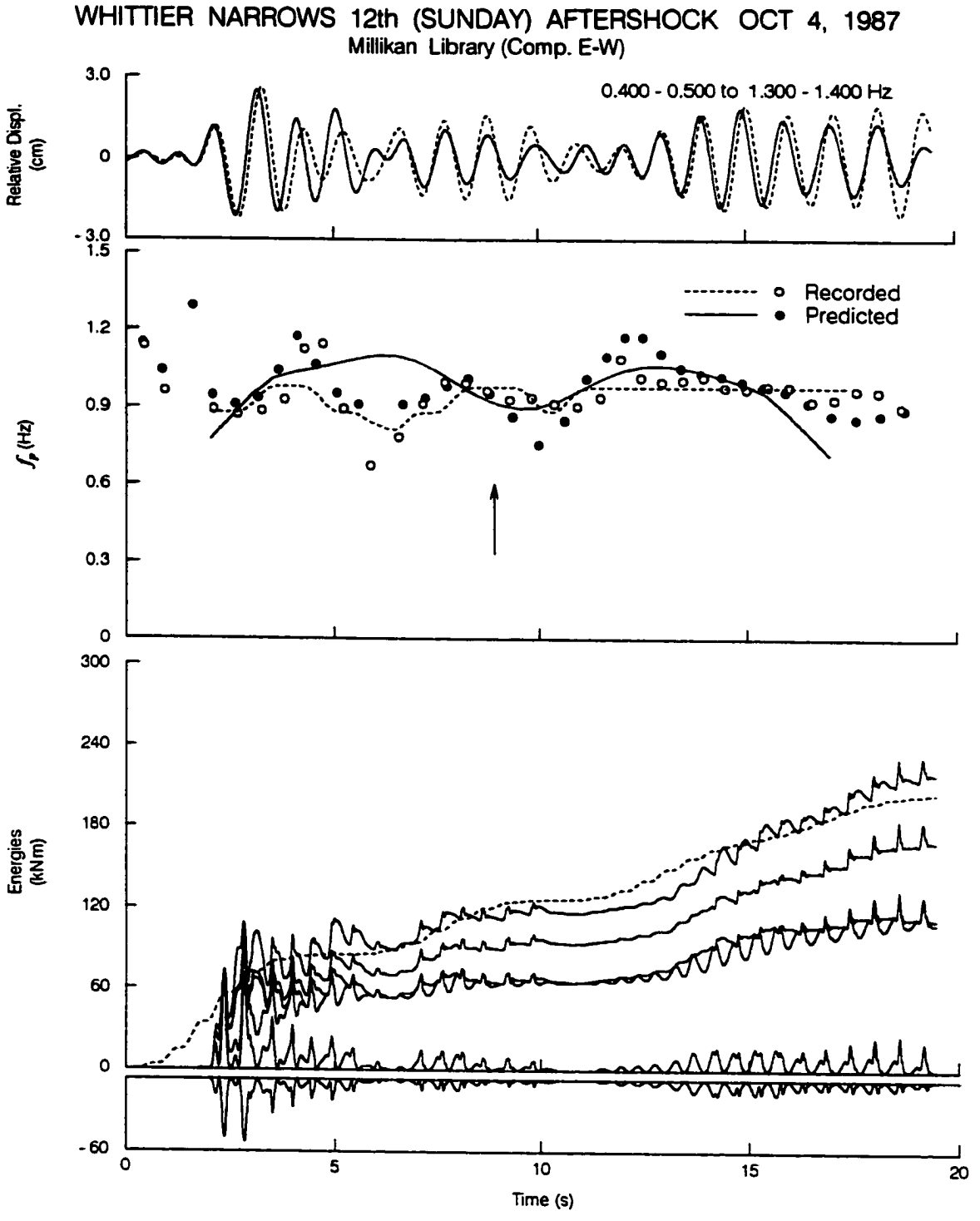

Fig. C.7a Same as Fig. C.4a, but for the 1987 Whittier -Narrows aftershock.

Reproduced with permission of the copyright owner. Further reproduction prohibited without permission.

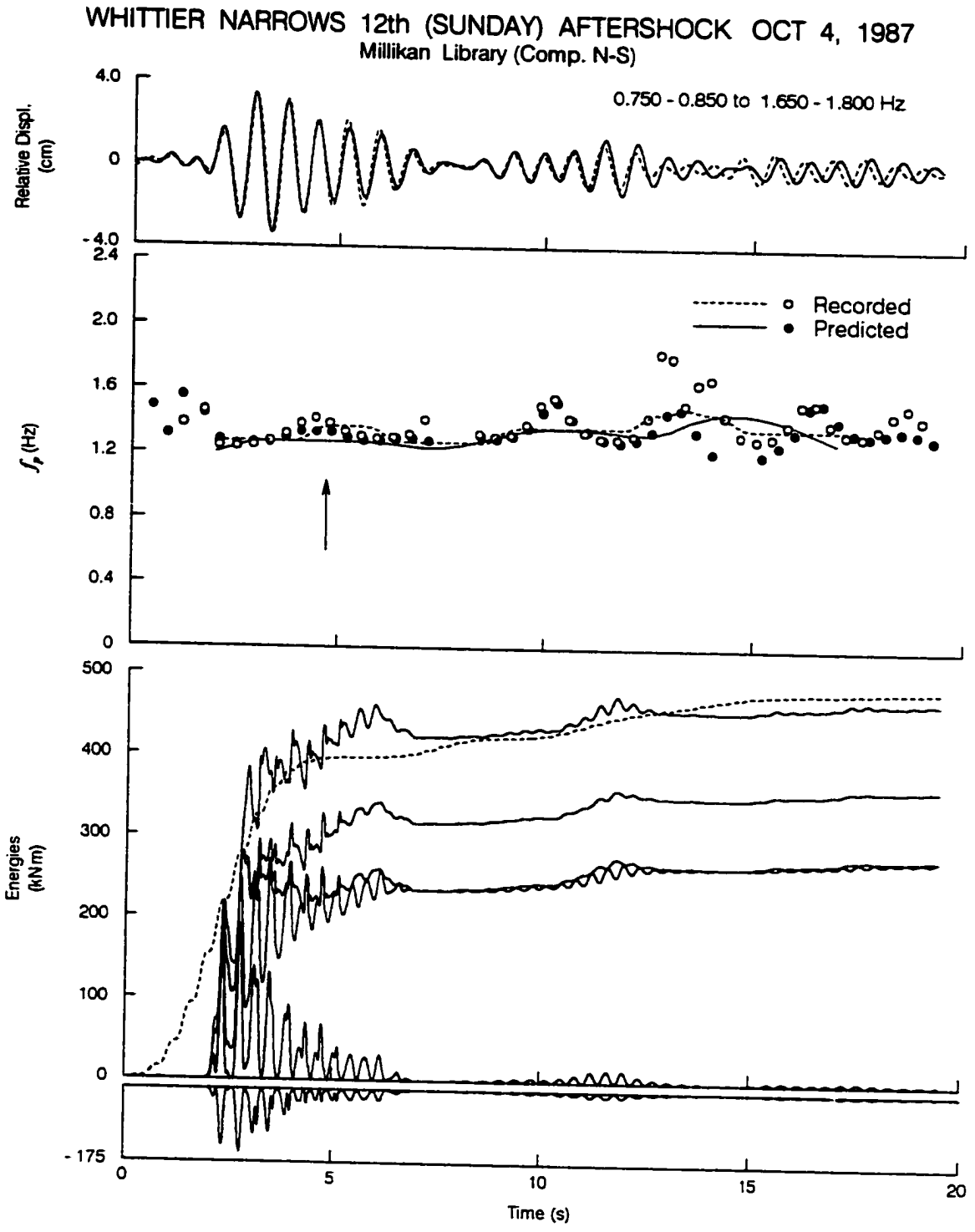

Fig. C.7b Same as Fig. C.7a, but for NS response.

Reproduced with permission of the copyright owner. Further reproduction prohibited without permission.

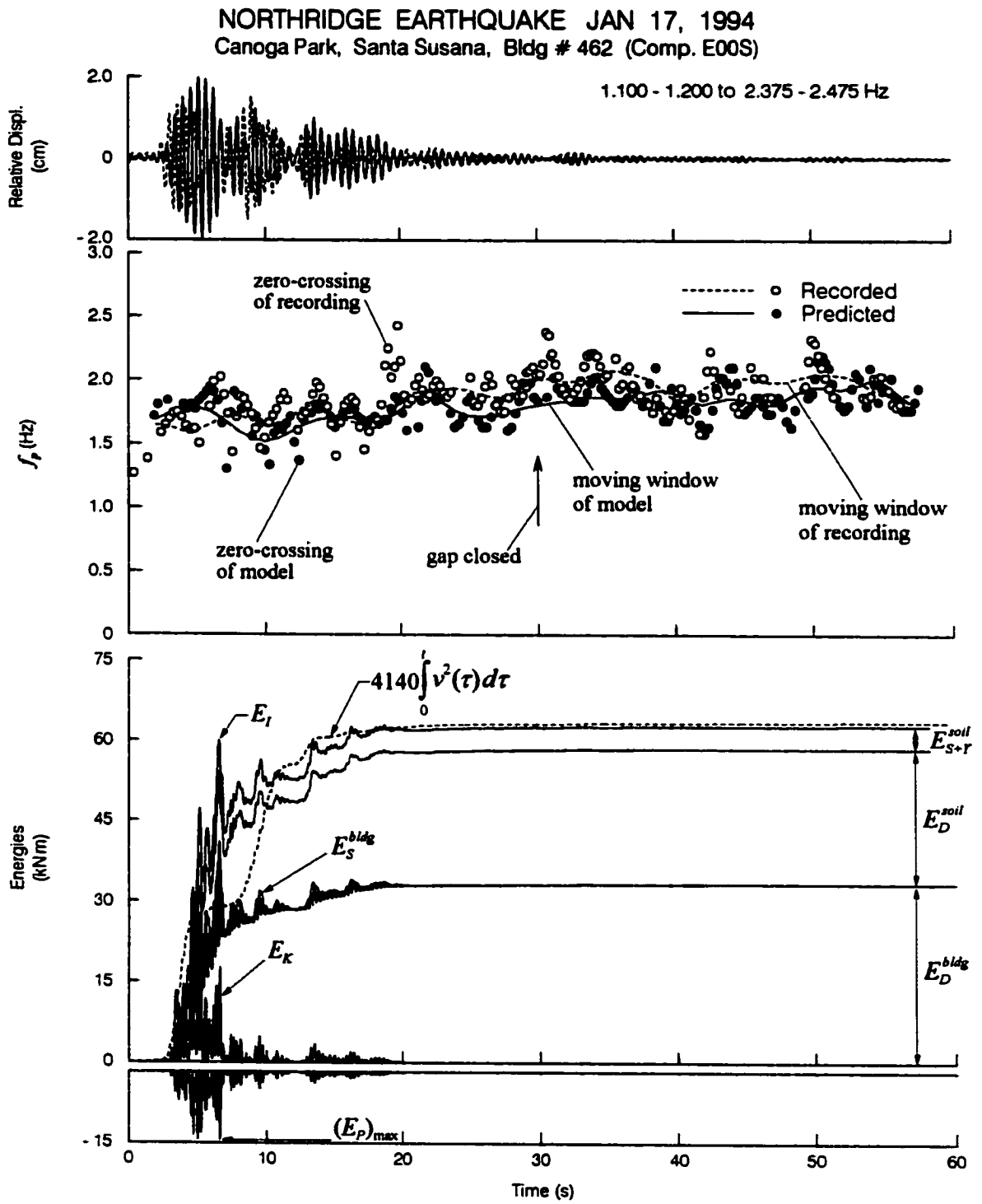

Fig. C.8a Top: comparison of recorded (dashed line) and predicted (solid line) EW relative displacement response at roof of ETEC building during the 1994 Northridge earthquake. Center: time dependent changes of the system frequency f_p computed from recorded (dashed line and open circles) and predicted (continuous line and solid dots) responses. Bottom: contributions to the system energy: E_{S+T}^{soil}, E_D^{soil}, E_S^{bldg}, E_D^{bldg}, E_K and E_P and their sum E_I. Input wave energy $a_0\int_0 v^2(\tau)d\tau$ is shown by dashed line.

Reproduced with permission of the copyright owner. Further reproduction prohibited without permission.

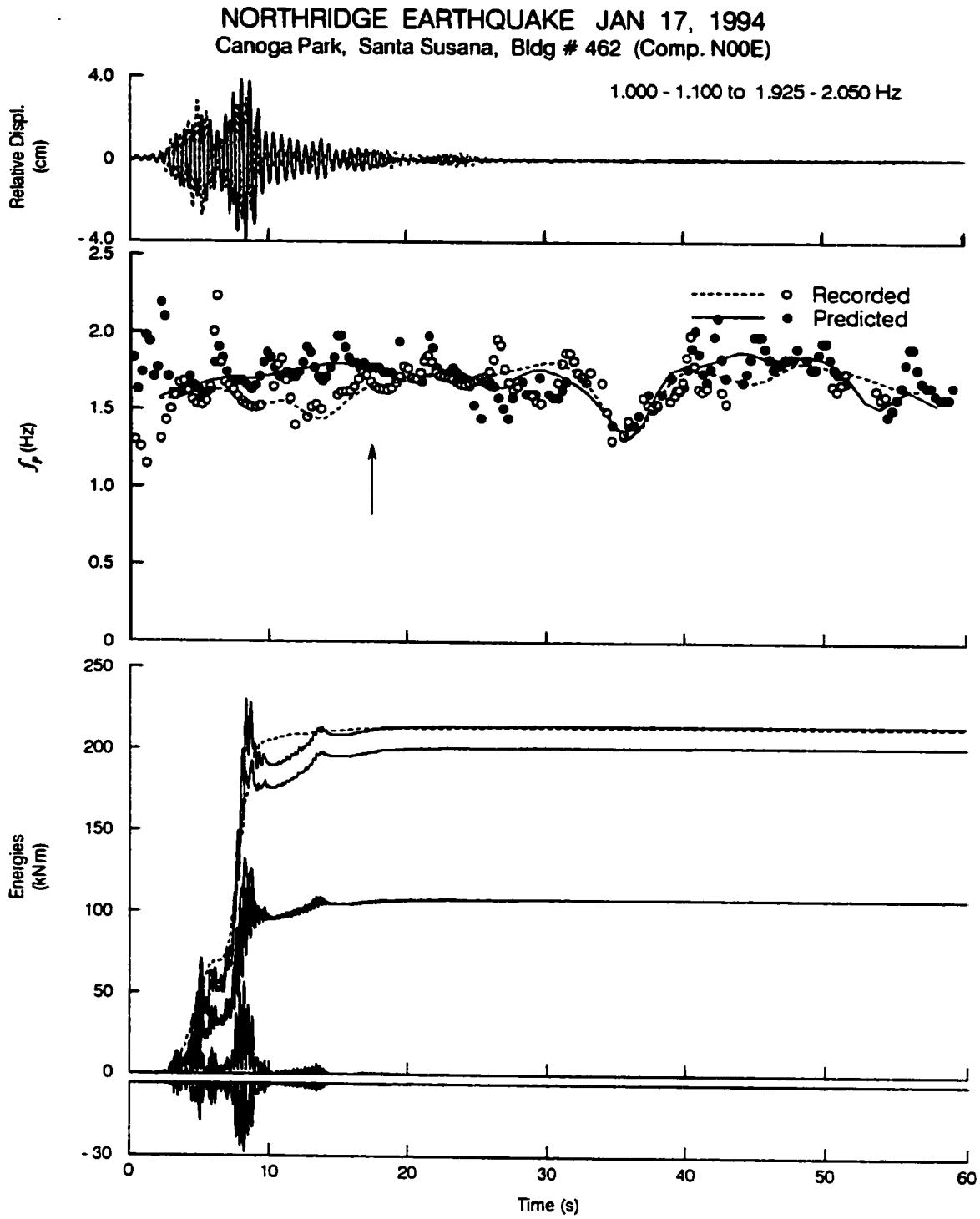

Fig. C.8b Same as Fig. C.8a, but for NS response.

Reproduced with permission of the copyright owner. Further reproduction prohibited without permission.

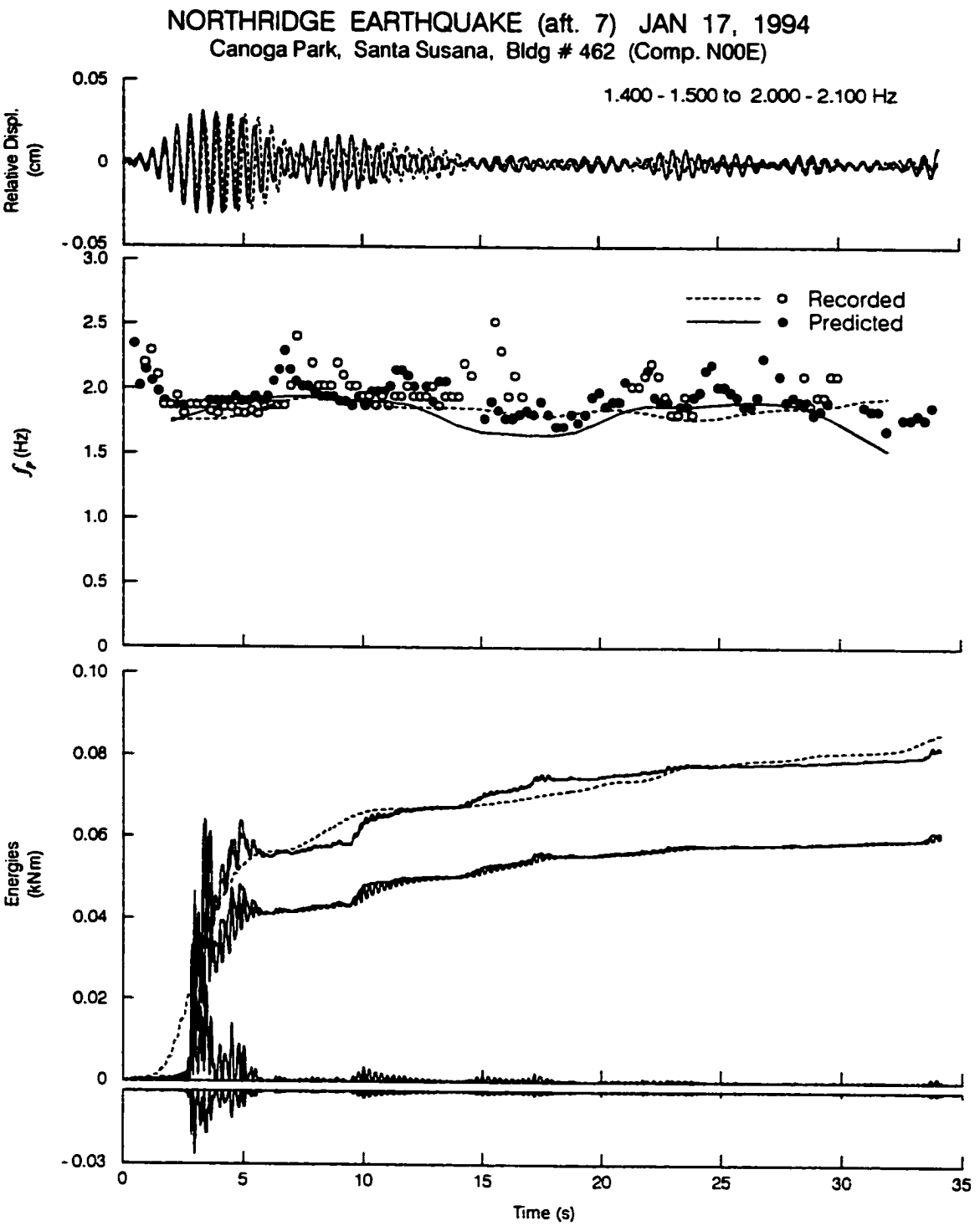

Fig. C.9b Same as Fig. C.9a, but for NS response.

Reproduced with permission of the copyright owner. Further reproduction prohibited without permission.

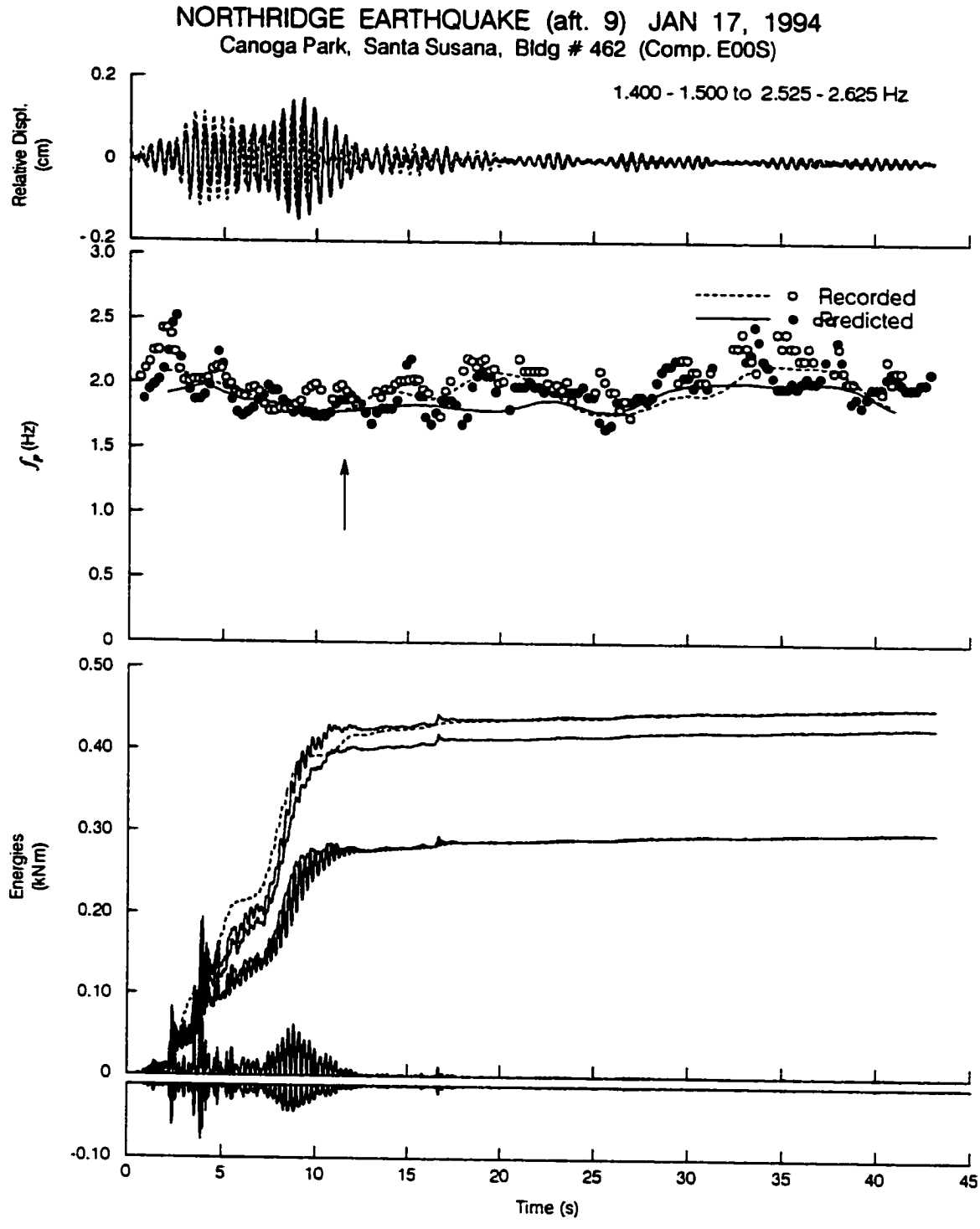

Fig. C.10a Same as Fig. C.8a, but for the 1994 Northridge aftershock #9.

Reproduced with permission of the copyright owner. Further reproduction prohibited without permission.

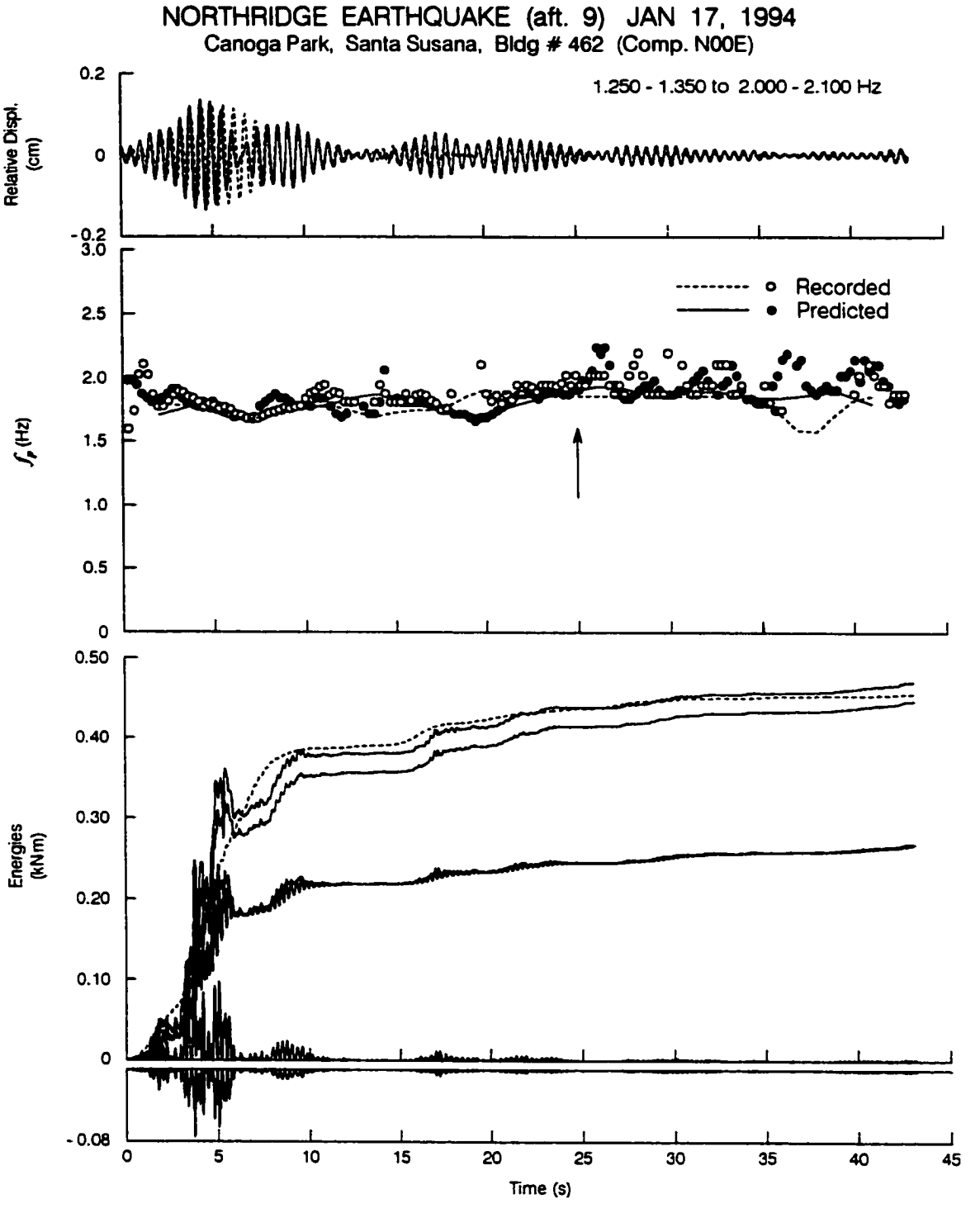

Fig. C.10b Same as Fig. C.10a, but for NS response.

Reproduced with permission of the copyright owner. Further reproduction prohibited without permission.

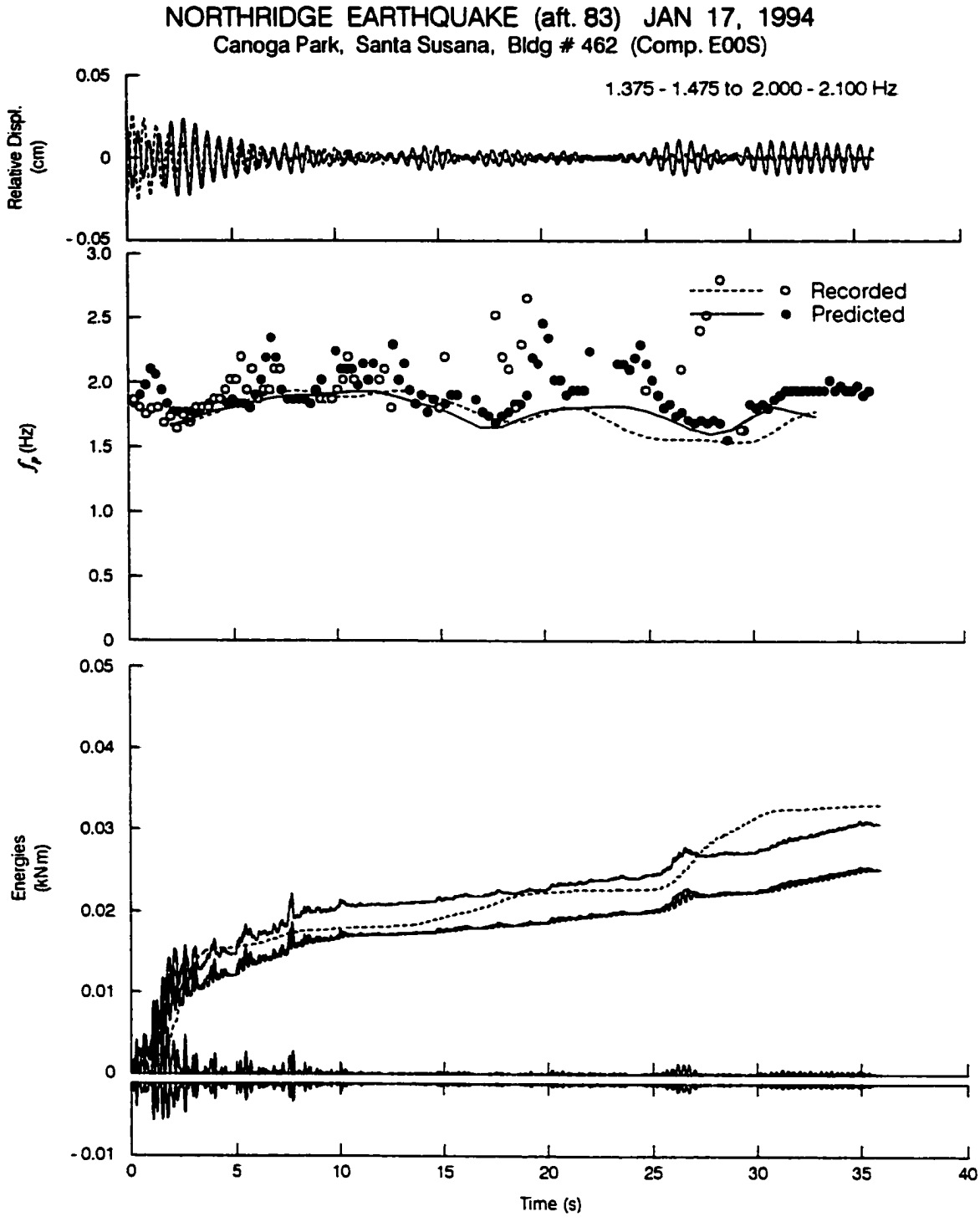

Fig. C.11a Same as Fig. C.8a, but for the 1994 Northridge aftershock #83.

Reproduced with permission of the copyright owner. Further reproduction prohibited without permission.

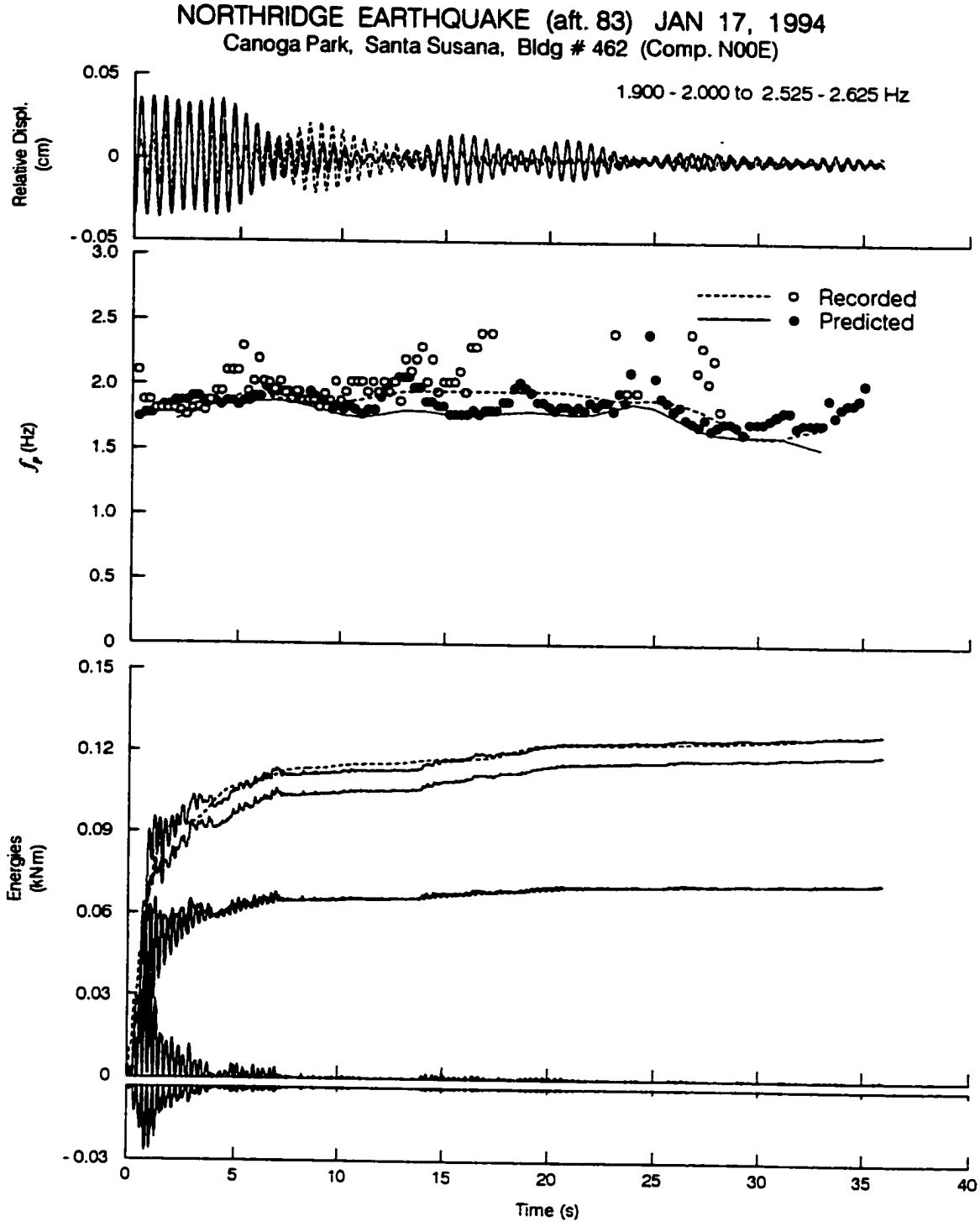

Fig. C.11b Same as Fig. C.11a, but for NS response.

Reproduced with permission of the copyright owner. Further reproduction prohibited without permission.

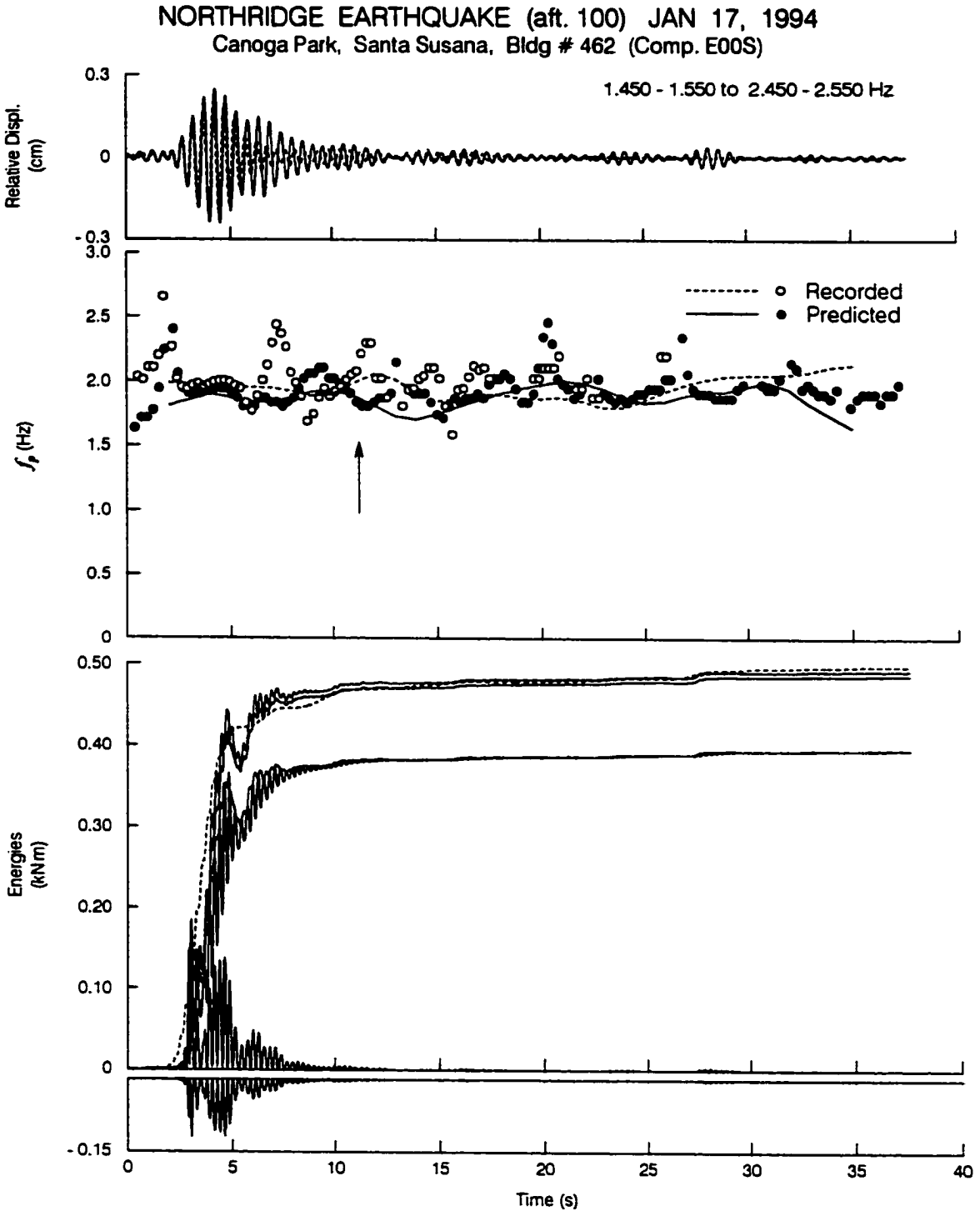

Fig. C.12a Same as Fig. C.8a, but for the 1994 Northridge aftershock #100.

Reproduced with permission of the copyright owner. Further reproduction prohibited without permission.

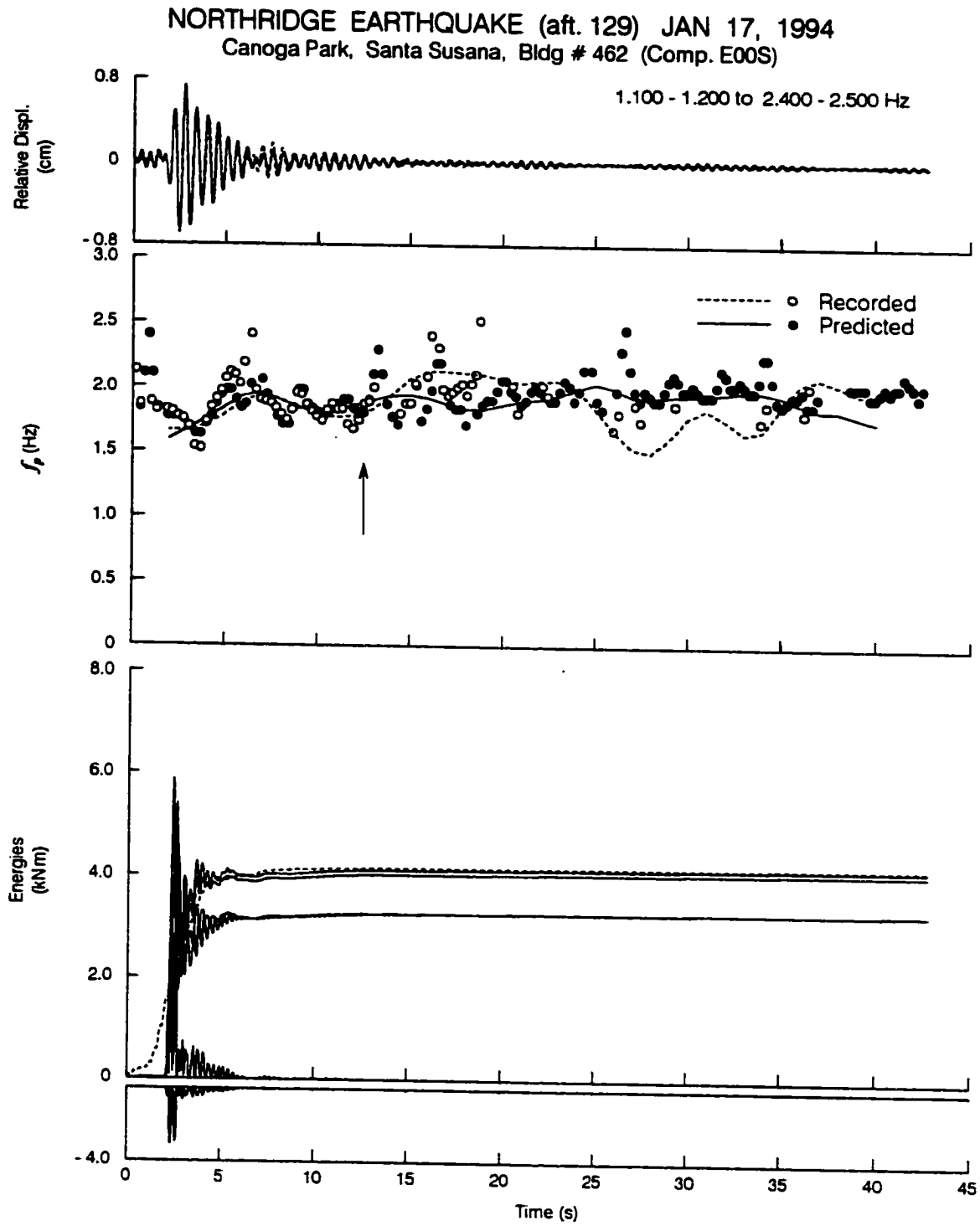

Fig. C.13a Same as Fig. C.8a, but for the 1994 Northridge aftershock #129.

Reproduced with permission of the copyright owner. Further reproduction prohibited without permission.

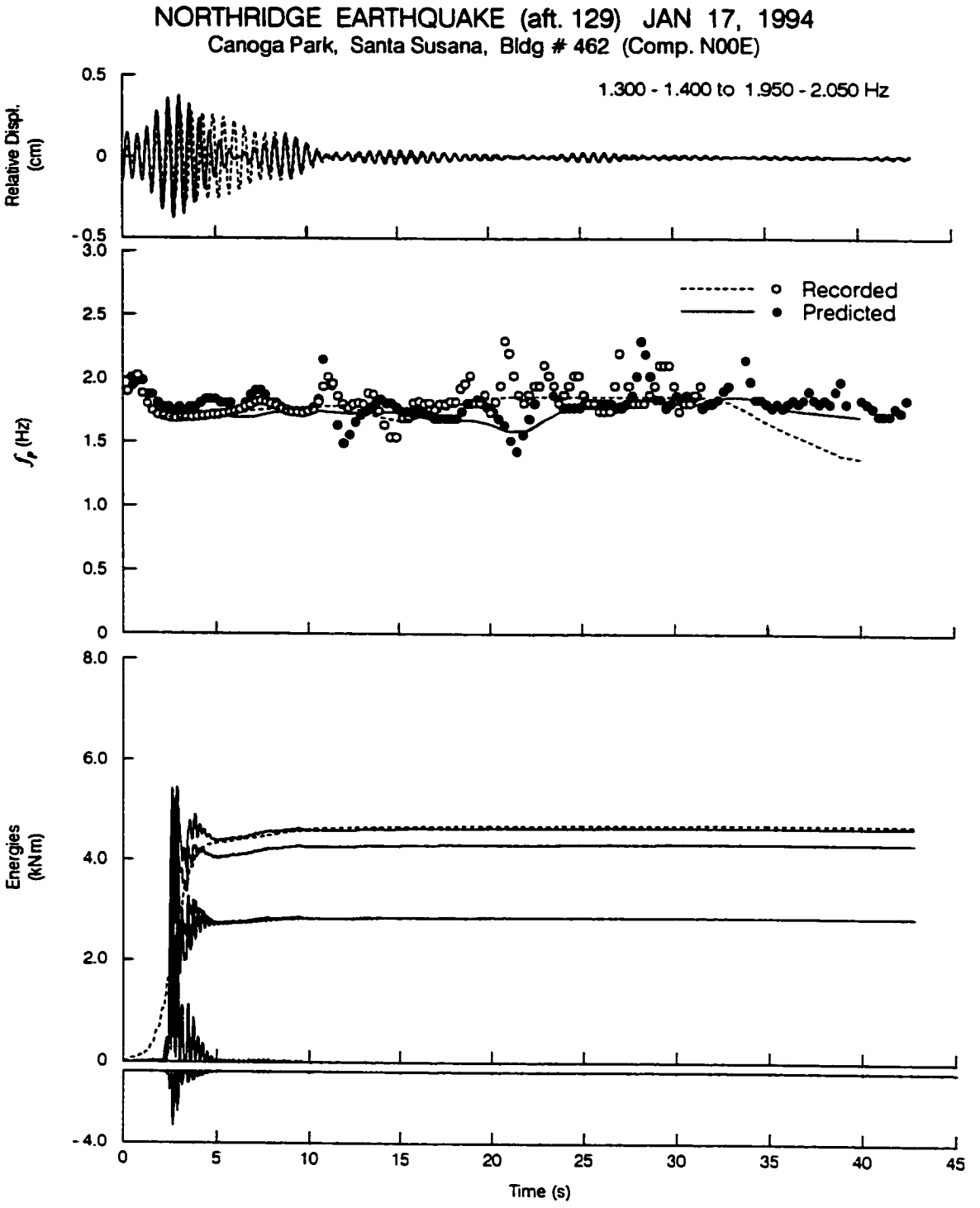

Fig. C.13b Same as Fig. C.13a, but for NS response.

Reproduced with permission of the copyright owner. Further reproduction prohibited without permission.

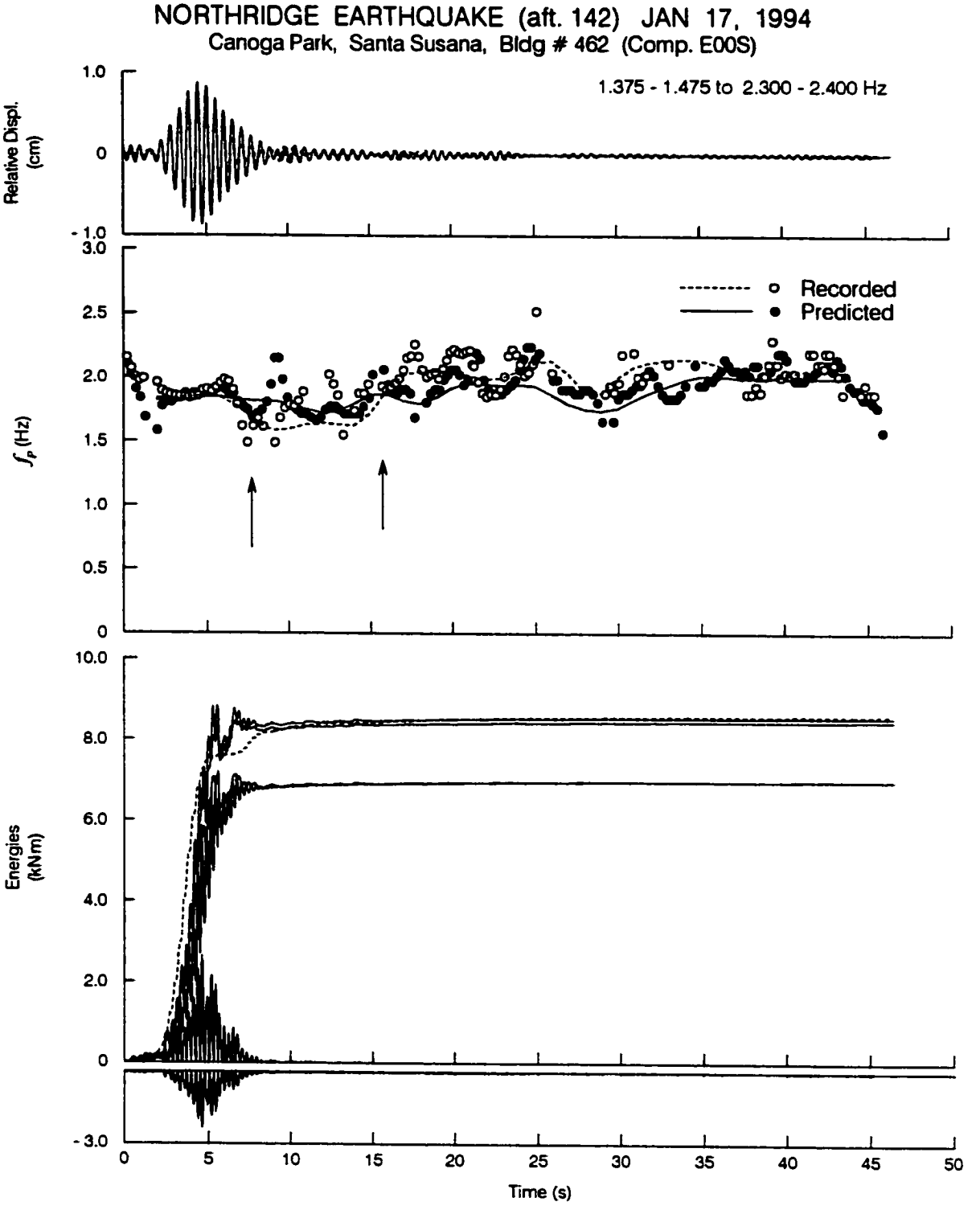

Fig. C.14a Same as Fig. C.8a, but for the 1994 Northridge aftershock #142.

Reproduced with permission of the copyright owner. Further reproduction prohibited without permission.

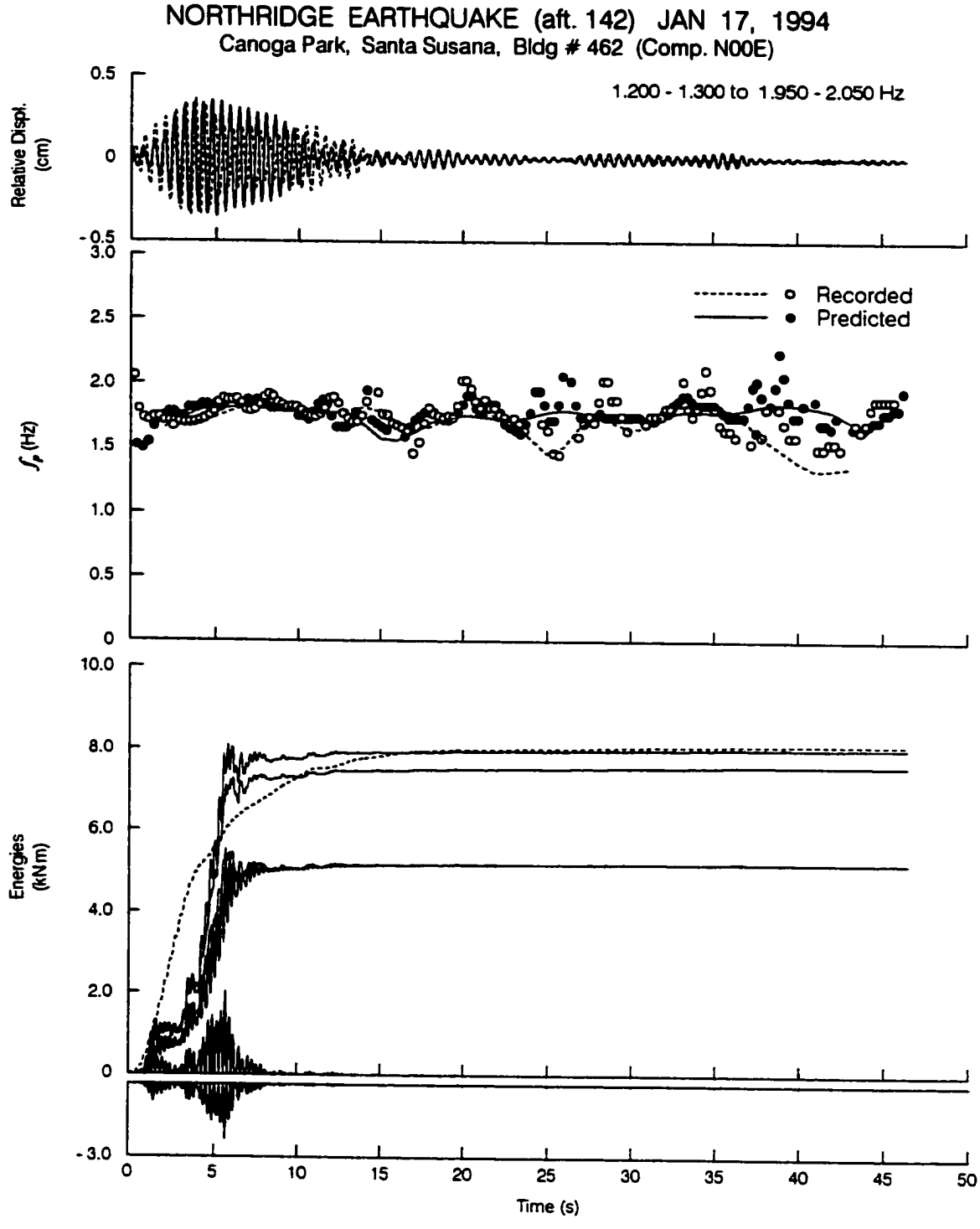

Fig. C.14b Same as Fig. C.14a, but for NS response.

Reproduced with permission of the copyright owner. Further reproduction prohibited without permission.

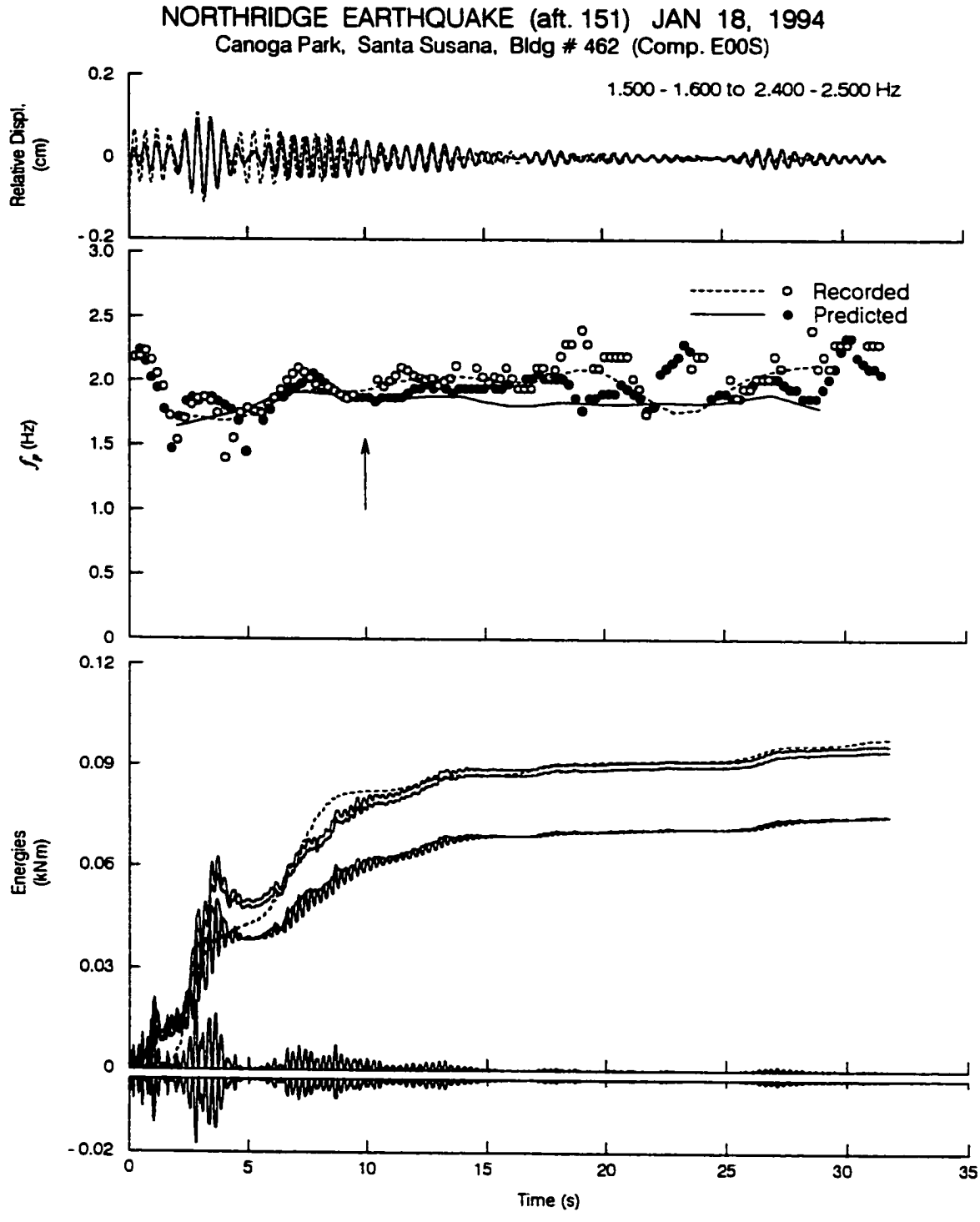

Fig. C.15a Same as Fig. C.8a, but for the 1994 Northridge aftershock #151.

Reproduced with permission of the copyright owner. Further reproduction prohibited without permission.

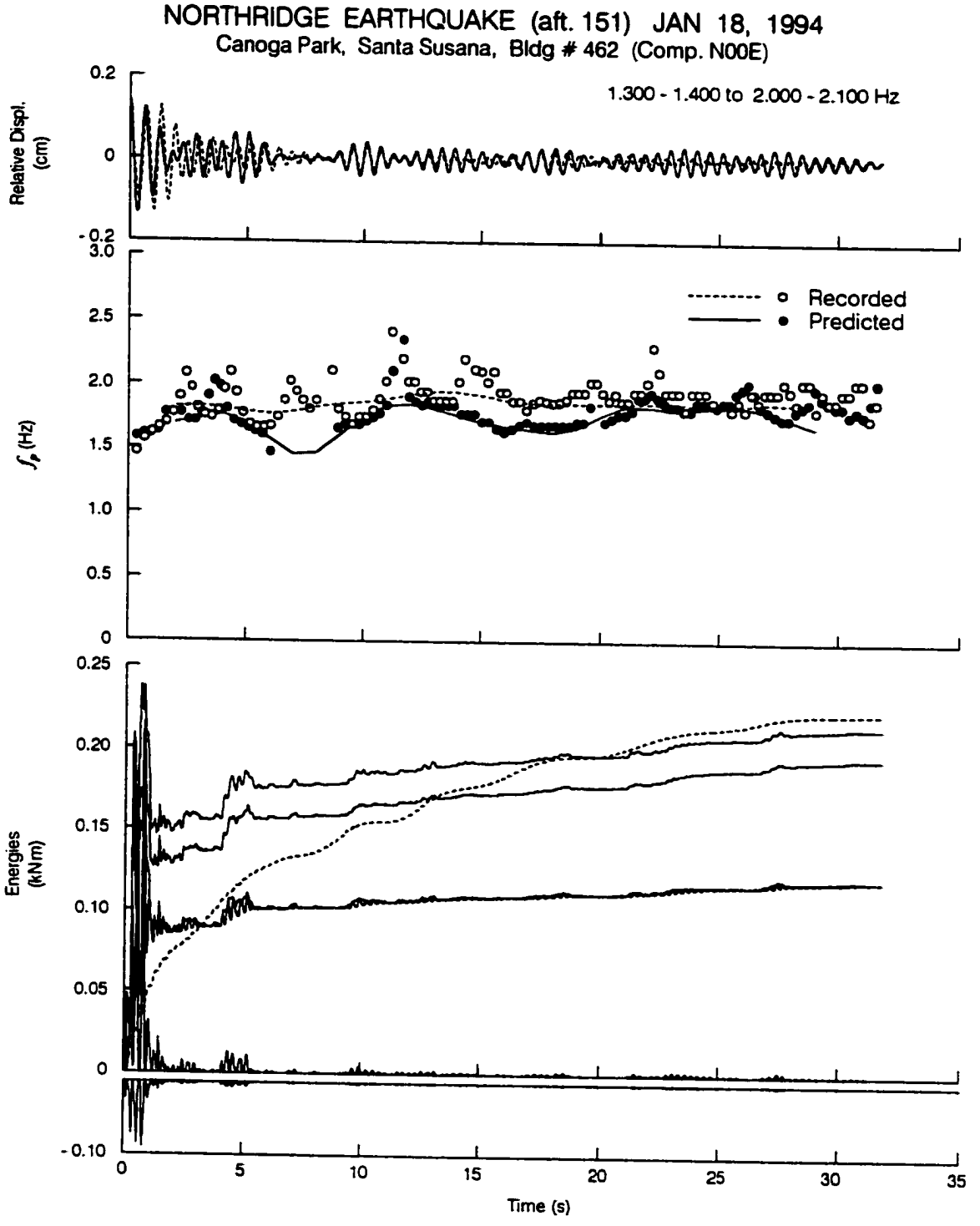

Fig. C.15b Same as Fig. C.15a, but for NS response.

Reproduced with permission of the copyright owner. Further reproduction prohibited without permission.

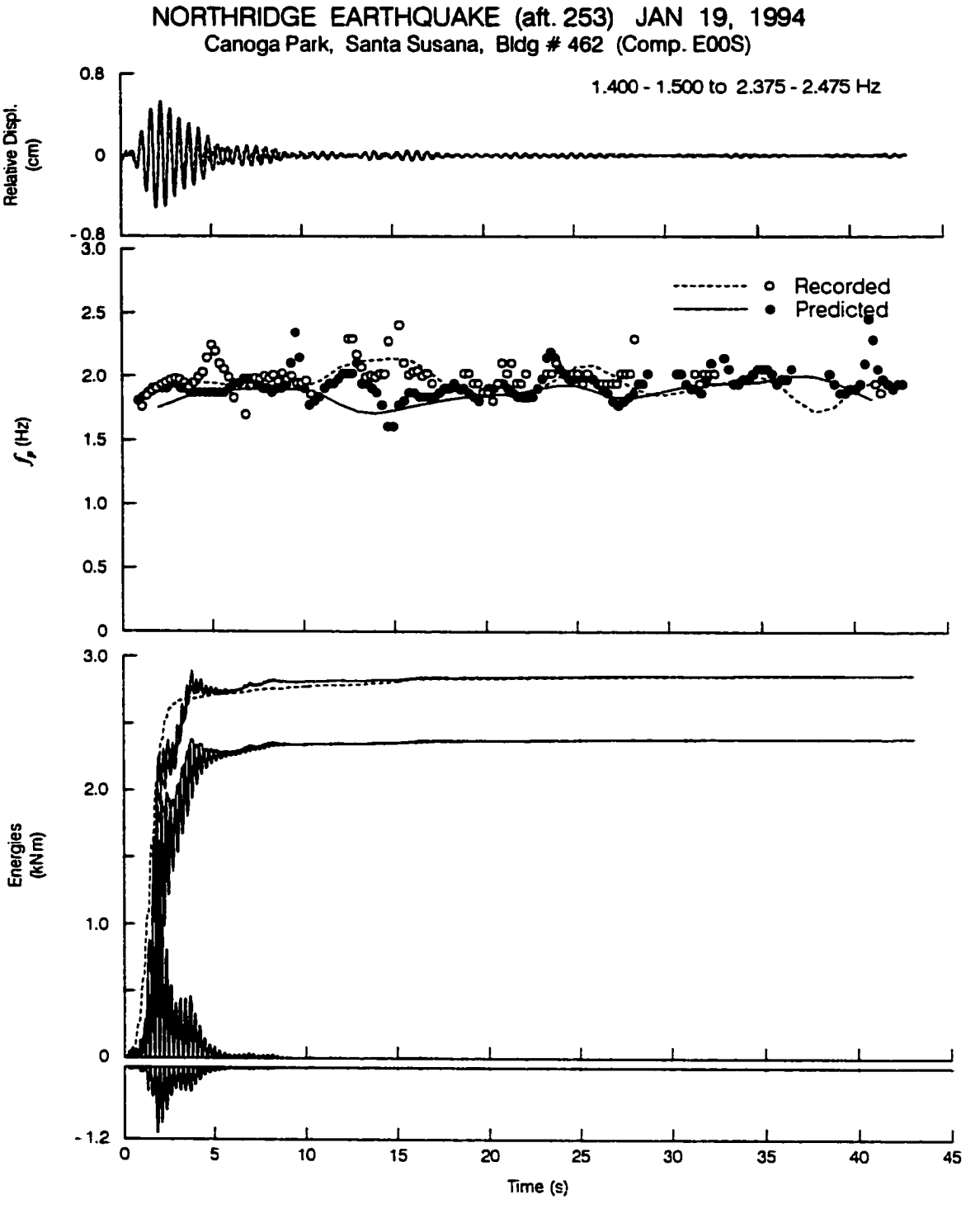

Fig. C.16a Same as Fig. C.8a, but for the 1994 Northridge aftershock #253.

Reproduced with permission of the copyright owner. Further reproduction prohibited without permission.

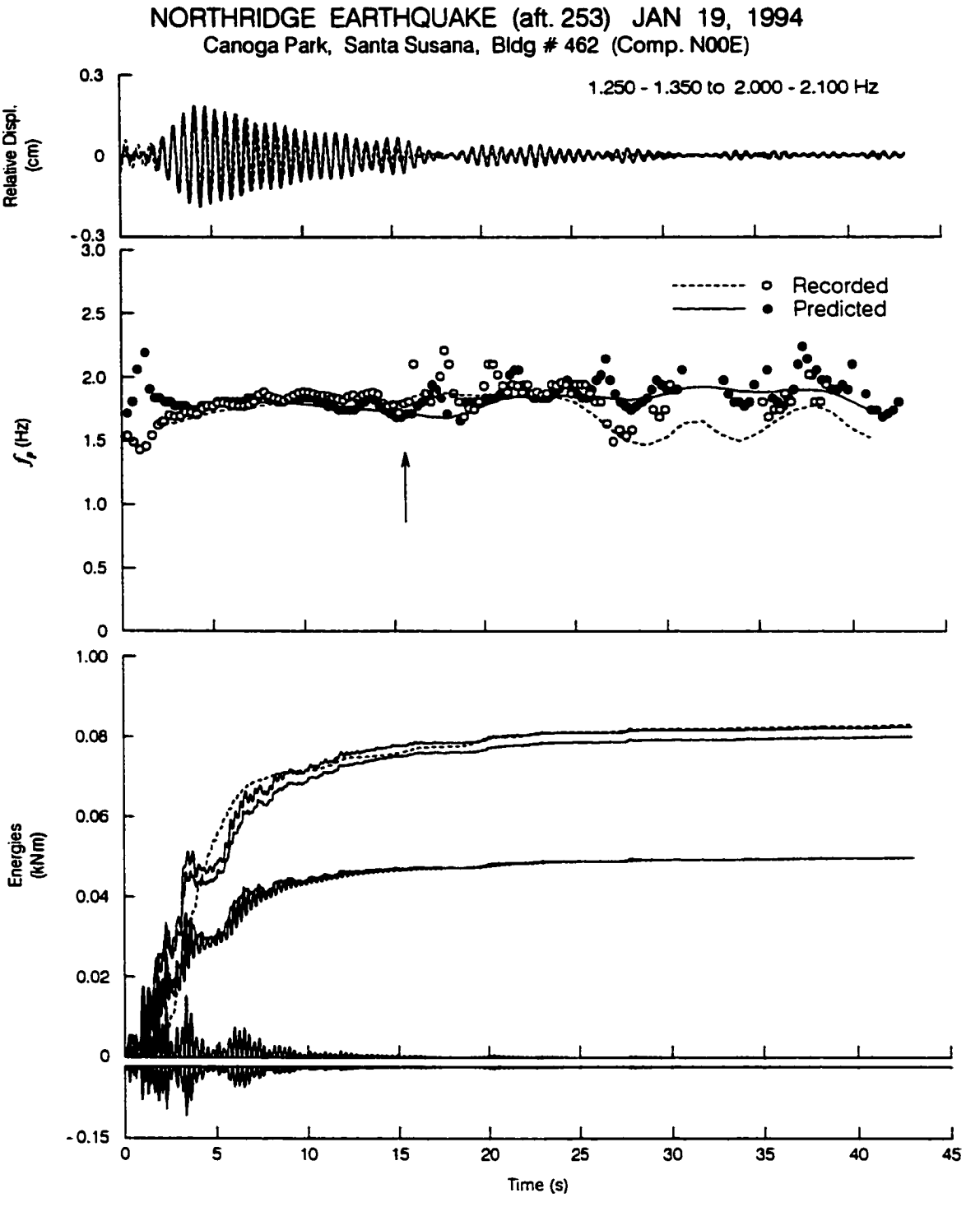

Fig. C.16b Same as Fig. C.16a, but for NS response.

Reproduced with permission of the copyright owner. Further reproduction prohibited without permission.

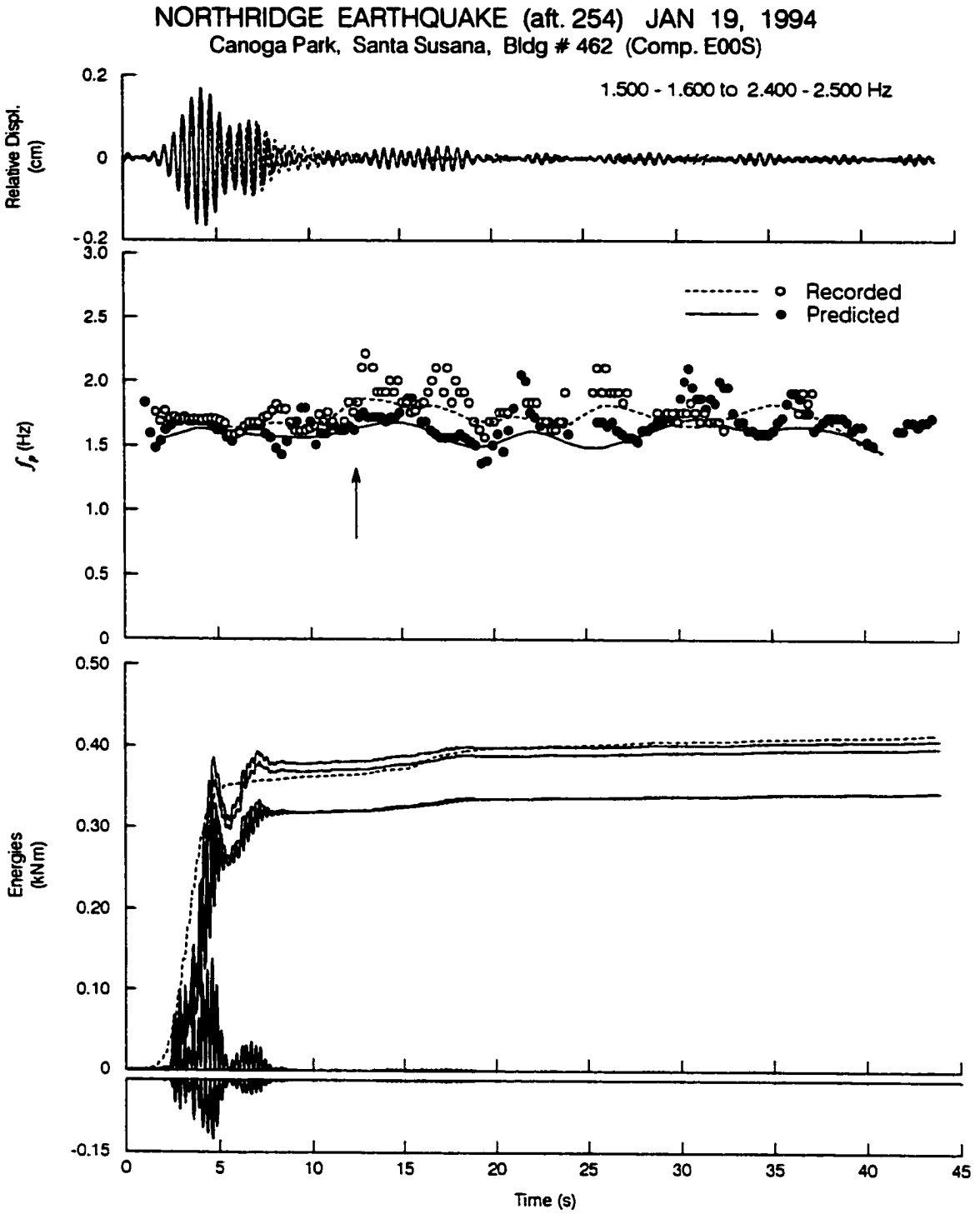

Fig. C.17a Same as Fig. C.8a, but for the 1994 Northridge aftershock #254.

Reproduced with permission of the copyright owner. Further reproduction prohibited without permission.

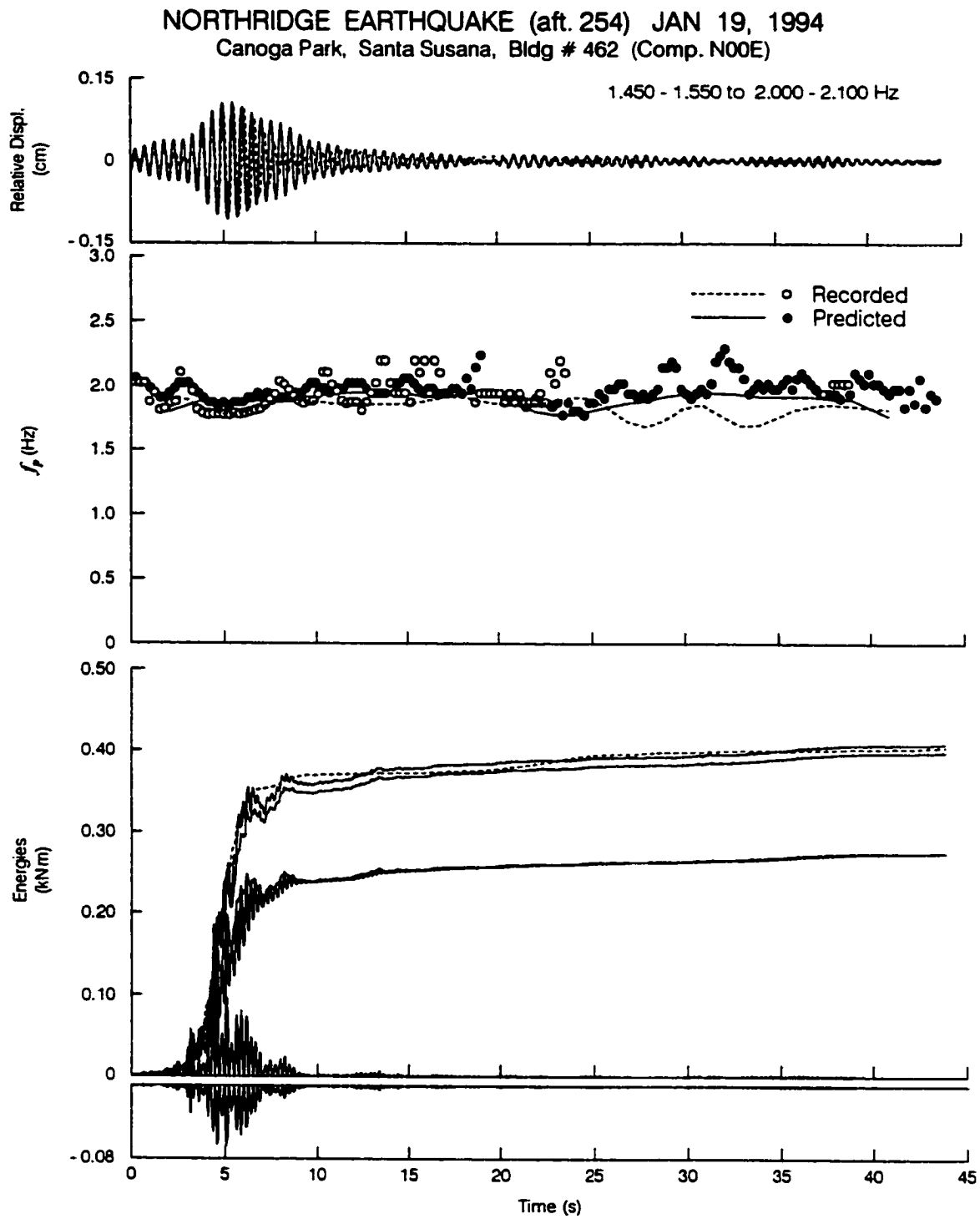

Fig. C.17b Same as Fig. C.17a, but for NS response.

Reproduced with permission of the copyright owner. Further reproduction prohibited without permission.

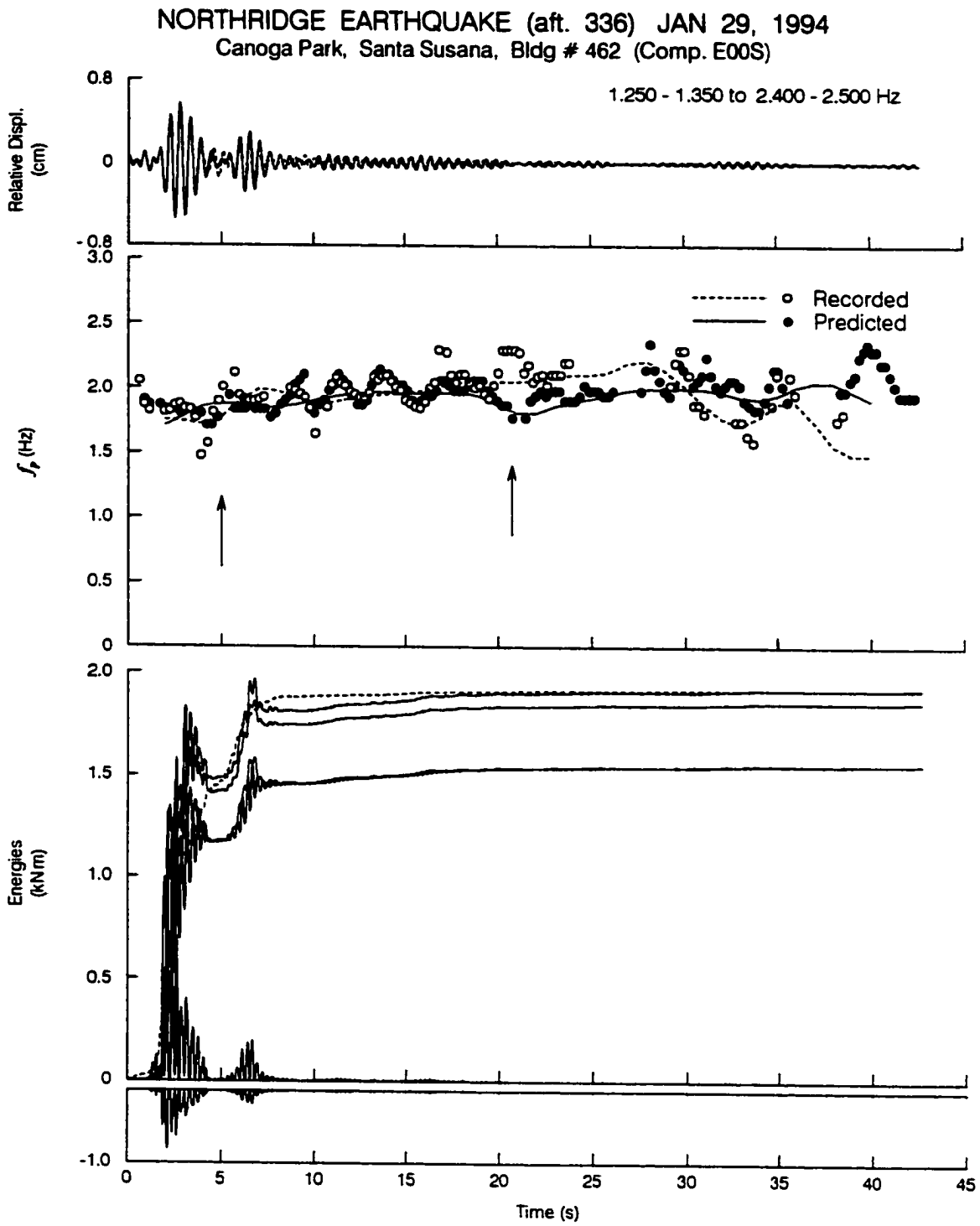

Fig. C.18a Same as Fig. C.8a, but for the 1994 Northridge aftershock #336.

Reproduced with permission of the copyright owner. Further reproduction prohibited without permission.

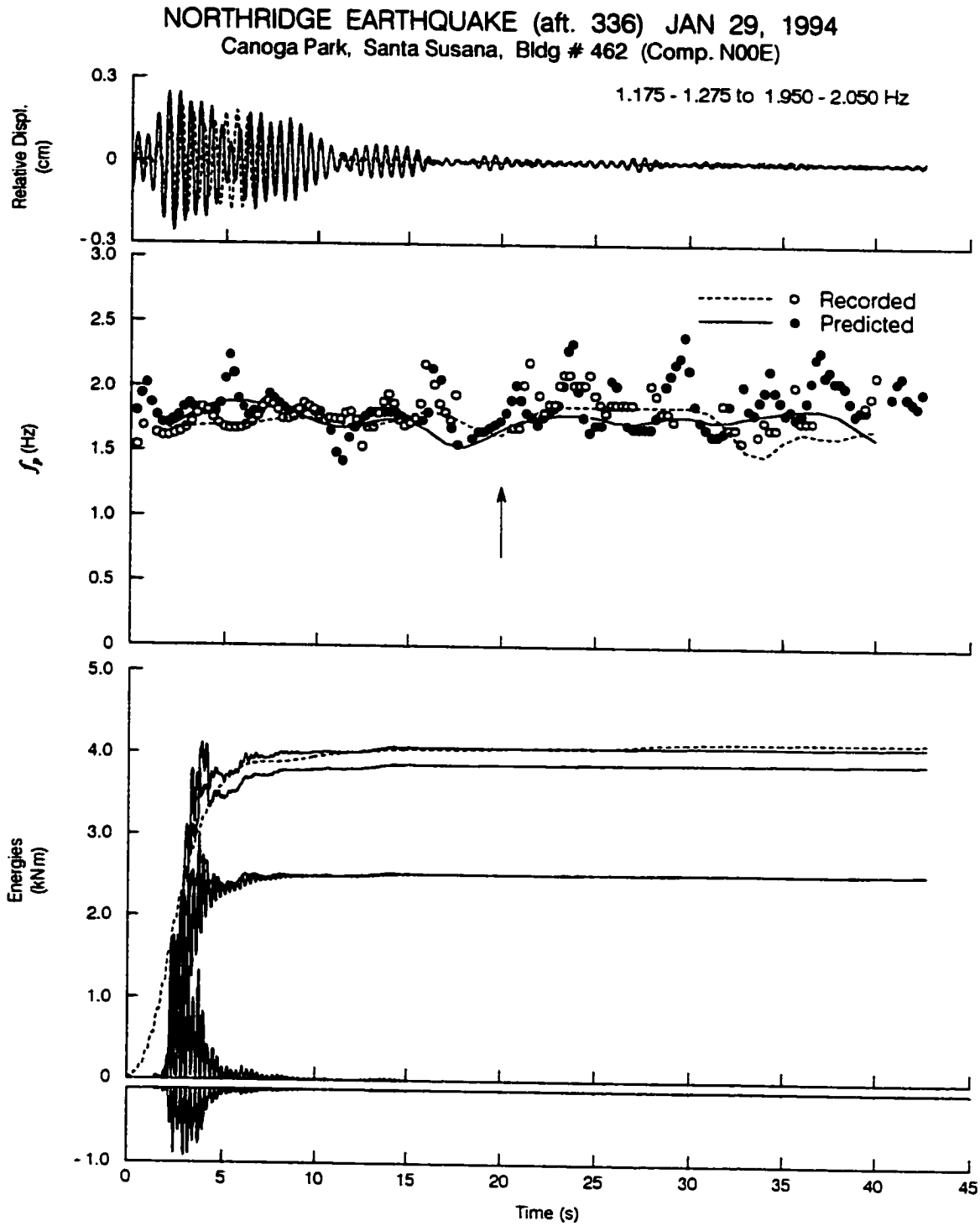

Fig. C.18b Same as Fig. C.18a, but for NS response.

Reproduced with permission of the copyright owner. Further reproduction prohibited without permission.

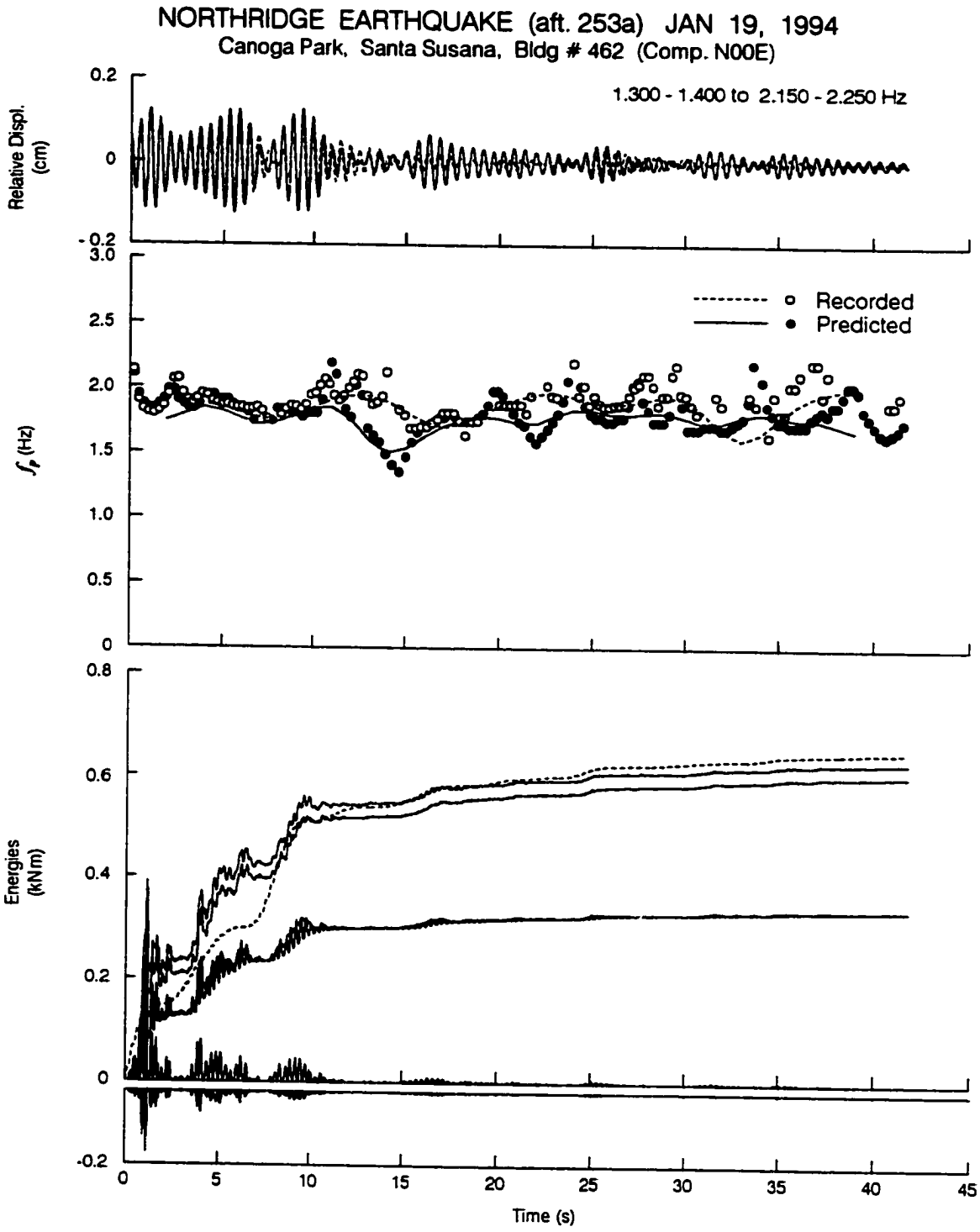

Fig. C.19b Same as Fig. C.19a, but for NS response.

Reproduced with permission of the copyright owner. Further reproduction prohibited without permission.